Lytic polysaccharide monooxygenases from *Myceliophthora thermophila* C1

Matthias Frommhagen

Lytic polysaccharide monooxygenases from *Myceliophthora thermophila* C1

Matthias Frommhagen

Propositions

1. The parameter t_{MF} enables a further discrimination of cellulose-active LPMOs.
   (*this thesis*)

2. The classification of LPMOs as AA (auxiliary activity) enzymes ignores their importance for lignocellulose degradation.
   (*this thesis*)

3. A protease with a high specific activity does not necessarily hydrolyze a protein to a large extent.

4. Call center employees who get provided with cartoons are perceived as more friendly, as smiling is discerned auditively through the phone.
   (Ohala, JJ, 1980, The acoustic origin of the smile, J. Acoust. Soc. Am. 68:33)

5. Trial and error experiments are underestimated for their effectiveness.

6. Basic military obligation is a better tool for integration than an obligatory integration course.

Propositions belonging to the thesis, entitled

'Lytic polysaccharide monooxygenases

from *Myceliophthora thermophila* C1'

Matthias Frommhagen

Wageningen, 8th September 2017.

Lytic polysaccharide monooxygenases from *Myceliophthora thermophila* C1

Matthias Frommhagen

Thesis committee

Promotors

Prof. Dr H. Gruppen
Professor of Food Chemistry
Wageningen University & Research

Prof. Dr W.J.H. van Berkel
Personal chair at Biochemistry
Wageningen University & Research

Co-promotor

Dr M.A. Kabel
Assistant professor, Laboratory of Food Chemistry
Wageningen University & Research

Other members

Prof. Dr J. van der Oost, Wageningen University & Research
Prof. Dr V.G.H. Eijsink, Norwegian University of Life Sciences, Ås, Norway
Dr F. Hollmann, Delft University of Technology
Dr S. Kralj, DuPont Industrial Biosciences, Leiden

This research was conducted under the auspices of the Graduate School VLAG (Advanced studies in Food Technology, Agrobiotechnology, Nutrition and Health Sciences).

Lytic polysaccharide monooxygenases from *Myceliophthora thermophila* C1

Matthias Frommhagen

Thesis

submitted in fulfilment of the requirements for the degree of doctor

at Wageningen University

by the authority of the Rector Magnificus,

Prof. Dr A.P.J. Mol,

in the presence of the

Thesis Committee appointed by the Academic Board

to be defended in public

on Friday 8 September 2017

at 11 a.m. in the Aula.

Matthias Frommhagen

Lytic polysaccharide monooxygenases from *Myceliophthora thermophila* C1, 194 pages.

PhD thesis, Wageningen University, Wageningen, the Netherlands (2017)

With references, with summary in English

ISBN 978-94-6343-643-4

DOI http://dx.doi.org/10.18174/420143

Abstract

Current developments aim at the effective enzymatic degradation of plant biomass polysaccharides into fermentable monosaccharides for biofuels and biochemicals. Recently discovered lytic polysaccharide monooxgygenases (LPMOs) boost the hydrolytic breakdown of lignocellulosic biomass, especially cellulose, due to their oxidative mechanism. At the beginning of this thesis, only few LPMOs were characterized and many aspects related to their catalytic performance were unknown. Hence, in this thesis, we investigated AA9 LPMOs from *Myceliophthora thermophila* C1. This fungus encodes 22 putative AA9 LPMOs and we hypothesized that these enzymes differ in their substrate preference and mode of action towards plant cell wall polysaccharides.

We demonstrated that *Mt*LPMO9A oxidizes xylan associated to cellulose, which is the only published LPMO comprising this capability known so far. We also showed that *Mt*LPMOs from *M. thermophila* C1 differ in their substrate preference and C1-/C4-regioselectivity. Moreover, we described the use of reversed phase (RP)-UHPLC in combination with non-reductive 2-aminobenzamide (2-AB) labeling to separate and identify C4-oxidized gluco-oligosaccharides.

All characterized *Mt*LPMOs differ in their reducing agent preference. The highest amount of non-oxidized and oxidized gluco-oligosaccharides from cellulose were released by *Mt*LPMOs in the presence of reducing agents with a 1,2-benzenediol or 1,2,3-benzenetriol moiety. The latter compounds can be formed from lignin-building blocks by using polyphenol oxidases (PPOs), such as *Mt*PPO7 from *M. thermophila* C1, which boost the LPMO-driven lignocellulose oxidation. Sequence analysis of genomes of 336 Ascomycota and 208 Basidiomycota revealed a high correlation between *Mt*PPO7-like and AA9 LPMO-like genes. Finally, a β-glucosidase-assisted method was developed to quantify the catalytic performance of the C1-oxidizing *Mt*LPMO9B and *Mt*LPMO9D. The catalytic performance of both *Mt*LPMOs was strongly dependent on pH and temperature. Notably, pH mainly affected the reducing agent dependency whereas temperature influenced the operational stability of both *Mt*LPMOs.

In summary, our study contributed to the further understanding of LPMO-driven lignocellulose degradation.

Table of contents

Chapter I

General Introduction

1.1 Relevance of this research

The industrial development of the last centuries has led to a rising demand of energy through the increased use of fuel, materials and chemicals. Nowadays, this energy is mainly derived from fossil resources which leads to the emission of carbon dioxide contributing to global warming.

A milestone of the last years was the replacement of the historic 'Kyoto Protocol' by the ratification of the new 'Paris Agreement' by the United Nations Framework Convention on Climate Change (UNFCCC). One of the aims of the new agreement is to not exceed the global average temperature rise of 2°C in order to minimize the effects of climate change [1]. Hence, it is essential to develop new strategies to ensure an alternative energy supply without increasing the carbon dioxide emission. A key strategy aims at the use of alternative energy sources such as wind, hydroelectric, geothermal and solar power, as well as plant biomass biorefinery. The biorefinery concept aims at the degradation of plant biomass into smaller building blocks that can be used for the production of biochemicals and biofuels. Still, carbon dioxide emission will occur, but now plants can make use of this carbon dioxide to produce new biomass. Such a closed cycle is seen as an environmentally friendly contribution to a green and circular economy.

In order to degrade non-edible plant biomass for the production of biofuels and biomaterials, enzymes are seen as effective and green catalysts. However, plant biomass mainly consists of plant cell wall materials which are difficult to degrade by enzymes due to the complex lignocellulose structure. For many years it was assumed that enzyme degradation of lignocellulose was steered by hydrolytic enzymes only. Hence, the current commercial enzyme cocktails contain high amounts of various hydrolytic enzymes. Recently, a new class of enzymes, namely lytic polysaccharide monooxygenases (LPMOs), were discovered that have been shown to enhance the activity of hydrolytic enzymes in degrading lignocellulosic plant cell wall compounds [2, 3]. The discovery of these LPMOs is expected to open new ways for degrading complex lignocelluloses. Therefore, it can be expected that the composition of future commercial enzyme cocktails will completely change due to the incorporation of LPMOs. At the beginning of this research, only little was known about LPMOs and only a few of them were characterized. Therefore, this thesis aimed at studying various features of multiple LPMOs from the fungus *Myceliophthora thermophila* C1, such as activity, mode of action and substrate specificity.

1.2 Plant cell wall

1.2.1 Plant cell wall architecture

The plant cell wall is composed of a middle lamella, a primary and a secondary cell wall. Both primary and secondary cell walls are built of various polysaccharides, such as cellulose and hemicellulose, the aromatic polymer lignin and structural proteins [4]. All components are present in varying proportions within the cell wall, but in general, the polysaccharides are the most abundant components. Variations in the plant cell wall structure and composition, as discussed below, are dependent on the year and location of the harvest, developmental stage of the plant and part of the plant (e.g. leaf or stem) [5].

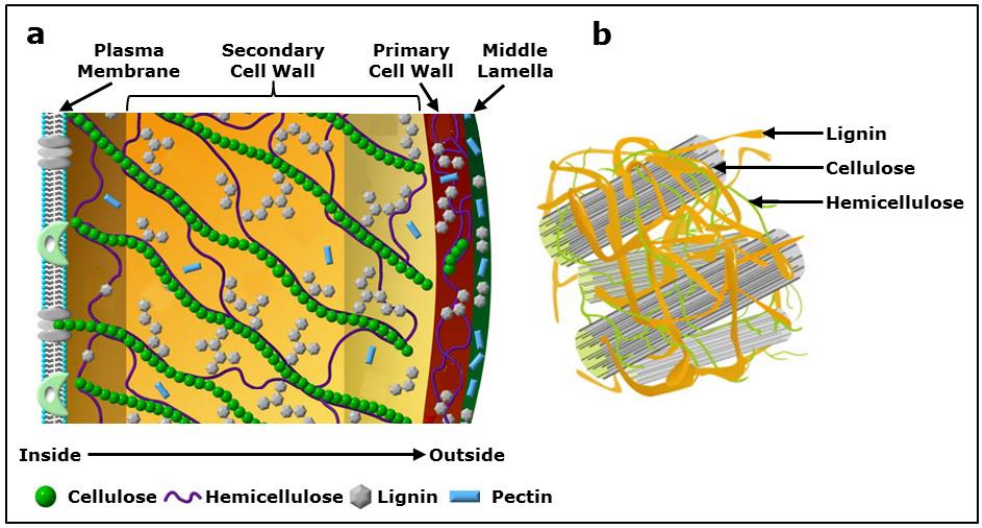

Figure 1.1 Plant cell wall models. **a** Model of the four plant cell wall compartments (based on Achyuthan *et al*. [6]). **b** Interaction of structural elements in the secondary plant cell wall (based on Vanholme *et al*. [7]).

The middle lamella is a very flexible cell wall compartment and represents the first synthesized layer of the plant cell wall. This layer mainly contains pectins and has a high water binding capacity [8]. The flexibility of this layer allows cells to expand. The next layer is the primary cell wall, which is the major part of the plant cell wall in fruits and vegetables [9]. The primary cell wall is mainly composed of polysaccharides and classified into Type I and II, based on the structure. The Type I cell wall is present in dicots and to a certain degree in monocots as well [10]. This Type I consists of cellulose microfibrils, which are embedded in a network built of xyloglucan and, to a lesser extent, glucuronoarabinoxylans (GAXs), as well as pectins such as homogalacturonans and rhamnogalacturonan I [11, 12]. At a later developmental stage, Type I cell wall components are further crosslinked with structural proteins [11]. Type II cell walls are present in Poaceae and in related monocots. In these Type II cell walls, cellulose is embedded in a network of GAXs and, to a lower extent, pectins, glucomannans and xyloglucans [10, 13].

Relevant for lignocellulosic plant biorefinery is the secondary plant cell wall, which represents the main part of the dry matter of lignocellulosic feedstocks. Examples of the latter are grass-like agricultural by-products or hard- and softwoods. The secondary cell wall represents the third layer of the cell wall and contains cellulose and hemicellulose [10]. This hemicellulose is majorly represented by (acetylated) GAXs in grasses and hard woods or mannans in soft woods and will be further explained in **Section 1.2.3**. In addition, the secondary cell wall is further fortified by non-(hemi)cellulose compounds such as lignin or suberin (**Figure 1.1**) [14].

The interactions within and between secondary cell wall components, such as cellulose and hemicellulose, are presented separately in **Section 1.2.5**.

1.2.2 Cellulose

Cellulose is mainly produced by photosynthetic higher plants and algae, but there are also non-photosynthetic organisms such as some bacteria species, marine invertebrates or fungi that are able

to synthesize cellulose [15, 16]. In general, cellulose is simply described as a homogeneous linear polymer of β-(1→4)-linked glucan chains which aggregate into microfibrils via hydrogen bonds and van der Waals forces [17].

The structure of cellulose itself is highly polymorph. Alternate (rotated by 180°) glucosyl units are linked to form a flat ribbon (**Figure 1.2**). Hydrogen bonds between the *O*3-H···*O*5' tighten this conformation [15]. Several of these glucan chains are aligned in parallel and form one sheet [18]. The sheets are stacked on top of each other with a stagger over the whole distance row of microfibrils. The type of stagger depends on the crystal form I_α, which is the predominant form found in algae and bacteria, and I_β that is present in plants [15, 17, 19, 20]. Dependent on the source, these crystalline forms vary in their proportion and type of hydrogen bonds between oxygen atoms (*O*2, *O*3, *O*5 and *O*6) [15, 17, 19, 21]. In general, 12-32 glucan chains form one microfibril which is twisted and forms a diamond or rectangular shape in higher plants, such as wood (**Figure 1.2**) [16, 18]. These microfibrils also differ in length which is a result from the glucan chains that have either a very high DP (14,000-15,000) in the secondary cell wall (e.g. cotton) or a shorter DP (between 500 and 8,000) in the primary cell wall [22].

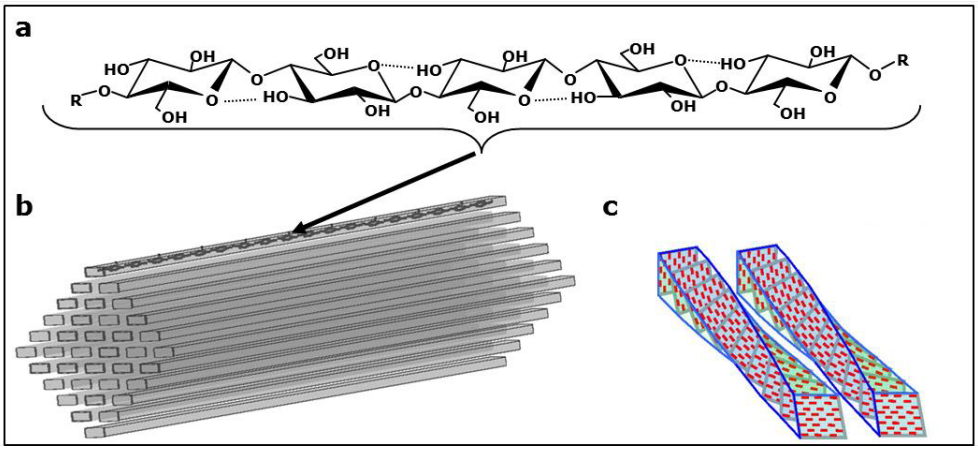

Figure 1.2 Simplified structural overview of cellulose. **a** The backbone structure of cellulose consists of β-(1→4)-linked glucan chains. Dotted lines indicate hydrogen bonds (*O*3-H...*O*5') between glycosyl units. **b** Structure of the cellulose microfibril (based on Horn *et al*. [23]). **c** Schematic presentation of two adjacent twisted microfibrils (based on Fernandez *et al*. [18]).

The interaction between the glucan chains and the described packing is not completely coherent within cellulose, which leads to the formation of crystalline and amorphous regions. For example, varying and less strict hydrogen bonds between surface chains of the microfibril allows intermolecular interaction with external molecules in the plant, which were hypothesized to be, for example, hemicelluloses [24]. In addition, pretreatments (e.g. alkaline extraction conditions or heating) can change the structure of cellulose and, based on the crystallinity, lead to the formation of allomorphs, such as type II, III or IV [20, 22]. These crystalline allomorphs of cellulose differ in their X-ray diffraction pattern and solid-state nuclear magnetic resonance (NMR) spectral properties [20].

1.2.3 Hemicellulose

Unlike cellulose, hemicellulose comprises very heterogeneous polymers. Hemicelluloses can have different backbones and show structural side-chain variations, like different types and distributions of substituents along the backbone. In addition, backbones of hemicelluloses are strongly associated with cellulose via hydrogen bonding, especially the ones with a low degree of substitution or a block-wise distribution of substituents along the backbone [25, 26]. The backbone structure as well as the type and pattern of substituents vary between different plant species and tissues (**Figure 1.1**).

Xylans are a diverse group of polysaccharides, which constitute about 20 to 30% (w/w) of the dry matter content in dicotyl plants, such as hardwoods, and can account for up to 50% (w/w) in cereals and grasses [29]. Xylans are further divided into homoxylans, which are present in algae and seaweed, and more complex heteroxylans that are part of the cell wall of higher plants [29]. The backbone of heteroxylan consists of β-(1→4)-linked xylosyl residues [28, 30]. Notably, mono- and dicotyledons differ in their heteroxylan structure.

The heteroxylans in monocotyledons, like grasses and cereals, are substituted by arabinosyl residues at either the *O*-2, *O*-3 or both positions of the xylosyl backbone and are known as arabinoxylans (**Figure 1.3a**). To a lesser extent, these xylans can be substituted by glucuronosyl and 4-*O*-methyl-glucuronosyl residues, referred to as glucuronoarabinoxylans (GAX) (**Figure 1.3a**). GAXs are further acetylated, via the *O*-2, *O*-3 or both positions of the xylosyl backbone, and the amount of acetyl groups ranges from less than 1% to 4% (w/w) of the dry matter content, depending on the source [31]. Furthermore, many more variations exist in the xylan structure, such as ester-linked ferulic and *p*-coumaric acid substitutions than can be further crosslinked to lignin (**Section 1.2.5**) [28, 29, 32, 33]. Glucuronoxylans (GX) are present in hardwoods, such as beech, birch and aspen wood. In general, the β-(1→4)-linked xylosyl backbone is substituted by α-(1→2)-linked 4-*O*-methyl-glucuronosyl residues [28, 29, 34-36]. Moreover, these GXs are highly acetylated in a range from 8 to 17%, based on the dry matter content (**Figure 1.3**) [31].

Xyloglucans are mostly found in the primary cell walls of higher plants, such as dicots (e.g. fruit and vegetables) or soft- (e.g. spruce) and hardwoods (e.g. poplar) [29, 31]. As an example, the poplar primary cell wall is composed of up to 6% (w/w) of xyloglucan whereas the xyloglucan content is less than 1% (w/w) in the secondary cell wall, based on the dry matter content [37]. In contrast, between 20 and 25% (w/w) of the dry matter is xyloglucan in the primary cell wall of *Arabidopsis thaliana* [29]. The backbone of xyloglucan consists of β-(1→4)-linked glycosyl residues that are substituted with xylosyl residues. These xylosyl residues are often extended with galactosyl and fucosyl residues, to a varying degree (**Figure 1.3b**). Despite these varying substitutions, xyloglucans comprise repeating substituted backbone units, which led to the introduction of a one-letter code (**G**, **X**, **L**, ...) for an eased identification and characterization (**Figure 1.3b**) [27].

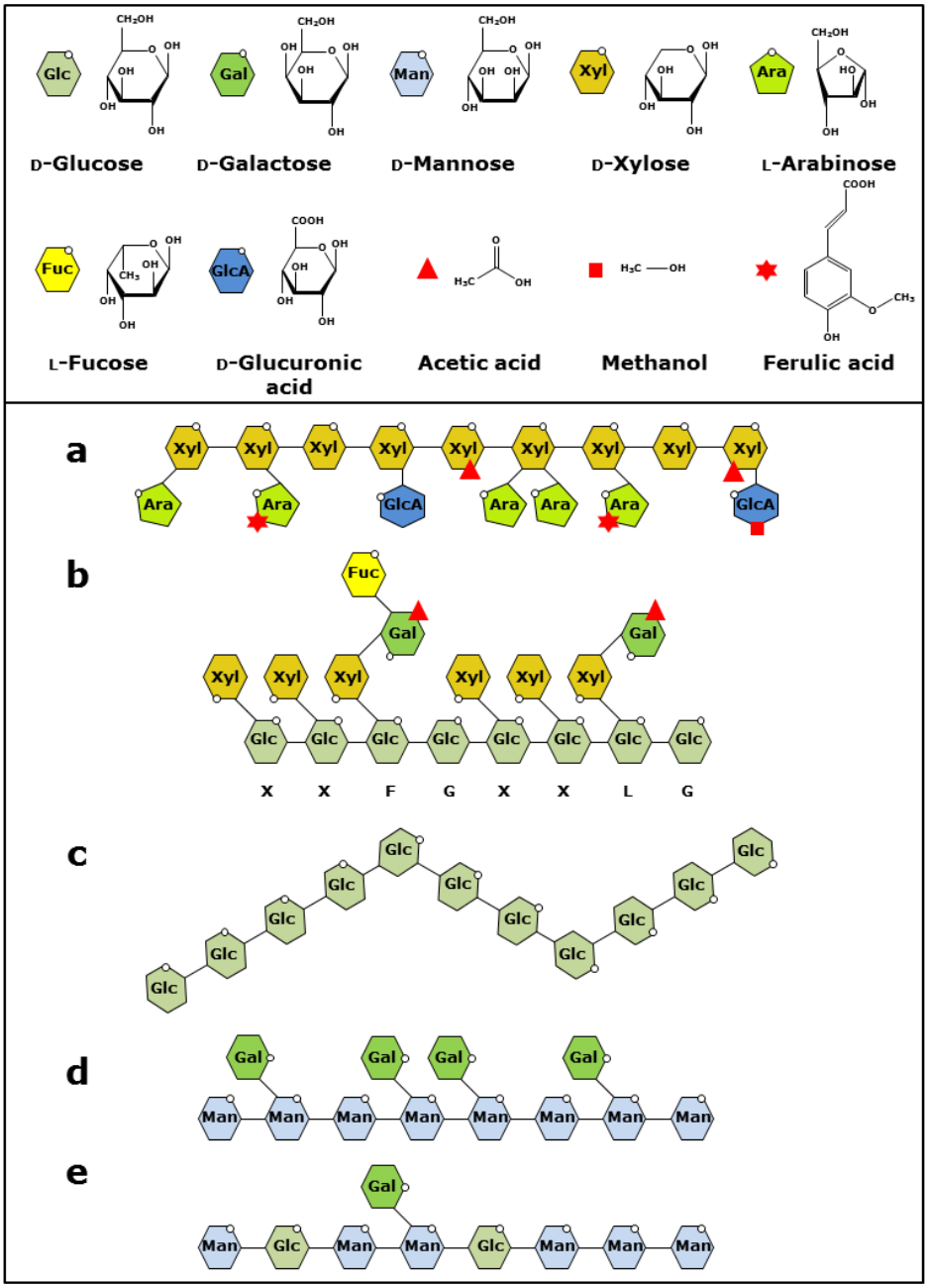

Figure 1.3 Structural presentation of hemicelluloses present in plant cell walls. **a** Glucuronoarabinoxylan (GAX), **b** xyloglucan (letters under the molecule indicate common side chains according to Fry *et al*. [27]), **c** mixed β-(1⟶3, 1⟶4)-linked glucan **d** galactomannan and **e** galactoglucomannan. Structures are modified and based on Scheller *et al*. [28]. Structural units are shown in the legend on the top.

Mixed β-(1→3, 1→4)-linked glucans are mainly present in the primary cell wall of cereal kernels, such as oat and barley [28]. Depending on the source, the content of β-glucan ranges from 3 to 12% (w/w) based on the total dry matter content [29]. In general, three to four β-(1→4)-linked glycosyl units are linked with each other via β-(1→3)-linkages, but longer β-(1→4)-linked segments have also been reported (**Figure 1.3c**) [38, 39].

Mannans and glucomannans mainly consist of β-(1→4)-linked mannosyl units which can be *O*2 and *O*3 acetyl-esterified. Next to these mannosyl units, the backbone can also contain glycosyl units as reported for glucomannans and galactomannans (**Figure 1.3d** and **e**) [40]. Glucomannans are present in soft- and hardwoods, algae species and mosses, whereas galactomannans are majorly present in softwoods, such as conifers [29, 31, 41, 42]. Mannans in hardwoods represent 3-5% of the dry matter content, whereas the seeds of *Mimosa* species can contain up to 20% galactomannans [29].

Pectins are highly heterogeneous polymers which consist of a plethora of different monosaccharides that show a great variability in linkage type [43]. The three backbone structures are homogalacturonan, xylogalacturonan and rhamnogalacturonan I, whereas the side chain substructures are arabinan, galactan and rhamnogalacturonan II [43].

1.2.4 Lignin and aromatic compounds

Lignin is an aromatic heteropolymer accounting for 10 to 15% (w/w) of the total dry matter content of grasses and up to 30% of soft- and hardwoods [44, 45]. The basic building block for the biosynthesis of lignin are the three phenylpropane monomers (monolignols) coniferyl, sinapyl and *p*-coumaryl alcohol (**Figure 1.4**). The resulting guaiacyl (G), syringyl (S) and *p*-hydroxyphenyl (H) structural units are linked with each other by C-C and C-O bonds and form a complex 3D-network. Softwoods mostly comprise lignin with G units, whereas hardwoods have both G and S units [46]. In contrast, grasses comprise all three structural units G, S and H [46]. The most abundant bond in the lignin of grasses and of soft- and hardwoods is the β-*O*-4 aryl ether linkage, which represents approximately 80% of the interunit linkages [44, 45]. Other linkages are, for example, β-5 phenyl coumaran, β-β' pinoresinol, 5-5' biphenyl, β-1 diaryl propane etc. [47-49]. Notably, the amount of lignin increases with the growing time (aging) of plants and, also, interunit linkages of lignin may further be formed. In the plant cell wall, lignin is built into a network with hemicellulose via ester and ether linkages. These linkages are formed between lignin and residues of hemicellulose, which comprise glucuronic acid or arabinosyl-ferulic acid substituents [50-52].

Apart from lignin, plants contain several other aromatic compounds that are mainly non-cell wall components, which can partly be linked to the plant cell wall. For example, non-esterified aromatic compounds, like *p*-coumaric acid, ferulic acid, *p*-hydroxybenzoic acid and caffeic acid, are present in a range from 1 to 3.5% (w/w) of the dry matter content in grasses, such as oat and wheat [53]. Another class of aromatic compounds in grasses are flavonoids such as anthocyanins, which account for up to 2% of the dry matter content [54]. Flavonoids typically consist of two aromatic rings, which are connected via cyclic, aromatic or aliphatic carbon structures, and have a variety of different substitutions, such as hydroxyl or methoxy groups [54]. Other relevant aromatic compounds are tannins, which account for up to 12% (w/w) of the dry matter content in the leaves of some softwoods, and stilbenoids, which are present in a range from 0.2 to 2% in canes of fruits [55, 56].

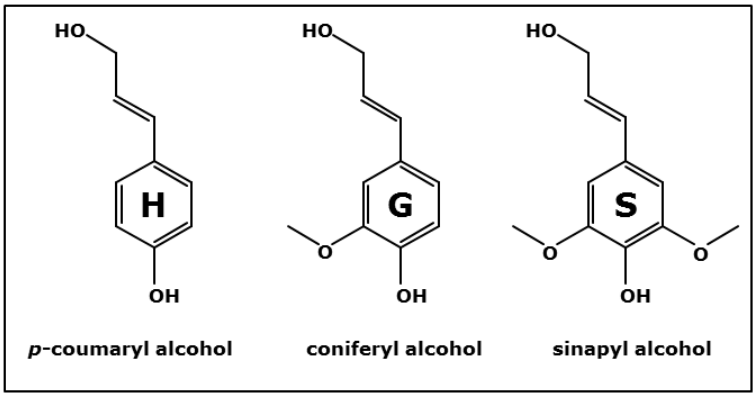

Figure 1.4 Structural units of lignin. Lignin is synthesized from the monolignols *p*-coumaryl, coniferyl and sinapyl alcohol, which form the H, G and S units in lignin, respectively.

1.2.5 Interaction of cell wall components

The rigidity of the primary and secondary cell wall is not only based on the structural features of cell wall components but also on the interactions between these components. These molecular interactions between cell wall components can be classified into non-covalent and covalent interactions.

Non-covalent interactions are built of polysaccharides that are linked with each other via a restricted segment (junctions zones) [14]. Typically, these polysaccharides are non-cellulosic and comprise a linear backbone [14]. Importantly, some of these non-cellulosic polysaccharides, such as the low-substituted xylan or xyloglucan mentioned in **Section 1.2.3**, are also able to associate to the surface of cellulosic microfibrils (**Figure 1.1**) [14, 25, 26].

Covalent interactions are formed by a variety of different cell wall components and stabilize intra- and intermolecular structures. For example, intermolecular covalent interactions are built between hemicelluloses as well as between hemicelluloses and lignin by ester and ether linkages [57]. The ester and ether linkages are either formed directly, or indirectly via dimerization of substituents, such as ferulic acid or hydrocinnamic acids [51, 58]. Several other forms of described or proposed interactions (e. g. between proteins and polysaccharides) will not be further described here [14, 59].

1.3 Enzymes involved in plant cell wall degradation

The complexity of the plant cell wall is reflected in the existence of a wide range of cell wall degrading enzymes, which are expressed by different organisms like bacteria and fungi. The discovery and description of an increasing amount of cell wall degrading enzymes, in particular enzymes that show activity towards different carbohydrates, led to the establishment of the CAZy database [60]. This database classifies carbohydrate active enzymes into families based on their amino acid sequence identity. As an example, enzymes that show hydrolytic activity towards glycosidic bonds of polysaccharides, such as hemicellulose and cellulose, are summarized as glycoside hydrolase (GH) families (**Table 1.1**). The CAZy database also hosts proteins classified as carbohydrate-binding modules (CBMs). These CBMs specially bind to carbohydrates and do not possess catalytic activities (further explained in **Section 1.4.3.2** Auxiliary modules).

1.3.1 Cellulose degrading enzymes

The degradation of cellulose is catalyzed by the action of three different classes of cellulases: endoglucanases (endo-β-1,4-glucanases), exoglucanases (cellobiohydrolases (CBHs)) and β-1,4-glucosidases. The latter hydrolyze soluble cello-oligosaccharides into glucose and are predominantly found in the GH1 and GH3 families [61]. Based on the CAZy database, an overview of the classification of cellulose degrading enzymes is given in **Table 1.1** [60].

Endoglucanases are described as crucial for the degradation of internal β-(1→4)-linked glucan bonds in cellulose and are distributed over various GH families, such as GH5, 7, 12 or 45. In contrast, cellobiohydrolases degrade the β-(1→4)-linked glucan chain from the reducing (CBH1) and non-reducing end (CBH2) and are found in the GH6 and GH7 families [61, 62]. Notably, the classification of cellulose degrading enzymes into these categories is oversimplified since endoglucanases have already been shown to cleave cellulose randomly or processively and cellobiohydrolases also vary in their mode of action from strictly exoacting to highly processive [61-64].

Other enzyme or protein classes that are involved in the degradation of cellulose are, for example, expansins, swollenins and lytic polysaccharide monooxygenases (LPMOs) [65-67]. These enzymes are less studied and recently summarized as non-hydrolytic cellulose active proteins (NHCAPs) [68]. In particular, LPMOs possess a different catalytic mechanism compared to classical cellulose hydrolases, which is explained in detail in **Section 1.4** [3, 69].

1.3.2 Hemicellulose degrading enzymes

The hemicellulose backbone is highly heterogeneous and its degradation demands a variety of enzymes with different substrate specificities. In addition, the backbone-decorations differ in degree, linkage type and monosaccharide composition, which demands a variety of accessory enzyme activities. An overview is shown in **Table 1.1**.

The β-(1→4)-linked xylan backbone is cleaved by endo-β-1,4-xylanases and the released xylo-oligosaccharides are further degraded by β-xylosidases (e.g. family GH3, 43 or 54) [70]. The activity of endo-β-1,4-xylanases, which are mainly present in the CAZy family GH10, 11 and 30, towards xylans depends on the type of substitutions present [60, 61]. Some of these enzymes can degrade a substituted xylan backbone (e.g. GH10 xylanases), whereas others tolerate only a low degree of substitution (e.g. GH11 xylanases) [61]. The degradation of the side chain is catalyzed by a plethora of enzymes like α-glucuronidases (e.g. family GH67 or GH115) or α-arabinofuranosidases (e.g. family GH43, 51, 54 etc.) (**Table 1.1**) [61, 71, 70].

The backbone of xyloglucan is cleaved by endo-β-1,4-glucanases, which are present in the GH5, 12, 16 and 44 families [61]. The activity of these enzymes depends on the type of substitution linked to the backbone of xyloglucan. Therefore, endo-β-1,4-glucanases are divided into nonspecific (randomly cleaving) and specific glucanases [61]. Further, β-glucosidases (GH1 and GH3) take part in the degradation of xylogluco-oligosaccharides into glucose. Similar to xylan, several enzymes show activity towards xyloglucan side chains such as α-fucosidases (GH95), α-xylosidases (GH31) and α-galactosidases (GH27 and GH36) (**Table 1.1**) [72-74].

Other enzymes that are involved in the degradation of hemicelluloses, such as mannan and mixed β-(1→3, 1→4)-linked glucans, are β-mannanases (e.g. family GH26) and β-mannosidases (GH1, 2 and 5), as well as specific β-(1,3), β-(1,3-1,4) and β-(1,4) endoglucanases, respectively (**Table 1.1**) [39, 75, 76].

Furthermore, a plethora of additional esterases are involved in side chain cleavages, such as methyl esterases and acetyl esterases. Moreover, esterases such as ferulic/coumaric acid esterases cleave the linkages between ferulic/*p*-coumaric acid and hemicelluloses. These additional enzymes will not be further explained in this thesis.

The presence of highly substituted (hairy) and less substituted (smooth) regions in pectins demands a plethora of enzymes and accessory enzymes for the degradation of side chains, which will not be extensively discussed here. In short, the glycosidic bonds of pectin are cleaved via hydrolysis by polygalacturonases (PGs), whereas pectin lyases and pectic lyases non-hydrolytically catalyze (β-elimination) the degradation of uronic acid containing polysaccharide chains [60, 61].

Table 1.1 Selected glycoside hydrolase (GH) families taking part in cellulose and hemicellulose degradation[a]

Group	Major substrate	Enzyme	CAZy family[a]
cellulose	cellulose	endo-β-1,4-glucanases	GH5, 7, 12, 45
		cellobiohydrolases	GH6, 7
		β-1,4-glucosidases	GH1, 3
hemicellulose	xylan	endo-β-1,4-xylanases	GH5, 8, 10, 11, 30, 43
	(arabino-)xylan	α-(arabino)furanosidases	GH3, 43, 51, 54, 62, 127
	xylan	α-glucuronidases	GH67, 115
	xylan	β-xylosidases	GH3, 30, 39, 43, 52, 54
	xyloglucan, mixed β-(1→3, 1→4)-linked glucans	endo-β-1,4-glucanases	GH5, 12, 16, 44, 74
	xyloglucan	β-1,4-glucosidases	GH1, 3
	xyloglucan	α-galactosidases	GH27, 36
	xyloglucan	α-xylosidases	GH31
	xyloglucan	α-fucosidases	GH95
	mixed β-(1→3, 1→4)-linked glucans	endo-β-(1,3-1,4)-glucanases	GH9, 26
	mannan	β-mannanases	GH26, 113, 134
	mannan	β-mannosidases	GH1, 2, 5

[a] based on CAZy [60]

1.3.3 Enzymes active towards lignin and aromatic plant compounds

A variety of different enzymes is required to enable the degradation of lignin and aromatic compounds, which are present in plants such as hardwood, softwoods or Poaceae species. Based on their catalytic mechanism, the majority of these enzymes are oxidoreductases and classified under the Enzyme Commission (EC) number 1 [77].

Members of lignin modifying enzymes, such as laccases and peroxidases, are now also added to the CAZy database and classified as auxiliary activity (AA) families 1 and 2, respectively [60]. Both enzyme groups act towards lignin and lignin substructures by a different catalytic mechanism. As an example, laccases (EC 1.10.3.2) are reported to directly oxidize *o*- and *p*-diphenols, whereas these

enzymes are also able to oxidize larger lignin substructures via oxidation of small molecular weight (charge transfer) compounds (mediators) (**Figure 1.5a** and **b**) [78, 79]. The latter has been described as the laccase-mediator system (LMS). Peroxidases are further divided into manganese peroxidases (MnP, EC 1.11.1.13), lignin peroxidases (LiP, EC 1.11.1.14) and versatile peroxidases (VP, EC 1.11.1.16). These heme-containing enzymes generate peroxides (R-O-O-R') to catalyze oxidative reactions. MnPs oxidize Mn(II) to Mn(III) in the presence of H_2O_2 and the formed chelated Mn(III) is highly reactive and proposed to attack lignin substructures [80]. LiPs are described to directly oxidize compounds such as the C_α-C_β-linkage of lignin substructures based on a H_2O_2-dependent reaction, which involves a long range electron transfer [81, 82]. In addition, versatile peroxidases have been described to comprise the catalytic mechanism of both MnPs and LiPs [83, 84].

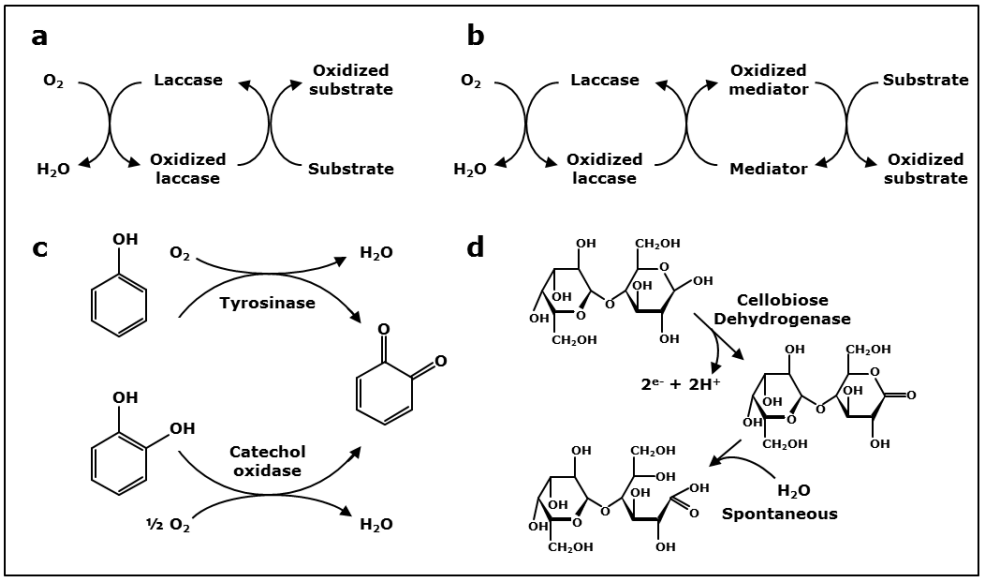

Figure 1.5 Schematic presentation of the catalytic mechanism of oxidoreductases. Reaction scheme of laccase-catalyzed redox cycles for the oxidation of substrates in the **a** absence and **b** presence of mediators. **c** Reactivities of tyrosinases (top) and catechol oxidases (bottom) towards aromatic compounds. **d** Schematic presentation of the cellobiose dehydrogenase (CDH) activity towards cellobiose. The oxidation of cellobiose by CDH leads to the formation of a δ-lactone, which further hydrolyzes into its carboxylic acid in the presence of water. Schematic presentations are based on Adinarayana *et al*., Henriksson *et al*. and Solem *et al*. [78, 92, 93].

Another class of enzymes taking part in the degradation of lignin are peroxide generating enzymes such as aryl-alcohol oxidases (AAOs, EC 1.1.3.7) and glucose oxidases (GOs, EC 1.1.3.4), which are both AA3 family members [85]. These enzymes have been reported to act in synergy with lignin modifying enzymes such as laccases and peroxidases and, furthermore, are family members of the flavin containing GMCs (glucose-methanol-choline oxidases) [86-90]. Moreover, cellobiose dehydrogenase (CDH, EC 1.1.99.18), which is an electron generating GMC member, has been reported to act in synergy with peroxidases during lignin degradation (**Figure 1.5d**) [91]. Aromatic plant compounds, other than lignin, are known to be oxidized directly by the well-described tyrosinases (EC 1.14.18.1) and catechol oxidases (EC 1.10.3.1), which are also referred to as polyphenol oxidases (PPOs). Tyrosinases oxidize monophenols at the *o*-position into *o*-diphenols by

their monophenolase activity (**Figure 1.5c**) [94]. Tyrosinases also exhibit diphenolase activity, which is characterized by the oxidation of these *o*-diphenols into *o*-quinones. Catechol oxidases are described to catalyze only the oxidation of *o*-diphenols into *o*-quinones [95]. However, studies already indicated that minimal differences in the amino acid sequence in the active site of tyrosinases and catechol oxidases can change their ability to exhibit either monophenolase or diphenolase activities (**Figure 1.5c**) [93, 96].

1.4 Lytic Polysaccharide Monooxygenases (LPMOs)

In this section, lytic polysaccharide monooxygenases are discussed in detail. The information about LPMOs is based on literature published until the end of 2013, the year in which this project was initialized. Recent literature (2013-2017) is discussed in **Chapter VII** of this thesis, together with the major findings of our research.

1.4.1 Discovery of polysaccharides oxidizing LPMOs

In 2010, the catalytic function of LPMOs was unraveled for the first time [69]. In contrast, the observation of their function has been described even decades earlier. In 1950, Reese *et al*. gave first indications about the existence of certain undefined enzymes ("C_1"), now known as LPMOs, by investigating the growth of thirty different cellulolytic and non-cellulolytic bacteria and fungi in the presence of cellulose derivatives [97]. Their results built the fundament of their proposed "C_1-C_x-theory" presented in **Figure 1.6**. This theory describes the ability of non-cellulolytic organisms to degrade 'shorter linear polyanhydroglucosyl chains' by their "C_x" enzyme into smaller soluble molecules, which were absorbed by the organisms [97]. However, these non-cellulolytic organisms lacked the ability to degrade native cellulose. For the degradation of native cellulose into shorter linear glucose chains, a second "C_1" enzyme was proposed, which seemed only present in cellulolytic organisms [97]. Although this theory was approved only decades later, it presents a milestone in the understanding of cellulose degradation until today. Later, in 1974, Eriksson *et al*. described an enzyme secreted by *Sporotrichum pulverulentum*, which was able to oxidize cellulose [98]. In addition, the presence of this oxidative enzyme in a cellulolytic enzyme mixture enhanced the cellulose hydrolysis two-fold compared to the hydrolysis of cellulose by a non-oxidative cellulolytic enzyme mixture only. Based on their results, they suggested multiple scenarios how the oxidative enzyme was able to enhance cellulose degradation. One scenario described the insertion of uronic acid moieties into cellulose, which caused a breakage of hydrogen bonds and led to either the "swelling of cellulose" or a structural "disorder in crystalline cellulose" [98]. With the current knowledge, it seems likely that Eriksson *et al*. also reported LPMO activity.

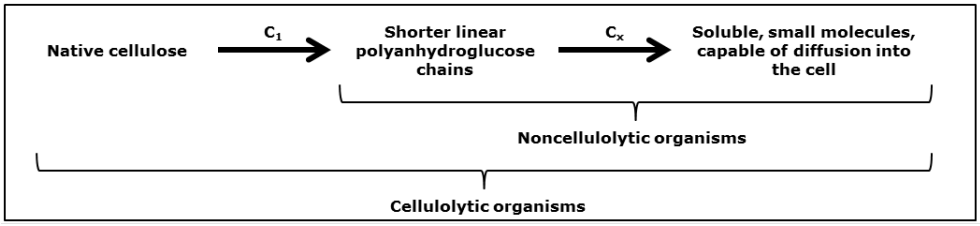

Figure 1.6 Illustration of the "C_1-C_x-theory" based on Reese *et al*. [97]

In the late 2000s, genome analysis and isolation coupled to protein expression and purification enabled new ways for enzyme identification and characterization and accelerated the search for the "C_1" or cellulose-oxidizing enzyme. An overview of enzymes that are related to the discovery of LPMOs is presented in **Table 1.2**. Notably, the first gene, the cellulose-growth-specific *cel*1 gene from the fungus *Agaricus bisporu*s, was isolated and characterized in 1992 [99]. Although not known at that time, *cel*1 was the first identified AA9 LPMO sequence (UniProtKB: Q00023; CAZy [60]). In the following years, two more LPMOs were characterized. The cellulase CEL1 from *Streptomyces reticuli*, also referred to as Avicelase, released cellobiose from cellulose and CEL1 from *Trichoderma reesei,* which was named EGIV due to its endoglucanase activity (**Table 1.2**) [100, 101]. Interestingly, the high amino acid sequence similarity of CEL1 from *A. bisporus* and EGIV from *T. reesei* led to a new classification of both cellulases as 'glycosyl hydrolase family 61' (GH61) in 1997 [100]. In 2001, a first study was published that determined the activity of a GH61 in detail by incubating a variety of substrates with a homologously expressed and purified Cel61A (previously EGIV) from *T. reesei* [102]. This study showed a small endoglucanase activity of Cel61A towards crystalline and amorphous cellulose (**Table 1.2**). Similarly, the discovered GH61 from *Aspergillus kawachii* (*Ak*Cel61) with a appended CBM1 showed a low activity towards cellulose derivatives [103].

In 2007 , the work of Merino *et al.* launched intensive research efforts in the LPMO field by demonstrating the beneficial effect of adding GH61 members from *Thielavia terrestis* to a cellulolytic enzyme cocktail of *T. reesei* (**Table 1.2**) [2]. As an example, 5% (w/w) supplementation of the cellulolytic enzyme cocktail with GH61B reduced the enzyme load needed to achieve 90% cellulose conversion by 1.4-fold [2]. However, no or only a negligible activity of the GH61 members towards pure cellulose derivatives was determined [2]. Three years later, this data was further supported by Harris *et al*., who incorporated a GH61 member in a cellulolytic enzyme producing strain from *T. reesei*, which led to a reduction of the protein load by 2-fold compared to the activity of the untreated strain (**Table 1.2**) [3]. In 2008, the first crystal structure of a Cel61B from *Hypocrea jecorina* was published, but still the possible catalytic role of this enzyme was unknown [104].

Finally in 2010, a *breakthrough* was achieved by the work of Vaaje-Kolstad *et al*., who first revealed the catalytic mechanism behind the activity of an AA10 LPMO which showed activity towards chitin [69]. They presented the mode of action and the crystal structure of a bacterial chitin-binding protein family 21 (CBP21) from *Serratia marcescens*. In the CAZy enzyme database, CBP21 was formerly classified as a member of the carbohydrate-binding module family 33 (CBM33) [60]. The discovery of Vaaje-Kolstad *et al*. accelerated related research in the field and other LPMOs that oxidized cellulose were discovered and recognized as 'LPMOs' shortly thereafter [107-110].

Although the degradation of chitin was not investigated in this thesis, it is necessary to mention that the discovery of cellulose oxidizing LPMOs was proceeded by the investigation of enzymes that took part in chitin degradation in the 1990s. Similar to the discovery of cellulose oxidizing LPMOs, chitin-binding proteins such as CHBs (*Streptomyces spp*.), CHBB (*Bacillus amyloliquefaciens*) and CBP21 have been found to be important for the degradation of chitin several years before the underlying catalytic mechanism was finally uncovered by Vaaje-Kolstad *et al.* in 2010 [111-119].

Table 1.2 Characterized cellulose active enzymes related to the discovery of LPMOs until 2010

Organism	Enzyme	Activity reported	Characterization	Year	Reference
Agaricus bisporus	cel1 gene	not active	-cellulose-growth-specific cel1 gene with appended cellulose binding domain (CBM) -first identified AA9 LPMO sequence	1992	[60, 99, 105]
Streptomyces reticuli	CEL1, Avicelase	cellobiose release from crystalline cellulose	-first study that tested enzyme activity of a purified LPMO	1995	[101]
Trichoderma reesei	CEL1, EGIV	small endoglucanase activity	-high amino acid sequence similarity to described CEL1 in *A. bisporus* -new GH-family proposed: 'glycosyl hydrolase family 61' (GH61)	1997	[100]
Cryptococcus neoformans	CAP60 gene	not investigated	-capsule-associated gene CAP60 -amino acid sequence similarity to described CEL1 in *A. bisporus* -CAP60 considered important for the virulence of the fungus	1998	[106]
Trichoderma reesei	Cel61A, EGIV	endoglucanase activity towards crystalline and amorphous cellulose	-activity tested by incubating Cel61A with a variety of substrates	2001	[102]
Aspergillus kawachii	AkCel61	low activity towards cellulose and its derivatives	-appended CBM1 -activity of purified enzymes tested	2007	[103]
Trichoderma terrestis/ Trichoderma reesei	GH61 members, GH61B	no or negligible hydrolytic activity towards cellulose and hemicelluloses	-expression of multiple GH61 members from *Trichoderma terrestis* in *Trichoderma reesei* -increased pretreated corn stover hydrolysis through GH61 addition in cellullolytic enzyme cocktail -reduced enzyme load (1.4-fold) through GH61B addition to cellullolytic enzyme cocktail of *T.reesei*	2007	[2]
Hypocrea jecorina	Cel61B	catalytic role unknown	-first crystal structure of GH61 enzyme	2008	[104]
Trichoderma terrestis	GH61B, GH61E, GH61G	weak endoglucanase activity	-reduced enzyme load (2-fold) through GH61E addition to cellullolytic enzyme cocktail of *T.reesei* -increased pretreated corn stover hydrolysis (PCS) through GH61 addition in cellullolytic enzyme cocktail -crystal structure of GH61B	2010	[3]
Trichoderma aurantiacus	GH61A	weak endoglucanase activity	-reduced enzyme load (1.6 to 1.9-fold) through GH61E addition to cellullolytic enzyme cocktail of *T.reesei* (PCS)	2010	[3]

1.4.2 Classification

As described above, the glycosyl hydrolase family 61 was first proposed in 1997 [100]. Proteins and protein domains with chitin-binding properties were first classified into several carbohydrate-binding module families, such as family 33 (CBM33). The CBM33 family mainly comprises bacterial and viral, as well as some eukaryotic non-catalytic chitin-binding proteins (CBPs) [118, 120, 121]. Later, it was recognized that these proteins demand electrons for their oxygen-dependent cleavage of polysaccharides, which led to the classification of CBM33 and GH61 members as (lytic) polysaccharide monooxygenases [23, 110]. In 2013, LPMOs were reclassified as auxiliary activities (AA) [60]. Based on their amino acid sequence similarities, known LPMOs were further categorized into AA families 9, 10, 11 and, later, 13 [60]. AA9 members are the classical 'GH61' LPMOs, which are active towards cellulose. CBM33 members were classified as AA10. A phylogenetic distinct LPMO family has been characterized as AA11 [122]. In addition to the AA classification, AA9 members have been proposed for further sub-classification, based on the phylogenetic relationship between regioselectivity and sequence [123].

Table 1.3 Crystal structures of AA9 and AA10 LPMOs published until the end of 2013

Enzyme	PDB-Code	Organism	AA-class	Year	Reference	
Cel61B	2VTC	*Hypocrea jecorina*	AA9	2008	Karkehabadi *et al*.	[104]
GH61E	3EII 3EJA	*Thielavia terrestis*	AA9	2010	Harris *et al*.	[3]
GH61A	2YET 3ZUD	*Thermoascus aurantiacus*	AA9	2011	Quinlan *et al*.	[109]
PMO-2 NCU01050	4EIR	*Neurospora crassa*	AA9	2012	Li *et al*.	[124]
PMO-3 NCU07898	4EIS	*Neurospora crassa*	AA9	2012	Li *et al*.	[124]
*Pc*GH61D	4B5Q	*Phanerochaete chrysosporium*	AA9	2013	Wu *et al*.	[125]
*Sm*CBP21	2LHS 2BEM 2BEN	*Serratia marcescens*	AA10	2005	Vaaje-Kolstad *et al*.	[118]
CBM33	3UAM	*Burkholderia pseudomallei*	AA10	2011	SSGCID[a]	[128]
*Ef*CBM33A	4A02	*Enterococcus faecalis*	AA10	2012	Vaaje-Kolstad *et al*.	[129]
CBM33	2XWX	*Vibrio cholerae*	AA10	2012	Wong *et al*.	[127]
CBM33	2YOX	*Bacillus amyloliquefaciens*	AA10	2013	Hemsworth *et al*.	[130]

[a]SSGCID, Seattle Structural Genomics Center for Infectious Disease

1.4.3 Structure of AA9 and AA10

Interestingly, structures of both AA9 (formerly GH61) and AA10 (formerly CBM33) were determined before the catalytic mechanism was revealed in 2010. **Table 1.3** summarizes crystal structures of AA9 and AA10 LPMOs that were known by the end of 2013. The first crystal structure of an AA9 and

AA10 LPMO was published in 2008 and 2005, respectively [104, 118]. Initial crystal structures and experimental approaches presented a variety of possible metal ions that were present in the active site such as Mn, Cu, Ni, Mg, and Zn [3, 104, 107]. In 2011, Quinlan *et al*. showed that Cu was actually present in the metal binding site by using X-ray crystallography. From that time onwards, crystal structures of LPMOs show the presence of Cu consistently [109, 121].

In general, LPMOs share an overall low sequence identity [60]. Nevertheless, several conserved structure similarities were identified between AA9 and AA10 LPMOs (**Figure 1.7**). All LPMOs feature a conserved immunoglobulin-like β-sheet core, which lays roughly perpendicular to an extended flat face and can be enlarged by an α-helical loop [3, 118, 124]. In contrast to glycosyl hydrolases, LPMO structures do not comprise large surface clefts but feature a relatively planar surface and a conical-like tip [124-126]. The copper ion is coordinated by a N-terminal histidine, a further side chain histidine and, depending on the AA class, a third aromatic amino acid. The latter is a tyrosine and phenylalanine in AA9 and AA10 LPMOs, respectively (**Figure 1.7c** and **d**). The residues involved in the copper coordination are forming the so-called 'histidine brace' [123].

Structural features of AA9 LPMOs are further highlighted in the following sections. In addition, AA10 LPMOs will also be further described due to the structural similarities of AA9 and AA10 LPMOs.

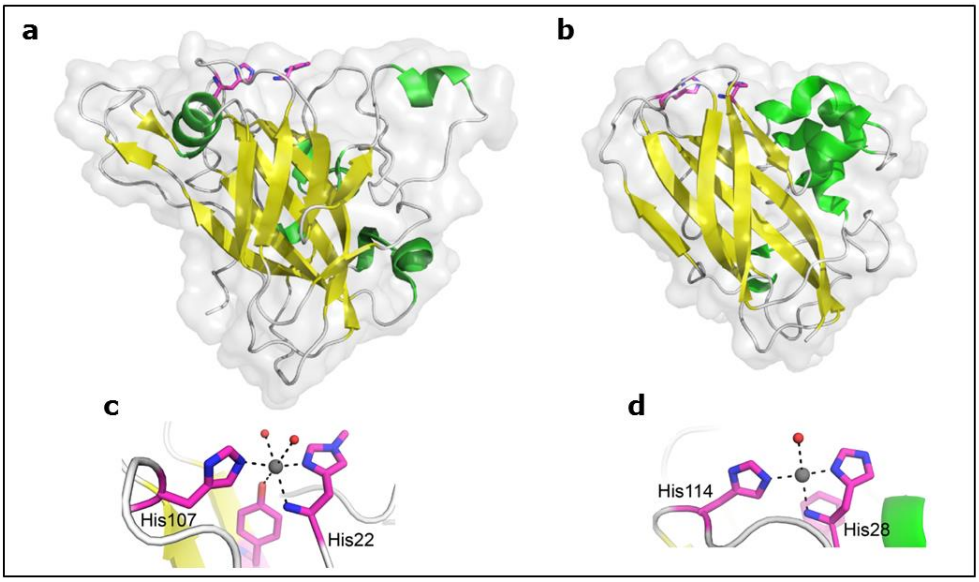

Figure 1.7 Structure of AA9 and AA10 LPMOs. **a** Structure of the cellulose oxidizing *Ta*GH61A (AA9) which has been used to demonstrate that LPMOs are copper-containing enzymes [109]. **b** First crystal structure of the chitin oxidizing CBP21 (AA10) [118]. The enlargement shows the conserved aromatic amino acids of **c** *Ta*GH61A and **d** CBP21, which take part in the coordination of the copper ion (grey). Water molecules are indicated by red balls. The figures are based on Horn *et al*. [23].

1.4.3.1 Planar surface with metal binding site

AA9 LPMOs contain multiple extended loops, which are involved in shaping the potential substrate-binding surface (**Figure 1.8**) [125]. The long C-terminal loop (LC loop) often does not contain secondary structural elements. The LC loop interacts, for example, with a shorter LS loop via

hydrophobic interactions. These interactions contribute to an additional stabilization of the loops. The L2 loop is the most diverse loop in the AA9 family and varies in length and presence of secondary structures, such as helices [124, 125]. Furthermore, the L2 loop can contain several aromatic amino acids, such as Tyr residues, which are expected to play a role in substrate binding and recognition (**Figure 1.8** and **1.9**) [124]. LPMOs are secreted proteins and can be subject of posttranslational modifications, such as multiple disulfide bonds and N-glycosylation sites. Some of the loops, such as the L2 loop, build disulfide bridges with the conserved β-sheet core [125]. In addition, some AA9 members contain 5-10 monosaccharide units (e.g. PMO-3) and it was suggested that glycosylations in the planar face could potentially impact the substrate binding, as shown for a CBM1 by using molecular dynamics simulations [124, 131].

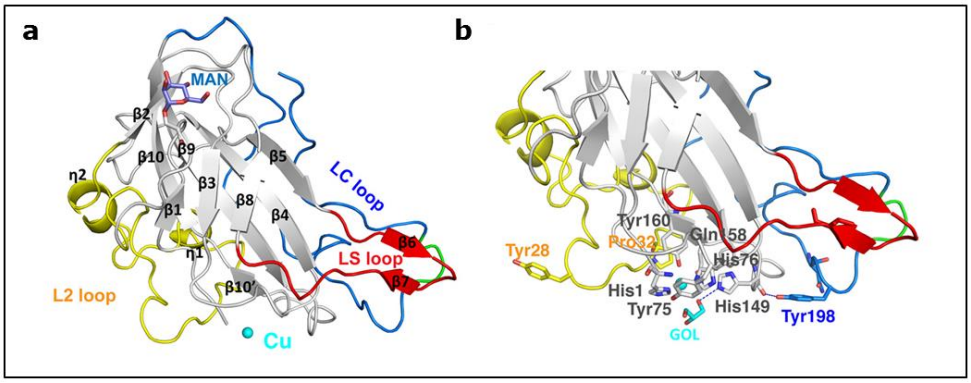

Figure 1.8 Structural features of the AA9 *Pch*GH61D. **a** LPMO typical conserved β-sheet core and **b** close up of amino acids residues involved in coordination of the copper ion (light blue). The three loops L2, LS and LC, which are involved in shaping the substrate binding site, are highlighted in yellow, red and blue, respectively. The glycerol molecule is shown in cyan (marked as GOL). Picture adapted from Wu *et al.* [125].

As already mentioned, three aromatic amino acids are involved in the copper coordination and the formation of the histidine brace in AA9 LPMOs. A detailed view was obtained from the first crystal structure of an AA9 LPMO (Cel61B), which indicated that the metal ion was coordinated by two histidines (His1 and His89) and a tyrosine (Tyr176) [104]. In 2010, it was first suggested that the planar surface of GH61E interacts with the polysaccharide involving the N-terminal His1 and His68, which coordinate the metal ion [3]. In addition, mutation of either His1 or His68 resulted in a complete loss of the enzyme activity. In contrast, mutation of a closely interacting Tyr153 did not inactivate the enzyme, but significantly decreased its activity instead [3]. Further, it was already indicated that the Tyr153 of GH61E is a Phe in CBP21, which turned out to be one of the major differences between fungal AA9 and bacterial AA10 LPMOs [3]. With the presence of more crystal structures, other aromatic amino acids (e.g. Tyr) came into focus due to their potential involvement in the substrate binding and possible influence on the C1-/C4-regioselectivity of the LPMOs (**Figure 1.9**). By using molecular dynamics simulations it was shown that the tyrosines in *Pc*GH61 (Tyr28, Tyr75 and Tyr198) in the planar surface interact with cellulose and, thus, play a potential role in the substrate binding [125]. An overview of aromatic amino acids present in the planar surface of the AA9 and AA10 LPMOs is shown in **Figure 1.9**.

In general, fungal AA9 LPMOs contain a τ-N-methylated histidine (His1) which is involved in the coordination of Cu. In contrast, bacterial AA10 LPMOs and AA9 LPMOs produced in 'foreign' hosts, such as *Pichia pastoris*, do not contain this τ-N-methylation [124, 125, 130]. The impact of this methylation on the activity of the LPMO has been discussed controversially, but its function was still unclear until the end of 2013. Nevertheless, all determined LPMOs either with or without a τ-N-methylation at the His1 were active, which led to the conclusion that this posttranslational modification is not strictly necessary for LPMO activity [125].

Compared to AA9 LPMOs, bacterial AA10 LPMOs have only two conserved histidines, but feature more hydrophilic residues in the planar face such as Thr, Gln or Ser (**Figure 1.9**) [121, 124]. Several of these hydrophilic residues have been shown to be important for chitin recognition, since the chitin surface (N-acetylglucosamine) is more hydrophilic compared to that of cellulose (**Figure 1.9d**) [118, 121]. In contrast, the bacterial cellulose oxidizing AA10 CelS2 from *S. coelicolor* has a sequence insertion which contains three Tyr and one Trp as aromatic residues and, therefore, is less hydrophilic in the planar phase. The latter might contribute to the ability of CelS2 to oxidize cellulose instead of chitin [108, 124]. Despite the conserved β-sheet core, AA10 LPMOs contain more helical secondary structures than AA9 members [124].

1.4.3.2 Auxiliary modules

Carbohydrate binding modules (CBMs) are structurally diverse protein domains, which can be found appended to carbohydrate-active enzymes. Previously, CBMs were known as cellulose-binding domains (CBDs) [60, 132]. Based on their amino acid sequence identity, CBMs have further been categorized into CAZy-CBM family 1, 2, or, as mentioned above, 33 [60]. Appended CBMs have been described to be involved in substrate recognition and interaction and, thereby, they can influence the activity of enzymes [133]. Similar to LPMOs, CBMs contain aromatic amino acids (e.g. Tyr in CBM1) in the substrate binding site that play an important role in the recognition of substrates like cellulose [131]. Furthermore, studies indicated an impact of the (*N*- or *O*-) glycosylation on the substrate binding affinity, which has also been discussed for LPMOs [124, 131]. Until the end of 2013, the impact of appended CBMs on the LPMO activity had not been investigated in detail.

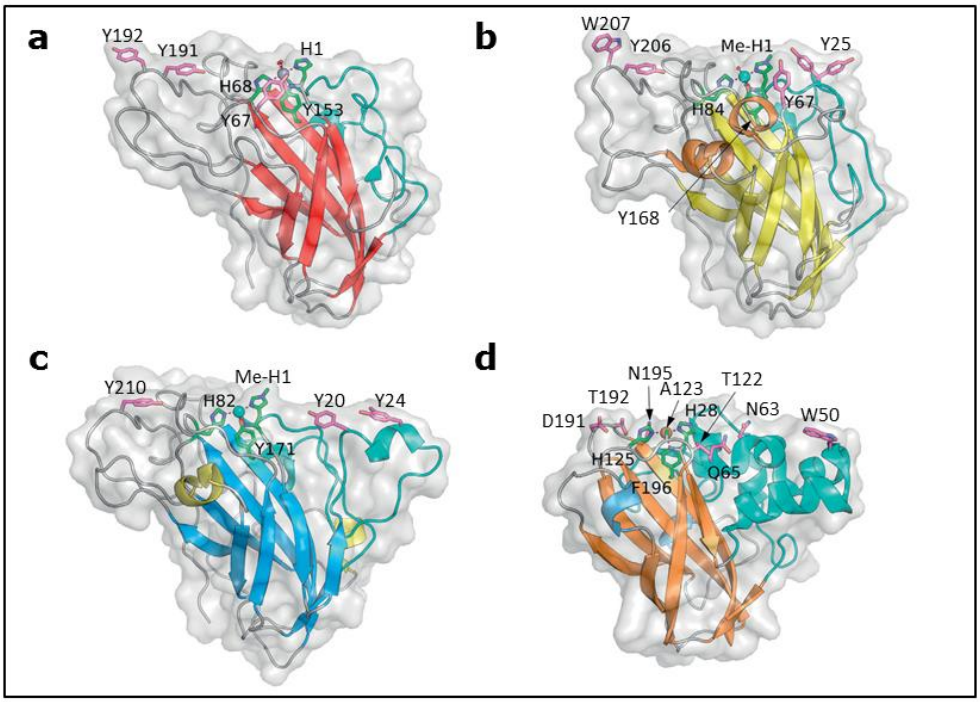

Figure 1.9 Representative AA9 PMOI, AA9 PMOII, AA9 PMOIII and AA10 structures. **a** PMOI member from *T. terrestis* (GH61E, PDB-id: 3EII), **b** PMOII member from *N. crassa* (PMO-2, PDB-id: 4EIR), **c** PMOIII member from *N. crassa* (PMO-3, PDB-id: 4EIS), **d** AA10 member from *B. amyloliquefaciens* (CBM33, PDB-id: 2YOX). Amino acids coordinating the metal binding are indicated in green and additional amino acids which are proposed to be involved in the substrate binding are highlighted in cyan. The pictures are based on Hemsworth *et al*. [123].

1.4.4 Substrates and C1-/C4-regioselectivity

The first C1-/C4-regioselectivity was described for CBP21, an AA10 LPMO from *Serratia marcescens.* This AA10 member oxidized chitin at the C1-carbon position, which led to the cleavage of the β-(1→4)-linked N-aceylglucosamine (GlcNAc) chain [69]. In 2011, the bacterial AA10 CelS2 from *Streptomyces coelicolor* was described to cleave cellulose by oxidizing the C1-carbon position [108]. In the same year, the first AA9 LPMO (*Ta*GH61) was characterized and it was shown that this LPMO oxidized cellulose at the C1 as well as at the C4 position. Shortly afterwards, the number of AA9 and AA10 LPMOs with known C1-/C4-regioselectivity grew rapidly [107, 110]. **Table 1.4** shows an overview of AA9 and AA10 LPMOs with known C1-/C4-regioselectivities. It should be noted that nowadays more LPMOs have been expressed and characterized, but their C1-/C4-regioselectivity was not experimentally determined until the end of 2013 [134].

1.4.5 Reaction mechanism and polysaccharide oxidation

Before LPMOs were described as copper containing oxygenases, isotope labeling ($H_2{}^{18}O$ and $^{18}O_2$) indicated that one of the two oxygens introduced into the oxidized glucan chain derived from water and the other one from molecular oxygen (**Figure 1.10**) [69]. In addition, it was shown that the AA10 CBP21 demanded electrons provided by reducing agents, such as ascorbic acid or reduced glutathione [69].

Table 1.4 Experimentally determined C1-/C4-regioselectivity of LPMOs until 2013[a]

Enzyme (AA class)	Organism	Substrate	Regio-selectivity	Year	Reference	
CBP21 (AA10)	*Serratia marcescens*	chitin	C1	2010	Vaaje-Kolstad *et al.*	[69]
CelS2 (AA10)	*Streptomyces coelicolor* A3(2)	cellulose	C1	2011	Forsberg *et al*.	[108]
TaGH61 (AA9)	*Thermoascus aurantiacus*	cellulose	C1/(C6)	2011	Quinlan *et al*.	[109]
NCU01050 (AA9)	*Neurospora crassa*	cellulose	C4	2011	Phillips *et al*.	[110]
NCU07898 (AA9)			C1/C4			
NCU08760 (AA9)			C1			
*Pc*GH61D (AA9)	*Phanerochaete chrysosporium*	cellulose	C1	2011	Westereng *et al*.	[107]
*Ef*CBM33A (AA10)	*Enterococcus faecalis*	chitin	C1	2012	Vaaje-Kolstad *et al*.	[129]
*Pa*GH61A (AA9)	*Podospora anserina*	cellulose	C1/C4	2013	Bey *et al*.	[135]
*Pa*GH61B (AA9)			C1[b]; (C6)			

[a] Only LPMOs with known C1-/C4-regioselectivity until the 2013 are listed

[b] C1 only with CDH as electron donor

Until 2013, it was known that bacterial AA10 LPMOs cleave cellulose and chitin by the oxidation of the C1-carbon atom, whereas AA9 members oxidize either the C1, C4 or both the C1 and C4 position (**Table 1.4**). Depending on the type of oxidation, released gluco-oligosaccharides are oxidized either at the reducing (C1) or non-reducing end (C4) (**Figure 1.11**). The oxidation of the C1-carbon atom leads to the formation of an unstable δ-lactone (-2 Da), which is converted into an aldonic acid in the presence of water (+ 16 Da) [69]. The oxidation of the C4-postion leads to the formation of a more stable 4-ketoaldose (-2 Da), which tautomerizes into a geminal diol depending on the pH (first shown by B. Westereng, 4th Workshop on Enzymatic Hydrolysis of Insoluble Carbohydrates, Holbæk, Denmark, 2013) [109]. Furthermore, early studies indicated the presence of gemdiols resulting from oxidation of the C6-carbon atom. However, this C6-oxidation would not lead to a chain cleavage of the polysaccharide and further studies revealed that LPMOs only oxidize the C1- and the C4-carbon atom of the β-(1→4)-linked glucan chain [109, 110, 135].

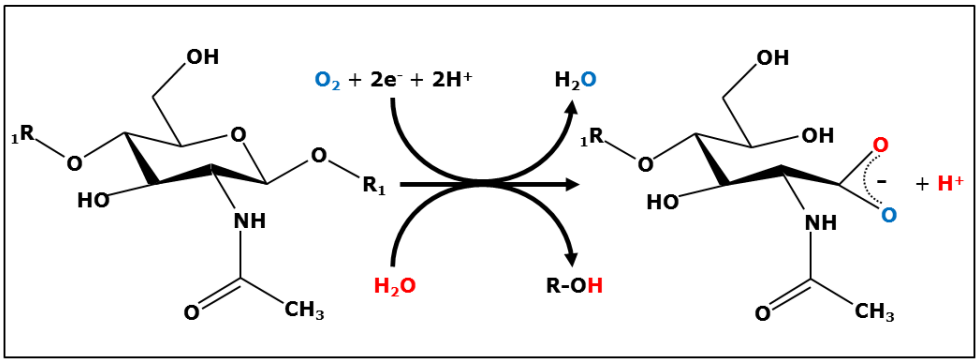

Figure 1.10 Reaction scheme of the *Sm*CBP21 catalyzed oxidation of chitin. The oxidation of chitin leads to the formation of an aldonic acid. The carboxylic acid of the aldonic acid contains one oxygen, which derives from molecular oxygen (blue) and a second oxygen from water (red). The figure is based on Vaaje-Kolstad *et al*. [69].

1.4.5.1 Electron donors of LPMOs

As already mentioned, all discovered LPMOs demand electrons provided by small molecular weight compounds, and ascorbic acid was by far the one most used for LPMO activity assays [69, 136]. Later, it became apparent that other electron donation systems are also possible. One example is the co-action of LPMOs with cellobiose dehydrogenase (CDH). Already in 2011, it was shown that deletion of the highly expressed CDH-1 gene from the cellulolytic fungus *N. crassa* resulted in a decreased cellulose degradation. Moreover, the addition of a purified CDH from *Myceliophthora thermophila* to a CDH lacking *N. crassa* strain improved the cellulose degradation up to 2-fold [110]. The latter study showed the direct beneficial interaction of CDH-2 on the activity of three AA9 LPMOs (NCU01050, NCU07898 and NCU08760) (**Table 1.4**) [110].

CDH itself catalyzes the oxidation of cellobiose or other oligosaccharides (e.g. DP2-5) to the corresponding lactones [110, 137]. Similar to C1-oxidized products from LPMOs, CDH generated lactones are instable and spontaneously convert to aldonic acids in the presence of water (**Figure 1.5**). The oligosaccharide oxidation takes place in the flavin domain (FAD) of the CDH and leads to the reduction of the flavin ($FADH_2$). The electrons of the reduced flavin are subsequently transferred to the heme domain, which is appended to the cytochrome domain. Finally, the electrons are transferred from the heme domain to the LPMO [110, 138]. In addition, studies have shown that LPMOs and CDH are co-expressed on various substrates, which indicates the relevance of this interaction in nature [139, 140].

Until the end of 2013, it was not clear how electrons from either reducing agents or CDHs are transferred to LPMOs. A major point of discussion was that the close binding of LPMOs to the surface of cellulose or chitin makes the catalytic copper center inaccessible even for smaller reductants. Therefore, it was hypothesized that reduction of the catalytic copper center takes place before the binding of the LPMO to the polysaccharide or, alternatively, electrons are continuously transported to the catalytic copper center by an electron tunneling. Li *et al*. suggested two possible scenarios how fungal LPMOs could accommodate an internal electron tunneling [124]. In the first scenario, electrons are transferred through an internal conserved ionic network (hydrogen bond network), which connects the copper ligand Tyr with the surface exposed Lys under involvement of conserved Tyr residues. In a second scenario, electrons are provided by aromatic residues which are

in the proximity of the histidines [124]. In addition, computational simulation studies showed that the heme domain of a CDH could potentially bind to a hydrophilic conserved surface patch. The electrons could be transferred to the catalytic copper center by one of the above proposed scenarios [124].

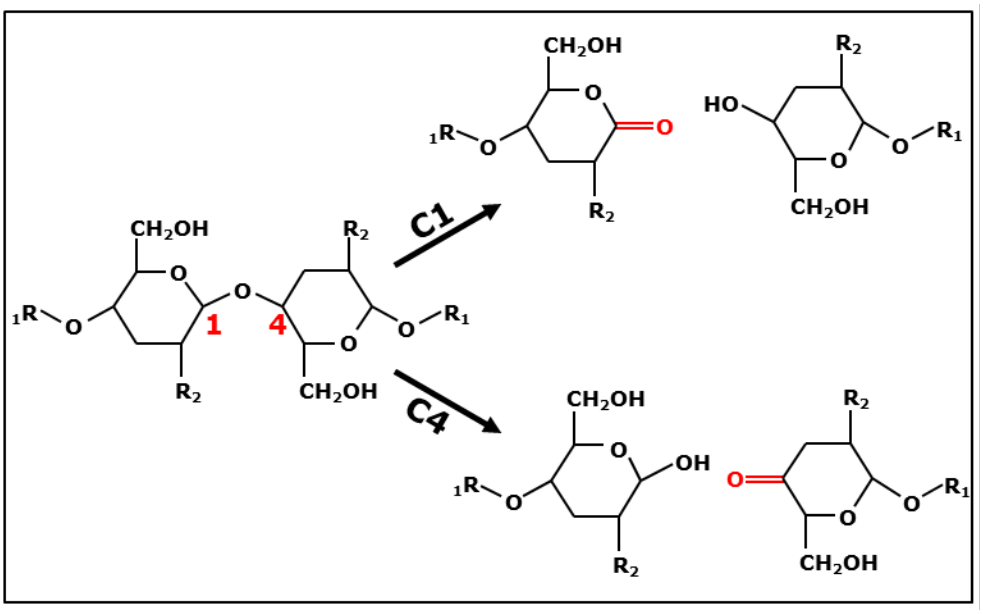

Figure 1.11 Oxidation of the β-(1→4)-linked glucan at the C1- or C4-carbon position by LPMOs leads to the formation of non-oxidized and C1- or C4-oxidized products. See **Section 1.4.5** for details.

1.4.5.2 Catalytic mechanism of LPMOs

The detailed catalytic mechanism of the oxidation of the β-(1→4)-linked glucan chain by LPMOs was not unraveled until 2013. The most detailed reaction pathway was proposed by Phillips *et al.* in 2011 [110] who based the catalytic mechanism on the reaction pathway of copper monooxygenases as described above [141, 142]. A key step described the one electron reduction (**A, Figure 1.12**) of the Cu(II) to Cu(I) by either the CDH or another external reducing agent. The Cu(I) binds molecular oxygen (**B, Figure 1.12**) and the electron is internally transferred to the bound oxygen, which results in the formation of a copper superoxo intermediate (**C, Figure 1.12**). In a next step, the copper superoxo intermediate subtracts a hydrogen atom from the C1-carbon or the C4-carbon atom of the polysaccharide (**D, Figure 1.12**), which leads to the formation of a copper hydroperoxo intermediate and a radical at the C1- or C4-carbon atom. A second reduction leads to the cleavage of the O-O bond of the copper hydroperoxo intermediate and the release of water (**E, Figure 1.12**). The formed copper oxo radical couples to the substrate radical and thereby hydroxylates the C1- or C4-position (**F, Figure 1.12**). Subsequently, an additional oxygen atom destabilizes the β-(1→4)-linkage, which leads to the elimination of a non-oxidized and an oxidized glucan chain. The latter elimination could be enabled by a conserved histidine acting as an acid, which is located next to the copper binding side. It was also suggested that a direct two electron reduction of oxygen to a Cu-OOH intermediate might be able to abstract a hydrogen [110]. However, this approach was not underpinned since neither did peroxide enable the reaction nor was the reaction inhibited by catalase addition [110].

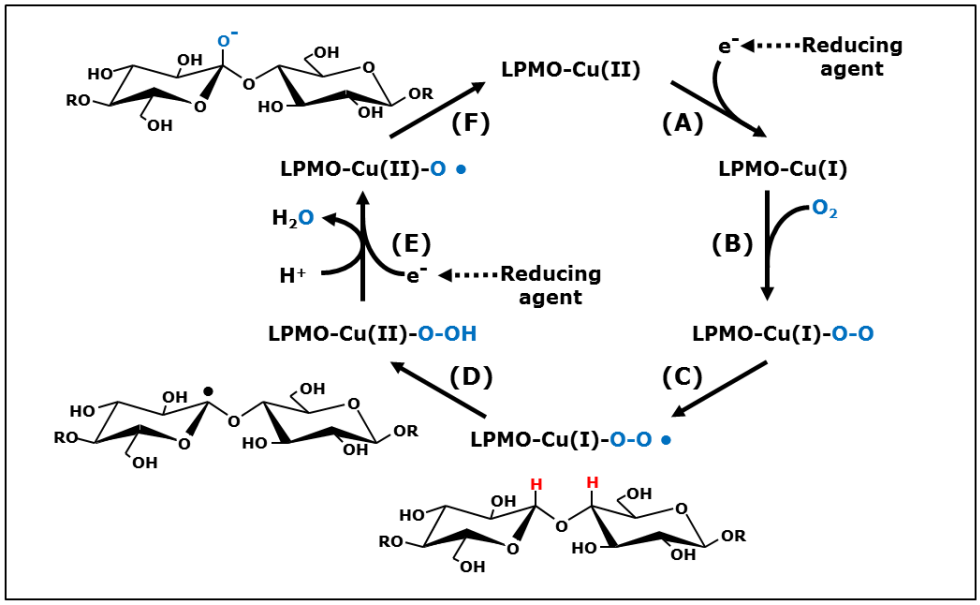

Figure 1.12 Reaction mechanism as proposed by Phillips *et al.* in 2011 [110].

1.4.6 Analytical methods for the determination of chitin and cellulose oxidizing LPMOs

Qualitative and quantitative techniques for the analysis of non-oxidized oligosaccharides for the characterization of enzymes that are active towards cellulose or chitin have been developed over the past decades. Techniques that were used to determine cellulolytic enzyme activity were, for example, high performance anion exchange chromatography (HPAEC), high performance liquid chromatography coupled to mass spectrometry (HPLC-MS), matrix-assisted laser desorption ionization-time of flight mass spectrometry (MALDI-TOF MS) or nuclear magnetic resonance (NMR) spectroscopy [30, 143, 144]. However, the catalytic mechanism of LPMOs challenged the development of techniques for the analysis of oxidized oligosaccharides due to the lack of standards and a limited solubility of released products, which can have a higher degree of polymerization (DP ≥ 6). The structural variability of oxidized oligosaccharides ranges from the presence of δ-lactones and aldonic acids (C1-oxidation) to 4-ketoaldoses and geminal diols (C4-oxidation). An overview of available methods used for determination of LPMO activity until 2013 is presented in **Table 1.5**.

The first described AA10 LPMO (*Sm*CBP21) cleaved chitin by oxidizing the C1-carbon atom. The released chito-oligosaccharides were determined by a variety of techniques such as hydrophilic interaction liquid chromatography coupled to MS, HPLC and MALDI-TOF MS (**Table 1.5**) [69]. Furthermore, the simultaneous use of *Sm*CBP21 and chitinase (ChiC) led to the degradation of most C1-oxidized chito-oligosaccharides into chitobionic acid, which was quantified by using HPLC [69]. Shortly afterwards, a study showed the identification of released C1-oxidized gluco-oligosaccharides from cellulose incubated with an AA10 LPMO (*Sc*CelS2) by using HPAEC and MALDI-TOF MS [108]. A more complex approach was the derivatization of released non-oxidized and oxidized oligosaccharides from the incubation of RAC with an AA9 LPMO. These oligosaccharides were first

Table 1.5 Selected techniques for the determination of released oxidized oligosaccharides from chitin and cellulose incubated with AA9 and AA10 LPMOs, respectively

Analytical Technique[a]	Column/ type of separation[b]	Type of Analysis	Further specification	Substrate	Regio-selectivity	Reference	
MALDI-TOF MS	-	Qualitative	Derivatization by using isotope labeling ($H_2{}^{16}O$ or $^{18}O_2$)	Chitin	C1	Vaaje-Kolstad *et al.*	[69]
HPLC-UV	Amide-80 column, HIC	Partially quantitative	Analysis of $(GlcNAc)_2$ by using chitinase (ChiC)	Chitin	C1	Vaaje-Kolstad *et al.*	[69]
UHPLC-MS	BEH amide column, HIC	Qualitative	Chitin-oligosaccharides	Chitin	C1	Vaaje-Kolstad *et al.*	[69]
HPAEC-CAD	Hypercarb column, AEC	Qualitative	Fractionation of cello-oligosaccharides	Cellulose	C1	Forsberg *et al.*	[108]
MALDI-TOF MS	-	Qualitative	Cello-oligosaccharides	Cellulose	C1	Forsberg *et al.*	[108]
HPAEC-PAD	PA-200 HPAEC column, CarboPack PA1 column, AEC	Qualitative	Cello-oligosaccharides	Cellulose	C1 / C4	Phillips *et al.*, Forsberg *et al.*	[108, 110]
MALDI-TOF MS and MALDI-TOF/TOF MS	-	Qualitative	*Per*-methylated cello-oligosaccharides	Cellulose	C1 (C6[a])	Quinlan *et al.*	[109]
HPAEC-PAD & Post column	CarboPac PA1 column, AEC	Quantitative	Aldonic acid from cellulolytic enzymes cocktail	Cellulose	C1	Cannella *et al.*	[145]
HPLC-RI-UV	Phenomenex Rezex ROA column, IEC	Quantitative	Aldonic acid from cellulolytic enzymes cocktail	Cellulose	C1	Cannella *et al.*	[145]
HPLC-MS	Acquity UPLC BEH amide column, SeQuant ZIC-HILIC column, HIC	Qualitative	Lactones and aldonic acid separation	Cellulose	C1 / C4 (C6[c])	Westereng *et al.*, Phillips *et al.*	[110, 146]
PGC-LC-CAD/PAD	Hypercarb PGC	Qualitative	Lactones and aldonic acid separation	Cellulose	C1	Westereng *et al.*	[146]
NMR	-	Qualitative	Identification of purified oxidized gluco-oligosaccharides	Cellulose	C1	Westereng *et al.*	[146]
HPLC-MS	HILIC column, HIC	Qualitative	Derivatization of aldonic acids with isotope labeling $^{16}O_2$ and $^{18}O_2$	Cellulose	C1	Beeson *et al.*	[136]
HPAEC-PAD	PA-200 column, PA-20 column, AEC	Qualitative	Oxidation with I_2 or reduction with $NaBH_4$ in combination with TFA hydrolysis	Cellulose	C4 (not C6[d])	Beeson *et al.*	[136]

[a] MALDI-TOF MS, matrix-assisted laser desorption ionization-time of flight mass spectrometry; (U)HPLC, ultra high performance liquid chromatography; HILIC, hydrophilic interaction liquid chromatography; HPAEC-CAD, high performance anion exchange chromatography-charged aerosol detection; PAD, pulsed amperometric detection; RI, refractive index; PGC, porous graphitized carbon

[b] HIC, hydrophobic interaction chromatography, AEC, anion exchange chromatography; IEC, ion exclusion chromatography

[c] Putative C6-oxidation was shown to be C4-oxidation by Beeson *et al.* [136]

permethylated and afterwards analyzed by MALDI-TOF/TOF MS analysis (**Table 1.5**) [109]. This approach led to the identification of C1-oxidized and putative C6-oxidized gluco-oligosaccharides. Follow-up studies indicated that the C6-oxidation was actually a C4-oxidation [110]. A later study proved that released putative C6-oxidized gluco-oligosaccharides were oxidized at the C4-carbon atom by using a hypoiodite and sodium borohydride based derivatization technique (**Table 1.5**) [136].

The availability of the standards gluconic and cellobionic acid (DP1-2) helped the analysis of C1-oxidized oligosaccharides. Nevertheless, C1-oxidized gluco-oligosaccharides had not been quantified to determine the catalytic performance of LPMOs until the end of 2013 (**Table 1.5**) [69, 145, 146]. In addition, only a limited number of LPMOs were identified as C4-oxidizing enzymes and analysis was far from quantitative.

As an alternative approach, a fluorimetric assay was developed to determine the activity of LPMOs by measuring the release of hydrogen peroxide (H_2O_2) [134]. Therefore, the LPMO was incubated with a reducing agent such as ascorbate or CDH, a horseradish peroxidase (HRP) and Amplex Red (10-acetyl-3,7-dihydroxyphenoxazine), which is the fluorogenic substrate for HRP. Upon LPMO reduction by the reducing agent, the LPMO converts molecular oxygen (O_2) to H_2O_2. In the presence of HRP, Amplex Red reacts one-to-one with H_2O_2 to the resorufin. The released resorufin is highly fluorescent and can be determined by fluorescence spectroscopy [134]. This assay was used to determine the activity of LPMOs in the absence of a substrate like cellulose [134]. Noteworthy, this assay cannot be used to determine the activity of LPMOs towards complex biomass due to turbidity. Furthermore, the determination of the activity of LPMOs in cellulolytic enzyme mixtures by using the Amplex Red assay is limited due to the possible presence of other H_2O_2 producing enzymes, such as peroxidases which are described in **Section 1.3.2**.

1.5 *Myceliophthora thermophila* C1

The degradation of complex biomass requires a plethora of naturally occurring enzymes. In contrast, commercially produced enzymes, such as hydrolases, derive from a rather small number of filamentous fungi such as *Trichoderma reesei* or *Aspergillus species* [147]. In this thesis, the fungus *Myceliophthora thermophila* C1 (formerly *Chrysosporium lucknowence* C1) was used for the production of carbohydrate active enzymes. This Ascomycota strain was isolated in Russia and further developed for the commercial production of enzymes, which are, for example, used for the degradation of biomass [148, 149].

In total, around 200 putative carbohydrate active enzymes were annotated in the genome of *M. thermophila* C1 [148]. Interestingly, 55 of these carbohydrate active enzymes are expected to take part in the degradation of cellulose (**Figure 1.13**) [148]. Remarkably, *M. thermophila* C1 comprises 26 putative LPMOs, of which 22 and 4 were annotated as AA9 and AA11 subfamily members, respectively (**Figure 1.13**) [150]. It has already been shown in previous research, which used a related *M. thermophila* strain and the fungus *Thelavia terrestis,* that the type of substrate alters the expression profile of fungal LPMOs [150]. Therefore, it was expected that LPMOs of *M. thermophila* C1 differ in their substrate specificity and mode of action.

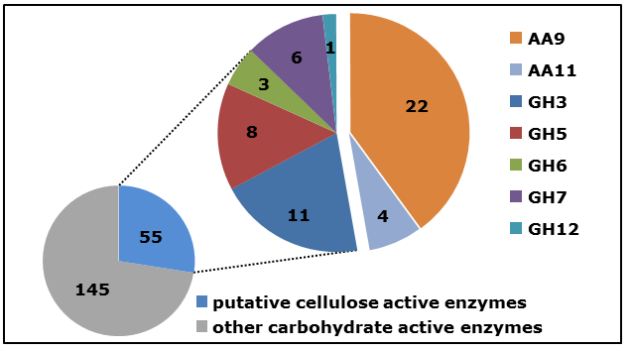

Figure 1.13 Overview of cellulose active enzymes present in *M. thermophila* C1

1.6 Project aim

This project aims at the characterization of LPMOs from *Myceliophthora thermophila* C1 and their potential use in biomass degradation. Therefore, several LPMOs will be purified and investigated for their mode of action towards plant cell wall materials such as cellulose. It is hypothesized that the plethora of LPMOs expressed by *M. thermophila* C1 differ in their catalytic behavior and mode of action towards plant cell wall materials. In addition, LPMOs will be characterized through the identification and quantification of released non-oxidized and oxidized gluco-oligosaccharides from plant cell wall components, such as cellulose and hemicellulose.

1.7 Outline of this thesis

The background and aim of this project is described in **Chapter I**. The cell wall architecture is thoroughly described, which helps to understand the variation in mode of action of the newly discovered LPMO enzymes. The details given comprise the knowledge of LPMOs at the time of the beginning of this thesis (2013).

The activity of the first purified LPMO (*Mt*LPMO9A) from *Myceliophthora thermophila* C1 is presented in **Chapter II**. This chapter describes that *Mt*LPMO9A is the first enzyme which is capable of oxidizing xylan in addition to cellulose. Moreover, we show that *Mt*LPMO9A acts in strong synergy with endoglucanase I from *T. viride*.

In **Chapter III**, three LPMOs from the fungus *Myceliophthora thermophila* C1, *Mt*LPMO9A, *Mt*LPMO9B and *Mt*LPMO9C are shown to differ in their substrate preference, C1-/C4-regioselectivity and reducing agent specificity.

Chapter IV describes the use of reversed phase (RP)-UHPLC in combination with non-reductive 2-aminobenzamide (2-AB) labeling to separate C4-oxidized gluco-oligosaccharides from their non-oxidized counterparts. Coupling of RP-UHPLC to UV detection and subsequent mass spectrometry allowed the identification of both labeled non-oxidized and C4-oxidized oligosaccharides formed by LPMO activity.

In **Chapter V** we describe a new class of polyphenol oxidases (PPOs) that are able to attack lignin building blocks and, thereby, boost the action of LPMOs. In addition, we show that *Mt*PPO7, unlike PPOs described so far (e.g. tyrosinases), is highly active towards methoxylated phenolic compounds.

In **Chapter VI**, the impact of temperature and pH on the activity of *Mt*LPMO9B and *Mt*LPMO9C towards cellulose is presented. In addition, we quantify the release of C1-oxidized gluco-oligosaccharides by a newly developed β-glucosidase-assisted method.

Finally (**Chapter VII**), we discuss the relevance of this research for the use of LPMOs in second generation biorefinery. Furthermore, new findings in the LPMO field (2013-2017) and results obtained in this thesis are discussed.

References

1. UNFCCC United Nations Framework Convention on Climate Change. Paris Agreement. United Nations. Paris: 2015.
2. Merino ST, Cherry J. Progress and challenges in enzyme development for biomass utilization. Biofuels. Olsson L, editor. Berlin, Heidelberg: Springer Berlin Heidelberg; 2007. p. 95-120.
3. Harris PV, Welner D, McFarland KC, Re E, Navarro Poulsen JC, Brown K *et al*. Stimulation of lignocellulosic biomass hydrolysis by proteins of glycoside hydrolase family 61: structure and function of a large, enigmatic family. Biochem. 2010;49(15):3305-16.
4. Cassab GI, Varner JE. Cell Wall Proteins. Ann. Rev. Plant Physiol. Plant Mol. Biol. 1988;39(1):321-53.
5. McCann MC, Wells B, Roberts K. Complexity in the spatial localization and length distribution of plant cell-wall matrix polysaccharides. J. Microsc. 1992;166(1):123-36.
6. Achyuthan KE, Achyuthan AM, Adams PD, Dirk SM, Harper JC, Simmons BA *et al*. Supramolecular self-assembled chaos: Polyphenolic lignin's barrier to cost-effective lignocellulosic biofuels. Molecules. 2010;15(12):8641.
7. Vanholme R, Van Acker R, Boerjan W. Potential of *Arabidopsis* systems biology to advance the biofuel field. Trends Biotechnol. 2010;28(11):543-7.
8. Reiter W-D. Biosynthesis and properties of the plant cell wall. Curr. Opin. Plant Biol. 2002;5(6):536-42.
9. Fischer RL, Bennett AB. Role of cell wall hydrolases in fruit ripening. Ann. Rev. Plant Physiol. Plant Mol. Biol. 1991;42(1):675-703.
10. Carpita NC, McCann MC. Maize and sorghum: genetic resources for bioenergy grasses. Trends Plant Sci. 2008;13(8):415-20.
11. Carpita NC, Gibeaut DM. Structural models of primary cell walls in flowering plants: consistency of molecular structure with the physical properties of the walls during growth. Plant J. 1993;3(1):1-30.
12. Hoffman M, Jia Z, Peña MJ, Cash M, Harper A, Blackburn AR *et al*. Structural analysis of xyloglucans in the primary cell walls of plants in the subclass *Asteridae*. Carbohydr Res. 2005;340(11):1826-40.
13. Gordon AH, Lomax JA, Dalgarno K, Chesson A. Preparation and composition of mesophyll, epidermis and fibre cell walls from leaves of perennial ryegrass (*Lolium perenne*) and italian ryegrass (*Lolium multiflorum*). J. Sci. Food Agric. 1985;36(7):509-19.
14. Harris PJ, Stone BA. Chemistry and molecular organization of plant cell walls. Biomass Recalcitrance. Himmel ME, editor. Blackwell Publishing Ltd.; 2009. Chapt. 4, p. 61-93.
15. Jarvis M. Chemistry: Cellulose stacks up. Sci. 2003;426(6967):611-2.
16. Zhang Y-HP, Lynd LR. Toward an aggregated understanding of enzymatic hydrolysis of cellulose: Noncomplexed cellulase systems. Biotechnol. Bioeng. 2004;88(7):797-824.
17. Nishiyama Y, Langan P, Chanzy H. Crystal structure and hydrogen-bonding system in cellulose I_β from synchrotron X-ray and neutron fiber diffraction. J. Am. Chem. Soc. 2002;124(31):9074-82.
18. Fernandes AN, Thomas LH, Altaner CM, Callow P, Forsyth VT, Apperley DC *et al*. Nanostructure of cellulose microfibrils in spruce wood. Proc. Natl. Acad. Sci. U.S.A. 2011;108(47):E1195-E203.
19. Nishiyama Y, Sugiyama J, Chanzy H, Langan P. Crystal structure and hydrogen bonding system in cellulose I_α from synchrotron X-ray and neutron fiber diffraction. J. Am. Chem. Soc. 2003;125(47):14300-6.
20. Mittal A, Katahira R, Himmel ME, Johnson DK. Effects of alkaline or liquid-ammonia treatment on crystalline cellulose: changes in crystalline structure and effects on enzymatic digestibility. Biotechnol. Biofuels. 2011;4:41.
21. Atalla RH, Vanderhart DL. Native cellulose: A composite of two distinct crystalline forms. Sci. 1984;223(4633):283-5.
22. Mohnen D, Bar-Peled M, Somerville C. Biosynthesis of plant cell walls. Biomass Recalcitrance. Himmel M, editor. Oxford: Blackwell Publishing; 2008. p. 94-187.

23. Horn SJ, Vaaje-Kolstad G, Westereng B, Eijsink V. Novel enzymes for the degradation of cellulose. Biotechnol. Biofuels. 2012;5(1):45.
24. Viëtor RJ, Newman RH, Ha M-A, Apperley DC, Jarvis MC. Conformational features of crystal-surface cellulose from higher plants. Plant J. 2002;30(6):721-31.
25. Kabel MA, van den Borne H, Vincken J-P, Voragen AGJ, Schols HA. Structural differences of xylans affect their interaction with cellulose. Carbohydr. Polym. 2007;69(1):94-105.
26. Vincken JP, de Keizer A, Beldman G, Voragen AGJ. Fractionation of xyloglucan fragments and their interaction with cellulose. Plant Physiol. 1995;108(4):1579-85.
27. Fry SC, York WS, Albersheim P, Darvill A, Hayashi T, Joseleau J-P *et al*. An unambiguous nomenclature for xyloglucan-derived oligosaccharides. Physiol. Plant. 1993;89(1):1-3.
28. Scheller HV, Ulvskov P. Hemicelluloses. Ann. Rev. Plant Biol. 2010;61(1):263-89.
29. Ebringerová A, Hromádková Z, Heinze T. Hemicellulose. Adv. Polym. Sci. 2005;186:1-67.
30. Appeldoorn MM, Kabel MA, Van Eylen D, Gruppen H, Schols HA. Characterization of oligomeric xylan structures from corn fiber resistant to pretreatment and simultaneous saccharification and fermentation. J. Agric. Food Chem. 2010;58(21):11294-301.
31. Gírio FM, Fonseca C, Carvalheiro F, Duarte LC, Marques S, Bogel-Łukasik R. Hemicelluloses for fuel ethanol: A review. Bioresour. Technol. 2010;101(13):4775-800.
32. Kühnel S, Pouvreau L, Appeldoorn MM, Hinz SWA, Schols HA, Gruppen H. The ferulic acid esterases of *Chrysosporium lucknowense* C1: Purification, characterization and their potential application in biorefinery. Enzyme Microb. Technol. 2012;50(1):77-85.
33. Hatfield RD, Marita JM, Frost K. Characterization of *p*-coumarate accumulation, *p*-coumaroyl transferase, and cell wall changes during the development of corn stems. J. Sci. Food Agric. 2008;88(14):2529-37.
34. Darvill JE, McNeil M, Darvill AG, Albersheim P. Structure of plant cell walls: XI. Glucuronoarabinoxylan, a second hemicellulose in the primary cell wall of suspension-cultured sycamore cells. Plant Physiol. 1980;66(6):1135-9.
35. Naran R, Chen G, Carpita NC. Novel rhamnogalacturonan I and arabinoxylan polysaccharides of flax seed mucilage. Plant Physiol. 2008;148(1):132-41.
36. Zablackis E, Huang J, Müller B, Darvill AG, Albersheim P. Characterization of the cell-wall polysaccharides of *Arabidopsis thaliana* leaves. Plant Physiol. 1995;107(4):1129-38.
37. Park YW, Baba Ki, Furuta Y, Iida I, Sameshima K, Arai M *et al*. Enhancement of growth and cellulose accumulation by overexpression of xyloglucanase in poplar. FEBS Lett. 2004;564(1–2):183-7.
38. Bulone V, Fincher GB, Stone BA. In vitro synthesis of a microfibrillar (1→3)-β-glucan by a ryegrass (*Lolium multiflorum*) endosperm (1→3)-β-glucan synthase enriched by product entrapment. Plant J. 1995;8(2):213-25.
39. Fry SC, Nesselrode BHWA, Miller JG, Mewburn BR. Mixed-linkage (1→3,1→4)-β-D-glucan is a major hemicellulose of *Equisetum* (horsetail) cell walls. New Phytologist. 2008;179(1):104-15.
40. Gilbert HJ, Stålbrand H, Brumer H. How the walls come crumbling down: Recent structural biochemistry of plant polysaccharide degradation. Curr. Opin. Plant Biol. 2008;11(3):338-48.
41. Popper ZA. Evolution and diversity of green plant cell walls. Curr. Opin. Plant Biol. 2008;11(3):286-92.
42. Popper ZA, Fry SC. Primary cell wall composition of Bryophytes and Charophytes. Ann. Bot. 2003;91(1):1-12.
43. Ridley BL, O'Neill MA, Mohnen D. Pectins: Structure, biosynthesis, and oligogalacturonide-related signaling. Phytochem. 2001;57(6):929-67.
44. del Rio JC, Rencoret J, Prinsen P, Martinez AT, Ralph J, Gutierrez A. Structural characterization of wheat straw lignin as revealed by analytical pyrolysis, 2D-NMR, and reductive cleavage methods. J. Agric. Food Chem. 2012;60(23):5922-35.
45. Rencoret J, Marques G, Gutiérrez A, Nieto L, Santos JI, Jiménez-Barbero J *et al*. HSQC-NMR analysis of lignin in woody (*Eucalyptus globulus* and *Picea abies*) and non-woody (*Agave sisalana*) ball-milled plant materials at the gel state. Holzforschung. 2009;63(6).
46. Chen F, Dixon RA. Lignin modification improves fermentable sugar yields for biofuel production. Nat. Biotechnol. 2007;25(7):759-61.
47. Mäkelä MR, Marinović M, Nousiainen P, Liwanag AJM, Benoit I, Sipilä J *et al*. Aromatic metabolism of filamentous fungi in relation to the presence of aromatic compounds in plant biomass. Adv. Appl. Microbiol. Academic press; 2015. Chapter 2, p. 63-137.
48. Stewart JJ, Akiyama T, Chapple C, Ralph J, Mansfield SD. The effects on lignin structure of overexpression of ferulate 5-hydroxylase in hybrid poplar (1). Plant Physiol. 2009;150(2):621-35.
49. Boerjan W, Ralph J, Baucher M. Lignin biosynthesis. Ann. Rev. Plant Biol. 2003;54(1):519-46.
50. Takahashi N, Koshijima T. Ester linkages between lignin and glucuronoxylan in a lignin-carbohydrate complex from beech (*Fagus crenata*) wood. Wood Sci. Technol. 1988;22(231-241):231-41.

51. Lam TBT, Kadoya K, Iiyama K. Bonding of hydroxycinnamic acids to lignin: ferulic and *p*-coumaric acids are predominantly linked at the benzyl position of lignin, not the β-position, in grass cell walls. Phytochem. 2001;57(6):987-92.
52. Jacquet G, Pollet B, Lapierre C, Mhamdi F, Rolando C. New Ether linked ferulic acid conferyl alcohol dimers identified 1995. J. Agric. Food Chem. 1995;43(10):2746-51.
53. Cherney JH, Anliker KS, Albrecht KA, Wood KV. Soluble phenolic monomers in forage crops. J. Agric. Food Chem. 1989;37(2):345-50.
54. Dykes L, Rooney LW. Phenolic compounds in cereal grains and their health benefits. Cereal Foods World. 2007;52(3):105-11.
55. Haslam E. Vegetable tannins – Lessons of a phytochemical lifetime. Phytochem. 2007;68(22–24):2713-21.
56. Pawlus AD, Sahli R, Bisson J, Rivière C, Delaunay J-C, Richard T *et al*. Stilbenoid profiles of canes from *Vitis* and *Muscadinia* species. J. Agric. Food Chem. 2013;61(3):501-11.
57. Ralph J, Bunzel M, Marita JM, Hatfield RD, Lu F, Kim H *et al*. Peroxidase-dependent cross-linking reactions of *p*-hydroxycinnamates in plant cell walls. Phytochem. Rev. 2004;3(1):79-96.
58. Iiyama K, Lam TBT, Stone BA. Covalent cross-links in the cell wall. Plant Physiol. 1994;104(2):315-20.
59. Cooper JB, Varner JE. Cross-linking of soluble extensin in isolated cell walls. Plant Physiol. 1984;76:414-7.
60. Lombard V, Golaconda Ramulu H, Drula E, Coutinho PM, Henrissat B (2014) The Carbohydrate-active enzymes database (CAZy) in 2013. Nucleic. Acids Res. 42:D490–D495.
61. Kubicek CP, Starr TL, Glass NL. Plant cell wall–degrading enzymes and their secretion in plant-pathogenic fungi. Ann. Rev. Phytopathol. 2014;52(1):427-51.
62. Jung J, Sethi A, Gaiotto T, Han JJ, Jeoh T, Gnanakaran S *et al*. Binding and movement of individual Cel7A cellobiohydrolases on crystalline cellulose surfaces revealed by single-molecule fluorescence imaging. J. Biol. Chem. 2013;288(33):24164-72.
63. Kurašin M, Väljamäe P. Processivity of cellobiohydrolases is limited by the substrate. J. Biol. Chem. 2011;286(1):169-77.
64. Teeri TT. Crystalline cellulose degradation: New insight into the function of cellobiohydrolases. Trends Biotechnol. 1997;15(5):160-7.
65. Gourlay K, Hu J, Arantes V, Andberg M, Saloheimo M, Penttilä M *et al*. Swollenin aids in the amorphogenesis step during the enzymatic hydrolysis of pretreated biomass. Bioresour. Technol. 2013;142:498-503.
66. Gourlay K, Hu J, Arantes V, Penttilä M, Saddler JN. The use of Carbohydrate Binding Modules (CBMs) to monitor changes in fragmentation and cellulose fibre surface morphology during cellulase and swollenin induced deconstruction of lignocellulosic substrates. J. Biol. Chem. 2015; 290(5):2938-2945.
67. Saloheimo M, Paloheimo M, Hakola S, Pere J, Swanson B, Nyyssönen E *et al*. Swollenin, a *Trichoderma reesei* protein with sequence similarity to the plant expansins, exhibits disruption activity on cellulosic materials. Eur. J. Biochem. 2002;269(17):4202-11.
68. Ekwe E, Morgenstern I, Tsang A, Storms R, Powlowski J. Non-hydrolytic cellulose active proteins: Research progress and potential application in biorefineries. Ind. Biotechnol. 2013;9(3):123-31.
69. Vaaje-Kolstad G, Westereng B, Horn SJ, Liu Z, Zhai H, Sorlie M *et al*. An oxidative enzyme boosting the enzymatic conversion of recalcitrant polysaccharides. Sci. 2010;330(6001):219-22.
70. Schäfer A, Konrad R, Kuhnigk T, Kämpfer P, Hertel H, König H. Hemicellulose-degrading bacteria and yeasts from the termite gut. J. Appl. Bacteriol. 1996;80(5):471-8.
71. Ryabova O, Vršanská M, Kaneko S, van Zyl WH, Biely P. A novel family of hemicellulolytic α-glucuronidase. FEBS Lett. 2009;583(9):1457-62.
72. de Vries RP, Visser J. *Aspergillus* enzymes involved in degradation of plant cell wall polysaccharides. Microbiol. Mol. Biol. Rev. 2001;65(4):497-522.
73. Hayashi T. Xyloglucans in the primary cell wall. Annu. Rev. Plant Physiol. Plant Mol. Biol. 1989;40(1):139-68.
74. Pauly M, Andersen LN, Kauppinen S, Kofod LV, York WS, Albersheim P *et al*. A xyloglucan-specific endo-β-1,4-glucanase from *Aspergillus aculeatus*: Expression cloning in yeast, purification and characterization of the recombinant enzyme. Glycobiology. 1999;9(1):93-100.
75. Hagglund P, Sabini E, Boisset C, Wilson K, Chanzy H, Stalbrand H. Degradation of mannan I and II crystals by fungal endo-beta-1,4-mannanases and a beta-1,4-mannosidase studied with transmission electron microscopy. Biomacromolecules. 2001;2(3):694-9.
76. Lafond M, Navarro D, Haon M, Couturier M, Berrin J-G. Characterization of a broad-specificity β-glucanase acting on β-(1,3)-, β-(1,4)-, and β-(1,6)-glucans that defines a new glycoside hydrolase family. Appl. Environ. Microbiol. 2012;78(24):8540-6.
77. (IUBMB) IUoBaMB. Biochemical nomenclature, and Enzyme nomenclature. Eur. J. Biochem. 1993;213(1):1.
78. Adinarayana K, Francisco JP, Antonio B, Miguel A. Laccases and their applications: A patent review. Recent Pat. Biotechnol. 2008;2(1):10-24.
79. Camarero S, Ibarra D, Martínez MJ, Martínez ÁT. Lignin-derived compounds as efficient laccase mediators for decolorization of different types of recalcitrant dyes. Appl. Environ. Microbiol. 2005;71(4):1775-84.
80. Hofrichter M. Review: Lignin conversion by manganese peroxidase (MnP). Enzyme Microb. Technol. 2002;30(4):454-66.

81. Hammel KE, Jensen KA, Mozuch MD, Landucci LL, Tien M, Pease EA. Ligninolysis by a purified lignin peroxidase. J. Biol. Chem. 1993;268(17):12274-81.
82. Umezawa T, Higuchi T. Mechanism of aromatic ring cleavage of β-O-4 lignin substructure models by lignin peroxidase. FEBS Lett. 1987;218(2):255-60.
83. Pérez-Boada M, Ruiz-Dueñas FJ, Pogni R, Basosi R, Choinowski T, Martínez MJ *et al*. Versatile peroxidase oxidation of high redox potential aromatic compounds: Site-directed mutagenesis, spectroscopic and crystallographic investigation of three long-range electron transfer pathways. J. of Mol. Biol. 2005;354(2):385-402.
84. Ruiz-Dueñas FJ, Morales M, García E, Miki Y, Martínez MJ, Martínez AT. Substrate oxidation sites in versatile peroxidase and other basidiomycete peroxidases. J. Exp. Bot. 2009;60(2):441-52.
85. Hernández-Ortega A, Ferreira P, Martínez AT. Fungal aryl-alcohol oxidase: a peroxide-producing flavoenzyme involved in lignin degradation. Appl. Microbiol. Biotechnol. 2012;93(4):1395-410.
86. Cavener DR. GMC oxidoreductases. J. Mol. Biol. 1992;223(3):811-4.
87. Ferreira P, Hernandez-Ortega A, Herguedas B, Martínez ÁT, Medina M. Aryl-alcohol oxidase involved in lignin degradation: A mechanistic study based on steady and pre-steady state kinetics and primary and solvent isotope effects with two alcohol substrates. J. Biol. Chem. 2009;284(37):24840-7.
88. Goswami P, Chinnadayyala SSR, Chakraborty M, Kumar AK, Kakoti A. An overview on alcohol oxidases and their potential applications. Appl. Microbiol. Biotechnol. 2013;97(10):4259-75.
89. Guillén F, Martinez AT, Martínez MJ. Production of hydrogen peroxide by aryl-alcohol oxidase from the ligninolytic fungus *Pleurotus eryngii*. Appl. Microbiol. Biotechnol. 1990;32(4):465-9.
90. Ruiz-Dueñas FJ, Martínez ÁT. Microbial degradation of lignin: How a bulky recalcitrant polymer is efficiently recycled in nature and how we can take advantage of this. Microb. Biotechnol. 2009;2(2):164-77.
91. Huang F, Fang J, Lu X, Gao P, Chen J. Synergistic effects of cellobiose dehydrogenase and manganese-dependent peroxidases during lignin degradation. Chin. Sci. Bull. 2001;46(23):1956.
92. Henriksson G, Johansson G, Pettersson G. A critical review of cellobiose dehydrogenases. J. Biotechnol. 2000;78(2):93-113.
93. Solem E, Tuczek F, Decker H. Tyrosinase versus catechol oxidase: One asparagine makes the difference. Angew. Chem. Int. Ed. 2016;55(8):2884-8.
94. Konrad L. Tyrosinase: Molecular and active-site structure. Enzymatic browning and its prevention. ACS Symp. Ser: Am. Chem. Soc.; 1995. p. 64-80.
95. Lerch K. Neurospora tyrosinase: Structural, spectroscopic and catalytic properties. Mol. Cell. Biochem. 1983;52(2):125-38.
96. Goldfeder M, Kanteev M, Adir N, Fishman A. Influencing the monophenolase/diphenolase activity ratio in tyrosinase. Biochim. Biophys. Acta Proteins Proteomics. 2013;1834(3):629-33.
97. Reese ET, Siu RGH, Levinson HS. The biological degradation or soluble cellulose derivatives and its relationship to the mechanism of cellulose hydrolysis. J. Bacteriol. 1950;59(4):485-97.
98. Eriksson K-E, Pettersson B, Westermark U. Oxidation: An important enzyme reaction in fungal degradation of cellulose. FEBS Lett. 1974;49(2):282-5.
99. Raguz S, Yaguea E, Wood DA, Thurston CF. Isolation and characterization of a cellulose-growth-specific gene from *Agaricus bisporus*. Gene. 1992;119(2):183-90.
100. Saloheimo M, Nakari-SetäLä T, Tenkanen M, Penttilä M. cDNA cloning of a *Trichoderma reesei* cellulase and demonstration of endoglucanase activity by expression in yeast. Eur. J. Biochem. 1997;249(2):584-91.
101. Schrempf H, Walter S. The cellulolytic system of *Streptomyces reticuli*. Int. J. Biol. Macromol. 1995;17(6):353-5.
102. Karlsson J, Saloheimo M, Siika-aho M, Tenkanen M, Penttilä M, Tjerneld F. Homologous expression and characterization of *Cel*61A (EG IV) of *Trichoderma reesei*. Eur. J. Biochem. 2001;268(24):6498-507.
103. Koseki T, Mese Y, Fushinobu S, Masaki K, Fujii T, Ito K *et al*. Biochemical characterization of a glycoside hydrolase family 61 endoglucanase from *Aspergillus kawachii*. Appl. Microbiol. Biotechnol. 2007;77(6):1279.
104. Karkehabadi S, Hansson H, Kim S, Piens K, Mitchinson C, Sandgren M. The first structure of a glycoside hydrolase family 61 member, *Cel*61B from *Hypocrea jecorina*, at 1.6 A resolution. J. Mol. Biol. 2008;383(1):144-54.
105. Armesilla AL, Thurston CF, Yagüe E. *CEL*1: A novel cellulose binding protein secreted by *Agaricus bisporus* during growth on crystalline cellulose. FEMS Microbiol. Lett. 1994;116(3):293-9.
106. Chang YC, Kwon-Chung KJ. Isolation of the third capsule-associated gene, CAP60, required for virulence in *Cryptococcus neoformans*. Infect. Immun. 1998;66(5):2230-6.
107. Westereng B, Ishida T, Vaaje-Kolstad G, Wu M, Eijsink VG, Igarashi K *et al*. The putative endoglucanase *Pc*GH61D from *Phanerochaete chrysosporium* is a metal-dependent oxidative enzyme that cleaves cellulose. PloS One. 2011;6(11):e27807.
108. Forsberg Z, Vaaje-Kolstad G, Westereng B, Bunaes AC, Stenstrom Y, MacKenzie A *et al*. Cleavage of cellulose by a CBM33 protein. Protein Sci. : A Publication of the Protein Society. 2011;20(9):1479-83.

109. Quinlan RJ, Sweeney MD, Lo Leggio L, Otten H, Poulsen JC, Johansen KS *et al*. Insights into the oxidative degradation of cellulose by a copper metalloenzyme that exploits biomass components. Proc. Natl. Acad. Sci. U.S.A. 2011;108(37):15079-84.
110. Phillips CM, Beeson WT, Cate JH, Marletta MA. Cellobiose dehydrogenase and a copper-dependent polysaccharide monooxygenase potentiate cellulose degradation by *Neurospora crassa*. ACS Chem. Biol. 2011;6(12):1399-406.
111. Chu HH, Hoang V, Hofemeister J, Schrempf H. A *Bacillus amyloliquefaciens* ChbB protein binds β- and α-chitin and has homologues in related strains. Microbiol. 2001;147:1793-803.
112. Eijsink VGH, Vaaje-Kolstad G, Vårum KM, Horn SJ. Towards new enzymes for biofuels: lessons from chitinase research. Trends Biotechnol. 2008;26(5):228-35.
113. Kolbe S, Fischer S, Becirevic A, Hinz P, Schrempf H. The *Streptomyces reticuli* α-chitin-binding protein CHB2 and its gene. Microbiol. 1998;144:1291-7.
114. Saito A, Miyashita K, Biuković G, Schrempf H. Characteristics of a *Streptomyces coelicolor* A3(2) extracellular protein targeting chitin and chitosan. Appl. Environ. Microbiol. 2001;67(3):1268-73.
115. Schnellmann J, Zeltins A, Blaak H, Schrempf H. The novel lectin-like protein CHB1 is encoded by a chitin-inducible *Streptomyces olivaceoviridis* gene and binds specifically to crystalline α-chitin of fungi and other organisms. Mol. Microbiol. 1994;13(5):807-19.
116. Suzuki K, Suzuki M, Taiyoji M, Nikaidou N, Watanabe T. Chitin Binding Protein (CBP21) in the culture supernatant of *Serratia marcescens* 2170. Biosci. Biotechnol. Biochem. 1998;62(1):128-35.
117. Vaaje-Kolstad G, Horn SJ, van Aalten DM, Synstad B, Eijsink VG. The non-catalytic chitin-binding protein CBP21 from *Serratia marcescens* is essential for chitin degradation. J. Biol. Chem. 2005;280(31):28492-7.
118. Vaaje-Kolstad G, Houston DR, Riemen AH, Eijsink VG, van Aalten DM. Crystal structure and binding properties of the *Serratia marcescens* chitin-binding protein CBP21. J. Biol. Chem. 2005;280(12):11313-9.
119. Watanabe T, Kimura K, Sumiya T, Nikaidou N, Suzuki K, Suzuki M *et al*. Genetic analysis of the chitinase system of *Serratia marcescens* 2170. J. Bacteriol. 1997;179(22):7111-7.
120. Henrissat B, Davies G. Structural and sequence-based classification of glycoside hydrolases. Curr. Opin. Struct. Biol. 1997;7(5):637-44.
121. Aachmann FL, Sorlie M, Skjak-Braek G, Eijsink VG, Vaaje-Kolstad G. NMR structure of a lytic polysaccharide monooxygenase provides insight into copper binding, protein dynamics, and substrate interactions. Proc. Natl. Acad. Sci. U.S.A. 2012;109(46):18779-84.
122. Hemsworth GR, Henrissat B, Davies GJ, Walton PH. Discovery and characterization of a new family of lytic polysaccharide monooxygenases. Nat. Chem. Biol. 2014;10.
123. Hemsworth GR, Davies GJ, Walton PH. Recent insights into copper-containing lytic polysaccharide mono-oxygenases. Curr. Opin. Struct. Biol. 2013;23(5):660-8.
124. Li X, Beeson WT, Phillips CM, Marletta MA, Cate JHD. Structural basis for substrate targeting and catalysis by fungal polysaccharide monooxygenases. Structure. 2012;20(6):1051-61.
125. Wu M, Beckham GT, Larsson AM, Ishida T, Kim S, Payne CM *et al*. Crystal structure and computational characterization of the lytic polysaccharide monooxygenase GH61D from the Basidiomycota fungus *Phanerochaete chrysosporium*. J. Biol. Chem. 2013;288(18):12828-39.
126. Davies G, Henrissat B. Structures and mechanisms of glycosyl hydrolases. Structure. 1995;3(9):853-9.
127. Wong E, Vaaje-Kolstad G, Ghosh A, Hurtado-Guerrero R, Konarev PV, Ibrahim AFM *et al*. The *Vibrio cholerae* colonization factor GbpA possesses a modular structure that governs binding to different host surfaces. PLoS Pathog. 2012;8(1):e1002373.
128. Crystal structure of a chitin binding domain from Burkholderia pseudomallei. RCSB PDB. 2011. www.rcsb.org. Accessed: February 2017
129. Vaaje-Kolstad G, Bøhle LA, Gåseidnes S, Dalhus B, Bjørås M, Mathiesen G *et al*. Characterization of the chitinolytic machinery of *Enterococcus faecalis* V583 and high-resolution structure of its oxidative CBM33 Enzyme. J. Mol. Biol. 2012;416(2):239-54.
130. Hemsworth GR, Taylor EJ, Kim RQ, Gregory RC, Lewis SJ, Turkenburg JP *et al*. The copper active site of CBM33 polysaccharide oxygenases. J. Am. Chem. Soc. 2013;135(16):6069-77.
131. Taylor CB, Talib MF, McCabe C, Bu L, Adney WS, Himmel ME *et al*. Computational investigation of glycosylation effects on a family 1 carbohydrate-binding module. J. Biol. Chem. 2012;287(5):3147-55.
132. Gilkes NR, Henrissat B, Kilburn DG, Miller RC, Warren RA. Domains in microbial beta-1,4-glycanases: sequence conservation, function, and enzyme families. Microbiol. Rev. 1991;55(2):303-15.
133. Cantarel BL, Coutinho PM, Rancurel C, Bernard T, Lombard V, Henrissat B. The Carbohydrate-active enZymes database (CAZy): An expert resource for glycogenomics. Nucleic Acids Res. 2009;37:D233-D8.
134. Kittl R, Kracher D, Burgstaller D, Haltrich D, Ludwig R. Production of four *Neurospora crassa* lytic polysaccharide monooxygenases in *Pichia pastoris* monitored by a fluorimetric assay. Biotechnol. Biofuels. 2012;5(1):79.

135. Bey M, Zhou S, Poidevin L, Henrissat B, Coutinho PM, Berrin JG *et al*. Cello-oligosaccharide oxidation reveals differences between two lytic polysaccharide monooxygenases (family GH61) from *Podospora anserina*. Appl. Environ. Microbiol. 2013;79(2):488-96.
136. Beeson WT, Phillips CM, Cate JH, Marletta MA. Oxidative cleavage of cellulose by fungal copper-dependent polysaccharide monooxygenases. J. Am. Chem. Soc. 2012;134(2):890-2.
137. Langston JA, Shaghasi T, Abbate E, Xu F, Vlasenko E, Sweeney MD. Oxidoreductive cellulose depolymerization by the enzymes cellobiose dehydrogenase and glycoside hydrolase 61. Appl. Environ. Microbiol. 2011;77(19):7007-15.
138. Sygmund C, Kracher D, Scheiblbrandner S, Zahma K, Felice AKG, Harreither W. Characterization of the two *Neurospora crassa* cellobiose dehydrogenases and their connection to oxidative cellulose degradation. Appl. Environ. Microbiol. 2012;78.
139. Hori C, Igarashi K, Katayama A, Samejima M. Effects of xylan and starch on secretome of the basidiomycete *Phanerochaete chrysosporium* grown on cellulose. FEMS Microbiol. Lett. 2011;321(1):14-23.
140. Yakovlev I, Vaaje-Kolstad G, Hietala AM, Stefańczyk E, Solheim H, Fossdal CG. Substrate-specific transcription of the enigmatic GH61 family of the pathogenic white-rot fungus *Heterobasidion irregulare* during growth on lignocellulose. Appl. Environ. Microbiol. 2012;95(4):979-90.
141. Solomon EI, Ginsbach JW, Heppner DE, Kieber-Emmons MT, Kjaergaard CH, Smeets PJ *et al*. Copper dioxygen (bio)inorganic chemistry. Faraday Discuss. 2011;148:11-108.
142. Klinman JP. The copper-enzyme family of dopamine β-monooxygenase and peptidylglycine α-hydroxylating monooxygenase: Resolving the chemical pathway for substrate hydroxylation. J. Biol. Chem. 2006;281(6):3013-6. doi:10.1074/jbc.R500011200.
143. Leijdekkers AGM, Huang J-H, Bakx EJ, Gruppen H, Schols HA. Identification of novel isomeric pectic oligosaccharides using hydrophilic interaction chromatography coupled to traveling-wave ion mobility mass spectrometry. Carbohydr. Res. 2015;404:1-8.
144. Kabel MA, de Waard P, Schols HA, Voragen AGJ. Location of O-acetyl substituents in xylo-oligosaccharides obtained from hydrothermally treated *Eucalyptus* wood. Carbohydr. Res. 2003;338(1):69-77.
145. Cannella D, Hsieh C-wC, Felby C, Jørgensen H. Production and effect of aldonic acids during enzymatic hydrolysis of lignocellulose at high dry matter content. Biotechnol. Biofuels. 2012;5(1):26.
146. Westereng B, Agger JW, Horn SJ, Vaaje-Kolstad G, Aachmann FL, Stenstrom YH *et al*. Efficient separation of oxidized cello-oligosaccharides generated by cellulose degrading lytic polysaccharide monooxygenases. J. Chromatogr. A. 2013;1271(1):144-52.
147. Sørensen HR, Pedersen S, Viksø-Nielsen A, Meyer AS. Efficiencies of designed enzyme combinations in releasing arabinose and xylose from wheat arabinoxylan in an industrial ethanol fermentation residue. Enzyme Microb. Technol. 2005;36(5–6):773-84.
148. Hinz SWA, Pouvreau L, Joosten R, Bartels J, Jonathan MC, Wery J *et al*. Hemicellulase production in *Chrysosporium lucknowense* C1. J. Cereal Sci. 2009;50(3):318-23.
149. Verdoes JC, Punt PJ, Burlingame R, Bartels J, Dijk Rv, Slump E *et al*. Original research: A dedicated vector for efficient library construction and high throughput screening in the hyphal fungus *Chrysosporium lucknowense*. Ind. Biotechnol. 2007;3(1):48-57.
150. Berka RM, Grigoriev IV, Otillar R, Salamov A, Grimwood J, Reid I *et al*. Comparative genomic analysis of the thermophilic biomass-degrading fungi *Myceliophthora thermophila* and *Thielavia terrestris*. Nat. Biotechnol. 2011;29(10):922-7.

Chapter II

Discovery of the combined oxidative cleavage of plant xylan and cellulose by a new fungal polysaccharide monooxygenase

Based on: Frommhagen M, Sforza S, Westphal AH, Visser J, Hinz SWA, Koetsier MJ, van Berkel WJH, Gruppen H, Kabel MA. Discovery of the combined oxidative cleavage of plant xylan and cellulose by a new fungal polysaccharide monooxygenase. *Biotechnology for Biofuels*. 2015; 8:101.

Abstract

Many agricultural and industrial food by-products are rich in cellulose and xylan. Their enzymatic degradation into monosaccharides is seen as a basis for the production of biofuels and bio-based chemicals. Lytic polysaccharide monooxygenases (LPMOs) constitute a group of recently discovered enzymes, classified as the auxiliary activity subgroups AA9, AA10, AA11 and AA13 in the CAZy database. LPMOs cleave cellulose, chitin, starch and β-(1→4)-linked substituted and non-substituted glucosyl units of hemicellulose under formation of oxidized gluco-oligosaccharides.

Here, we demonstrate a new LPMO, obtained from *Myceliophthora thermophila* C1 (*Mt*LPMO9A). This enzyme cleaves β-(1→4)-xylosyl bonds in xylan under formation of oxidized xylo-oligosaccharides, while it simultaneously cleaves β-(1→4)-glucosyl bonds in cellulose under formation of oxidized gluco-oligosaccharides. In particular, *Mt*LPMO9A benefits from the strong interaction between low substituted linear xylan and cellulose. *Mt*LPMO9A shows a strong synergistic effect with endoglucanase I (EGI) with a 16-fold higher release of detected oligosaccharides, compared to the oligosaccharides release of *Mt*LPMO9A and EGI alone.

Now, for the first time, we demonstrate the activity of a lytic polysaccharide monooxygenase (*Mt*LPMO9A) that shows oxidative cleavage of xylan in addition to cellulose. The ability of *Mt*LPMO9A to cleave these rigid regions provides a new paradigm in the understanding of the degradation of xylan-coated cellulose. In addition, *Mt*LPMO9A acts in a strong synergism with endoglucanase I. The mode of action of *Mt*LPMO9A is considered to be important for loosening the rigid xylan-cellulose polysaccharide matrix in plant biomass, enabling increased accessibility to the matrix for hydrolytic enzymes. This discovery provides new insights in how to boost plant biomass degradation by enzyme cocktails for biorefinery applications.

2.1 Background

Effective degradation of plant polysaccharide biomass into monosaccharides, which are useful building blocks for biochemicals or biofuels, requires a variety of enzymes. Commercial enzyme cocktails for plant cell wall degradation mostly comprise enzymes produced by filamentous fungi, like *Aspergillus* and *Trichoderma* strains. In addition, the commercially available fungus *Myceliophthora thermophila* C1 is a good candidate for the production of thermo-tolerant carbohydrate-active enzymes [1]. Still, improvements of already existing enzyme cocktails are required for a more efficient degradation of plant biomass and a decrease in costs for the production of biochemicals and biofuels.

In general, plant cell walls are composed of a primary and secondary layer, which are both build from various polymers such as polysaccharides, lignins and proteins. The polysaccharides of the plant cell wall are cellulose fibrils and hemicellulose [2-5]. Cellulose is a homogeneous linear polymer of β-(1→4) linked glucosyl units and, depending on the source, exceeding a degree of polymerization (DP) over 10.000 [6]. These β-(1→4) linked glucosyl chains are forming microfibrills via hydrogen bonds and Van der Waals forces [7]. Depending on these interactions, cellulose is composed of crystalline and amorphous regions [8]. Lignin is an aromatic heteropolymer consisting of the three monolignols coniferyl, sinapyl and p-coumaryl alcohol, which are methoxylated in various degrees. The network of lignin in the plant cell wall is build up by ester and ether linkages with hemicellulose [9, 10, 3]. Hemicellulose is, unlike cellulose, a very heterogeneous polymer. The hemicellulose structure differs between species of mono- and dicotyls and, depending on the source, can consist of a xylan, mannan, xyloglucan or β-glucan backbone [11-16]. The majority of these backbones are composed of β-(1→3, 1→4) linked xylosyl, β-(1→4) linked mannosyl and β-(1→3, 1→4) linked glucosyl residues, respectively. In addition, these backbones show structural side-chain variations, which can differ in i.e. type of substituent or distribution along the backbone [17]. Such hemicelluloses are strongly associated with cellulose via hydrogen-bonding, especially the ones with a low degree of substitution or a block-wise distribution of substituents along the backbone [2, 4]. The cellulose-associated hemicelluloses block cellulases to reach their substrate, which is likely to contribute to the defense of plants against microbial attack, and hinder the deconstruction of cellulose by industrial enzymes into fermentable monosaccharides [18, 19]. Hence, degradation of cellulose-associated hemicelluloses is essential to improve hydrolysis of cellulose present in plant biomass.

It has been known for a long time that enzymatic degradation of cellulosic plant biomass can be achieved by a variety of glycoside hydrolases (GHs; EC.3.2.1.-), which are all listed in the Carbohydrate-Active enZYmes (CAZy, [20]) database. However, the effectiveness of hydrolases on cellulose is limited, due to hydrogen bonds between the glucan chains of the rather crystalline cellulose. Recently, it was demonstrated that the breakdown of crystalline polysaccharides could be boosted by the action of lytic polysaccharide monooxygenases (LPMOs). These LPMOs are classified as subgroups AA9, AA10, AA11 and AA13 in the CAZy database [21]. The LPMOs exhibit oxidative cleavage between β-(1→4)-glucosyl units in chitin, cellulose, hemicellulosic glucan and soluble cellodextrines under formation of oxidized gluco-oligosaccharides [22-26]. Depending on the type of LPMO, products released are gluco-oligosaccharides that are oxidized at either the reducing (C1) or

the non-reducing (C4) end. Although not relevant for degradation of plant cell walls, very recently starch-active LPMO has been reported, cleaving between α-(1→4)-glucosyl units in starch under formation of C1-oxidized dextrins [26, 27]. This finding illustrates that LPMO activities cover a broader range of substrates than earlier conceived. So far, no LPMO active on xylans has been reported.

In the present research, a new enzyme LPMO activity is described, which can be considered to be highly important for the concerted degradation of plant cellulose associated with xylan. In brief, we propose that the thermo-tolerant enzyme *Mt*LPMO9A from *M. thermophila* C1 cleaves cellulose-associated xylan under formation of oxidized xylo-oligosaccharides. In addition, to evaluate the enhanced cellulose accessibility, the synergistic effect of *Mt*LPMO9A with an endoglucanase I was determined.

2.2 Results

2.2.1 Enzyme purity

From the *M. thermophila* C1 genome, protein *Mt*LPMO9A was predicted to be an LPMO belonging to subfamily AA9 [21]. Since the addition of LPMOs to a cellulase cocktail was found to considerably increase the release of glucose from cellulose [28, 29], it was of interest to analyze the mode of action of *Mt*LPMO9A in further detail. Hereto, *Mt*LPMO9A was expressed and produced in a protease/(hemi-)cellulase-free *M. thermophila* C1 strain with Dyadic technology (Dyadic NL, Wageningen, The Netherlands). *Mt*LPMO9A was purified to apparent homogeneity using multiple chromatographic steps. The purified enzyme showed a single band in SDS-PAGE with an apparent molecular mass of 23 ± 1 kDa (**Additional Figure 2.1**), in good agreement with the predicted mass of *Mt*LPMO9A (22,755.3 Da; without signal peptide).

To further analyze the purified *Mt*LPMO9A preparation, the enzyme was subjected to LC/UV/ESI mass spectrometry. The elution pattern (**Figure 2.1**) showed a main and a shallow peak, of which the latter was due to protein denaturation by the LC conditions applied. MS-analysis of both the main and shallow peak showed exactly the same protein mass based on the multi-charged ion patterns corresponding to a mass of 22765.3 ± 0.1 Da. The *Mt*LPMO9A protein comprised ± 99.5% (65% + 34.5%, from the main and shallow peak, respectively) of the total protein present based on UV (214 nm), and 94.7% based on total ion current (TIC) in the full mass range. In conclusion, *Mt*LPMO9A was obtained in an extremely pure form.

2.2.2 Structural model of *Mt*LPMO9A

A structural model of *Mt*LPMO9A was generated based on the available structure of *Tt*PMO1 from *Thielavia terrestis* [29] (Protein Data Bank entry: 3EII), which shared 75% amino acid sequence identity. The *Mt*LPMO9A model (**Figure 2.2**) shows a highly conserved β-sheet core, whereas the loops differ from the *Tt*PMO1 structure reported. The divalent metal ion in the active site is coordinated by the three amino acids His1, His68 and Tyr153. The tyrosine (Tyr67) above the coordination site is typical for the PMO1 subgroup of the AA9 family [30]. Of the amino acids proposed to form the flat area of the *Tt*PMO1 substrate-binding site, only one tyrosine is replaced by an asparagine in *Mt*LPMO9A (Asn191). This tyrosine is also not conserved in other LPMO structures available in the Protein Data Bank. Based on the structural model shown in **Figure 2.2**,

*Mt*LPMO9A comprises two disulfide bridges Cys126-Cys208 (-2 Da) and Cys38-Cys156 (-2 Da). The predicted mass of *Mt*LPMO9A (22,755.3 Da; amino acid sequence without signal peptide) is 10 Da lower than the actual mass determined by ESI-MS (22765.3 Da). Based on this calculation, *Mt*LPMO9A is expected to contain a methylated N-terminal histidine (predicted mass from the amino acid sequence +14 Da for the methyl group bound to the histidine).

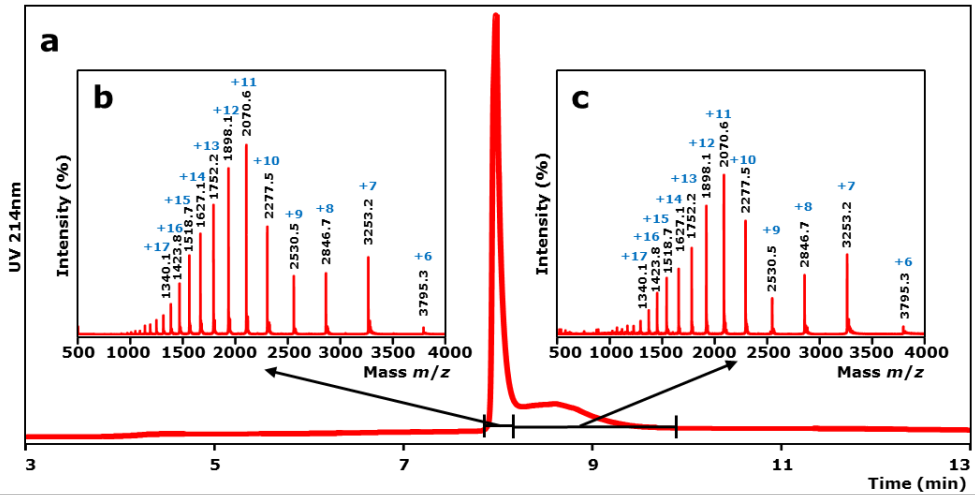

Figure 2.1 LC/ESI-MS analysis of MtLPMO9A. Purified *Mt*LPMO9A was analyzed by LC/UV/ESI-MS using an ACQUITY UPLC separation system and a SYNAPT ion mobility mass spectrometer. **a** Chromatographic profile of purified *Mt*LPMO9A (UV 214 nm). **b** and **c** ESI MS spectra (*m/z* values) of the main peak (**b**) and a shallow peak (**c**) observed by UV. The main and shallow peak showed exactly the same mass spectrum corresponding to the same protein with an *m/z* of 22765 Da. The main and shallow peak together featured about 99.5% of the total area measured in the UV trace at 214 nm and 94.7% of the total area measured in the total ion current (TIC) mass chromatogram (See Methods). Blue numbers represent different charge states of *Mt*LPMO9A.

2.2.3 Activity of *Mt*LPMO9A on amorphous cellulose

The activity of *Mt*LPMO9A was assayed on regenerated amorphous cellulose (RAC), both in the absence and presence of the external electron donor ascorbic acid. From HPAEC and MALDI-TOF MS analysis (**Figure 2.3**) it can be concluded that in the presence of ascorbic acid, RAC is degraded by *Mt*LPMO9A and that both C1 and C4 oxidized gluco-oligosaccharides ($GlcOS_n^{\#}$ and $GlcOS_n$*, respectively) and non-oxidized gluco-oligosaccharides ($GlcOS_n$) were formed. Furthermore, in the absence of ascorbic acid no oxidized and non-oxidized gluco-oligosaccharides were found, which indicates that both hydrolytic and oxidative cleavage activity towards RAC are absent (**Additional Figure 2.2**). The annotation by HPAEC of oxidized gluco-oligosaccharides was performed using the published elution pattern of C1- and C4-oxidized gluco-oligosaccharides formed by NCU01050 or NCU08760 from *Neurospora crassa* [22, 31]. In addition, the formation of oxidized gluco-oligosaccharides was confirmed by the masses identified with MALDI-TOF MS (**Figure 2.3c**), based on previously proposed LPMO cleaving mechanisms [31-33]. In short, oxidation at C1 of the pyranose ring leads to formation of an unstable δ-lactone, which in the presence of water converts to an aldonic acid. Lactone formation results in a 2 Da lower mass compared to the non-oxidized gluco-oligosaccharides, while aldonic acid formation results in a 16 Da higher mass (**Figure 2.3b** and **c**,

marked with [#]). Some of these acid groups may exchange an H-ion for a Li-ion, leading to a double Li-adduct yielding to an additional mass of 6 Da (**Figure 2.3c**, marked with [§]). Such double adducts have also been described for galacturonic acid oligosaccharides in MALDI-TOF MS [34]. Similarly, oxidation at the C4 position leads to a 4-ketoaldose (**Figure 2.3c**, marked with *), which is rather stable. It corresponds, like the lactone, to a 2 Da lower mass compared to the non-oxidized gluco-oligosaccharides [23, 32].

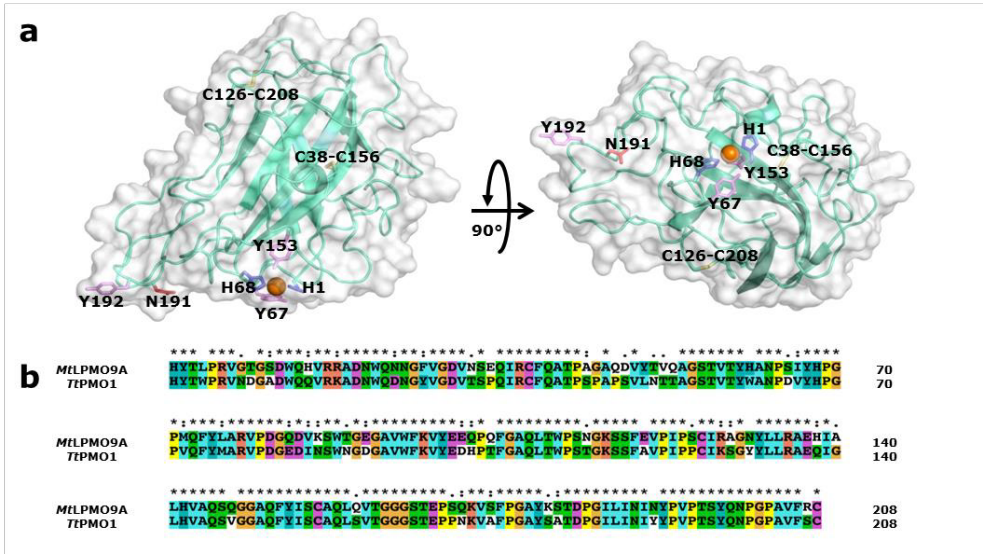

Figure 2.2 Structural model of *Mt*LPMO9A. **a** Structural model of *Mt*LPMO9A generated using the available template structure of *Tt*PMO1 from *Thielavia terrestis* (PDB-id: 3EII) [29]. The divalent metal ion (orange) in the flat face is coordinated by two histidines (His1 and His68; blue) and one tyrosine (Tyr153, magenta), which is typical for LPMOs belonging to subgroup AA9 of the CAZy database [30]. Compared to *Tt*PMO1, Tyr191 is replaced by Asn191 in the flat face. Two disulfide bridges Cys126-Cys208 and Cys38-Cys156 are conserved and expected to be crucial for the thermo-tolerance of *Mt*LPMO9A. **b** Sequence alignment of *Mt*LPMO9A and *Tt*PMO1 (PDB-id: 3EII), which scored the highest in a Blast search using the *Mt*LPMO9A sequence against the Protein Data Bank (75% amino acid identity).

Unexpectedly, besides oxidized and non-oxidized gluco-oligosaccharides, also masses of C1 and C4 oxidized xylo-oligosaccharides ($XOS_n^{\#}$ and XOS_n*, respectively) and non-oxidized xylo-oligosaccharides (XOS_n) were observed (**Figure 2.3c**), although Avicel is known to contain around 2% (w/w) of xylan [35]. This striking observation suggested that *Mt*LPMO9A is capable of oxidatively cleaving xylan next to cellulose. Based on the proposed LPMO cleaving mechanism for gluco-oligosaccharides as described above, the oxidation of the C1 and C4 position of xylo-oligosaccharides leads to a 2 Da lower mass compared to non-oxidized xylo-oligosaccharides. Xylo-oligosaccharides oxidized at the C1 position are, like C1 oxidized gluco-oligosaccharides, unstable δ-lactones, which hydrolyse in water to the corresponding aldonic acids ($XOS_n^{\#}$; +16 Da).

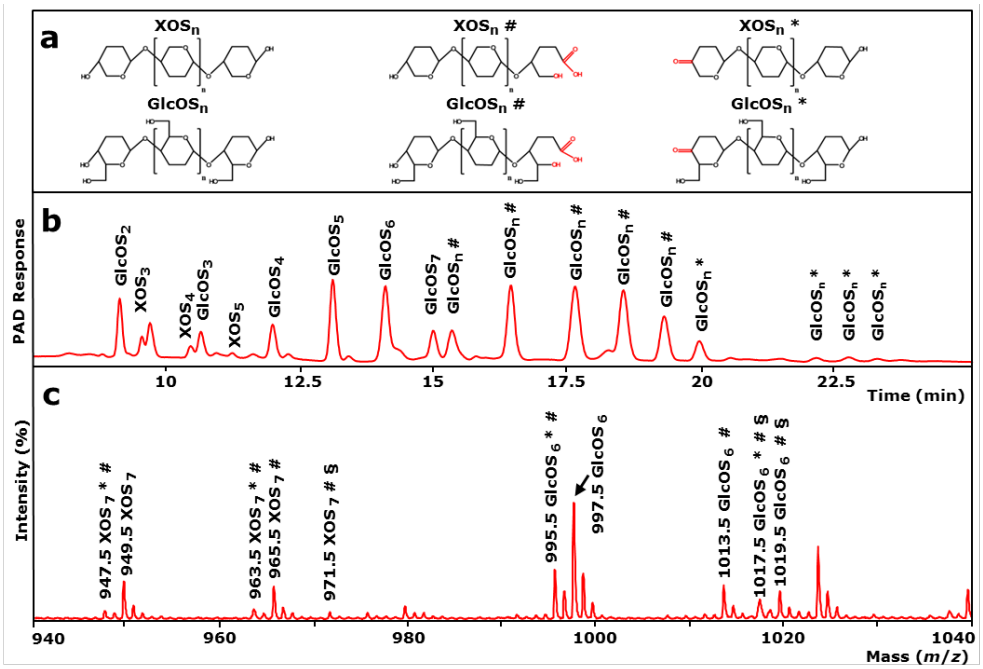

Figure 2.3 Activity of *Mt*LPMO9A on amorphous cellulose. **a** Structure and nomenclature used: XOS_n and $GlcOS_n$, non-oxidized xylo- and gluco-oligosaccharides; $XOS_n^{\#}$ and $GlcOS_n^{\#}$, xylo- and gluco-oligosaccharides oxidized at the C1-carbon atom; XOS_n* and $GlcOS_n$*, xylo - and gluco-oligosaccharides oxidized at the C4-carbon atom. **b** HPAEC elution pattern of regenerated amorphous cellulose (RAC) after incubation with *Mt*LPMO9A (5 mg g^{-1} substrate). Samples were incubated in a 50 mM ammonium acetate buffer (pH 5.0) for 24 h at 52°C with ascorbic acid addition (1 mM). In the presence of ascorbic acid, oxidized $GlcOS_n^{\#}$ * are formed by *Mt*LPMO9A (marked either with $^{\#}$ or *), of which the masses were analyzed by MALDI-TOF MS. Using RAC as a substrate, small amounts of non-oxidized XOS_n are detected by HPAEC. **c** MALDI-TOF mass spectrum of RAC incubated with *Mt*LPMO9A with ascorbic acid. Clusters of oxidized $GlcOS_n^{\#}$ * are determined as their lithium (Li) adducts. The insert shows masses of $XOS_n^{\#}$ * and $GlcOS_n^{\#}$ * oxidized either at C4 leading to a keto-group (* -2 Da) or C1 leading to a lactone ($^{\#}$ -2Da). The δ-lactones are unstable in water and hydrolyse to the corresponding aldonic acids ($^{\#}$ +16 Da). Double Li-adducts (one Li-adduct and one additional Li exchanged for H on the acid-group) are C1 oxidized products (§).

2.2.4 Activity of *Mt*LPMO9A on three types of xylans

The observation that *Mt*LPMO9A generates oxidized xylo-oligosaccharides from RAC next to oxidized gluco-oligosaccharides is new and such an action of LPMOs has not been described for other LPMOs. Therefore, wheat arabinoxylan (WAX), birchwood glucuronoxylan (BiWX) and oat spelt xylan (OSX) were incubated with *Mt*LPMO9A in the absence or presence of ascorbic acid. The products formed were determined by using HPAEC and MALDI-TOF MS (**Additional Figures 2.3-2.5**). Remarkably, both in the absence and presence of ascorbic acid, no oxidized xylo-oligosaccharides were observed. In fact, non-oxidized xylo-oligosaccharides were released, which most likely pointed at the presence of a minor xylanolytic hydrolase impurity.

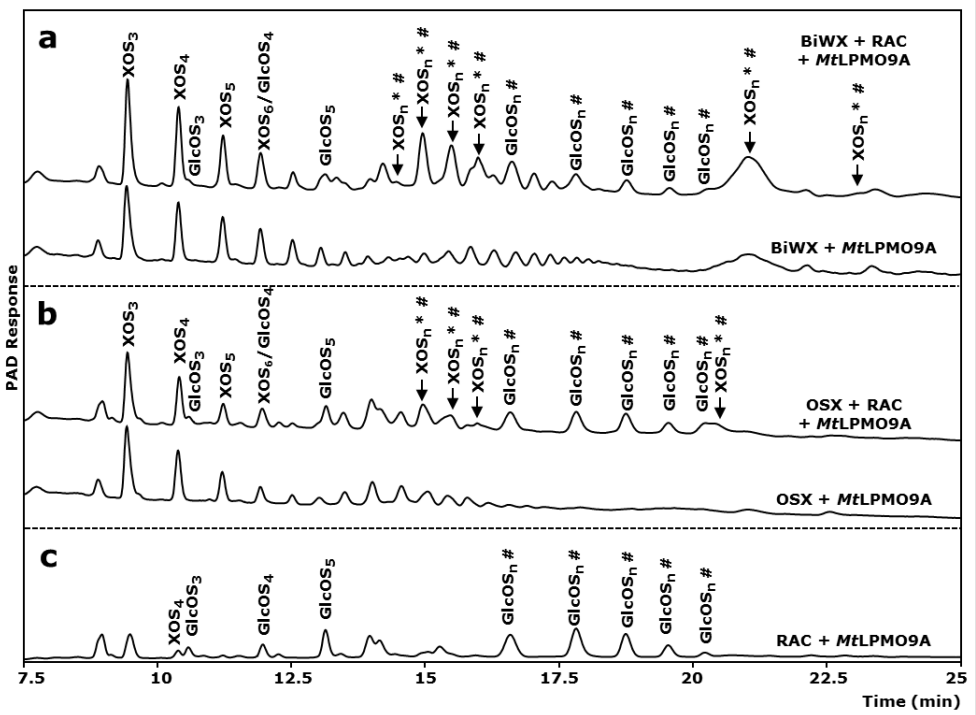

Figure 2.4 HPAEC elution pattern of xylan-RAC-mixtures incubated with *Mt*LPMO9A. **a** Birchwood xylan (BiWX) and **b** oat spelt xylan (OSX) (2mg mL^{-1}) in the presence and absence of regenerated amorphous cellulose (RAC; 2 mg mL^{-1}) after incubation with *Mt*LPMO9A (12.5 mg g^{-1} substrate). **c** HPAEC elution pattern of RAC after incubation with *Mt*LPMO9A (12.5 mg g^{-1} substrate). Samples were incubated in a 50 mM ammonium acetate buffer (pH 5.0) with ascorbic acid addition (1 mM). Incubation with *Mt*LPMO9A of the two xylans and xylan-RAC-mixtures, in the presence of ascorbic acid, results in the formation of non-oxidized linear xylo-oligosaccharides (XOS_n) and substituted xylo-oligosaccharides. Incubation of xylan-RAC-mixtures with *Mt*LPMO9A in the presence of ascorbic acid results in the formation of non-oxidized gluco-oligosaccharides ($GlcOS_n$) and oxidized gluco-oligosaccharides ($GlcOS_n^{\#}$). The incubation of *Mt*LPMO9A with BiWX-RAC- and OSX-RAC-mixture in the presence of ascorbic acid results in the formation of numerous products (black arrow, indicated as oxidized xylo-oligosaccharides $XOS_n^{\#}$*), which are not present if *Mt*LPMO9A was incubated with BiWX, OSX or RAC alone. The results of MALDI-TOF MS analysis of BiWX-RAC- and OSX-RAC-mixture incubated with *Mt*LPMO9A in the presence of ascorbic acid are shown in **Figure 2.5**.

2.2.5 Activity of *Mt*LPMO9A on xylan-RAC-mixtures

Since *Mt*LPMO9A generated oxidized xylo-oligosaccharides from RAC next to oxidized gluco-oligosaccharides, but not if xylan as substrate was used alone, the mode of action of *Mt*LPMO9A on xylan-rich cellulosic biomass was further investigated. Hereto, RAC was separately mixed with wheat arabinoxylan (WAX), birchwood glucuronoxylan (BiWX) or oat spelt xylan (OSX). *Mt*LPMO9A was added in the absence and presence of ascorbic acid. The products were determined using HPAEC and MALDI-TOF MS (**Figures 2.4** and **2.5**, **Additional Figure 2.5**). In the absence of ascorbic acid, only non-oxidized xylo-oligosaccharides were formed from incubating RAC with BiWX, OSX or WAX. In the presence of ascorbic acid, however, the OSX-RAC- and BiWX-RAC-mixtures incubated with *Mt*LPMO9A showed formation of non-oxidized and oxidized xylo-oligosaccharides and of non-

oxidized and oxidized $GlcA_{me}$-xylo-oligosaccharides (4-*O*-methylglucuronic acid attached to xylo-oligosaccharides) next to non-oxidized and oxidized gluco-oligosaccharides (**Figure 2.4**). MALDI-TOF MS confirmed the formation of xylo-oligosaccharides and xylo-oligosaccharides oxidized at C1 ($XOS_n^{\#}$; + 16 Da) and at C4 (XOS_n*; -2 Da). From the WAX-RAC-mixture in the presence of ascorbic acid the formation of oxidized and non-oxidized gluco-oligosaccharides was observed (**Additional Figure 2.5**), but no oxidized xylo-oligosaccharides.

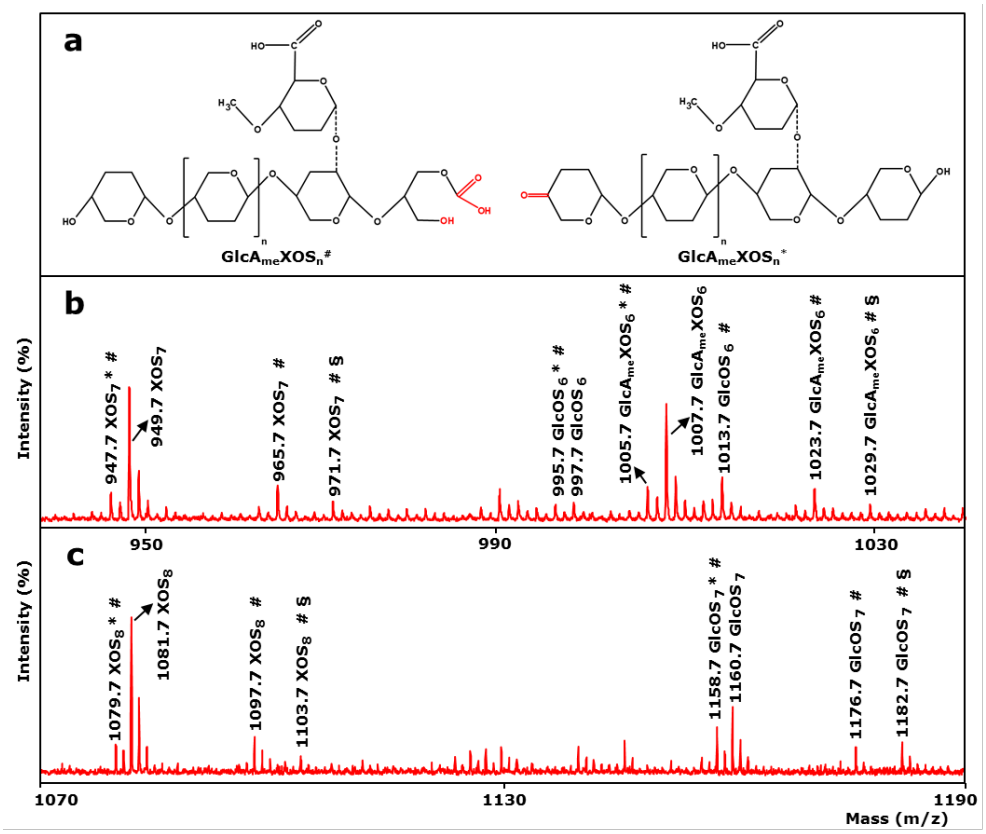

Figure 2.5 MALDI-TOF MS spectra of xylan-RAC-mixtures incubated with *Mt*LPMO9A. **b** Birchwood xylan (BiWX; 2 mg mL^{-1}) and **c** oat spelt xylan (OSX; 2 mg mL^{-1}) in the presence of regenerated amorphous cellulose (RAC; 2 mg mL^{-1}) after incubation of *Mt*LPMO9A (10 mg g^{-1} substrate). Samples were incubated in a 50 mM ammonium acetate buffer (pH 5.0) for 24 h at 52°C with ascorbic acid addition (1 mM). *Mt*LPMO9A incubation of BiWX and OSX with RAC addition releases non-oxidized and oxidized xylo- and gluco-oligosaccharides (XOS_n, $XOS_n^{\#}$ *; $GlcOS_n$, $GluOS_n^{\#}$ *). The presence of C4-oxidized XOS_n*, and $XOS_n^{\#}$ oxidized at C1 to an aldonic acid ($^{\#}$ + 16 Da) is shown. Non-oxidized $GlcOS_n$ and oxidized $GlcOS_n^{\#}$ * are less detectable due to abundance of xylo-oligosaccharides present. From BiWX also 4-*O*-methylglucoronic acid containing non-oxidized XOS_n ($GlcA_{me}XOS_n$) and 4-*O*-methylglucoronic acid containing oxidized $XOS_n^{\#}$ * ($GlcA_{me}XOS_n^{\#}$ *) are formed. **a** Illustrated structure of 4-*O*-methylglucoronic acid containing C1- and C4-oxidized XOS_n ($GlcA_{me}XOS_n^{\#}$, $GlcA_{me}XOS_n$*, respectively). Masses represent lithium-adducts only. Double Li-adducts are determined for C1 oxidized products (§ + 6 Da). MALDI-TOF MS analysis of BiWX and OSX in the presence of RAC after incubation of *Mt*LPMO9A without ascorbic acid did not reveal detectable amounts of oxidized products (data not shown).

2.2.6 Synergy with EGI

The synergy of *Mt*LPMO9A with a pure EGI from *Trichoderma viride* [36, 37] in degrading RAC is shown in **Figure 2.6**. The release of $GlcOS_n$ by EGI in the presence of *Mt*LPMO9A is around 16 and 8 times higher compared to the activity of pure EGI and pure *Mt*LPMO9A alone, respectively (based on the total HPAEC-area of $GlcOS_{2-5}$). The observed strong synergy between an LPMO and a cellulase has not been reported before.

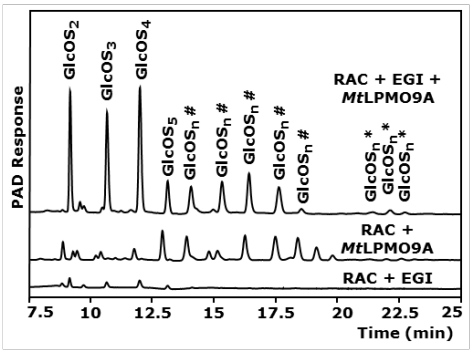

Figure 2.6 HPAEC elution patterns of RAC incubated with *Mt*LPMO9A and EGI. Regenerated amorphous cellulose (RAC, 2 mg mL^{-1}) before and after incubation with *Mt*LPMO9A (10 mg g^{-1} substrate) and/or endoglucanase I from *T. viride* (EGI) (100 µg g^{-1} substrate). Samples were incubated in a 50 mM ammonium acetate buffer (pH 5.0) for 24 h at 52°C with ascorbic acid addition (1 mM). In the presence of ascorbic acid, mainly oxidized gluco-oligosaccharides ($GlcOS_n^{\#}$ *) are formed by *Mt*LPMO9A from RAC (marked either with # for C1 or * for C4 oxidation). Incubation of EGI with RAC results in hardly detectable non-oxidized gluco-oligosaccharides (DP2-5). The combined addition of EGI and *Mt*LPMO9A results in a 16-fold higher release of non-oxidized $GlcOS_n$ (based on comparison of the sum of AUC of $GlcOS_{2-4}$ determined by HPAEC) from RAC compared to EGI incubated with RAC only.

2.3 Discussion

LPMOs constitute a new class of oxidative enzymes, which are expected to play a crucial role in the degradation of lignocellulosic biomass [23-25, 27]. We purified a new LPMO from the commercially applied fungus *Myceliophthora thermophila* C1 and investigated its degradation capacity on a wide range of substrates (**Table 2.1**). We show for the first time an LPMO that is able to oxidize substrates with a β-(1→4)-linked xylan backbone, in the presence of cellulose and the electron donor ascorbic acid.

For the formation of oxidized xylo-oligosaccharides by *Mt*LPMO9A in the presence of ascorbic acid, the addition of cellulose to xylans is essential. During incubations without ascorbic acid no oxidized xylo- and gluco-oligmers were detected. We considered the idea that the formation of glucyl radical intermediates of cellulose by *Mt*LPMO9A [31, 32] might have oxidized the xylan backbone. This hypothesis, however, seemed to be unlikely since also other LPMOs cleave cellulose under the formation of oxidized gluco-oligosaccharides via glucyl radical intermediates, but the formation of oxidised xylo-oligosaccharides has not been reported [23, 28]. We showed that the oxidized xylo-oligosaccharides detected were not from RAC only. Specifically, oxidized $GlcA_{me}$-xylo-oligosaccharides from the cleavage of BiWX and OSX were also detected, but only if RAC was

incubated *together* with BiWX or OSX (**Figures 2.4** and **2.5**). Hence, we hypothesize that *Mt*LPMO9A uses the cellulose to bind while oxidizing neighbouring xylan-chains. This idea is strengthened by the observation that in contrast to RAC-BiWX and RAC-OSX-mixtures, oxidized xylo-oligosaccharides are not formed with RAC-WAX mixtures. Unlike WAX, both BiWX and OSX consist of large sequences of unsubstituted xylosyl residues [4, 38]. Such long linear unsubstituted xylans are reported to associate with cellulose via hydrogen-bonding [2, 4]. WAX, on the other hand, has a high degree of arabinosyl-substituents present on the β-(1→4)-linked xylan backbone [39], which has been shown to prevent association with cellulose-chains [4]. Here, we show for the first time a LPMO, which benefits from the strong interaction between low substituted linear xylan and cellulose. The discovered activity of *Mt*LPMO9A provides a new paradigm in the understanding of the degradation of xylan-coated cellulose.

Table 2.1 *Mt*LPMO9A oxidation on various polysaccharide substrates

Substrate	**Occurrence of oxidation**			
	without Ascorbic Acid		**with 1 mM Ascorbic Acid**	
	$GlcOS_n^{\#*}$ [a]	**$XOS_n^{\#*}$** [b]	**$GlcOS_n^{\#*}$**	**$XOS_n^{\#*}$**
Cellulose				
Avicel[c]	-	-	+	+
RAC[c]	-	-	+	+
Hemicellulose				
Glucan				
Xyloglucan[d]	-	-	+	-
β-Glucan barley	-	-	+	-
β-Glucan oat spelt	-	-	+	-
Xylan				
OSX[e]	-	-	-	-
BiWX[e]	-	-	-	-
WAX[e]	-	-	-	-
Oligosaccharides				
Gluco-oligosaccharides[f]	-	-	-	-
Xylo-oligosaccharides[f]	-	-	-	-
Galactomannan[g]	-	-	-	-
RAC/Hemicellulose combination				
RAC + BiWX	-	-	+	+
RAC + OSX	-	-	+	+
RAC + WAX	-	-	+[h]	-

[a] Gluco-oligosaccharides oxidized at the C1 ($GlcOS_n^{\#}$) or C4 position ($GlcOS_n^{*}$)

[b] Xylo-oligosaccharides oxidized at the C1 ($XOS_n^{\#}$) or C4 position (XOS_n^{*})

[c] Regenerate amorphous cellulose (RAC), crystalline cellulose (Avicel)

[d] Xyloglucan from tamarind seed

[e] Oat spelt xylan (OSX), birch wood xylan (BiWX), wheat arabinoxylan (WAX)

[f] β-(1→4)-linked gluco- and xylo-oligosaccharides, degree of polymerisation 2-5

[g] β-(1→4)-linked-D-mannosyl backbone from guar (medium viscosity), purchased from Megazyme (Bray, Ireland)

[h] Corrected, published as (-)

Recently, *Nc*LPMO9C from *N. crassa* expressed in *P. pastoris* was described to have an activity on hemicellulosic β-(1→4)-linked glucans [24]. We found that *Mt*LPMO9A showed a similar mode of action on hemicellulosic β-(1→4)-linked glucans and β-(1→3, 1→4)-linked glucans (**Additional Figure 2.6-2.7**). However, formation of oxidized xylo-oligosaccharides so far has only been observed for *Mt*LPMO9A.

Based on their amino acids in the substrate binding site, LPMOs of the AA9 class are further divided into the subgroups PMOI, PMOII and PMOIII [30]. *Mt*LPMO9A shows most similarity with subgroup PMOI and has the highest amino acid sequence identity with *Tt*PMO1 (75%). Like *Tt*PMO1 [29], *Mt*LPMO9A considerably enhances glucose release from cellulose when added to a cellulase-cocktail. Additionally, *Mt*LPMO9A shows a strong synergistic effect with EGI on amorphous cellulose as shown in the present study. During enzyme purification, the oxidative activity of *Mt*LPMO9A was separated from a strong hydrolytic activity towards cellulose (data not shown). Probably, *Mt*LPMO9A and the enzyme responsible for this hydrolytic activity are closely working together *in vivo*. Possibly, during the evolution of fungi, the development of enzymes containing both oxidative activities and synergism with hydrolases enabled a more efficient degradation of a wider range of substrates present in nature.

2.4 Conclusions

The enzymatic degradation of cellulose and xylan rich agricultural and industrial food by-products into monosaccharides is seen as a basis for the production of biofuels and bio-based chemicals. Now, for the first time, we demonstrate the activity of a lytic polysaccharide monooxygenase (*Mt*LPMO9A), that shows oxidative cleavage of xylan in addition to cellulose and that acts in synergism with endoglucanase I. The ability of *Mt*LPMO9A to cleave the xylan coated cellulose regions is considered to be important for loosening the rigid plant polysaccharide matrix in plant biomass, enabling an increased accessibility for hydrolytic enzymes. This discovery provides new insights in how fungi degrade plant cell wall structures by using both oxidative activity and synergism with hydrolases and, in addition, how to boost hydrolytic enzyme cocktails for biorefinery applications.

2.5 Methods

2.5.1 Enzyme expression, production and purification

*Mt*LPMO9A from *Myceliophthora thermomphila* C1 (UniProt: KP901251) was over-expressed in a protease/(hemi-)cellulase free C1-expression host (LC strain) [40, 41]. The C1-strain was grown aerobically in 2-L fermentors using a medium containing glucose and ammonium sulfate, and enriched with essential salts [41]. Enzyme production was performed under glucose limitation in a fed-batch process (pH 6.0; 32°C) as described previously [40] and resulted in an *Mt*LPMO9A-rich crude enzyme extract. The crude enzyme extract was dialyzed against 10 mM potassium phosphate buffer (pH 7.0). *Mt*LPMO9A was purified using an AKTA-Explorer preparative chromatography system (GE Healthcare, Uppsala, Sweden). As a first step, 3 g of the dialyzed crude enzyme mixture (50 mg mL^{-1}) was subjected to a self-packed Source15Q column (100 x 70 mm internal diameter, GE Healthcare), pre-equilibrated in 20 mM potassium phosphate buffer (pH 7.0). After protein

application, the column was washed with 3 column volumes of 20 mM potassium phosphate buffer (pH 7.0). Elution was performed with a linear gradient of 0-1 M NaCl in 20 mM potassium phosphate buffer (pH 7.0) over five column volumes at 25 mL min^{-1}. The eluate was monitored at 220 and 280 nm. Fractions (20 mL) were collected and immediately stored on ice. Peak fractions were pooled and concentrated using ultrafiltration (Amicon Ultra, molecular mass cut-off of 3 kDa, Merck Millipore, Cork, Ireland) at 4°C. The concentrated pools were subjected to SDS-PAGE (**Additional Figure 2.1**). For further purification (2nd step), the *Mt*LPMO9A-containing pool (fraction AEC-I, **Additional Figure 2.1**) was loaded onto a self-packed Superdex TM-75 column (100 x 3 cm internal diameter, GE Healthcare) and eluted at 5 mL min^{-1} with a 10 mM potassium phosphate buffer (pH 7.0) containing 150 mM NaCl. Fractions (5 mL) were immediately stored on ice. Peak fractions were pooled and concentrated by ultrafiltration as described above.

The *Mt*LPMO9A preparation thus obtained (partially purified fraction SEC-I; **Additional Figure 2.1**) was further subjected (3rd step) to a Resource Q column (30 x 16 mm internal diameter, GE Healthcare), pre-equilibrated in 20 mM potassium phosphate buffer (pH 7.0). After protein application, the column was washed with 20 column volumes of starting buffer. Elution at 6 mL min^{-1} was performed with a linear gradient of 0-1 M NaCl in 20 mM potassium phosphate buffer (pH 7.0) over 20 column volumes. Elution was monitored at 220 and 280 nm. Fractions (3 mL) were immediately stored on ice. Peak fractions were pooled and concentrated by ultrafiltration as described above.

2.5.2 Protein identification

Sequencing of the *Mt*LPMO9A coding sequence was carried out by The Scripps Research Institute, USA.

2.5.3 Protein content

To analyze protein contents the BCA Protein Assay Kit (Thermo Scientific, Rockford, IL, USA) was used with bovine serum albumin (BSA) as calibration.

2.5.4 SDS-PAGE

The protein purity was analyzed by using sodium dodecyl sulfate polyacrylamide gel electrophoresis (SDS-PAGE). Therefore, proteins were reduced with β-mercaptoethanol, heated for 10 min and loaded on 12% polyacrylamide gels (Mini-PROTEAN TGX Gels, Bio-Rad Laboratories, Hempel Hempstead, UK). In addition, a protein marker (Protein All Blue Standards, Bio-Rad Laboratories) was loaded for mass calibration. Gels were stained with the EZBlue Gel Staining Reagent (Sigma Aldrich, Steinheim, Germany).

2.5.5 LC/ESI-MS

Purified *Mt*LPMO9A (2.5 mg mL^{-1} in 0.1% (v/v) trifluoroacetic acid (TFA) in H_2O) was analyzed by liquid chromatography/electronspray ionization-mass spectrometry (LC/ESI-MS) using an ACQUITY UPLC separation system (Waters, Milford, MA, USA) equipped with a C4-reversed phase column (UPLC BEH C4 1.7 µm, 2.1 x 100 mm, Waters) coupled to a PLC LG 500 photodiode array detector (Waters) and to a SYNAPT G2-Si High Definition Mass Spectrometer (Waters). Gradient elution with eluent A (H_2O + 1% (v/v) acetonitrile + 0.1% (v/v) TFA) and eluent B (acetonitrile + 0.1% (v/v) TFA) was performed according to the following steps: From 0 to 2 min isocratic 90% A, from 2 to 12 min gradient from 90% A to 25% A, from 12 to 15 min gradient from 25% A to 100% B, from 12 to 15 min isocratic at 100% B, then re-equilibration to the initial conditions. The flow rate and the injection

volume were 0.35 mL min^{-1} and 2 µL, respectively. The photodiode array detector was operated at a sampling rate of 40 points sec^{-1} in the range 200-400 nm, resolution 1.2 nm. The SYNAPT mass spectrometer was operated in the positive ion mode (resolution mode), capillary voltage 3 kV, sampling cone 30 V, source temperature 150°C, desolvation temperature 500°C, cone gas flow (N_2) 200 L h^{-1}, desolvation gas flow (N_2) 800 L h^{-1}, acquisition in the full scan mode, scan time 0.3 sec, interscan time 0.015 sec, acquisition range 150-4000 *m/z*.

2.5.6 Substrates incubated with *Mt*LPMO9A

OSX, BiWX, Avicel PH-101, xylo-oligosaccharides (DP1-5) and β-(1→4)-linked gluco-oligosaccharides (DP1-5) were obtained from Sigma-Aldrich (Steinheim, Germany). WAX (medium viscosity), β-(1→3, 1→4)-linked-glucan from barley (medium viscosity) and oat spelt (medium viscosity) were purchased from Megazyme (Bray, Ireland). Xyloglucan (XG; from tamarind seed) was obtained from Dainippon Sumitomo Pharma (Osaka, Japan). Regenerated amorphous cellulose (RAC) was prepared from Avicel PH-101 by adapting a method described elsewhere [42]. Briefly, Avicel PH-101 (100 mg) was moistened with 0.6 mL water. Next, 10 mL 86.2% (w/v) *ortho*-phosphoric acid was slowly added followed by rigorously stirring for 30 min until the cellulose was completely dissolved. The dissolved cellulose precipitated during step-wise addition of 40 mL water. After centrifugation (4000 x *g*, 12 min, 4°C), the pellet obtained was washed twice with water and neutralized (pH 7.0) with 2 M sodium carbonate. The pellet was washed again with water (three times) and the final pellet was suspended in water to a dry matter content of 1.4 ± 0.1% (w/w) RAC suspension.

2.5.7 *Mt*LPMO9A activity assays

Substrates (1-2 mg mL^{-1}, see **Figure** captions) were dissolved in 50 mM ammonium acetate buffer (pH 5.0), with or without addition of ascorbic acid (final concentration of 1 mM). *Mt*LPMO9A was added (12.5 µg mg^{-1} substrate) and incubated for 24 h at 50°C in a head-over-tail rotator in portions of 1 mL total volume (Stuart rotator, Bibby Scientific, Stone, UK) at 20 rpm. Supernatants of all incubations, including substrates incubated with and without ascorbic acid in the absence of *Mt*LPMO9A, were analyzed by HPAEC and MALDI-TOF MS.

2.5.8 Structural modelling

An alignment was made of the amino acid sequence of *Mt*LPMO9A and the amino acid sequence of PMO1 from *Thielavia terrestis*, which scored highest in a Blast search using the *Mt*LPMO9A sequence against the Protein Data Bank (75% amino acid identity). Using this alignment and the available structure of *Tt*PMO1 (PDB-id: 3EII) as template, structural models were obtained for *Mt*LPMO9A using the Modeller program version 9.14 [43]. Thirty comparative models were generated, after which the model with lowest corresponding DOPE score [44] was selected for image generation using Pymol (Pymol, The PyMOL Molecular Graphics System, Version 1.5.0.4 Schrödinger, LLC, New York, NY, USA).

2.5.9 Oligosaccharides analysis

Oligosaccharides were analyzed by high-performance anion-exchange chromatography (HPAEC) with pulsed amperometric detection (PAD). The HPAEC system (ICS-5000, Dionex, Sunnyvale, CA, USA) was equipped with a combination of a CarboPac PA1 guard column (50 mm x 2 mm i.d., Dionex) and a CarboPac PA1 analytical column (250 mm x 2 mm i.d., Dionex). The flow rate was 0.3 mL min^{-1} (20°C). Samples were kept at 6°C in the autosampler and the injection volume was 10 µL. Elution was performed by using two mobile phases: 0.1 M NaOH and 1 M NaOAc in 0.1 M NaOH.

The gradient elution program was as follows: 0-30 min, linear gradient 0-400 mM NaOAc; 30-40 min linear gradient 400-1000 mM NaOAc; followed by a cleaning step and equilibration (15 min) of the column with the starting conditions. Soluble gluco- and xylo-oligosaccharides (degree of polymerisation 1-5) as well as glucuronic and gluconic acid were used as standards (Sigma-Aldrich).

2.5.10 MALDI-TOF MS

For matrix-assisted laser desorption ionization – time of flight mass spectrometry (MALDI-TOF MS), an Ultraflex workstation using FlexControl 3.3 (Bruker Daltonics) equipped with a nitrogen laser of 337nm was used. The pulsed ion extraction was set on 80 ns. Ions were accelerated to a kinetic energy of 25 kV and detected in positive reflector mode with a set reflector voltage of 26 kV. The lowest laser energy required was used to obtain a good signal-to-noise ratio. A total of 200 spectra were collected for each measurement. The mass spectrometer was calibrated by using a mixture of maltodextrins (Avebe, Veendam, The Netherlands) in a mass range (*m*/*z*) of 500-2500. The peak spectra were processed by using FlexAnalysis software version 3.3 (Bruker Daltonics). Prior to analysis, samples were desalted by adding AG 50W-X8 Resin (Bio-Rad Laboratories). To obtain lithium (Li)-adducts, the supernatant was dried under nitrogen and re-suspended in 20 mM LiCl [28]. Each lithium-enriched sample of a volume of 1 µL was mixed with 1 µL of matrix solution (12 mg mL^{-1} 2,5-dihydroxy-benzoic acid (Bruker Daltonics) in 30% (v/v) acetonitrile in H_2O), applied on a MTP 384 massive target plate (Bruker Daltonics) and dried under a stream of warm air.

References

1. Hinz SWA, Pouvreau L, Joosten R, Bartels J, Jonathan MC, Wery J *et al*. Hemicellulase production in *Chrysosporium lucknowense* C1. J. Cereal Sci. 2009;50(3):318-23.
2. Vincken JP, de Keizer A, Beldman G, Voragen AGJ. Fractionation of xyloglucan fragments and their interaction with cellulose. Plant Physiol. 1995;108(4):1579-85.
3. Lam TBT, Kadoya K, Iiyama K. Bonding of hydroxycinnamic acids to lignin: ferulic and *p*-coumaric acids are predominantly linked at the benzyl position of lignin, not the β-position, in grass cell walls. Phytochem. 2001;57(6):987-92.
4. Kabel MA, Van den Borne H, Vincken JP, Voragen AGJ, Schols HA. Structural differences of xylans affect their interaction with cellulose. Carbohydr. Polym. 2007;69(1):94-105.
5. Carpita NC, Gibeaut DM. Structural models of primary cell walls in flowering plants: consistency of molecular structure with the physical properties of the walls during growth. Plant J. 1993;3(1):1-30.
6. Zhang YHP, Lynd LR. Toward an aggregated understanding of enzymatic hydrolysis of cellulose: Noncomplexed cellulase systems. Biotechnol. Bioeng. 2004;88(7):797-824.
7. Parthasarathi R, Bellesia G, Chundawat SPS, Dale BE, Langan P, Gnanakaran S. Insights into hydrogen bonding and stacking interactions in cellulose. J. Phys. Chem. A. 2011;115(49):14191-202.
8. Mansfield SD, Mooney C, Saddler JN. Substrate and enzyme characteristics that limit cellulose hydrolysis. Biotechnol. Prog. 1999;15(5):804-16.
9. Jacquet G, Pollet B, Lapierre C, Mhamdi F, Rolando C. New ether linked ferulic acid conferyl alcohol dimers identified in grass straws. J. Agric. Food Chem. 1995;43(10):2746-51.
10. Takahashi N, Koshijima T. Ester linkages between lignin and glucuronoxylan in a lignin-carbohydrate complex from beech (*Fagus crenata*) wood. Wood Sci. Technol. 1988;22(231-241):231-41.
11. Hoffman M, Jia Z, Peña MJ, Cash M, Harper A, Blackburn Ii AR *et al*. Structural analysis of xyloglucans in the primary cell walls of plants in the subclass *Asteridae*. Carbohydr. Res. 2005;340(11):1826-40.
12. Popper ZA, Fry SC. Primary cell wall composition of *Bryophytes* and *Charophytes*. Ann. Bot. 2003;91(1):1-12.
13. Bochicchio R, Reicher F. Are hemicelluloses from *Podocarpus lambertii* typical of gymnosperms? Carbohydr. Polym. 2003;53(2):127-36.
14. Capek P, Kubačková M, Alföldi J, Bilisics L, Lišková D, Kákoniová D. Galactoglucomannan from the secondary cell wall of *Picea abies* L. Karst. Carbohydr. Res. 2000;329(3):635-45.
15. Vogel J. Unique aspects of the grass cell wall. Curr. Opin. Plant Biol. 2008;11(3):301-7.

16. Smith BG, Harris PJ. The polysaccharide composition of Poales cell walls: Poaceae cell walls are not unique. Biochem. Syst. Ecol. 1999;27(1):33-53.
17. Ebringerová A, Hromádková Z, Heinze T. Hemicellulose. Adv. Polym. Sci. 2005;186:1-67.
18. Yang B, Wyman CE. Effect of xylan and lignin removal by batch and flowthrough pretreatment on the enzymatic digestibility of corn stover cellulose. Biotechnol. Bioeng. 2004;86(1):88-95.
19. Jeoh T, Ishizawa CI, Davis MF, Himmel ME, Adney WS, Johnson DK. Cellulase digestibility of pretreated biomass is limited by cellulose accessibility. Biotechnol. Bioeng. 2007;98(1):112-22.
20. CAZy. Glycoside Hydrolase family classification. 2014. doi:www.cazy.org/Glycoside-Hydrolases.html. Accessed 27 March 2015.
21. Levasseur A, Drula E, Lombard V, Coutinho PM, Henrissat B. Expansion of the enzymatic repertoire of the CAZy database to integrate auxiliary redox enzymes. Biotechnol. Biofuels. 2013;6:41.
22. Vu VV, Beeson WT, Phillips CM, Cate JH, Marletta MA. Determinants of regioselective hydroxylation in the fungal polysaccharide monooxygenases. J. Am. Chem. Soc. 2014;136(2):562-5.
23. Isaksen T, Westereng B, Aachmann FL, Agger JW, Kracher D, Kittl R *et al*. A C4-oxidizing lytic polysaccharide monooxygenase cleaving both cellulose and cello-oligosaccharides. J. Biol. Chem. 2014;289(5):2632-42.
24. Agger JW, Isaksen T, Varnai A, Vidal-Melgosa S, Willats WG, Ludwig R *et al*. Discovery of LPMO activity on hemicelluloses shows the importance of oxidative processes in plant cell wall degradation. Proc. Natl. Acad. Sci. U.S.A. 2014;111(17):6287-92.
25. Forsberg Z, Rohr AK, Mekasha S, Andersson KK, Eijsink VG, Vaaje-Kolstad G *et al*. Comparative study of two chitin-active and two cellulose-active AA10-type lytic polysaccharide monooxygenases. Biochem. 2014;53(10):1647-56.
26. Lo Leggio L, Simmons TJ, Poulsen J-CN, Frandsen KEH, Hemsworth GR, Stringer MA *et al*. Structure and boosting activity of a starch-degrading lytic polysaccharide monooxygenase. Nat. Commun. 2015;6:5961.
27. Vu VV, Beeson WT, Span EA, Farquhar ER, Marletta MA. A family of starch-active polysaccharide monooxygenases. Proc. Natl. Acad. Sci. U.S.A. 2014;111(38):13822-7.
28. Westereng B, Ishida T, Vaaje-Kolstad G, Wu M, Eijsink VG, Igarashi K *et al*. The putative endoglucanase *Pc*GH61D from *Phanerochaete chrysosporium* is a metal-dependent oxidative enzyme that cleaves cellulose. PLoS ONE. 2011;6(11):e27807.
29. Harris PV, Welner D, McFarland KC, Re E, Navarro Poulsen JC, Brown K *et al*. Stimulation of lignocellulosic biomass hydrolysis by proteins of glycoside hydrolase family 61: structure and function of a large, enigmatic family. Biochem. 2010;49(15):3305-16.
30. Hemsworth GR, Davies GJ, Walton PH. Recent insights into copper-containing lytic polysaccharide mono-oxygenases. Curr. Opin. Struct. Biol. 2013;23(5):660-8.
31. Phillips CM, Beeson WT, Cate JH, Marletta MA. Cellobiose dehydrogenase and a copper-dependent polysaccharide monooxygenase potentiate cellulose degradation by *Neurospora crassa.* ACS Chem. Biol. 2011;6(12):1399-406.
32. Beeson WT, Phillips CM, Cate JH, Marletta MA. Oxidative cleavage of cellulose by fungal copper-dependent polysaccharide monooxygenases. J. Am. Chem. Soc. 2012;134(2):890-2.
33. Kim S, Stahlberg J, Sandgren M, Paton RS, Beckham GT. Quantum mechanical calculations suggest that lytic polysaccharide monooxygenases use a copper-oxyl, oxygen-rebound mechanism. Proc. Natl. Acad. Sci. U.S.A. 2014;111(1):149-54.
34. Guillotin SE, Van Kampen J, Boulenguer P, Schols HA, Voragen AGJ. Degree of blockiness of amide groups as indicator for difference in physical behavior of amidated pectins. Biopolym. 2006;82(1):29-37.
35. Van Gool MP. Targeted discovery and functional characterisation of complex-xylan degrading enzymes. PhD Thesis. Wageningen University, Wageningen, The Netherlands; 2012.
36. Beldman G, Voragen AGJ, Rombouts FM, Searle-van Leeuwen MF, Pilnik W. Adsorption and kinetic behavior of purified endoglucanases and exoglucanases from *Trichoderma viride.* Biotechnol. Bioeng. 1987;30(2):251-7.
37. Vincken J-P, Beldman G, Voragen AGJ. Substrate specificity of endoglucanases: what determines xyloglucanase activity? Carbohydr. Res. 1997;298(4):299-310.
38. Van Gool MP, van Muiswinkel GC, Hinz SW, Schols HA, Sinitsyn AP, Gruppen H. Two GH10 endo-xylanases from *Myceliophthora thermophila* C1 with and without cellulose binding module act differently towards soluble and insoluble xylans. Bioresour. Technol. 2012;119:123-32.
39. Van Gool MP, Vancsó I, Schols HA, Toth K, Szakacs G, Gruppen H. Screening for distinct xylan degrading enzymes in complex shake flask fermentation supernatants. Bioresour. Technol. 2011;102(10):6039-47.
40. Visser H, Joosten V, Punt PJ, Gusakov AV, Olson PT, Joosten R *et al*. Development of a mature fungal technology and production platform for industrial enzymes based on a *Myceliophthora thermophila* isolate, previously known as *Chrysosporium lucknowense* C1. Ind. Biotechnol. 2011;7:214–23.
41. Punt P, J, Burlingame R, Paul, Pynnonen C, M, Olson P, T, Wery J, Visser J, Heinrich *et al*. *Chrysosporium lucknowense* protein production system. Patent WO/2010/107303. 2010.

42. Zhang YHP, Cui J, Lynd LR, Kuang LR. A transition from cellulose swelling to cellulose dissolution by o-phosphoric acid: Evidence from enzymatic hydrolysis and supramolecular structure. Biomacromolecules. 2006;7(2):644-8.
43. Sali A. Comparative protein modeling by satisfaction of spatial restraints. Mol. Med. Today. 1995;1(6):270-7.
44. Eswar N, Webb B, Marti-Renom MA, Madhusudhan MS, Eramian D, Shen MY *et al*. Comparative protein structure modeling using MODELLER. Curr. Protoc. Protein Sci. 2007;(50):2.9.1-2.9.31.

Additional files

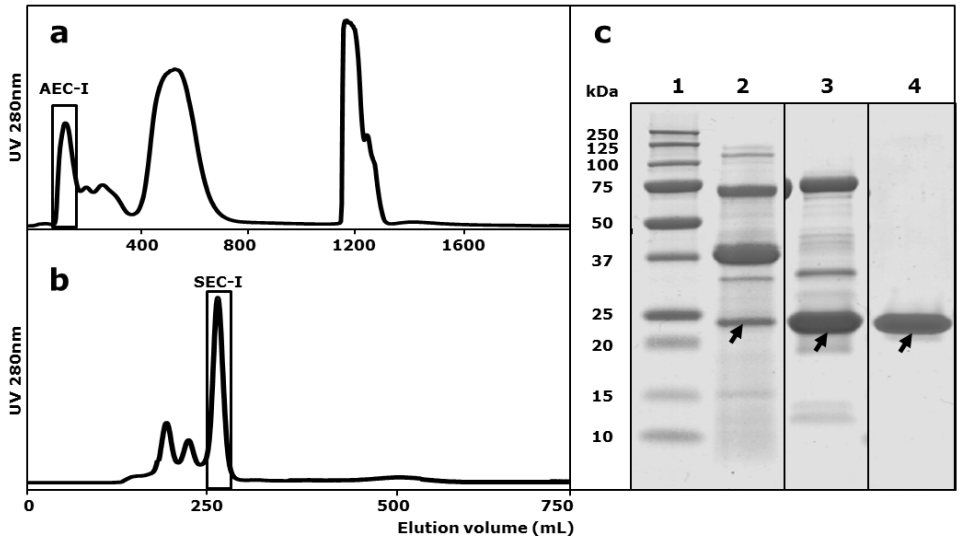

Additional Figure 2.1 a Anion exchange chromatography (AEC) elution profile (step 1) of crude enzyme extract containing expressed *Mt*LPMO9A. **b** Size exclusion chromatography (SEC) elution profile of Pool AEC-I (step 2). The framed columns indicate the *Mt*LPMO9A-containing fractions pooled and concentrated for further analysis. **c** SDS-PAGE of marker (lane 1; Precision Plus Protein, Bio-Rad Laboratories), the crude enzyme extract (lane 2), pooled fraction AEC-I (lane 3) and partially purified fraction SEC-I (lane 4). Protein bands corresponding to *Mt*LPMO9A are indicated by an arrow. For more details about protein purification see Methods.

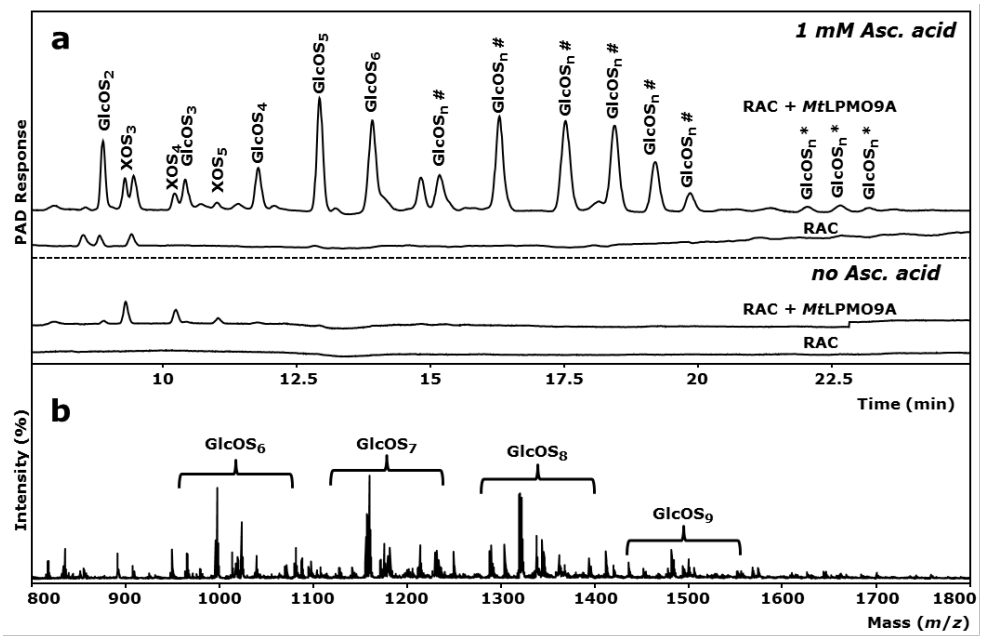

Additional Figure 2.2 Regenerated amorphous cellulose **a** (RAC; 2 mg mL^{-1}) before and after incubation with *Mt*LPMO9A (12.5 mg g^{-1} substrate). Samples were incubated in a 50 mM ammonium acetate buffer (pH 5.0) for 24 h at 52°C, either with ascorbic acid addition (1 mM) or without. In the presence of *Mt*LPMO9A and ascorbic acid, non-oxidized gluco-oligomers ($GlcOS_n$) and gluco-oligomers oxidized at C1 ($GlcOS_n^{\#}$) and C4 ($GlcOS_n$*) are formed from RAC. Neither non-oxidized nor oxidized gluco-oligomers were formed by *Mt*LPMO9A in the absence of ascorbic acid. In both incubations of RAC with *Mt*LPMO9A, either with or without ascorbic acid, traces of non-oxidized xylo-oligomers were formed (XOS_n). **b** MALDI-TOF mass spectrum of RAC incubated with *Mt*LPMO9A with ascorbic acid. Clusters of oxidized gluco-oligomers are determined as their lithium (Li) adducts. See **Figure 2.3** for more details.

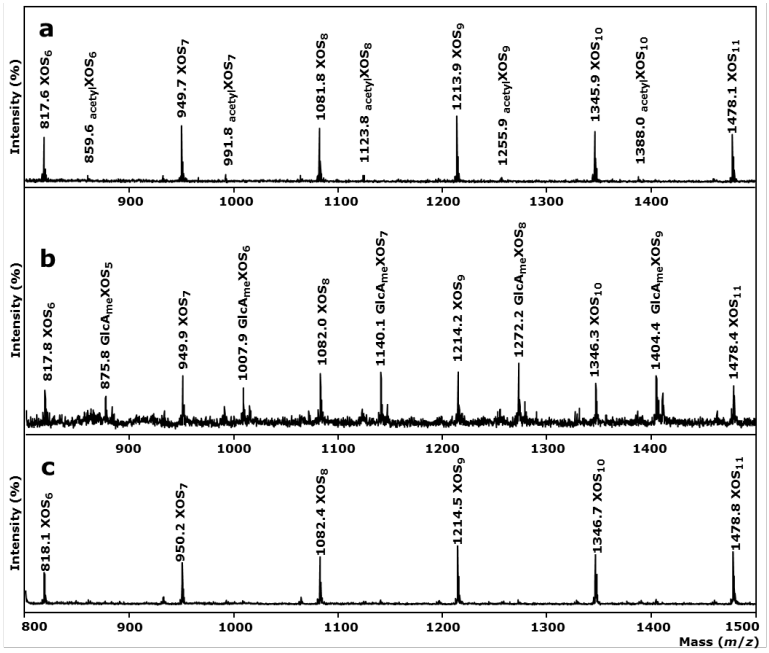

Additional Figure 2.3 Wheat arabinoxylan **a** (WAX), birchwood **b** (BiWX) and oat spelt **c** (OSX) xylan (2 mg mL^{-1}) after incubation with *Mt*LPMO9A (12.5 mg g^{-1} substrate). Samples were incubated in a 50 mM ammonium acetate buffer (pH 5.0) containing ascorbic acid addition (1 mM) for 24 h at 52°C. In all three incubations, *Mt*LPMO9A released non-oxidized xylo-oligomers (XOS_n). **a** incubation of WAX with *Mt*LPMO9A; formation of non-oxidized xylo-oligomers and traces of acetylated ($_{acetyl}XOS_n$) xylo-oligomers (+42 Da). **b** incubation of BiWX with *Mt*LPMO9A; formation of non-oxidized xylo-oligomers and xylo-oligomers ($Glc_{me}XOS_n$) substituted with 4-*O*-methyl-glucoronic acid (+191 Da). **c** incubation of OSX with *Mt*LPMO9A releases non-oxidized xylo-oligomers only. Masses represents lithium (Li) adducts only.

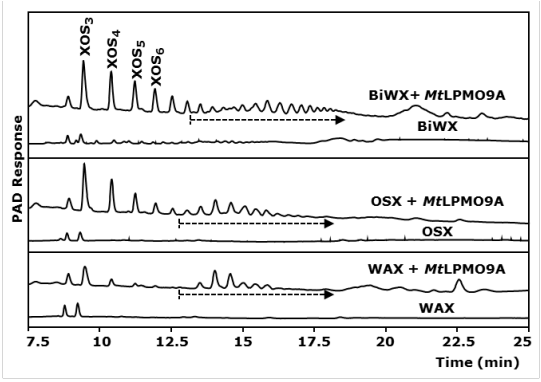

Additional Figure 2.4 Birchwood xylan (BiWX), oat spelt xylan (OSX) and wheat arabinoxylan (WAX) (2 mg mL^{-1}) before and after incubation with *Mt*LPMO9A (12.5 mg g^{-1} substrate). Samples were incubated in a 50 mM ammonium acetate buffer (pH 5.0) containing ascorbic acid addition (1 mM) for 24 h at 52°C. Incubation with *Mt*LPMO9A results in the formation of non-oxidized linear xylo-oligomers (XOS_n) and substituted xylo-oligomers (black dashed arrow).

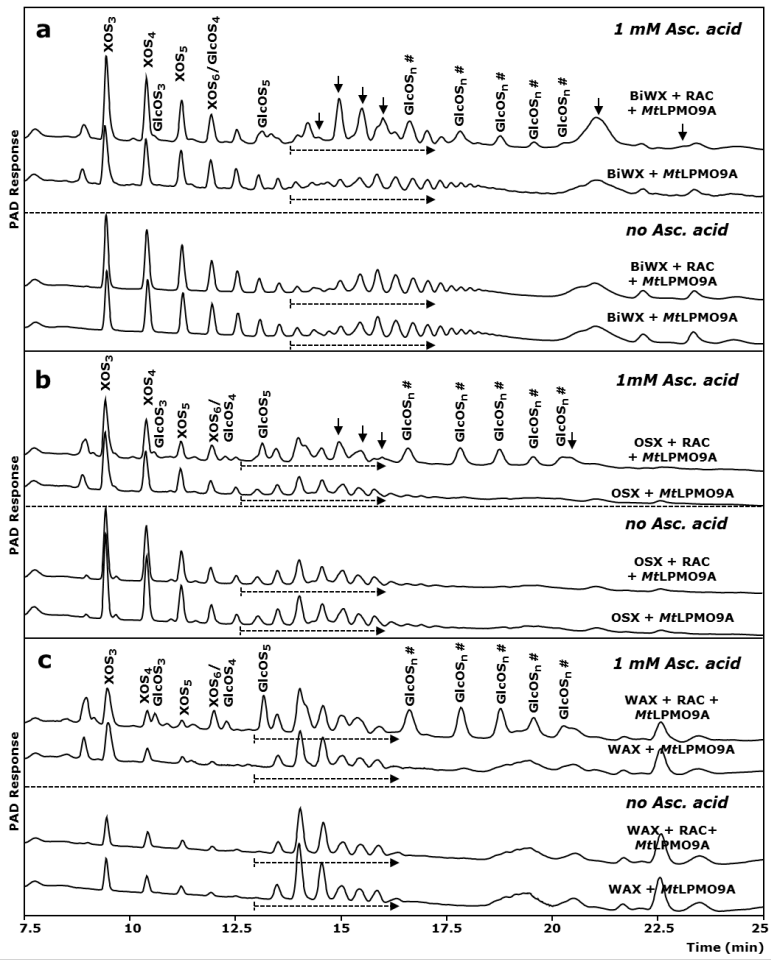

Additional Figure 2.5 Birchwood xylan **a** (BiWX), oat spelt xylan **b** (OSX) and wheat arabinoxylan **c** (WAX) (2 mg mL^{-1}) in the presence and absence of regenerated amorphous cellulose (RAC; 2 mg mL^{-1}) before and after incubation with *Mt*LPMO9A (12.5 mg g^{-1} substrate). Samples were incubated in a 50 mM ammonium acetate buffer (pH 5.0) with ascorbic acid addition (1 mM) or without for 24 h at 52°C. Incubation with *Mt*LPMO9A of all three xylans and xylan-RAC-mixtures, in the presence or absence of ascorbic acid, results in the formation of non-oxidized linear xylo-oligomers (XOS_n) and substituted xylo-oligomers (black dashed arrow). Incubation of xylan-RAC-mixtures with *Mt*LPMO9A in the presence of ascorbic acid results in the formation of non-oxidized gluco-oligomers ($GlcOS_n$) and C1-oxidized gluco-oligomers ($GlcOS_n^{\#}$). **a** + **b** The incubation of *Mt*LPMO9A with BiWX-RAC- and OSX-RAC-mixture in the presence of ascorbic acid results in the formation of numerous products (black arrow), which are not present if *Mt*LPMO9A is incubated with BiWX, OSX or RAC alone. The results of MALDI-TOF MS analysis of BiWX-RAC- and OSX-RAC-mixture incubated with *Mt*LPMO9A in the presence of ascorbic acid are shown in **Figure 2.4**.

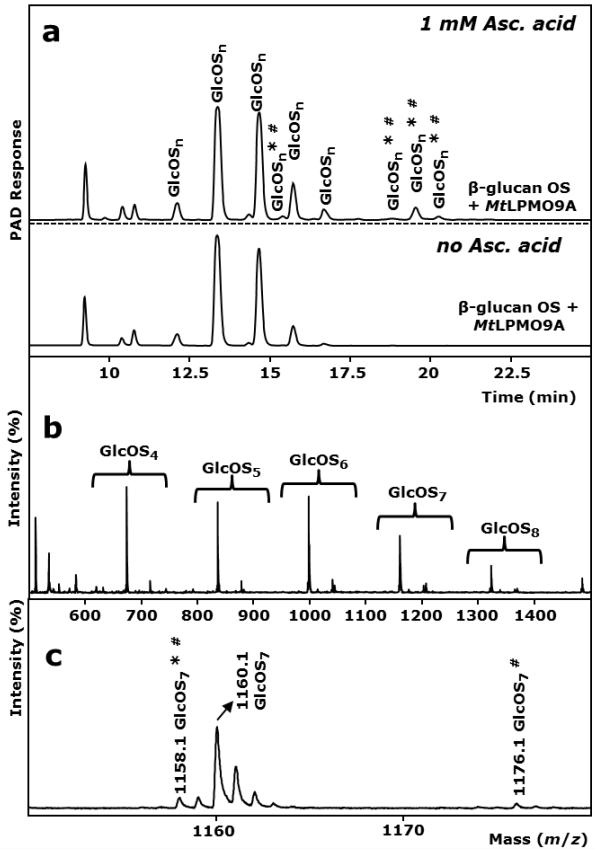

Additional Figure 2.6 HPAEC elution pattern **a** OS β-glucan before and after incubation with partially purified *Mt*LPMO9A fraction SEC-I (**Additional Figure 2.1**; 12.5 mg g^{-1} substrate), with addition of 1 mM ascorbic acid or without. **a** In the presence and absence of ascorbic acid, various non-oxidized β-gluco-oligomers ($GlcOS_n$) are formed by the partially purified *Mt*LPMO9A fraction. Incubation of oat spelt β-glucan with *Mt*LPMO9A in the presence of ascorbic acid results in the formation of oxidized gluco-oligomers ($GlcOS_n^{\#}$, $GlcOS_n$*). **b** MALDI-TOF mass spectrum of partially purified *Mt*LPMO9A incubated with oat spelt β-glucan in the presence of 1 mM ascorbic acid. Clusters of non-oxidized gluco-oligomers and gluco-oligomers, oxidized at C1 ($GlcOS_n^{\#}$) and C4 ($GlcOS_n$*) are determined. Enlargement **c** shows the presence of non-oxidized gluco-oligomers and gluco-oligomers, oxidized at C1 with an aldonic acid ($^{\#}$) and at C4 with a keto-group (*). Masses represent lithium (Li) adducts only.

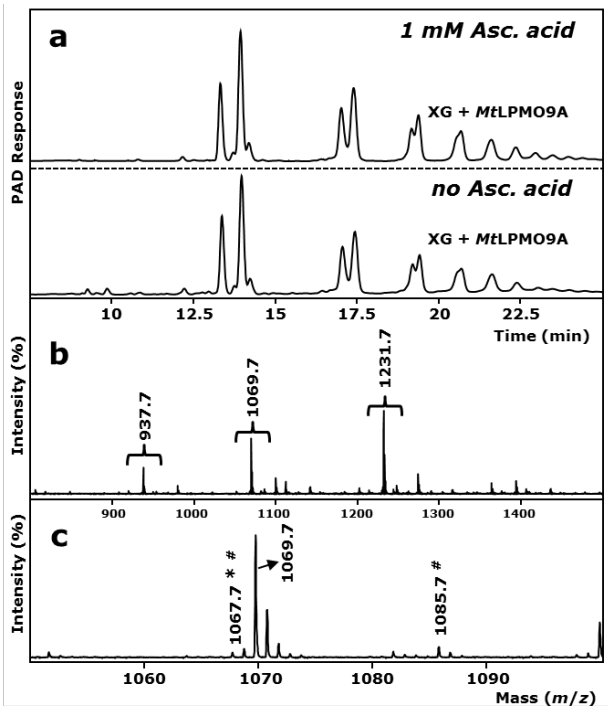

Additional Figure 2.7 HPAEC elution pattern **a** of xyloglucan from tamarind seed (2 mg mL^{-1}) after incubation with partially purified *Mt*LPMO9A fraction SEC-I (**Additional Figure 2.1**; 12.5 mg g^{-1} substrate). Samples were incubated in 50 mM ammonium acetate buffer (pH 5.0) for 24 h at 52°C, either with ascorbic acid addition (1 mM) or without. Numerous various non-oxidized xyloglucan-derived oligomers were formed if xyloglucan was incubated with *Mt*LPMO9A, either with ascorbic acid addition (1 mM) or without. **b** MALDI-TOF mass spectrum of xyloglucan incubated with *Mt*LPMO9A with 1 mM ascorbic acid addition. Clusters of non-oxidized and oxidized xyloglucan-derived oligomers are formed. **c** (enlargement of **b**) - In the presence of *Mt*LPMO9A and ascorbic acid, next to non-oxidized xyloglucan-derived oligomers, oligomers oxidized at the C1 ($^{\#}$) and C4 (*) position are formed. Masses represent lithium (Li) adducts only.

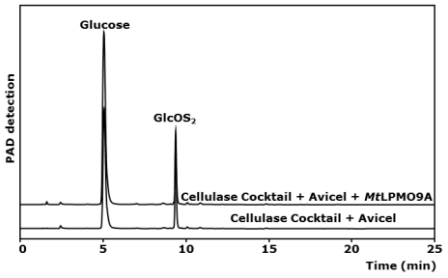

Additional Figure 2.8 HPAEC elution patterns of Avicel incubations with a cellulase cocktail (Dyadic, Wageningen, The Nederlands) with and without partially purified *Mt*LPMO9A addition (2.5 mg protein g^{-1} Avicel). The addition of *Mt*LPMO9A to a cellulase cocktail (5 mg protein g^{-1} Avicel) results in a 60% higher release of glucose (based on HPAEC-area) compared to the glucose release from Avicel by the cellulase cocktail alone. Samples were incubated in 50 mM acetate buffer (pH 5.0) at 52°C with ascorbic acid addition (1 mM).

Chapter III

Lytic polysaccharide monooxygenases from *Myceliophthora thermophila* C1 differ in substrate preference and reducing agent specificity

Based on: Frommhagen M, Koetsier MJ, Westphal AH, Visser J, Hinz SWA, Vincken J-P, van Berkel WJH, Kabel MA, Gruppen H. Lytic polysaccharide monooxygenases from *Myceliophthora thermophila* C1 differ in substrate preference and reducing agent specificity. *Biotechnology for Biofuels*. 2016; 9:186.

Abstract

Lytic polysaccharide monooxgygenases (LPMOs) are known to boost the hydrolytic breakdown of lignocellulosic biomass, especially cellulose, due to their oxidative mechanism. For their activity, LPMOs require an electron donor for reducing the divalent copper cofactor. LPMO activities are mainly investigated with ascorbic acid as a reducing agent, but little is known about the effect of plant-derived reducing agents on LPMOs activity.

Here, we show that three LPMOs from the fungus *Myceliophthora thermophila* C1, *Mt*LPMO9A, *Mt*LPMO9B and *Mt*LPMO9C, differ in their substrate preference, C1-/C4-regioselectivity and reducing agent specificity. *Mt*LPMO9A generated C1- and C4-oxidized, *Mt*LPMO9B C1-oxidized and *Mt*LPMO9C C4-oxidized gluco-oligosaccharides from cellulose. The recently published *Mt*LPMO9A oxidized, next to cellulose, xylan, β-(1→3, 1→4)-glucan and xyloglucan. In addition, *Mt*LPMO9C oxidized, to a minor extent, xyloglucan and β-(1→3, 1→4)-glucan from oat spelt at the C4 position. In total, 34 reducing agents, mainly plant-derived flavonoids and lignin building blocks, were studied for their ability to promote LPMO activity. Reducing agents with a 1,2-benzenediol or 1,2,3-benzenetriol moiety gave the highest release of oxidized and non-oxidized gluco-oligosaccharides from cellulose for all three *Mt*LPMOs. Low activities towards cellulose were observed in the presence of monophenols and sulfur-containing compounds.

Several of the most powerful LPMO reducing agents of this study serve as lignin building blocks or protective flavonoids in plant biomass. Our findings support the hypothesis that LPMOs do not only vary in their C1-/C4-regioselectivity and substrate specificity, but also in their reducing agent specificity. This work strongly supports the idea that the activity of LPMOs towards lignocellulosic biomass does not only depend on the ability to degrade plant polysaccharides like cellulose, but also on their specificity towards plant-derived reducing agents *in situ*.

3.1 Background

Plant biomass utilization is considered to be a green approach for the production of renewable biofuels and biochemicals. Hereto, current developments aim at the effective degradation of the plant biomass polysaccharides, mostly embedded in a lignocellulosic complex, into monosaccharides by using enzyme cocktails. These commercial enzyme preparations usually originate from fungi such as *Aspergillus* and *Trichoderma* strains. Alternatively, the ascomycete *Myceliophthora thermophila* C1 is used to produce plant polysaccharide degrading enzymes [1-3].

Lignocellulosic plant biomass is composed of the aromatic heteropolymer lignin and polysaccharides, such as hemicellulose and cellulose. In this research, we focus on the degradation of the highly recalcitrant polysaccharide cellulose. Cellulose is a homogenous polymer consisting of β-(1→4)-linked glucosyl chains. The interactions of these glucosyl chains via hydrogen bondings and van der Waal forces lead to the formation of crystalline cellulose regions [4]. These crystalline regions are difficult to access for most of the known hydrolytic cellulases listed in the Carbohydrate-Active enZyme (CAZy, [5]) database. The recently discovered lytic polysaccharide monooxygenases (LPMOs) are able to improve the hydrolytic breakdown of crystalline cellulose regions by their oxidative mechanisms [6, 7]. It has also been shown that certain LPMOs oxidize chitin, hemicellulosic glucan, soluble cellodextrins, xylan or starch [2, 8-12]. LPMOs are classified as "auxiliary activities" (AA) and are divided, based on their sequence similarity, into four CAZy subgroups: AA9, AA10, AA11 and AA13 [5].

The AA9 classified fungal LPMOs exhibit the oxidative cleavage of cellulose yielding products with either the C1- (lactones) or C4- (ketoaldoses) position oxidized, or mixtures of the two [6, 13-15]. The oxidative cleavage of substrates by LPMOs requires a divalent copper ion in the active site in addition to molecular oxygen and a reducing agent to oxidize one β-(1→4)-linkage between the glucosyl residues [15].

Most studies on the activity of LPMOs published so far have been carried out with ascorbic acid as reducing agent [2, 6, 10, 16, 17]. Besides ascorbic acid, other small molecular weight reducing agents have been described to donate electrons to LPMOs, such as hydroquinone, catechin, and gallic acid and the macromolecule lignin [9, 13, 14, 18-20]. Interestingly, it has been shown that reducing agents, especially the plant-derived diphenols, can be regenerated by GMC oxidoreductases [20]. Furthermore, flavocytochrome dependent cellobiose dehydrogenases (CDHs) are reported to provide LPMOs with electrons and, more recently, light excited photosynthetic pigments [21-23]. Literature is, however, ambiguous whether the type of reducing agent also influences the LPMO activity. On the one hand it has been shown that the addition of different reducing agents influences the amount of released oxidized and non-oxidized gluco-oligosaccharides from PASC (phosphoric acid swollen cellulose) incubated with LPMO [19, 20]. On the other hand, the addition of three different reducing agents to PASC incubated with *Pc*GH61D did not affect the amounts of products released [7]. Therefore, it remains unknown whether different LPMOs share the same preference for the same type of reducing agent. In addition, for fungi it has been shown that polysaccharide sources used for fungal growth influence the expression of LPMO-encoding genes [3]. Hence, we hypothesize that different LPMOs from *M. thermophila* C1 do not only vary in their C1-/C4-regioselectivity and substrate specificity, but also in their reducing agent specificity [3]. Therefore,

we investigated the effect of 34 different reducing agents, in particular plant-derived reducing agents, such as flavonoids or lignin building blocks, on the cellulose-degrading activity of three LPMOs from *M. thermophila* C1. One of these LPMOs is *Mt*LPMO9A, which has been shown to oxidize cellulose at the C1- and C4 position [2]. For the two other LPMOs, *Mt*LPMO9B and *Mt*LPMO9C, we also characterized the C1-/C4-regioselectivity and substrate specificity. Based on their chemical structure, all reducing agents were classified into five groups, partly reflecting their effect on the LPMO activity.

3.2 Results

3.2.1 Purification of *Mt*LPMO9B and *Mt*LPMO9C

*Mt*LPMO9B and *Mt*LPMO9C were produced in the homologous host *M. thermophila* C1 and purified from the culture broth supernatant in either three (*Mt*LPMO9B) or four (*Mt*LPMO9C) steps. Both final *Mt*LPMO9B and *Mt*LPMO9C preparations showed single bands on SDS-PAGE (**Additional Figure 3.1**) with apparent subunit molecular masses of 32 kDa and 25 kDa, respectively. The purified *Mt*LPMO9B and *Mt*LPMO9C preparations were further analyzed by LC/UV/ESI-MS. The weighted average masses of *Mt*LPMO9B and *Mt*LPMO9C were 32,765 Da and 24,640 Da, respectively. These values are somewhat higher than the theoretical molecular masses (30.6 kDa and 23.5 kDa, respectively) calculated from the respective amino acid sequences. However, ESI-MS spectra (*m/z* values) of *Mt*LPMO9B and *Mt*LPMO9C showed that both LPMOs were glycosylated by hexoses. In particular, up to 13 and 5 glycosyl units were attached to *Mt*LPMO9B and *Mt*LPMO9C, respectively (**Additional Figure 3.2**).

3.2.2 Mode of action of *Mt*LPMO9B and *Mt*LPMO9C on amorphous cellulose

The activities of the pure *Mt*LPMO9B and *Mt*LPMO9C enzymes were tested on regenerated amorphous cellulose (RAC), in both the presence and absence of ascorbic acid. Incubation of RAC in the presence and absence of ascorbic acid without LPMO addition did not cause auto-oxidation of RAC since no non-oxidized or oxidized gluco-oligosaccharides were detected by using HPAEC and MALDI-TOF MS. The products released from RAC, after incubation with *Mt*LPMO9B or *Mt*LPMO9C are shown in **Figure 3.1**. Besides non-oxidized gluco-oligosaccharides ($GlcOS_n$), only C1-oxidized gluco-oligosaccharides ($GlcOS_n^{\#}$) were formed upon incubation of RAC with *Mt*LPMO9B in the presence of ascorbic acid (**Figure 3.1b**). In contrast, RAC incubated with *Mt*LPMO9C in the presence of ascorbic acid yielded only C4-oxidized gluco-oligosaccharides ($GlcOS_n$*), besides non-oxidized gluco-oligosaccharides ($GlcOS_n$) (**Figure 3.1c**). For both enzymes, neither oxidized nor non-oxidized gluco-oligosaccharides were released from RAC in the absence of ascorbic acid, which showed that cellulolytic activity was completely absent (**Figures 3.1b** and **3.1c**). MALDI-TOF MS confirmed the annotation of the HPAEC eluted gluco-oligosaccharides (**Figures 3.1d** and **3.1e**, **Additional Figures 3.3a**, **3.3b**). For example, incubation of RAC with *Mt*LPMO9B released non-oxidized cellohexaose with a mass of 997 Da (lithium adduct) and C1-oxidized cellohexaose appeared either as a lactone (995 Da) or as the corresponding aldonic acid (1013 Da) (**Figure 3.1d**). Masses of lactonic acid double substituted with lithium were also detected (1019 and 1017 Da, probably due to double oxidation). In contrast, RAC incubated with *Mt*LPMO9C only formed the C4-oxidized ketoaldose (995 Da) of cellohexaose and non-oxidized cellohexaose (997 Da, **Figure 3.1e**). In summary, *Mt*LPMO9B oxidizes

cellulose at the C1- and *Mt*LPMO9C at the C4-position, while the previously characterized *Mt*LPMO9A oxidizes cellulose at the C1- and C4-positon [2].

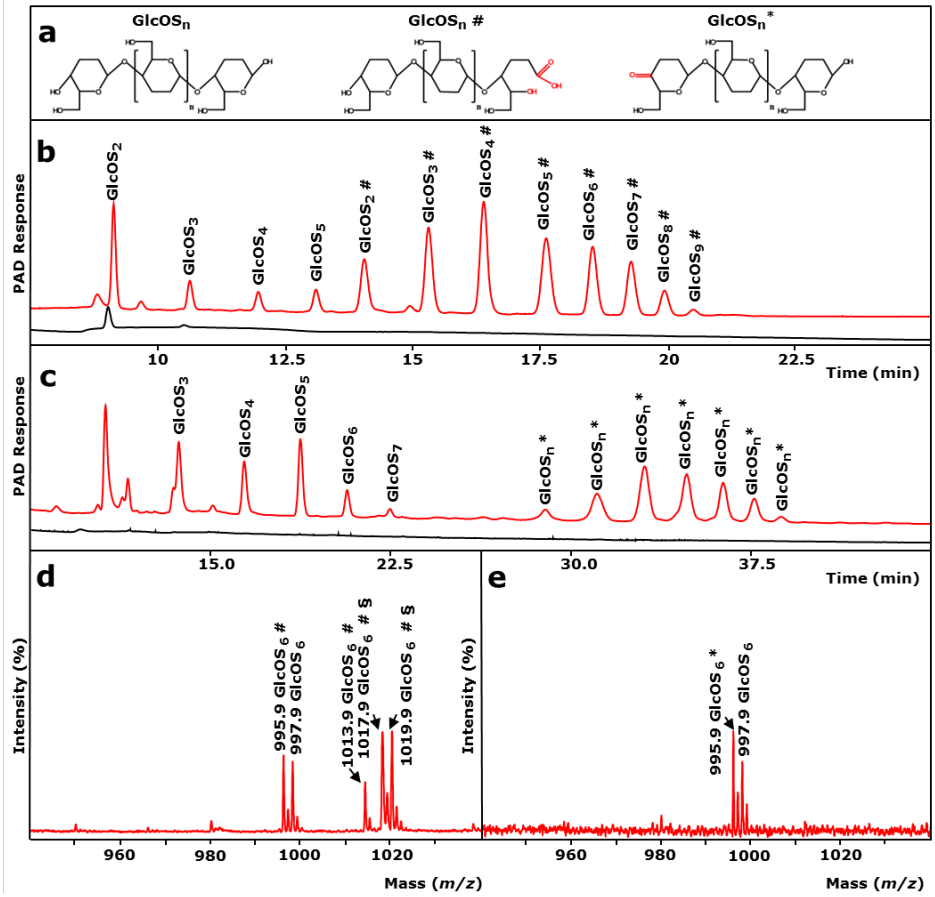

Figure 3.1 Activity of *Mt*LPMO9B and *Mt*LPMO9C on regenerated amorphous cellulose. **a** Structure and nomenclature of released non-oxidized and C1- and C4-oxidized gluco-oligosaccharides (GlcOS$_n$, GlcOS$_n$$^{\#}$, GlcOS$_n$*, respectively). HPAEC elution pattern of regenerated amorphous cellulose (RAC; 2 mg mL^{-1}) incubated with **b** *Mt*LPMO9B (10 mg g^{-1} substrate) and **c** *Mt*LPMO9C (10 mg g^{-1} substrate), in the presence (1 mM, red line) and absence of ascorbic acid (black line). A different gradient was used for the separation of **b** C1- and **c** C4-oxidised gluco-oligosaccharides (See Methods). The C4-oxidized gluco-oligosaccharides are known to be unstable under the alkaline conditions present during HPAEC analysis and undergo further derivatization to gemdiols, which are actually annotated as C4-oxidized gluco-oligosaccharides (GlcOS$_n$*) [34]. MALDI-TOF mass spectrum (*m/z* values) of RAC incubated with **d** *Mt*LPMO9B or **e** *Mt*LPMO9C, in the presence of ascorbic acid. **d** Double Li$^+$ adducts of C1-oxidized gluco-oligosaccharides are marked with **§**. **d** Oxidation of the C1-carbon atom results in the formation non-oxidized gluco-oligosaccharides (GlcOS$_n$) and C1-oxidized gluco-oligosaccharides present as a δ-lactone (-2 Da, marked as GlcOS$_n$$^{\#}$). Lactones are unstable and convert to aldonic acids by the addition of water, leading to a 16 Da higher mass compared to the non-oxidized gluco-oligosaccharide (+16 Da, marked as GlcOS$_n$$^{\#}$). Double Li$^+$ adducts of C1-oxidized gluco-oligosaccharides are marked with **§ (**GlcOS$_6$$^{\#}$**§,** 1019.9 Da and 1017.9 Da, probably due to double oxidation). **e** Oxidation of the C4-carbon atom results in the formation of non-oxidized gluco-oligosaccharides (GlcOS$_n$) and C4-oxidized gluco-oligosaccharides present as ketoaldoses (-2 Da, marked as GlcOS$_n$*). No gemdiols were formed. For more information see Methods.

3.2.3 Structure-based sequence alignment of *Mt*LPMO9A, *Mt*LPMO9B and *Mt*LPMO9C and structural models of *Mt*LPMO9B and *Mt*LPMO9C

Structure-based sequence alignments of *Mt*LPMO9A, *Mt*LPMO9B and *Mt*LPMO9C were constructed, based on the sequences of a C1- (*Pc*LPMO9D; PDB ID code 4B5Q), C4- (*Nc*LPMO9C; PDB ID code 4D7U) and C1- and C4- (*Ta*LPMO9A; PDB ID code 3ZUD) oxidizing LPMO as presented by Borisova *et al*. (**Figure 3.2**) [10, 14, 24, 25]. The three-dimensional structural models of *Mt*LPMO9B and *Mt*LPMO9C (**Figures 3.3a** and **3.3b**) were generated based on the available structure of *Nc*LPMO9C from *Neurospora crassa* [25] (Protein Data Bank entry: 4D7U). *Mt*LPMO9B is, unlike *Mt*LPMO9C and the previously published *Mt*LPMO9A [2], linked at the C-terminal end to a Carbohydrate Binding Module 1 (CBM1), which is not presented in the structural model of *Mt*LPMO9B. The sequences used for the structural-based alignments and models do not include the signal peptides and start from the N-terminal histidine (His1). The overall sequence identity of *Mt*LPMO9A, *Mt*LPMO9B and *Mt*LPMO9C ranges from 41 – 46%. All three *Mt*LPMOs share the LPMO typical β-sheet core, but differ in their loop regions L2 (10-49), LS (114-128) and LC (176-226) that are involved in shaping the substrate-binding surface (**Figure 3.2**) [2, 25, 26]. Interestingly, *Mt*LPMO9C and partly *Mt*LPMO9B contain an insertion, which forms the L3 (64-78) loop region (**Figure 3.2**). This L3 region is a typical structural characteristic of C4-oxidizing AA9 LPMOs [25-27]. Based on the model, *Mt*LPMO9B contains distal from the coordinated copper sphere an additional loop (Gly115-Asn121), which is not present in *Mt*LPMO9A and *Mt*LPMO9C (**Figures 3.2a** and **3.2b**). The copper ion in *Mt*LPMO9A, *Mt*LPMO9B and *Mt*LPMO9C is coordinated by His1-His68-Tyr153, His1-His79-Tyr170 and His1-His84-Tyr166, respectively (**Figure 3.2** and **3.3**)[2]. All three *Mt*LPMOs share two putative disulfide bridges, presumably involved in stabilizing the different loops regions such as Cys126–Cys208 (LS – LC) for *Mt*LPMO9A and Cys28-Cys178 (L2 – LC) for *Mt*LPMO9B (**Figure 3.3**)[2]. In addition, it is likely that the neighboring Cys18 and Cys49 of *Mt*LPMO9B form a second disulfide bond (L2 – L2) (**Figure 3.3**). The putative disulfide bridges of *Mt*LPMO9C between Cys39-Cys169 and Cys139-Cys221 are not expected to be involved in interlinking any of the four described loop regions (**Figure 3.2**). All three *Mt*LPMOs share the presence of several aromatic amino acid residues in the substrate binding surface, which were formerly used for classifying the AA9s into subgroups (**Figure 3.2** and **3.3**) [2, 28, 29].

3.2.4 Activity of *Mt*LPMO9B and *Mt*LPMO9C with various soluble and insoluble polysaccharides

Various soluble and insoluble substrates were incubated with purified *Mt*LPMO9B or *Mt*LPMO9C in the presence of ascorbic acid. The overview of the activities observed is presented in **Table 3.1**, which, for comparison, includes the activities of the previously published *Mt*LPMO9A [2]. Of all substrates tested, *Mt*LPMO9B showed only oxidative activity towards RAC, releasing C1-oxidized and non-oxidized gluco-oligosaccharides (**Figure 3.1b**). *Mt*LPMO9C oxidized RAC (**Figure 3.1c**) releasing C4-oxidized and non-oxidized gluco-oligosaccharides and showed also activity towards β-(1→3, 1→4)-glucan from oat spelt or xyloglucan from tamarind seed under the formation of C4-oxidized gluco-oligosaccharides and substituted C4-oxidized gluco-oligosaccharides (**Additional Figures 3.4**, **3.5**, **3.6**). No oxidized gluco-oligosaccharides were released from β-(1→3, 1→4)-glucan from barley incubated with *Mt*LPMO9B or *Mt*LPMO9C.

*Mt*LPMO9A has been described to cleave xylan associated with cellulose [2] forming oxidized xylo-oligosaccharides and oxidized gluco-oligosaccharides (**Table 3.1**). Hence, *Mt*LPMO9B and *Mt*LPMO9C

were also studied for their activity towards RAC-xylan-mixtures, in particular, RAC mixed with either birchwood xylan, oat spelt xylan or wheat arabinoxylan, in the presence and absence of ascorbic acid (**Table 3.1**). No oxidized xylo-oligosaccharides were released by *Mt*LPMO9B and *Mt*LPMO9C, which discriminates these enzymes from *Mt*LPMO9A.

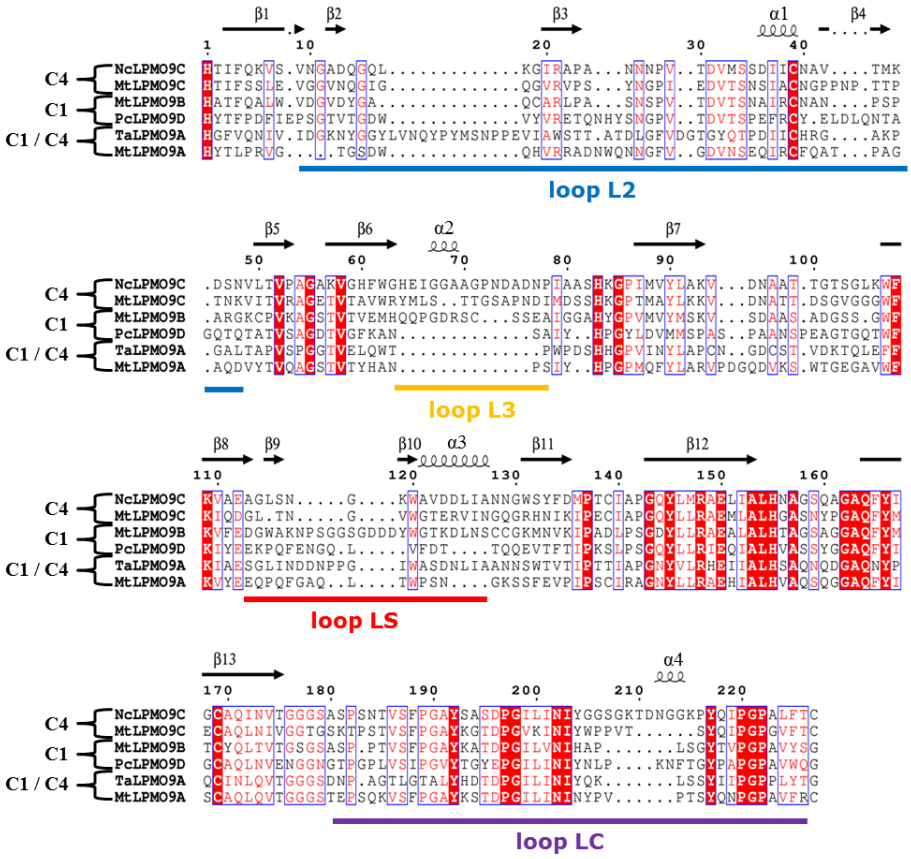

Figure 3.2 Structure-based sequence alignment of *Mt*LPMO9A, *Mt*LPMO9B and *Mt*LPMO9C. The structure-based sequence alignments of *Mt*LPMO9A, *Mt*LPMO9B and *Mt*LPMO9C were made by using three known sequences of a C1-(*Pc*LPMO9D; PDB ID code 4B5Q), C4-(*Nc*LPMO9C; PDB ID code 4D7U) and C1- and C4-(*Ta*LPMO9A; PDB ID code 3ZUD) oxidizing LPMO based on Borisova *et al*. [10, 14, 24, 25]. The β-strands (black arrow) and α-helices (black helix) are based on *Nc*LPMO9C and shown above the columns [25]. The bold colored lines below the columns are highlighting the amino acids of the four loop regions L2 (blue), L3 (yellow), Ls (red) and LC (purple), which are involved in shaping the substrate-binding site. The highly conserved amino acid residues are presented as white letters on a red background. Amino acid residues that have comparable chemical and physical properties are presented as red letters within blue frames. Sequences are presented without the signal sequence and start from the N-terminal histidine (His1). The structure-based sequence alignment was obtained by using ESPript [48].

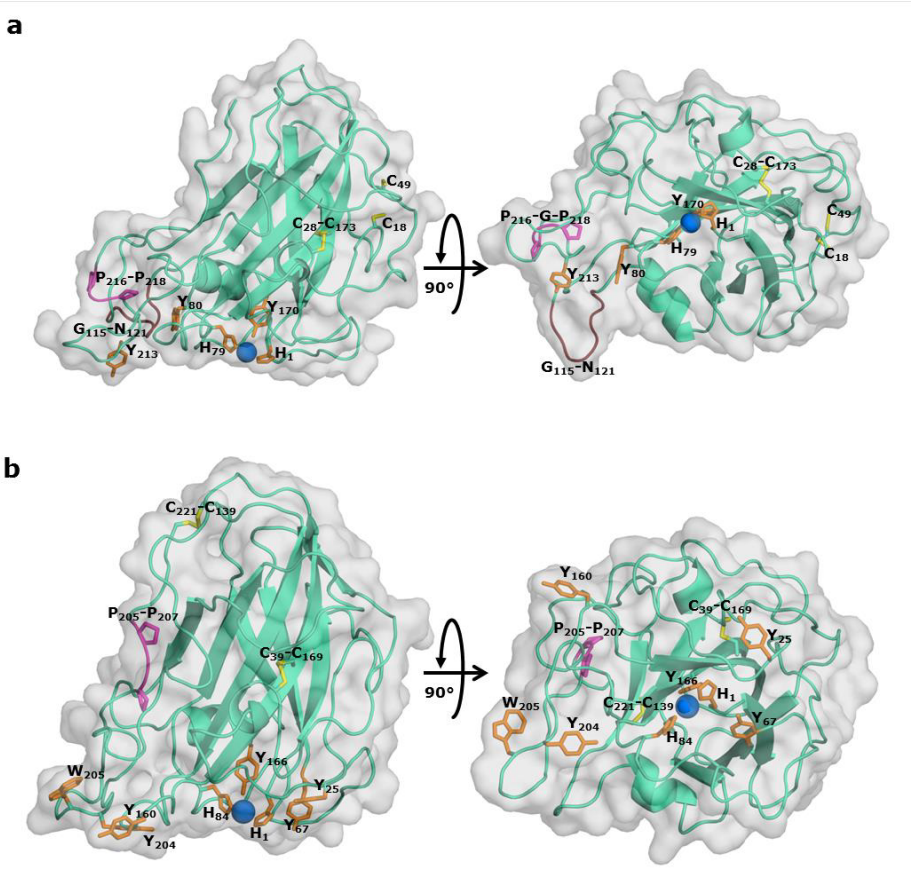

Figure 3.3 Structural models of *Mt*LPMO9B and *Mt*LPMO9C. The structural model of **a** *Mt*LPMO9B was generated based on the available structure of *Nc*LPMO9C from *Neurospora crassa* [25] (PDB entry: 4D7U). The amino acid sequence identity of *Mt*LPMO9B and *Mt*LPMO9C were, compared to *Nc*LPMO9C, 41% and 46%, respectively. The copper ion (blue) is coordinated by His1, His 79 and Tyr170 (orange). A disulfide bridge is located between Cys28-Cys178 (yellow) and it is likely that the neighboring Cys18 and Cys49 form a second disulfide bridge. The structural model of **b** *Mt*LPMO9C was, like *Mt*LPMO9B, generated based on *Nc*LPMO9C [25] (PDB entry: 4D7U). The copper ion (blue) is coordinated by His1, His84 and Tyr166 (orange). *Mt*LPMO9C contains two disulfide bridges between Cys39-Cys169 and Cys139-Cys221 (yellow). The highly conserved Gly-Pro-Gly triad (magenta) of *Mt*LPMO9B and *Mt*LPMO9C is located between Pro216-Pro218 and Pro205-Pro207, respectively. *Mt*LPMO9B contains, unlike *Mt*LPMO9C, an additional loop between Gly-115-Asn121 (brown).

3.2.5 Electron donor specificities of *Mt*LPMO9A, *Mt*LPMO9B and *Mt*LPMO9C

Based on the structural similarities of functional groups, the 34 reducing agents tested were classified into five groups (**Figure 3.4**). Monophenols, like sinapic acid (no. 5), are classified as group I. Group II comprises compounds with a benzenediol moiety, which represent the *ortho*-isomer 1,2-benzenediol, the *meta*-isomer 1,3-benzenediol and the *para*-isomer 1,4-benzenediol (**Figure 3.4**). Reducing agents with a 1,2,3-benzenetriol moiety are classified as group III. Reducing agents of group IV are sulfur-containing compounds, such as glutathione (no. 29) or L-cysteine (no. 30). Reducing agents of group V neither have a phenolic ring nor a sulfur atom.

Table 3.1 Oxidation of various polysaccharide substrates by *Mt*LPMO9A, *Mt*LPMO9B and *Mt*LPMO9C[a]

Substrate	Occurrence of oxidation (upon addition of 1mM ascorbic acid)							
	***Mt*LPMO9A**[b]		***Mt*LPMO9B**		***Mt*LPMO9C**		**no enzyme**	
	$GlcOS_n^{\#}$*[c]	**$XOS_n^{\#}$*[d]**	**$GlcOS_n^{\#}$**	**$XOS_n^{\#}$**	**$GlcOS_n$***	**XOS_n***	**$GlcOS_n$***	**XOS_n***
Cellulose								
RAC[e]	+	+	+	-	+	-	-	-
Hemicellulose								
Glucan								
Xyloglucan[f]	+	-	-	-	+	-	-	-
β-Glucan barley[f]	+	-	-	-	-	-	-	-
β-Glucan oat spelt[f]	+	-	-	-	+	-	-	-
Xylan								
OSX[g]	-	-	-	-	-	-	-	-
BiWX[g]	-	-	-	-	-	-	-	-
WAX[g]	-	-	-	-	-	-	-	-
Oligosaccharides								
Gluco-oligosaccharides[h]	-	-	-	-	-	-	-	-
Xylo-oligosaccharides[h]	-	-	-	-	-	-	-	-
RAC/Hemicellulose combination								
RAC + BiWX	+	+	+	-	+	-	-	-
RAC + OSX	+	+	+	-	+	-	-	-
RAC + WAX	+	-	+	-	+	-	-	-

[a] Oligosaccharides released and not released refers to + and -, respectively

[b] Data from Frommhagen *et al.* [2]

[c] Gluco-oligosaccharides oxidized at the C1 ($GlcOS_n^{\#}$) or C4 position ($GlcOS_n$*)

[d] Xylo-oligosaccharides oxidized at the C1 ($XOS_n^{\#}$) or C4 position (XOS_n*)

[e] Regenerated amorphous cellulose (RAC)

[f] Xyloglucan from tamarind seed, β-(1→3, 1→4)-glucan from barley and β-(1→3, 1→4)-glucan from oat spelt

[g] Oat spelt xylan (OSX), birchwood xylan (BiWX), wheat arabinoxylan (WAX)

[h] β-(1→4)-linked gluco- and xylo-oligosaccharides, degree of polymerization 2-5

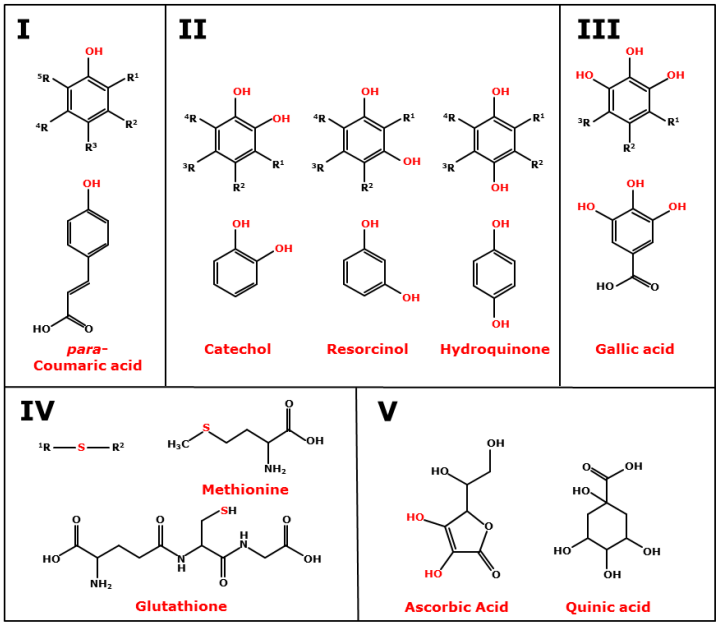

Figure 3.4 Structural classification of reducing agents into five groups. Group I, monophenols. Group II, *ortho*-, *meta*- or *para*-isomers of compounds bearing a benzenediol moiety. Group III, reducing agents with a 1,2,3-benzenetriol moiety. Group IV, sulfur-containing compounds. Group V, compounds with neither have a phenolic ring nor a sulfur atom.

An overview of the effect of 34 different reducing agents with corresponding codes (no.) on the amounts of oxidized and non-oxidized gluco-oligosaccharides released from RAC incubated with *Mt*LPMO9A, *Mt*LPMO9B or *Mt*LPMO9C is presented in **Table 3.2**. First, we determined from the HPAEC profiles the amounts, expressed as peak areas, of C1-oxidised gluco-oligosaccharides, C4-oxidized gluco-oligosaccharides and non-oxidized gluco-oligosaccharides formed (**Figure 3.5**). Subsequently, these amounts were presented as percentage of the corresponding amounts obtained by the same incubation, but with ascorbic acid (no. 33), which was set to 100% (**Table 3.2**). All 34 reducing agents were also incubated with RAC alone, which did not result in the release of oxidized or non-oxidized gluco-oligosaccharides, confirming the absence of auto-oxidation in the presence of the reducing agents, only.

Fourteen reducing agents (**Table 3.2**, bold), including ascorbic acid, were able to donate electrons to all three *Mt*LPMOs enabling the oxidative cleavage of RAC. Nevertheless, the LPMO activity based on the amounts of oxidized gluco-oligosaccharides formed, varied per reducing agent (**Figure 3.5**; **Table 3.2**). For all three *Mt*LPMOs, ascorbic acid was one of the best electron donors (**Table 3.2**). Besides ascorbic acid, compounds bearing a 1,2-benzenediol moiety (3-methylcatechol (no. 14), 3,4-dihydroxyphenylalanine (no. 21)) or 1,2,3-benzenetriol moiety (gallic acid (no. 26), epigallocatechin-gallate (no. 27)), gave the highest formation of oxidized and non-oxidized gluco-oligosaccharides. Interestingly, dopamine (no. 21) turned out to be one of the best electron donors for *Mt*LPMO9A (93% of the activity compared to ascorbic acid), but was a less efficient electron donor for *Mt*LPMO9B and *Mt*LPMO9C (46% and 6% compared to ascorbic acid, respectively). Some compounds bearing a 1,2-benzenediol moiety, for example quercetin or taxifolin (no. 23), and the

benzenetriol tannic acid (no. 28) did not donate electrons to all three *Mt*LPMOs. Out of seven monophenols, only sinapic acid (no. 5) acted as electron donor for all three *Mt*LPMOs, but less efficient (4-23%) compared to ascorbic acid (no. 33). A poor electron donating capacity was also found for sulfur-containing compounds, such as reduced glutathione (no. 29) and L-cysteine (no. 30) (**Table 3.2**). Both thiol compounds have already been described as LPMO electron donors in literature [7, 30]. In summary, the presence of different reducing agents strongly influences the release of oxidized and non-oxidized gluco-oligosaccharides from RAC for all three *Mt*LPMOs. Based on these findings, we conclude that *Mt*LPMO9A, *Mt*LPMO9B and *Mt*LPMO9C differ in their specificity towards reducingagents.

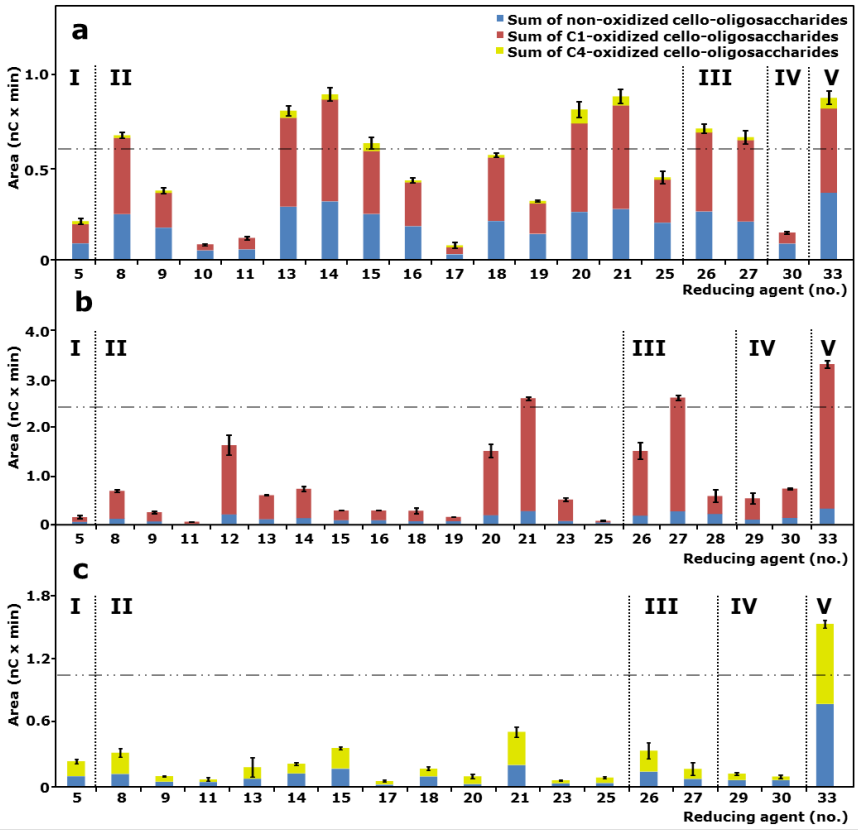

Figure 3.5 Released oligosaccharides from RAC incubated with three different *Mt*LPMOs. RAC was incubated with **a** *Mt*LPMO9A, **b** *Mt*LPMO9B and **c** *Mt*LPMO9C using different reducing agents. The total sum is shown of integrated peak areas of released C1- (red), C4- (yellow) oxidized and non-oxidized (blue) gluco-oligosaccharides after incubation of *Mt*LPMO9A, *Mt*LPMO9B and *Mt*LPMO9C (2.5, 5 and 2.5 mg g^{-1} substrate, respectively) with regenerated amorphous cellulose (RAC; 1.5 mg mL^{-1}) based on HPAEC. The reducing agents (1 mM) are numbered (X-axes) and specified in **Table 3.2**. Vertical dotted lines separate reducing agents of the 5 structural groups (**Figure 3.4**). Threshold (horizontal dashed dotted line) is set to 70% of the released products from RAC incubated with the *Mt*LPMOs in the presence of ascorbic acid (no. 33) (**Table 3.2**). See Methods for data analysis. All incubations were performed in duplicates, and the standard deviation is represented by error bars, which correspond to one cumulated SD (error bar = ± SDtot; with SDtot = $\sqrt{SD_1^2 + SD_2^2 + ...}$).

Table 3.2 Overview of electron donor specificity of *Mt*LPMO9A, *Mt*LPMO9B or *Mt*LPMO9C[a]

Group	No.	Reducing agent	*Mt*LPMO9A				*Mt*LPMO9B			*Mt*LPMO9C		
			activity compared to ascorbic acid %									
			C1-/ C4-ox & non-ox	C1-ox	C4-ox	non-ox	C1-/ C4-ox & non-ox	C1-ox	non-ox	C1-/ C4-ox & non-ox	C4-ox	non-ox
I	1	3-hydroxy-4-methoxycinnamic acid	0	0	0	0	0	0	0	0	0	0
	2	homovanillic acid	0	0	0	0	0	0	0	0	0	0
	3	naringin	0	0	0	0	0	0	0	0	0	0
	4	*p*-coumaric acid	0	0	0	0	0	0	0	0	0	0
	5	**sinapic acid**	23	23	31	24	4	3	14	15	12	18
	6	syringic acid	0	0	0	0	0	0	0	0	0	0
	7	vanillic acid	0	0	0	0	0	0	0	0	0	0
II	8	**(-)-epicatechin**	77	68	90	27	21	19	34	21	15	26
	9	**(+)-catechin**	43	47	41	24	7	6	17	6	5	7
	10	3,4-dihydroxybenzaldehyde	9	13	7	0	0	0	0	0	0	0
	11	**3,4-dihydroxybenzoic acid**	13	15	13	0	1	1	2	4	5	3
	12	3,4-dihydroxycinnamic acid	0	0	0	0	49	48	63	0	0	0
	13	**3,4-dihydroxyphenylacetic acid**	92	79	105	68	18	17	31	12	9	14
	14	**3-methylcatechol**	102	87	121	49	22	20	38	14	15	12
	15	**4-chlorocatechol**	72	68	75	74	8	7	24	24	21	26
	16	caffeic acid	49	49	52	20	8	7	26	0	0	0
	17	carminic acid	8	7	8	21	0	0	0	3	2	4
	18	**catechol**	65	57	75	26	8	7	18	11	12	10
	19	chlorogenic acid	36	38	36	25	4	3	18	0	0	0
	20	**dopamine hydrochloride**	93	71	105	132	46	45	57	6	2	10
	21	**L-3,4-dihydroxyphenylalanine**	101	75	123	86	79	78	84	33	26	41
	22	quercetin	0	0	0	0	0	0	0	0	0	0
	23	taxifolin	0	0	0	0	15	15	20	4	3	4
	24	resorcinol	0	0	0	0	0	0	0	0	0	0
	25	**hydroquinone**	51	55	51	25	2	1	10	5	4	7

Table 3.2 Overview of electron donor specificity of *Mt*LPMO9A, *Mt*LPMO9B or *Mt*LPMO9C[a]

Group	No.	Reducing agent	*Mt*LPMO9A				*Mt*LPMO9B			*Mt*LPMO9C		
			activity compared to ascorbic acid %									
			C1-/ C4-ox & non-ox	C1-ox	C4-ox	non-ox	C1-/ C4-ox & non-ox	C1-ox	non-ox	C1-/ C4-ox & non-ox	C4-ox	non-ox
III	26	**gallic acid**	81	72	94	38	46	45	54	22	18	26
	27	**(-)-epigallocatechin-gallate**	76	56	97	30	79	79	83	11	9	12
	28	tannic acid	0	0	0	0	18	13	66	0	0	0
IV	29	reduced glutathione	0	0	0	0	16	15	30	8	7	8
	30	**L-cysteine**	16	23	13	0	22	20	40	6	7	4
	31	allyl iso-thiocyanate	0	0	0	0	0	0	0	0	0	0
	32	D-methionine	0	0	0	0	0	0	0	0	0	0
V	33	**ascorbic acid**	100	100	100	100	100	100	100	100	100	100
		Peak Area (nC x min)[b]	(0.897)	(0.460)	(0.058)	(0.360)	(3.273)	(2.962)	(0.311)	(1.542)	(0.760)	(0.781)
	34	D-quinic acid	0	0	0	0	0	0	0	0	0	0

[a]The total sum of integrated peaks areas of released oxidized (C1-ox, C4-ox) and non-oxidized (non-ox) and both (ox & non-ox) gluco-oligosaccharides from RAC, incubated with either *Mt*LPMO9A, *Mt*LPMO9B *or Mt*LPMO9C in the presence of ascorbic acid, was taken as a reference and equals to 100% of the LPMO activity. The numbers correspond to the relative activity of *Mt*LPMO9A, *Mt*LPMO9B *or Mt*LPMO9C compared to ascorbic acid (total sum integrated peaks areas of released oxidized and non-oxidized gluco-oligosaccharides of a reducing agent compared to ascorbic acid (areas from **Figure 3.5**). Auto-oxidation of RAC was absent for all reducing agents tested based on the absence of oxidized or non-oxidized gluco-oligosaccharides. Reducing agents that can donate electrons to all three LPMOs are highlighted in bold. See Methods for details about the activity assays.

[b]Integrated peak areas of released C1-, C4-oxidized and non-oxidized gluco-oligosaccharides after incubation of *Mt*LPMO9A, *Mt*LPMO9B and *Mt*LPMO9C with RAC in the presence of 1 mM ascorbic acid based on HPAEC (**Figure 3.5**).

3.3 Discussion

The recently discovered LPMOs play a crucial role in the enzymatic degradation of lignocellulosic plant biomass. Here, we purified the C1-oxidizing *Mt*LPMO9B and C4-oxidizing *Mt*LPMO9C, two novel LPMOs from the filamentous fungus *M. thermophila* C1, and compared their catalytic properties with those of the C1- and C4-oxidizing *Mt*LPMO9A [2].

3.3.1 Protein mass

The difference in molecular mass between *Mt*LPMO9B and *Mt*LPMO9C results from the CBM1 linked to *Mt*LPMO9B. This CBM1 has a predicted mass, calculated from the amino acid sequence of 6811 Da. The weighted average mass of the purified *Mt*LPMO9B linked to CBM1 and *Mt*LPMO9C enzymes (32.765 Da and 24.640 Da, respectively), differ slightly from the predicted masses, calculated from the amino acid sequences (30.633 Da and 23.449 Da, respectively). Both *Mt*LPMO9B and *Mt*LPMO9C contain multiple glycosylations that were determined as hexoses based on LC/ESI-MS (**Additional Figure 3.2**). It is known that LPMOs can feature glycosylation in the substrate-binding site, though the glycosylation could also appear at the serine/threonine containing linker between the carbohydrate-binding module (CBM), the C-terminal end of the LPMO or at the binding site of the CBM [29, 31, 32].

3.3.2 Activity on cellulose

The total amount of released oxidized and non-oxidized gluco-oligosaccharides from RAC incubated with *Mt*LPMO9B is approximately three-times higher (based on total AUC) compared to the released products from RAC by the *Mt*LPMO9A using ascorbic acid as a reducing agent (**Figure 3.5**). We suggest that the CBM1 attached to *Mt*LPMO9B has a strong affinity to cellulose and supports the activity of *Mt*LPMO9B through the positioning of the *Mt*LPMO9B to the cellulose. Our finding is supported by previous studies which showed that LPMOs linked to a CBM release more oxidized gluco-oligosaccharides from cellulose compared to LPMOs without a CBM [17, 33]. In addition, it has been hypothesized that glycosylation could affect the binding to cellulose, altering the enzyme activity [29]. So far, it has only been demonstrated for CBMs that the glycosylation of proteins with mannose in the planar face can increase the substrate binding strength towards cellulose, and not yet for LPMOs [29, 32]. However, it has been reported that the removal of a CBM1 linked to *Nc*LPMO9C did not show any effect on the degradation rate of amorphous cellulose [25]. Still, a direct comparison of all three LPMOs regarding their activity on cellulose would require the absolute quantification of the released C1- and C4-oxidized gluco-oligosaccharides, which is so far not possible due to the lack of standards. Especially the quantification of C4-oxidized products has its limits due to the instability of these compounds under alkaline conditions during HPAEC analysis [34]. The release of high amounts of non-oxidized gluco-oligosaccharides observed in the HPAEC spectra is likely to derive, to a certain extent, from the decomposition of these labile C4-oxidized gluco-oligosaccharides into non-oxidized compounds (**Figure 3.1**) [34].

3.3.3 Substrate specificity and C1-/C4-regioselectivity

*Mt*LPMO9A, *Mt*LPMO9B and *Mt*LPMO9C were compared regarding their substrate specificity and C1-/C4-regioselectivity of oxidation using a wide range of polysaccharides (**Table 3.1**). The activity of *Mt*LPMO9A towards various polysaccharides has already been investigated previously, showing that

*Mt*LPMO9A oxidizes cellulose, besides β-(1→3, 1→4)-glucan from oat spelt or barley and xyloglucan from tamarind seed, at the C1 and C4 position. In addition, *Mt*LPMO9A also oxidized xylan in the presence of cellulose [2]. *Mt*LPMO9B oxidized RAC at the C1 position. The presence of the CBM1 linked to *Mt*LPMO9B is not expected to have an impact on the substrate specificity of *Mt*LPMO9B. It has been shown that the removal of a CBM1 linked to *Nc*LPMO9C, which has a broad substrate specificity, does not affect the ability to oxidize different polysaccharides such as cellulose, cellopentaose or xyloglucan [25]. Besides that, *Mt*LPMO9B shows a typical insertion, which forms the L3 loop region in C4-oxidizing AA9 LPMOs. Compared to the solely C4-oxidizing *Nc*LPMO9C, *Mt*LPMO9B shares within this L3 loop only a low sequence identity [10, 25]. The L3 loop is known to be an extension of the surface-binding site and involved in the binding of soluble polysaccharides such as xyloglucan and cello-oligosaccharides [25-27]. *Mt*LPMO9C also contains the L3 loop and is, like *Nc*LPMO9C, a C4-oxidizing AA9 LPMO (**Figure 3.2**). In addition to cellulose, *Mt*LPMO9C oxidizes to a lower extent hemicellulose like β-(1→3, 1→4)-glucan from oat spelt and xyloglucan from tamarind seed at the C4 position (**Additional Figures 3.4**, **3.5**, **3.6**). The previously published *Nc*LPMO9D (PDB-id: 4EIR) from *N. crassa* shares the highest sequence identity (83%) with *Mt*LPMO9C, but unlike *Mt*LPMO9C, it has not been tested if *Nc*LPMO9D is active on hemicellulose such as (1→3, 1→4)-glucan [15, 29].

3.3.4 Reducing agent specificity

We show here that three LPMOs from the same organism differ in their reducing agent specificity. Importantly, all three LPMOs are able to utilize various natural phenolic compounds as reducing agents. Most of these reducing agents are present in plants, either free or as lignin building blocks, such as sinapic acid (no. 5), or as flavonoids such as catechin (no. 9) and dopamine (no. 20). This finding is of high relevance as these reducing agents can act as intrinsic electron donors in plant biomass biorefinery [35].

For all three *Mt*LPMOs, phenolic compounds with 1,2-benzenediol and 1,2,3-benzenetriol moieties yielded the highest release of oxidized and non-oxidized gluco-oligosaccharides from cellulose compared to monophenols or sulfur containing compounds (**Figure 3.5**, **Table 3.2**). This observation may be related to the fact that the donation of an electron by one hydroxyl group leads to a dislocation of the π-electron sextet, which is energetically unfavorable. It has been shown that monophenols have a higher oxidation potential compared to compounds with 1,2-benzenediol and 1,2,3-benzenetriol moieties [20]. This high oxidation potential of monophenols hinders the reduction of the active site copper of LPMOs. In contrast to monophenols, phenolic compounds with 1,2-benzenediol and 1,2,3-benzenetriol moieties can stabilize the dislocation of π-electrons by their additional(s) hydroxyl groups due to the resonance effect [36]. Compared to monophenols, these compounds have a low reduction potential and are able to reduce the active site copper of the LPMOs [20]. In addition, the ability of such compounds to donate electrons is also influenced by other electron-donating or electron-withdrawing substituents attached to the aromatic ring [37, 38]. Remarkably, the number of reducing agents, that gave an activity of 70% or higher of the LPMO activity obtained with ascorbic acid, differed between the three LPMOs (**Figure 3.5**, **Table 3.2**). For *Mt*LPMO9A this number was eight (compounds with a benzenediol and benzenetriol moiety), but for *Mt*LPMO9B, this number was only two (**Figure 3.5**, **Table 3.2**). *Mt*LPMO9C oxidizes RAC in the presence of several reducing agents, but, in comparison to *Mt*LPMO9A and *Mt*LPMO9B, none of the reducing agents tested gave an activity of 70% or higher of the *Mt*LPMO9C-activity obtained with

ascorbic acid. Remarkably, we also found reducing agents with a 1,2-benzenediol moiety that are not able to reduce the active site copper of all three *Mt*LPMOs tested (**Table 3.2**). These findings cannot be explained by the oxidation potential of the reducing agents alone. Another explanation for the reducing agent preferences among the three LPMOs may result from differences in the protein structure. It has been formerly hypothesized that the binding site of electron donating proteins, such as CDHs, is located in the surface patch centered around the Pro-Gly-Pro triad, which is highly conserved within the LPMO family [21, 29]. However, recent analysis based on CDH docking studies and NMR revealed a direct interaction of the CDH with the LPMO involving a narrow surface patch around the His1, Ala80, His83 and His155 of *Nc*LPMO9C [21, 26]. Indeed, the surface charge distribution obtained from the homology models differs widely among the three *Mt*LPMOs, including shape and charge in the vicinity of the above described surface patch (**Figure 3.6**, **Additional Figure 3.7**). *Mt*LPMO9A is strongly positively charged in the vicinity of the copper ion compared to *Mt*LPMO9B and *Mt*LPMO9C (pH 5.0). The charge differences in the vicinity of the copper ion might contribute to the different electron donor specificities of the *Mt*LPMOs.

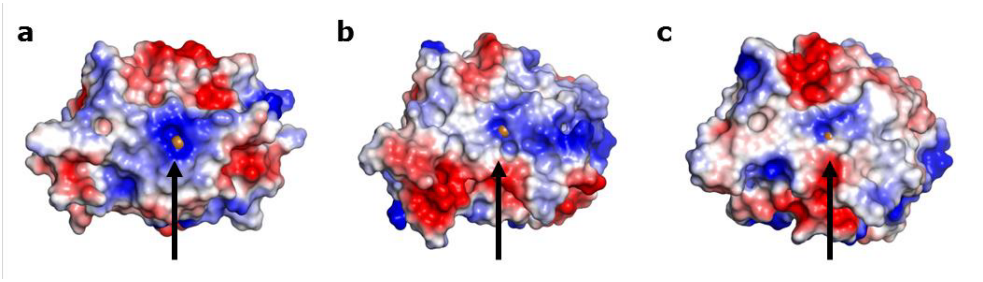

Figure 3.6 Cartoons of the surface charge distribution of the structural models of **a** *Mt*LPMO9A, **b** *Mt*LPMO9B and **c** *Mt*LPMO9C. Protein orientation: the flat substrate-binding site (**Figure 3.3**) is located to the front of all three LPMOs and the copper ion is indicated by the black arrow. Recent NMR studies revealed a direct interaction of the reductant CDH with a narrow surface patch in vicinity to the copper ion [26]. *Mt*LPMO9A is strongly positively charged in the vicinity of the copper ion compared to *Mt*LPMO9B and *Mt*LPMO9C based on the surface charge distribution (pH 5.0). The scaling from the negative and positive electrostatic potential regions are -5 for blue and +5 for the red regions. The electrostatic map was obtained from APBS plugin from PyMOL.

The incubations performed in this work have been conducted at a single time point (24 h) and at one pH (5.0). This pH plays an important role for the LPMO application due to the fact that cellulose cleaving cocktails produced by *M. thermophila* C1 have their pH optimum around pH 5.0. It can be expected that this pH does not represent the optimal condition for each reducing agent tested since redox potentials of reducing agents are pH dependent [37]. Furthermore, the product release determined at a single time point (24 h) does not give information about the progress of the LPMO reaction. The time point of 24 hours could lay in the initial rate period or already at the endpoint of the LPMO reaction, which highly depends on the reducing agents present during the reaction [17, 33]. We do not expect a release of non-oxidized or oxidized gluco-oligosaccharides after 24 h if no products have been released from RAC incubated with LPMOs before that time point (**Table 3.2**). Finally, the conditions chosen for all three LPMOs have been the same, which allows the comparison of the LPMO activity in the presence of different reducing agents and the chosen conditions can be considered as industrial relevant.

3.4 Conclusions

Our findings support the hypothesis that LPMOs do not only vary in their C1-/C4-regioselectivity and substrate specificity, but also in their reducing agent specificity. The mode of action of LPMOs is usually investigated in the presence of ascorbic acid. Here, we found that several reducing agents can donate electrons to the LPMOs with a similar efficiency as the commonly used ascorbic acid. Our findings are of high interest for industrial applications as most of these reducing agents are present in plant biomass and can act as intrinsic mediators in biorefinery processes.

3.5 Methods

3.5.1 Enzyme expression, production and purification

The purification and activity of *Mt*LPMO9A has been previously described [2]. The homologous expression of *Mt*LPMO9B and *Mt*LPMO9C was performed by using a low protease/low (hemi-)cellulose producing *Myceliophthora thermophila* C1 strain, which has been described elsewhere [39, 40]. The crude enzyme preparations obtained from the fermentation broth were dialyzed against 10 mM potassium phosphate buffer (pH 7.0). *Mt*LPMO9B and *Mt*LPMO9C were purified from the corresponding dialyzed enzyme preparations by using an ÄKTA-Explorer preparative chromatography system (GE Healthcare, Uppsala, Sweden).

*Mt*LPMO9B was purified in three subsequent chromatographic steps. For the first anion exchange step, the *Mt*LPMO9B-containing enzyme preparation was loaded on a Source 30Q column (50ml, GE Healthcare). A 20 mM potassium phosphate buffer (pH 7.8) was used to pre-equilibrate the column. Elution was performed using a linear gradient from 0 to 1 M NaCl in 20 mM potassium phosphate buffer (pH 7.8) at a flow rate of 10 mL min^{-1} and monitored at 220 and 280 nm. All fractions were collected and immediately stored on ice. Peak fractions were, based on UV (280 nm), pooled and concentrated by ultrafiltration (Amicon Ultra, molecular mass cut-off of 3 kDa, Merck Millipore, Cork, Ireland) at 4°C. The concentrated pools were analyzed by SDS-PAGE to determine the *Mt*LPMO9B-containing pool (expected molecular mass 30.6 kDa). After the first purification step, cation exchange chromatography purification was applied. The *Mt*LPMO9B containing pool was subjected to a Source 30S column (50 mL, GE Healthcare) for further purification (second step). A 20 mM sodium acetate buffer (pH 5.0) was used to pre-equilibrate the column. The elution was performed by using a linear gradient from 0 to 1 M NaCl in 20 mM sodium acetate (pH 5.0) at a flow rate of 5 mL min^{-1}. Elution was monitored at 220 and 280 nm. Fractions obtained (10 mL) were immediately stored on ice. Peak fractions were pooled, concentrated and analyzed by SDS-PAGE as described above. In a third purification step, the *Mt*LPMO9B-containing fraction was bound to a Source 30S column (50 mL, GE Healthcare) using a 10 mM sodium acetate buffer (pH 5.0) after pre-equilibration. After protein application, the column was washed with 20 column volumes of starting buffer. Elution was performed using a linear gradient from 0 to 1 M KCl in 20 mM sodium acetate (pH 5.0) at a flow rate of 5 mL min^{-1} and monitored at 220 and 280 nm. Fractions (3 mL) were immediately stored on ice. Peak fractions were pooled, concentrated and analyzed by SDS-PAGE as described above.

*Mt*LPMO9C was purified in four subsequent chromatographic steps. As a first size exclusion chromatography (SEC) purification step, the *Mt*LPMO9C-rich enzyme preparation (40 mg mL^{-1}) was loaded onto a self-packed Superdex TM-75 column (100 x 3 cm internal diameter, GE Healthcare) and eluted at 5 mL min^{-1} with a 10 mM potassium phosphate buffer (pH 7.0). Fractions (5 mL) were immediately stored on ice. Peak fractions were, based on UV (280 nm), pooled and concentrated by ultrafiltration as described above. The concentrated pools were analyzed by SDS-PAGE to determine the *Mt*LPMO9C-containing pool (expected molecular mass 23.5 kDa). For the second SEC purification step, the *Mt*LPMO9C-containing pool was loaded again on the Superdex TM-75 column under the same conditions. Fractions (5 mL) were immediately stored on ice. Peak fractions were pooled, concentrated and analyzed by SDS-PAGE to determine the *Mt*LPMO9C-containing pool as described above. The *Mt*LPMO9C-containing pool was dialyzed against a 20 mM Tris-HCl buffer (pH 8.4) using ultrafiltration (Amicon Ultra, molecular mass cut-off of 3 kDa). The dialyzed *Mt*LPMO9C fraction was, for the third purification step, subjected to a Resource Q column (30 x 16 mm internal diameter, GE Healthcare), which was pre-equilibrated in 20 mM Tris-HCl buffer (pH 8.4) (third step). Elution was performed with a linear gradient from 0 to1 M NaCl in 20 mM Tris-HCl (pH 8.4) over 20 column volumes at 6 mL min^{-1}. Fractions (3 mL) were immediately stored on ice. Peak fractions were pooled, concentrated and analyzed by SDS-PAGE to determine the *Mt*LPMO9C-containing pool as described above. The *Mt*LPMO9C containing fraction was dialyzed against a 20 mM potassium phosphate buffer (pH 7.0) using ultrafiltration (Amicon Ultra, molecular mass cut-off of 3 kDa) and subjected to a Resource Q column (30 x 16 mm internal diameter, GE Healthcare). The column was equilibrated using a 20 mM potassium phosphate buffer (pH 7.0) and elution was performed using a linear gradient over 20 column volumes at 6 mL min^{-1}. Fractions (3 mL) were immediately stored on ice. Peak fractions were pooled, concentrated and analyzed by SDS-PAGE as described above.

3.5.2 Protein analysis

The protein content of *Mt*LPMO9B and *Mt*LPMO9C was determined as described previously using a BCA Protein Assay Kit [2]. Furthermore, the purity of the enzymes was analyzed by sodium dodecyl sulfate polyacrylamide gel electrophoresis (SDS-PAGE) as described before [2]. Pure *Mt*LPMO9B and *Mt*LPMO9C fractions were analyzed by LC-mass spectrometry confirming the presence of the 2 LPMOs by 'The Scripps Research Institute' (San Diego, CA, USA).

3.5.3 LC/ESI-MS

Purified *Mt*LPMO9B- and *Mt*LPMO9C-preparations (2.5 mg mL^{-1} in 0.1% (v/v) trifluoroacetic acid) were analyzed by using a liquid chromatography/electron spray ionization-mass spectrometry (LC/ESI-MS) as described previously [2].

3.5.4 Reducing agents

Reducing agents were supplied by Sigma-Aldrich (Steinheim, Germany), unless stated otherwise. Taxifolin was purchased from Extrasynthese (Genay, France), catechol hydrate and chlorogenic acid from Thermo Fisher Scientific (Waltham, MA USA), tannic acid from BDH Chemical Ltd. (Poole, England) and naringin from Fluka Chemie (Buches, Switzerland).

3.5.4 Carbohydrates

OSX, BiWX, Avicel PH-101, xylo-oligosaccharides (DP1-5), β-(1→4)-linked gluco-oligosaccharides (DP1-5) were supplied by Sigma-Aldrich. WAX, β-(1→3, 1→4)-glucan from barley and oat spelt (both medium viscosity) were purchased from Megazyme (Bray, Ireland). Xyloglucan from tamarind seed

was obtained from Dainippon Sumitomo Pharma (Osaka, Japan). Regenerated amorphous cellulose (RAC) was prepared from Avicel PH-101 as described [2, 41]. Gluconic acid was purchased from Sigma-Aldrich and cellobionic acid ammonium salt from Toronto Research Chemicals (Toronto, Ontario, Canada).

3.5.5 *Mt*LPMO9A, *Mt*LPMO9B and *Mt*LPMO9C activity assays

Substrates (see figure captions) were dissolved in 50 mM ammonium acetate buffer (pH 5.0) to a concentration of 1-2 mg mL^{-1}, with or without addition of reducing agents listed in **Table 3.1** (final concentration of 1 mM). *Mt*LPMO9A, *Mt*LPMO9B or *Mt*LPMO9C were added (2.5-10.0 µg of protein mg^{-1} substrate, for details see figure captions) and incubated for 24 h at 50°C in a head-over-tail Stuart rotator in portions of 1 mL total volume (Bibby Scientific, Stone, UK) at 20 rpm. Supernatants of all incubations with and without reducing agent in the presence of LPMOs and of substrates incubated with and without reducing agents in the absence of LPMOs, were analyzed by HPAEC and MALDI-TOF MS. The enzyme reactions were stopped by storing samples at -24°C. All following sample treatments were performed on ice.

3.5.6 Structural modelling

The structural model of *Mt*LPMO9B was made using the available structure of *Nc*LPMO9C from *Neurospora crassa* [25] (Protein Data Bank entry: 4D7U) as a template, which scored highest in the BLAST search of *Mt*LPMO9B against the Protein Data Bank (41% amino acid identity). *Mt*LPMO9C was, like *Mt*LPMO9B, generated based on *Nc*LPMO9C [25] (PDB entry: 4D7U, 46% amino acid identity). All models were created by using Modeller version 9.14 [42]. Multiple comparative models were generated, after which the model with lowest corresponding DOPE score [43] was selected for image generation using Pymol (Pymol, The PyMOL Molecular Graphics System, Version 1.5.0.4 Schrödinger, New York, NY, USA). The following settings were applied to model the surface charge distribution of the LPMOs: The protonation states of the titratable groups at pH 5.0 of *Mt*LPMO9A, *Mt*LPMO9B and *Mt*LPMO9C, respectively, were calculated using H^{++}-server with default settings [44-47]. The server pdb-ouput files were used to generate a surface image colored by charge (range between -5 and 5) using the Pymol APBS-tool (Version 1.4r1 L, Schrödinger).

3.5.7 HPAEC

Enzyme digests were analyzed by high performance anion-exchange chromatography (HPAEC) with pulsed amperometric detection (PAD) using a HPAEC system (ICS-5000, Dionex, Sunnyvale, CA, USA) as described previously [2]. The temperature of the auto sampler was set to 6°C. For the analysis of C4-oxidized gluco-oligosaccharides released by *Mt*LPMO9C, a longer gradient was used. The gradient elution program was as follows: 0–45 min, linear gradient 0–250 mM NaOAc; 45–52 min isocratic gradient 400–1,000 mM NaOAc; followed by equilibration (13 min) of the column with the starting conditions. The assignment of the C1- and C4-oxidized gluco-oligosaccharides using HPAEC is based on previous publications [2, 8, 15, 17], while gluconic and cellobionic acids were assigned by available standards (See Methods). All incubations were performed in duplicates. Areas were analyzed to determine the effect of the reducing agents on the release of oxidized and non-oxidized gluco-oligosaccharides from RAC incubated with *Mt*LPMO9A *Mt*LPMO9B or *Mt*LPMO9C. Standard deviations are represented (**Figure 3.5**) by error bars, which correspond to one cumulated SD (error bar = ± SDtot; with SDtot = √SD12 + SD22 + ...).

3.5.8 MALDI-TOF MS

The analysis of substrates incubated with either *Mt*LPMO9B and *Mt*LPMO9C was performed using Matrix-assisted laser desorption ionization – time of flight mass spectrometry (MALDI-TOF MS, Bruker Daltonics) as described previously [2]. Masses of lithium-adducted C1- or C4- oxidized gluco-oligosaccharides for RAC incubated with *Mt*LPMO9B or *Mt*LPMO9C, respectively, were determined and assigned as described previously [2].

References

1. Hinz SWA, Pouvreau L, Joosten R, Bartels J, Jonathan MC, Wery J *et al.* Hemicellulase production in Chrysosporium lucknowense C1. J. Cereal Sci. 2009;50(3):318-23.
2. Frommhagen M, Sforza S, Westphal AH, Visser J, Hinz SW, Koetsier MJ *et al*. Discovery of the combined oxidative cleavage of plant xylan and cellulose by a new fungal polysaccharide monooxygenase. Biotechnol Biofuels. 2015;8:101.
3. Berka RM, Grigoriev IV, Otillar R, Salamov A, Grimwood J, Reid I *et al*. Comparative genomic analysis of the thermophilic biomass-degrading fungi *Myceliophthora thermophila* and *Thielavia terrestris*. Nat. Biotechnol. 2011;29(10):922-7.
4. Parthasarathi R, Bellesia G, Chundawat SPS, Dale BE, Langan P, Gnanakaran S. Insights into hydrogen bonding and stacking interactions in cellulose. J. Phys. Chem. A. 2011;115(49):14191-202.
5. CAZy (2014). Glycoside hydrolase family classification. Accessed 17 July 2016. http://www.cazy.org/Glycoside-Hydrolases.html
6. Vaaje-Kolstad G, Westereng B, Horn SJ, Liu Z, Zhai H, Sorlie M *et al.* An oxidative enzyme boosting the enzymatic conversion of recalcitrant polysaccharides. Sci. 2010;330(6001):219-22.
7. Westereng B, Ishida T, Vaaje-Kolstad G, Wu M, Eijsink VG, Igarashi K *et al.* The putative endoglucanase *Pc*GH61D from *Phanerochaete chrysosporium* is a metal-dependent oxidative enzyme that cleaves cellulose. PLoS ONE. 2011;6(11):e27807.
8. Vu VV, Beeson WT, Phillips CM, Cate JH, Marletta MA. Determinants of regioselective hydroxylation in the fungal polysaccharide monooxygenases. J. Am. Chem. Soc. 2014;136(2):562-5.
9. Isaksen T, Westereng B, Aachmann FL, Agger JW, Kracher D, Kittl R *et al.* A C4-oxidizing lytic polysaccharide monooxygenase cleaving both cellulose and cello-oligosaccharides. J. Biol. Chem. 2014;289(5):2632-42.
10. Agger JW, Isaksen T, Varnai A, Vidal-Melgosa S, Willats WG, Ludwig R *et al.* Discovery of LPMO activity on hemicelluloses shows the importance of oxidative processes in plant cell wall degradation. Proc. Natl. Acad. Sci. U.S.A. 2014;111(17):6287-92.
11. Forsberg Z, Rohr AK, Mekasha S, Andersson KK, Eijsink VG, Vaaje-Kolstad G *et al*. Comparative study of two chitin-active and two cellulose-active AA10-type lytic polysaccharide monooxygenases. Biochem. 2014;53(10):1647-56.
12. Vu VV, Beeson WT, Span EA, Farquhar ER, Marletta MA. A family of starch-active polysaccharide monooxygenases. Proc. Natl. Acad. Sci. U.S.A. 2014;111(38):13822-7.
13. Forsberg Z, Vaaje-Kolstad G, Westereng B, Bunaes AC, Stenstrom Y, MacKenzie A *et al*. Cleavage of cellulose by a CBM33 protein. Prot. Sci. : A Publication of the Protein Society. 2011;20(9):1479-83.
14. Quinlan RJ, Sweeney MD, Lo Leggio L, Otten H, Poulsen JC, Johansen KS *et al*. Insights into the oxidative degradation of cellulose by a copper metalloenzyme that exploits biomass components. Proc. Natl. Acad. Sci. U.S.A. 2011;108(37):15079-84.
15. Phillips CM, Beeson WT, Cate JH, Marletta MA. Cellobiose dehydrogenase and a copper-dependent polysaccharide monooxygenase potentiate cellulose degradation by *Neurospora crassa*. ACS Chem. Biol. 2011;6(12):1399-406.
16. Beeson WT, Phillips CM, Cate JH, Marletta MA. Oxidative cleavage of cellulose by fungal copper-dependent polysaccharide monooxygenases. J. Am. Chem. Soc. 2012;134(2):890-2.
17. Bennati-Granier C, Garajova S, Champion C, Grisel S, Haon M, Zhou S et *al*. Substrate specificity and regioselectivity of fungal AA9 lytic polysaccharide monooxygenases secreted by *Podospora anserina*. Biotechnol. Biofuels. 2015;8:90.
18. Rodriguez-Zuniga UF, Cannella D, Giordano RdC, Giordano RdLC, Jorgensen H, Felby C. Lignocellulose pretreatment technologies affect the level of enzymatic cellulose oxidation by LPMO. Green Chem. 2015;17(5):2896-903.
19. Westereng B, Cannella D, Wittrup Agger J, Jørgensen H, Larsen Andersen M, Eijsink VGH *et al*. Enzymatic cellulose oxidation is linked to lignin by long-range electron transfer. Nat. Sci. Rep. 2015;5:18561.
20. Kracher D, Scheiblbrandner S, Felice AKG, Breslmayr E, Preims M, Ludwicka K *et al.* Extracellular electron transfer systems fuel cellulose oxidative degradation. Sci. 2016, 352:1098–1101.
21. Tan T-C, Kracher D, Gandini R, Sygmund C, Kittl R, Haltrich D *et al*. Structural basis for cellobiose dehydrogenase action during oxidative cellulose degradation. Nat. Commun. 2015;6:7542.

22. Langston JA, Shaghasi T, Abbate E, Xu F, Vlasenko E, Sweeney MD. Oxidoreductive cellulose depolymerization by the enzymes cellobiose dehydrogenase and glycoside hydrolase 61. Appl. Environ. Microbiol. 2011;77(19):7007-15.
23. Cannella D, Mollers KB, Frigaard NU, Jensen PE, Bjerrum MJ, Johansen KS *et al*. Light-driven oxidation of polysaccharides by photosynthetic pigments and a metalloenzyme. Nat. Commun. 2016;7:11134.
24. Wu M, Beckham GT, Larsson AM, Ishida T, Kim S, Payne CM *et al*. Crystal structure and computational characterization of the lytic polysaccharide monooxygenase GH61D from the Basidiomycota fungus *Phanerochaete chrysosporium*. J. Biol. Chem. 2013;288(18):12828-39.
25. Borisova AS, Isaksen T, Dimarogona M, Kognole AA, Mathiesen G, Varnai A *et al.* Structural and functional characterization of a lytic polysaccharide monooxygenase with broad substrate specificity. J. Biol. Chem. 2015, 290(38):22955-69
26. Courtade G, Wimmer R, Røhr ÅK, Preims M, Felice AKG, Dimarogona M *et al.* Interactions of a fungal lytic polysaccharide monooxygenase with β-glucan substrates and cellobiose dehydrogenase. Proc. Natl. Acad. Sci. U.S.A. 2016;113(21):5922-7.
27. Frandsen KEH, Simmons TJ, Dupree P, Poulsen J-CN, Hemsworth GR, Ciano L *et al.* The molecular basis of polysaccharide cleavage by lytic polysaccharide monooxygenases. Nat. Chem. Biol. 2016;12,298-303.
28. Hemsworth GR, Davies GJ, Walton PH. Recent insights into copper-containing lytic polysaccharide mono-oxygenases. Curr. Opin. Struct. Biol. 2013;23(5):660-8.
29. Li X, Beeson IV WT, Phillips CM, Marletta MA, Cate JHD. Structural basis for substrate targeting and catalysis by fungal polysaccharide monooxygenases. Structure. 2012;20(6):1051-61.
30. Lo Leggio L, Simmons TJ, Poulsen J-CN, Frandsen KEH, Hemsworth GR, Stringer MA *et al.* Structure and boosting activity of a starch-degrading lytic polysaccharide monooxygenase. Nat. Commun. 2015;6: 5961.
31. Couturier M, Feliu J, Haon M, Navarro D, Lesage-Meessen L, Coutinho PM *et al*. A thermostable GH45 endoglucanase from yeast: impact of its atypical multimodularity on activity. Microb Cell Factories. 2011;10(1):1-12.
32. Taylor CB, Talib MF, McCabe C, Bu L, Adney WS, Himmel ME *et al.* Computational investigation of glycosylation effects on a family 1 carbohydrate-binding module. J. Biol. Chem. 2012;287(5):3147-55.
33. Crouch LI, Labourel A, Walton PH, Davies GJ, Gilbert HJ. The contribution of non-catalytic carbohydrate binding modules to the activity lytic polysaccharide monooxygenases. J. Biol. Chem. 2016.
34. Westereng B, Arntzen MØ, Aachmann FL, Várnai A, Eijsink VGH, Agger JW. Simultaneous analysis of C1 and C4 oxidized oligosaccharides, the products of lytic polysaccharide monooxygenases acting on cellulose. J. Chromatogr. A. 2016:46-54.
35. Wang W, Yang S, Hunsinger GB, Pienkos PT, Johnson DK. Connecting lignin-degradation pathway with pretreatment inhibitor sensitivity of *Cupriavidus necator*. Front. Microbiol. 2014;5.
36. Ingold CK. Principles of an electronic theory of organic reactions. Chem. Rev. 1934;15(2):225-74.
37. Steenken S, Neta P. One-electron redox potentials of phenols. Hydroxy- and aminophenols and related compounds of biological interest. J. Phys. Chem. 1982;86(18):3661-7.
38. Hansch C, Leo A, Taft RW. A survey of Hammett substituent constants and resonance and field parameters. Chem. Rev. 1991;91(2):165-95.
39. Visser H, Joosten V, Punt PJ, Gusakov AV, Olson PT, Joosten R *et al.* Development of a mature fungal technology and production platform for industrial enzymes based on a *Myceliophthora thermophila* isolate, previously known as *Chrysosporium lucknowense* C1. Ind. Biotechnol. 2011;7:214–23.
40. Punt P, J, Burlingame R, Paul, Pynnonen C, M, Olson P, T, Wery J, Visser J, Heinrich *et al*. *Chrysosporium lucknowense* protein production system. 2010. Patent WO/2010/107303
41. Zhang YHP, Cui J, Lynd LR, Kuang LR. A transition from cellulose swelling to cellulose dissolution by *o*-phosphoric acid: Evidence from enzymatic hydrolysis and supramolecular structure. Biomacromolecules. 2006;7(2):644-8.
42. Sali A. Comparative protein modeling by satisfaction of spatial restraints. Mol. Med. Today. 1995;1(6):270-7.
43. Eswar N, Webb B, Marti-Renom MA, Madhusudhan MS, Eramian D, Shen MY *et al.* Comparative protein structure modeling using MODELLER. Curr. Protoc. Protein Sci. 2007, 50:2.9.1-2.9.31.
44. Gordon JC, Myers JB, Folta T, Shoja V, Heath LS, Onufriev A. H++: A server for estimating pK(a)s and adding missing hydrogens to macromolecules. Nucleic Acids Res. 2005;33 (Web Server issue):W368-W71.
45. Anandakrishnan R, Aguilar B, Onufriev AV. H++ 3.0: Automating pK prediction and the preparation of biomolecular structures for atomistic molecular modeling and simulations. Nucleic Acids Res. 2012;40 (Web Server issue):W537-W41.
46. Myers J, Grothaus G, Narayanan S, Onufriev A. A simple clustering algorithm can be accurate enough for use in calculations of pKs in macromolecules. Proteins. 2006;63(4):928-38.
47. Onufriev A, Anandakrishnan R, Aguilar B, Gordon J, Myers J, Folta T *et al*. 2004-2005. http://biophysics.cs.vt.edu/H++. Accessed 22 July 2016.
48. Robert X, Gouet P. Deciphering key features in protein structures with the new ENDscript server. Nucleic Acids Res. 2014;42 (Web Server issue):W320-4.
49. Fry SC, York WS, Albersheim P, Darvill A, Hayashi T, Joseleau J-P *et al.* An unambiguous nomenclature for xyloglucan-derived oligosaccharides. Physiol. Plant. 1993;89(1):1-3.

Additional Files

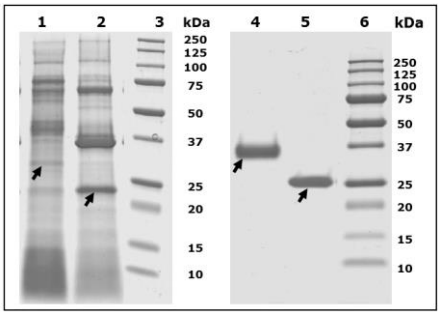

Additional Figure 3.1 SDS-PAGE of *Mt*LPMO9B and *Mt*LPMO9C fractions during enzyme purification. *Mt*LPMO9B and *Mt*LPMO9C were purified by multiple chromatographic steps from the crude enzyme extract of *Mt*LPMO9B (lane 1) and *Mt*LPMO9C (lane 2). The pools of *Mt*LPMO9B (lane 4) or *Mt*LPMO9C (lane 5), used for various experiments, showed a single protein band with apparent molecular masses of 32 and 25 kDa, respectively (black arrows). The Precision Plus Protein (Bio-Rad Laboratories) was used as a marker. (lane 3 and 6). For more details about protein purification see Methods.

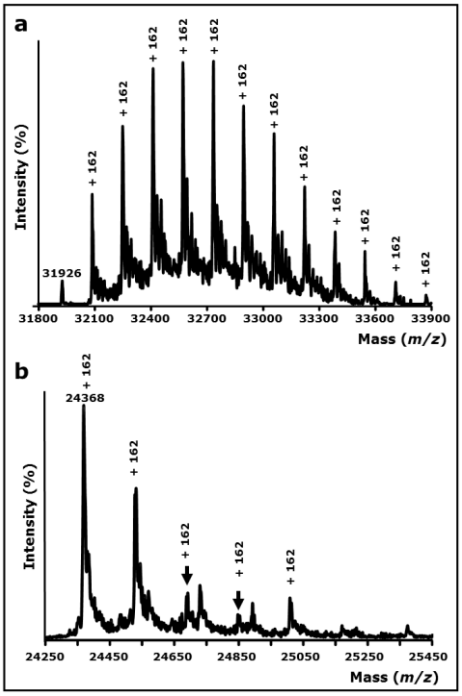

Additional Figure 3.2 LC/ESI-MS analysis of *Mt*LPMO9B and *Mt*LPMO9C. The purified **a** *Mt*LPMO9B- and **b** *Mt*LPMO9C-preparation was analyzed by LC/UV/ESI-MS using an AQUITY UPLC separation system and a SYNAPT ion mobiltiy mass spectrometer. The weighted average mass of *Mt*LPMO9B and *Mt*LPMO9C were 32,765 Da and 24,640 Da, respectively. ESI MS spectras (*m/z* values) of *Mt*LPMO9B and *Mt*LPMO9C show the presence of multiple glycations (+162 Da, hexose (180 Da) – water (18 Da)) of both LPMOs. Up to 13 and 5 glycosyl units are attached to *Mt*LPMO9B and *Mt*LPMO9C, respectively.

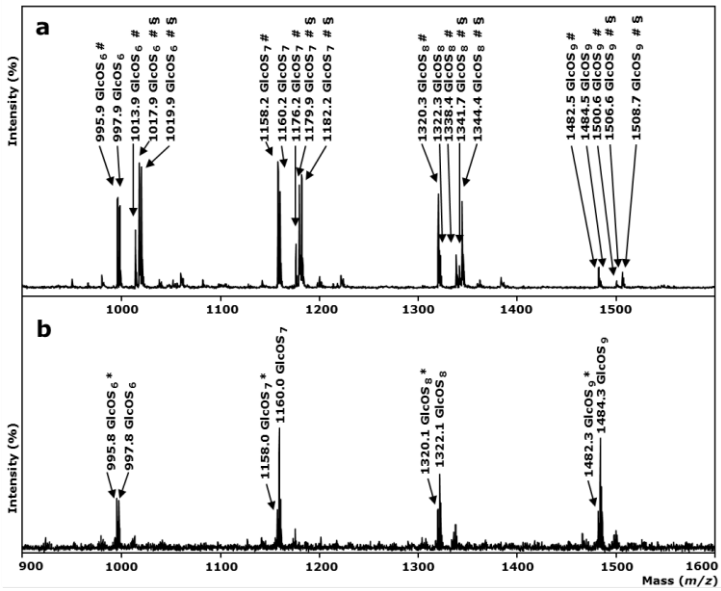

Additional Figure 3.3 MALDI-TOF mass spectrum of RAC incubated with *Mt*LPMO9B and *Mt*LPMO9C in the presence of ascorbic acid. **a** *Mt*LPMO9B incubated with RAC (RAC; 2 mg g^{-1}) in the presence of ascorbic acid. Clusters of C1-oxidized ($GlcOS_n^{\#}$) and non-oxidized ($GlcOS_n$) gluco-oligosaccharides were determined as their lithium (Li) adducts. Double Li-adducts are formed by exchanging a H^+ ion for another Li^+ ion (marked as $GlcOS_n^{\#}$§). **b** *Mt*LPMO9C incubated with RAC (RAC; 2 mg g^{-1}) in the presence of ascorbic acid. Clusters of gluco-oligosaccharides oxidized at the C4 position ($GlcOS_n$*) and non-oxidized gluco-oligosaccharides ($GlcOS_n$) were determined as their lithium adducts. **a** and **b** Clusters of non-oxidized and oxidized gluco-oligosaccharides differ by a mass difference of one glucose unit ($GluOS_1$, 180 Da – 16 Da = 162 Da). See **Figure 3.1** for more details.

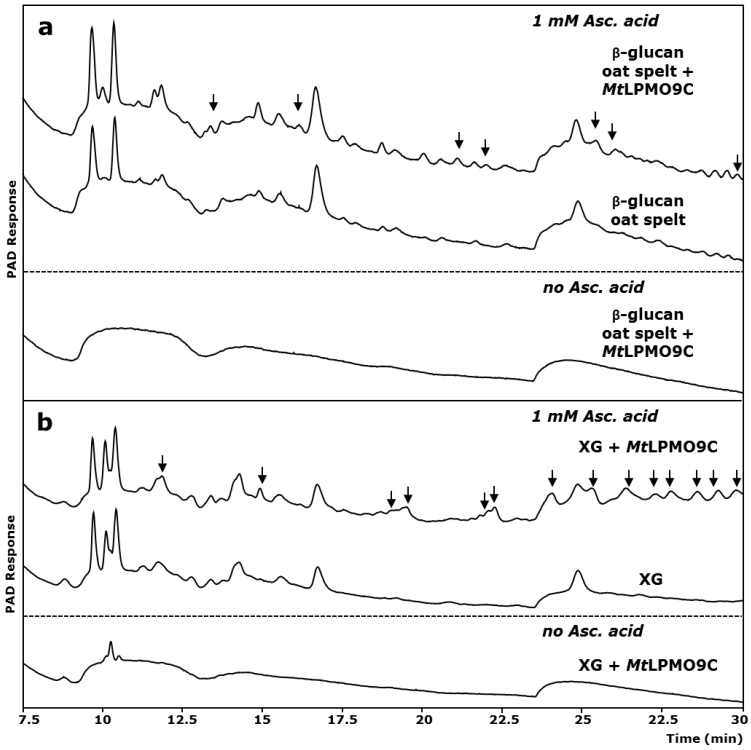

Additional Figure 3.4 HPAEC elution patterns of β-(1→3, 1→4)-glucan from oat spelt and xyloglucan incubated with *Mt*LPMO9C. Incubation of **a** oat spelt β-(1→3, 1→4)-glucan (2 mg mL^{-1}) and **b** xyloglucan from tamarind seed (XG; 2 mg mL^{-1}) with *Mt*LPMO9C (10 mg g^{-1} substrate) with ascorbic acid (1 mM) or without. Samples were incubated in a 50 mM ammonium acetate (pH 5.0) for 24 h at 52°C. **a** Numerous products (black arrows) were formed from oat spelt β-(1→3, 1→4)-glucan incubated with *Mt*LPMO9C in the presence of ascorbic acid compared to oat spelt β-(1→3, 1→4)-glucan without *Mt*LPMO9C addition in the presence of ascorbic acid. No oligosaccharides were released if oat spelt β-(1→3, 1→4)-glucan was incubated with *Mt*LPMO9C in the absence of ascorbic acid. **b** Incubation of XG with *Mt*LPMO9C in the presence of ascorbic acid released numerous products (black arrows) which were not present if XG was incubated with *Mt*LPMO9C in the absence of ascorbic acid. No oligosaccharides were formed from XG incubated with *Mt*LPMO9C in the absence of ascorbic acid.

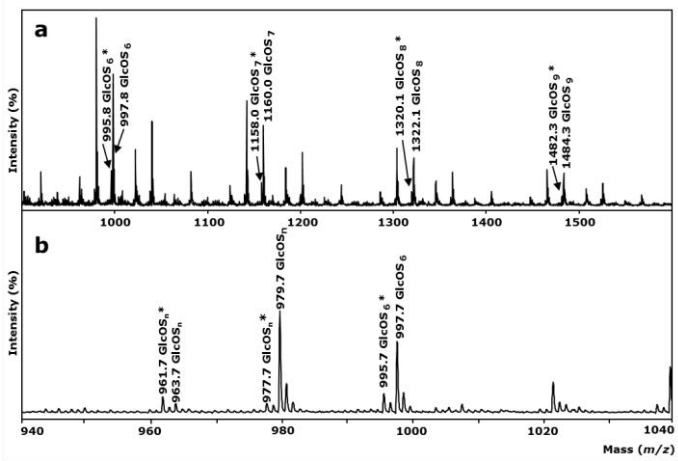

Additional Figure 3.5 MALDI-TOF mass spectrum of β-(1→3, 1→4)-glucan from oat spelt incubated with *Mt*LPMO9C. **a** *Mt*LPMO9B incubated with oat spelt β-(1→3, 1→4)-glucan (2 mg mL^{-1}) in the presence of ascorbic acid. Clusters of C4-oxidized ($GlcOS_n$*) and non-oxidized ($GlcOS_n$) gluco-oligosaccharides were determined as their lithium (Li) adducts. Clusters of non-oxidized and C4-oxidized gluco-oligosaccharides differ by a mass difference of one glucose unit ($GluOS_1$, 180 Da – 16 Da = 162 Da). **b** (enlargement of **a**) Several additional peaks were determined showing the characteristic 2 Da lower mass as reported for C4-oxidized products ($GluOS_n$* = $GluOS_n$ – 2 Da). See Methods for more details.

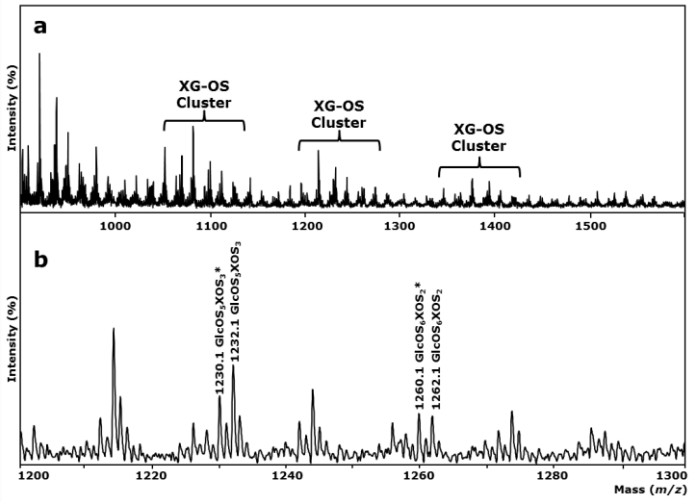

Additional Figure 3.6 MALDI-TOF mass spectrum of xyloglucan incubated with *Mt*LPMO9C. **a** *Mt*LPMO9C incubated with xyloglucan (2 mg mL^{-1}) in the presence of ascorbic acid. Xyloglucan oligosacchairde (XG-OS) clusters of C4-oxidized (XG-OS_n*) and non-oxidized (XG-OS_n) oligosaccharides were determined (*m/z* values) as their lithium (Li) adducts. **b** (enlargement of **a**) Several additional peaks were annotated showing the characteristic 2 Da lower mass as reported for C4-oxidized products ($GluOS_n$* = $GluOS_n$ – 2 Da). An identification of non-oxidized and C4-oxidized gluco-oligosaccharides of different substituted xyloglucan oligosaccharides based on Fry *et al*. (1993) remains limited due to the low amounts of products released from xyloglucan incubated with *Mt*LPMO9C (**Additional Figure 3.4**) and the therefore impossible MS^2-fragmentation [49]. Compounds annotated as $GluOS_nXOS_n$ indicate the number of expected hexoses and pentoses to be present in xyloglucan oligosaccharides. Samples were incubated in 50 mM ammonium acetate buffer (pH 5.0) containing 1 mM ascorbic acid for 24 h at 52°C. See Methods for more details.

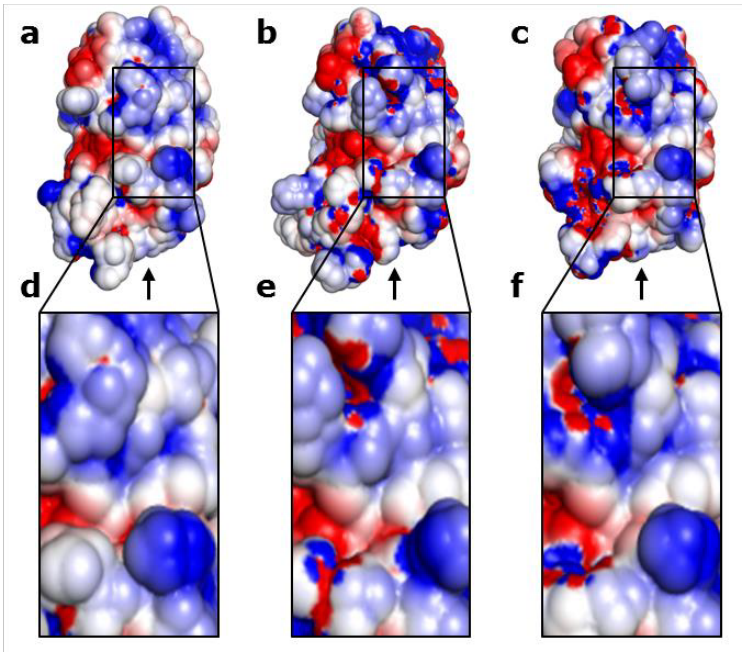

Additional Figure 3.7 Cartoons of the highly conserved surface patch near the Gly-Pro-Gly triad. Surface charge distribution and enlargement (in brackets) of **a** *Mt*LPMO9A (**d**), **b** *Mt*LPMO9B (**e**) and **c** *Mt*LPMO9C (**f**) emphasize the highly conserved surface patch near the Gly-Pro-Gly triad, positioned in the amino acid sequence around residue number 200 [21, 29]. The scaling from the negative and positive electrostatic potential regions are -5 for blue and +5 for the red regions. The electrostatic map was obtained from APBS plugin from PyMOL. Protein orientation: the flat substrate-binding site is located at the bottom of all three LPMOs indicated by the black arrow.

Chapter IV

RP-UHPLC-UV-ESI-MS/MS analysis of LPMO generated C4-oxidised gluco-oligosaccharides after non-reductive labeling with 2-aminobenzamide

Based on: Frommhagen M, van Erven G, Sanders M, van Berkel WJH, Kabel MA, Gruppen H. RP-UHPLC-UV-ESI-MS/MS analysis of LPMO generated C4-oxidised gluco-oligosaccharides after non-reductive labeling with 2-aminobenzamide. *Carbohydrate Research*. 2017; 448:191-199.

Abstract

Lytic polysaccharide monooxygenases (LPMOs) are able to cleave recalcitrant polysaccharides, such as cellulose, by oxidizing the C1 and/or C4 atoms. The analysis of the resulting products requires a variety of analytical techniques. Up to now, these techniques mainly focused on the identification of non-oxidized and C1-oxidized oligosaccharides. The analysis of C4-oxidized gluco-oligosaccharides is mostly performed by using high pressure anion exchange chromatography (HPAEC). However, the alkaline conditions used during HPAEC analysis lead to tautomerization of C4-oxidized gluco-oligosaccharides, which limits the use of this technique. Here, we describe the use of reverse phase-ultra high-performance liquid chromatography (RP-UHPLC) in combination with non-reductive 2-aminobenzamide (2-AB) labeling. Non-reductive 2-AB labeling enabled separation of C4-oxidized gluco-oligosaccharides from their non-oxidized counterparts. Moreover, RP-UHPLC does not require buffered mobile phases, which reduce mass spectrometry (MS) sensitivity. The latter is seen as an advantage over other techniques such as hydrophilic interaction liquid chromatography and porous graphitized carbon coupled to MS. RP-UHPLC coupled to UV detection and mass spectrometry allowed the identification of both labeled non-oxidized and C4-oxidized oligosaccharides. Non-reductive labeling kept the ketone at the C4-position of LPMO oxidized oligosaccharides intact, while selective reducing agents such as sodium triacetoxyborohydride (STAB) reduced this ketone group. Our results show that RP-UHPLC-UV-ESI-MS in combination with non-reductively 2-AB labeling is a suitable technique for the separation and identification of LPMO-generated C4-oxidized gluco-oligosaccharides.

4.1 Background

The use of lignocellulosic biomass, such as agricultural byproducts, is considered to be a green approach for the production of biofuels and biochemicals. Hereto, the (hemi)cellulose polysaccharides, which are the major constituents in addition to lignin, need to be degraded enzymatically to monosaccharides in one of the first steps of the biorefinery process. This enzymatic conversion has shown to be boosted by recently discovered lytic polysaccharide monooxygenases (LPMOs) [1].

Based on their regioselectivity, cellulose active LPMOs oxidize β-(1→4)-linked glucan chains at either the C1 or C4 position, or at both of these positions [1-5]. The oxidation of C1-atoms leads to formation of labile *δ*-lactones, which dissociate in water into aldonic acids. These compounds can be well separated by common oligosaccharide analysis methods, such as high-performance anion exchange chromatography (HPAEC) [3, 4, 6]. In contrast, LPMO-mediated C4-oxidation results in 4-ketoaldoses, which are present as their corresponding hydrates, geminal diols, in aqueous solutions [7, 8]. Unlike C1-oxidised oligosaccharides, C4-oxidised oligosaccharides undergo tautomerization in alkaline conditions and that limits their analysis by commonly used HPAEC, which requires alkaline eluents [6, 9]. Both C1- and C4-oxidised compounds are further identified by nuclear magnetic resonance (NMR) spectroscopy, by off-line mass spectrometric techniques, such as matrix-assisted laser desorption ionization-time of flight mass spectrometry (MALDI-TOF MS), or by direct infusion MS/MS^n [8-11] Nevertheless, for complex oligosaccharides mixtures a separation step prior to MS/MS^n improves identification [12-15].

So far, porous graphitized carbon liquid chromatography (PGC-LC) coupled to MS and charged aerosol detection (CAD) enabled identification of C4-oxidized gluco-oligosaccharides. This method allowed separation of non-oxidized and C4-oxidized gluco-oligosaccharides with a degree of polymerization up to 5 [8]. Still, the use of buffered mobile phases led to formation of multiple salt adducts and reduced MS sensitivity. Furthermore, C4-oxidized gluco-oligosaccharides could only be determined as geminal diols, but not as 4-ketoaldoses [8]. Alternatively, hydrophilic interaction liquid chromatography coupled to mass spectrometry (HILIC-MS) has been investigated, but resulted in co-elution of C4-oxidized gluco-oligosaccharides with their non-oxidized counterparts [8]. Hence, alternative methods are needed for the separation and identification of C4-oxidised oligosaccharides, which do not require the use of buffered eluents. In this work we propose RP-UHPLC-MS by using non-buffered eluents as an alternative technique for PGC-LC-MS and HILIC-MS.

To improve column affinity and enable UV-detection and MS^n-identification of oligosaccharides, labeling via reductive amination of sugar aldehydes has been shown to be a suitable procedure [15, 16]. Via reductive amination, an aldehyde, such as the reducing end of an oligosaccharide, reacts with a primary amine to which a chromophore or fluorophore is attached [17]. First, an imine (Schiff base) is formed that can isomerize into a glycosylamine [17]. Since these non-reduced intermediates are relatively unstable, selective reducing agents are used to convert the intermediates into stable secondary amines. Common reducing agents employed for this purpose are sodium cyanoborohydride ($NaBH_3CN$) and 2-picoline borane (pic-BH_3) [16, 17]. However, when reductive amination with common reducing agents is applied to label the reducing end of C4-oxidised

oligosaccharides, the ketone-group of C4-oxidized oligosaccharides will be reduced as well [18, 19]. Possibly, the milder reducing agent sodium triacetoxyborohydride (STAB, $NaBH(OAc)_3$), which has been reported to be unable to reduce ketones, has the ability to keep the C4-ketone intact [18]. So far, STAB has never been studied in relation with C4-oxidized oligosaccharide labeling.

Separation and identification of C4-oxidised oligosaccharides by using reversed phase coupled to MS with and without reductive amination has never been described. Here, we show how non-oxidized and C4-oxidized gluco-oligosaccharides can be identified by using non-reductive 2-AB labeling and RP-UHPLC-UV-ESI-MS. Furthermore, the developed method allows a clear separation of C4-oxidized gluco-oligosaccharides from there non-oxidized counterparts by using non-buffered eluents. In addition, alternative labeling approaches including the use of STAB and deuterated sodium borohydride are discussed.

4.2 Results and Discussion

4.2.1 Release of gluco-oligosaccharides from RAC incubated with *Mt*LPMO9C

In the absence of reducing agents, *Mt*LPMO9C is not active towards RAC [20]. Release of gluco-oligosaccharides from RAC incubated with *Mt*LPMO9C in the presence of 1 mM ascorbic acid was analyzed over an incubation-time of 72 h by using HPAEC. In the first 6 h of the incubation hardly any products were detected (**Figure 4.1**). An increase of released C4-oxidized gluco-oligosaccharides was observed after 6 h (**Figure 4.1c**), which reached a maximum between 18 to 30 h. The amount of C4-oxidized gluco-oligosaccharides with a higher degree of polymerization ($GluOS_{n+3}$*–$GluOS_{n+6}$*, annotation based on [20]) decreased after 30 h of incubation (**Figure 4.1b**), which has also been observed for other LPMOs [21]. After 6 h, the amount of non-oxidized gluco-oligosaccharides steadily increased the end of the incubation (**Figure 4.1b**).

The decrease of $GluOS_{n+3}$*–$GluOS_{n+6}$* is not expected to derive from the decomposition of these compounds due to the high pH used during HPAEC analysis. It is likely that *Mt*LPMO9C shows a low activity towards C4-oxidized gluco-oligosaccharides with a higher DP [20], although we did not determine any activity of *Mt*LPMO9C towards soluble cello-oligosaccharides with a degree of polymerization (DP) up to 5 [20]. In addition, after long incubation times the solubility of C4-oxidized gluco-oligosaccharides with longer DP could have decreased due to, for example, non-covalent interactions between these compounds and the remaining RAC material [14, 22]. This hypothesis was further studied by incubating non-oxidized gluco-oligosaccharides (DP3, DP4 and DP5) with RAC for 24, 48 and 72 h (**Additional Figure 4.1**). In particular, the amount of gluco-oligosaccharides with a longer DP, such as DP5, decreased significantly (up to 40%) when incubated with RAC for 72 h. This finding underpins the possible interaction of C4-oxidized gluco-oligosaccharides with a longer DP and RAC. Still, the decomposition of C4-oxidized gluco-oligosaccharides at high pH limits the use of HPAEC [8]. Therefore, we investigated the use of reversed phase UHPLC-MS as a suitable alternative.

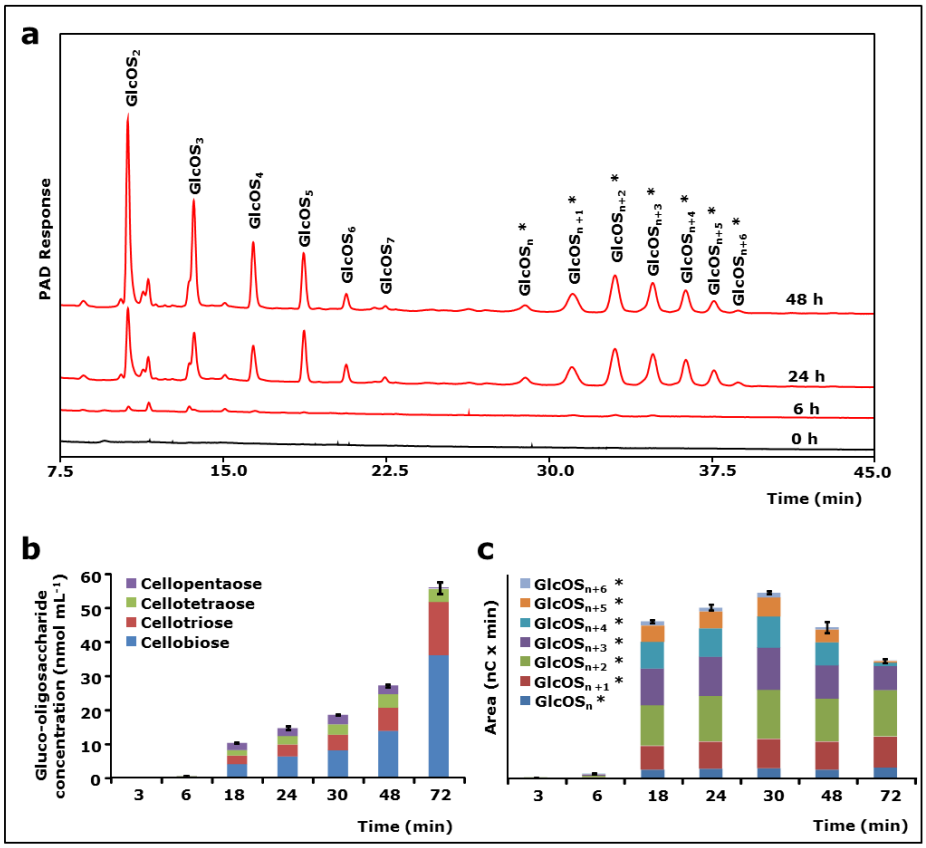

Figure 4.1 Activity of *Mt*LPMO9C on regenerated amorphous cellulose in time. **a** HPAEC elution pattern of regenerated amorphous cellulose (RAC; 2 mg mL^{-1}) incubated with *Mt*LPMO9C (15 mg g^{-1} substrate) in the presence of ascorbic acid (1 mM). The oxidation of the C4 carbon atom results in the formation of non-oxidized ($GlcOS_n$) and C4-oxidized gluco-oligosaccharides ($GlcOS_n$*). **b** Gluco-oligosaccharide concentration of released cellobiose, cellotriose, cellotetraose and cellopentaose from RAC incubated with *Mt*LPMO9C throughout 72 h. Minor amounts of released cellohexaose and cellopentaose were not quantified. **c** The total sum of integrated peak areas of released C4-oxidized gluco-oligosaccharides ($GlcOS_n$* - $GlcOS_{n+6}$*, annotation based on [20]) after incubation of RAC with *Mt*LPMO9C throughout 72 h based on HPAEC. Details are described in Methods.

4.2.2 2-AB labeling of non-oxidized and C4-oxidized gluco-oligosaccharides by reductive amination

Reductive labeling of gluco-oligosaccharides by using 2-AB has already been described before [16, 23]. Here, we applied this technique for the analysis of released gluco-oligosaccharides from RAC incubated with *Mt*LPMO9C. Therefore, a mixture of *Mt*LPMO9C-generated non-oxidized and C4-oxidized gluco-oligosaccharides and β-(1→4)-linked gluco-oligosaccharides standards (DP1-5) were labeled with 2-AB via reductive amination by using the mild reducing agent sodium triacetoxyborohydride (STAB). Labeled oligosaccharide mixtures were analyzed by using RP-UHPLC-UV-ESI-MS (**Figure 4.2**).

Clearly, labeled β-(1→4)-linked gluco-oligosaccharides standards from DP2 till 5 were well separated and well detectable by both UV and MS (**Figure 4.2a**). Glucose, although present in the mixture, was not detected because the 2-AB labeled form of this monosaccharide was not retained during the solid phase extraction (SPE) clean-up step of the samples prior to analysis (no further data shown). Positive mode MS and MS^2 analysis confirmed the presence of 2-AB labeled β-(1→4)-linked gluco-oligosaccharides of DP2-5 (DP2-AB, *m/z* 463; DP3-AB, *m/z* 625; DP4-AB, *m/z* 787; DP5-AB; *m/z* 949) (**Table 4.1**, **Figure 4.2**). The MS^2 fragmentation (**Figures 4.2c** and **d**; nomenclature based on [24]) showed sugar residue losses of *m/z* 162, which is typical for 2-AB labeled β-(1→4)-linked gluco-oligosaccharides. As an example, 2-AB labeled cellotetraose had a molecular weight of 786 (parent ion $[M+H]^+$ *m/z* 787). The *m/z* 162 sugar residue losses resulted in fragments of *m/z* 625, 463 and 301 (**Figure 4.2c**). The abundance of Y_1-ions (*m/z* 301, glycosyl unit attached to 2-AB) indicated that the β-(1→4)-linkages closest to the label were most susceptible to break in the positive mode of MS^2 analysis (**Figure 4.2**).

The *Mt*LPMO9C-generated non-oxidized gluco-oligosaccharides were also 2-AB labeled and, compared to the standards, their elution and MS/MS^2 spectra were similar (**Figures 4.2b-d**). Unfortunately, quantification of non-oxidized oligosaccharides was not possible due to the decrease of UV response with increasing DP (DP2-AB until DP6-AB), while molar amounts used during labeling were kept constant (0.5 µmol). Thus, quantification requires the use of calibration curves for each standard to overcome possible limitations such as a decreased solubility of gluco-oligosaccharides with a higher DP, which affects the labeling yield, or a decreased solubility of labeled gluco-oligosaccharides prior to analysis. The use of standards would also allow quantification of labeled gluco-oligosaccharides, which have different UV response factors (**Figure 4.2**).

In contrast to the detection of non-oxidized gluco-oligosaccharides, no 2-AB labeled C4-oxidized gluco-oligosaccharides were detected by RP-UHPLC-UV-ESI-MS in the supernatant of RAC incubated with *Mt*LPMO9C. Masses of the in previous research determined geminal diols of C4-oxidized gluco-oligosaccharides were also not detected. These results indicated that a reduction of the 4-ketoaldose occurred during the labeling. Apparently, STAB reduced ketones at the C4 position of oxidized gluco-oligosaccharides. The reduction of these ketones was further investigated by incubating *Mt*LPMO9C-generated non-oxidized and C4-oxidized gluco-oligosaccharides with STAB followed by HPAEC analysis. Only non-oxidized gluco-oligosaccharides were detected after STAB treatment in the HPAEC elution profile, as no peaks were present in the region where C4-oxidized gluco-oligosaccharides normally elute (based on **Figure 4.1** 28-40 min, data not shown). The proposed reaction pathway of the reduction of 4-ketoaldoses by STAB during 2-AB labeling is presented in **Additional Figure 4.2**. The effect of STAB on the reduction of 2-AB-labeled C4-oxidized gluco-oligosaccharides was further investigated by using 10 to 100 times lower concentrations of STAB. Low amounts of 2-AB labeled C4-oxidized gluco-oligosaccharides were only detected at the lowest STAB concentration used (**Additional Figure 4.3**).

The lowest concentration of STAB used also resulted in the formation of increasing amounts of non-reductively 2-AB labeled non-oxidized gluco-oligosaccharides, which could be identified as imines due to the determined two Da lower *m/z* of the Y-fragments compared to the reductively 2-AB labeled non-oxidized counterparts (**Table 4.1**). The two Da lower *m/z* of all fragments indicated that the *m/z* loss was positioned on the labeled sugar side and confirmed the presence of imines (*m/z* 299) instead of secondary amines (*m/z* 301) (**Table 4.1**). In addition, imines of non-reductively 2-AB

labeled C4-oxidized gluco-oligosaccharides were detected, which had the expected 2 Da lower *m/z* compared to their non-reductively 2-AB labeled non-oxidized counterparts (**Table 4.1**). However, MS^2 fragmentation was not possible due to the low abundance of these compounds.

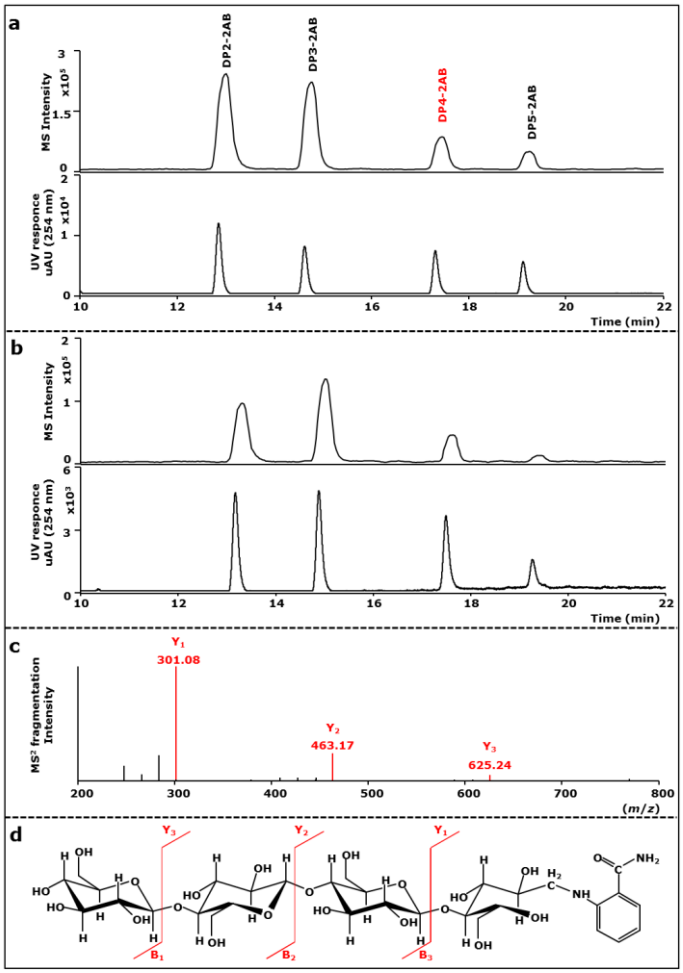

Figure 4.2 Identification of reductively labeled non-oxidized gluco-oligosaccharides. The reductively (in the presence of STAB) 2-AB labeled non-oxidized gluco-oligosaccharides were analyzed by RP-UHPLC-UV-ESI-MS **a** Upper graph – Extracted ion chromatogram (EIC) of reductively 2-AB labeled cellobiose (DP2-2AB), cellotriose (DP3-2AB), cellotetraose (DP4-2AB) and cellopentaose (DP5-2AB) with the *m/z* values of 463, 625, 787 and 949, respectively (**Table 4.1**) from a prepared standard (DP1-DP5). Lower graph – Elution profile of the four gluco-oligosaccharides based on UV (254 nm). **b** Upper graph – EIC of reductively 2-AB labeled cellobiose, cellotriose, cellotetraose and cellopentaose with the *m/z* values of 463, 625, 787 and 949, respectively (**Table 4.1**) from the supernatant of RAC incubated with *Mt*LPMO9C in the presence of ascorbic acid (48 h). Lower graph – Elution profile of the four gluco-oligosaccharides based on UV (254 nm). **c** MS^n spectrum, recorded in positive mode, showing determined B- and Y-fragments of reductively labeled cellotetraose (DP4-2AB, *m/z* 787). **d** Fragmentation pattern of reductively labeled cellotetraose based on determined MS^n fragments. See Methods for labeling procedure and RP-UHPLC-UV-ESI-MS determination.

Based on the strong reduction potential of STAB, the milder reducing agent ascorbic acid was used. Ascorbic acid has been previously described to be able to reduce imines to secondary amines [25]. Surprisingly, 2-AB labeled C4-oxidized gluco-oligosaccharides were detected as imines and not as expected secondary amines. Moreover, upon ascorbic acid addition, the formation of imines was clearly improved (**Additional Figure 4.3**). This raised the question if ascorbic acid improves or stabilizes the 2-AB labeling of non-oxidized gluco-oligosaccharides.

Until now, carbohydrate derivatization for MS analysis is mostly performed by reductive amination. Over 60 different amines have already been described to allow identification and characterization of labeled carbohydrates by this technique [17]. As an alternative to reductive amination, carbohydrate derivatization has also been performed with omitting the reduction step, allowing the detection of the imine form of labeled carbohydrates. Although these imines (Schiff base) are considered to be unstable, they have already been analyzed by using different techniques such as LC-MS and MALDI-TOF MS [17]. For instance, maltodextrins have been labeled by PFBAB (pentafluorobenzyl aminobenzoate) enabling MS analysis of very low concentrations (fmol) [26]. Another approach was the non-reductive amination of N-linked glycans by using aniline and the formed imines were stable enough to allow analysis by MALDI-TOF MS [27]. Although rarely applied, the given examples stimulated the development of a method that enabled the identification of C4-oxidized gluco-oligosaccharides as 2-AB imines after non-reductive labeling.

4.2.3 Identification of non-reductively 2-AB labeled non-oxidized and C4-oxidized gluco-oligosaccharides

Reductive labeling resulted in the loss of the C4-ketone of LPMO-generated C4-oxidised gluco-oligosaccharides. Still, intermediates of 2-AB labeled imines of C4-ketones were detected in the absence of a reduction step and became even more pronounced after ascorbic acid addition prior to labeling. Hence, this non-reductively labeling approach was tested with released non-oxidized and C4-oxidized gluco-oligosaccharides from RAC incubated with *Mt*LPMO9C and the RP-UHPLC-UV-ESI-MS results are shown in **Figure 4.3**.

All non-reductively 2-AB labeled non-oxidized oligosaccharides showed a complete baseline separation and their masses were confirmed by positive mode MS analysis (DP2-AB-NR, *m*/*z* 461; DP3-AB-NR, *m*/*z* 623; DP4-AB-NR, *m*/*z* 785; DP5-AB-NR; *m*/*z* 947) (**Table 4.1**). These determined *m*/*z* values were 2 Da lower compared to their reductively 2-AB labeled counterparts (with STAB addition) (**Table 4.1**). The 2 Da lower mass confirmed the formation of imines, which were not further reduced to amines due to the absence of STAB (**Additional Figure 4.2**). The addition of ascorbic acid prior to labeling did not reduce the formed imines into amines. Positive mode MS^2 fragmentation patterns of non-reductively 2-AB labeled non-oxidized gluco-oligosaccharides corresponded to their reductively labeled counterparts and showed the same typical sugar residue loss of *m*/*z* 162 (**Figures 4.2** and **4.3**).

Subsequently, non-reductively 2-AB labeled C4-oxidised oligosaccharides were analyzed by RP-UHPLC-UV-ESI-MS (**Figures 4.3** and **4.4**). Based on EIC (**Figure 4.4**), both non-reductively 2-AB labeled C4-oxidized cellotetraose (DP4-C4-ox-2AB-NR, *m*/*z* 783; **Table 4.1**) and cellopentaose (DP4-C4-ox-2AB-NR, *m*/*z* 945; **Table 4.1**) were identified. MS^n analysis of Y-fragments showed a sugar residue loss of *m*/*z* 162, which was also observed for above described non-oxidized gluco-

oligosaccharides (**Figures 4.4b** and **c**). Hence, our approach succeeded to identify the formation of C4-oxidised gluco-oligosaccharides as catalyzed by *Mt*LPMO9C.

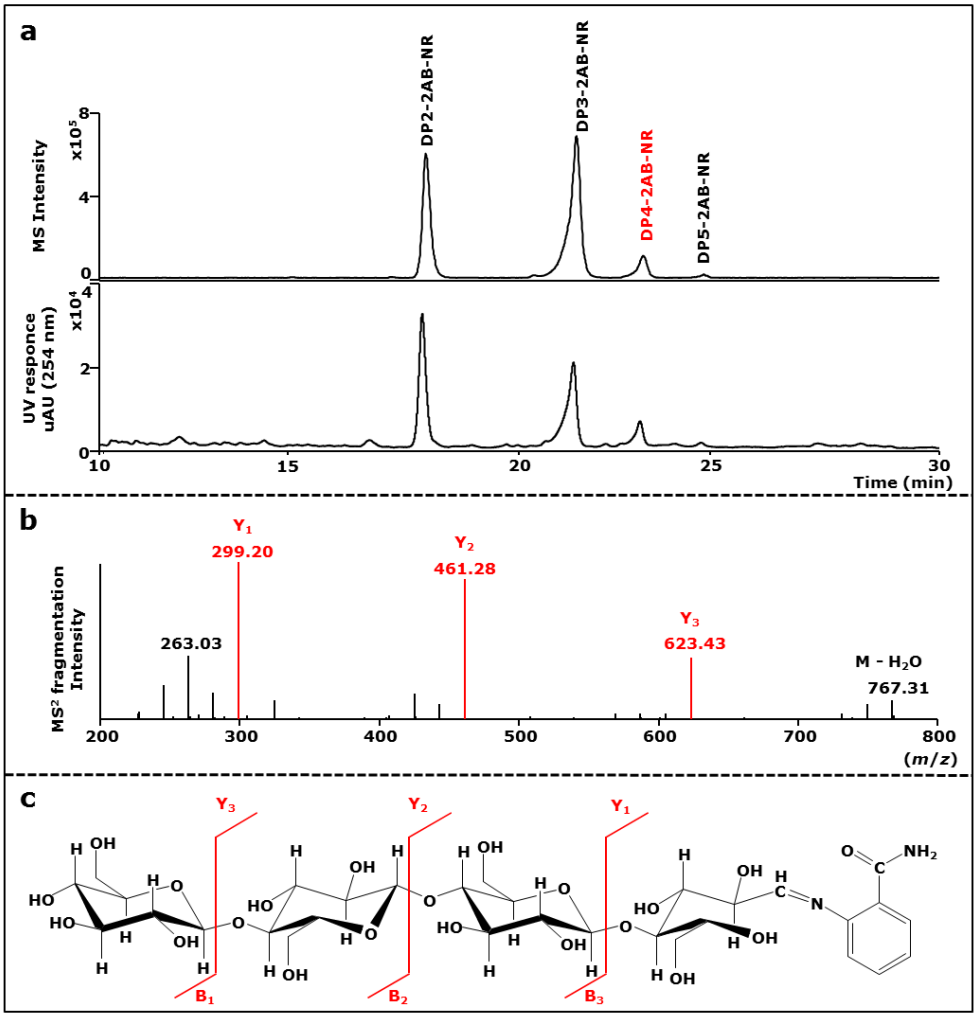

Figure 4.3 Identification of non-reductively labeled non-oxidized gluco-oligosaccharides. The non-reductively labeled non-oxidized gluco-oligosaccharides were analyzed by RP-UHPLC-UV-ESI-MS **a** Upper graph – EIC of non-reductively 2-AB labeled cellobiose (DP2-2AB-NR), cellotriose (DP3-2AB-NR), cellotetraose (DP4-2AB-NR) and cellopentaose (DP5-2AB-NR) with the *m/z* values of 461, 623, 785 and 947, respectively (**Table 4.1**). Lower graph – Elution profile of the four gluco-oligosaccharides based on UV (254 nm). **b** MS^n spectrum, recorded in positive mode, showing determined B- and Y-fragments of non-reductively labeled cellotetraose (DP4-2AB-NR, *m/z* 785). **c** Fragmentation pattern of non-reductively labeled cellotetraose based on determined MS^n fragments. See Methods for labeling procedure and RP-UHPLC-UV-ESI-MS determination.

The abundance of 2-AB labeled C4-oxidised oligosaccharides is much lower compared to their non-oxidized counterparts (**Figures 4.3** and **4.4**). Moreover, this low abundance of 2-AB labeled C4-oxidized gluco-oligosaccharides is also reflected by the UV signal, which hardly exceeded the

baseline noise. The low MS sensitivity for non-reductively 2-AB labeled C4-oxidized gluco-oligosaccharides likely results from the use of reductively 2-AB labeled cellobiose for MS optimization, which led to non-optimal MS settings. In the developed RP-UHPLC-MS method, the presence of the rather small 4-keto group (of 2-AB labeled C4-oxidized gluco-oligosaccharides) determined the elution time to a larger extent than the DP (**Figures 4.3a** and **4.4a**). Hence, it was concluded that the 4-keto group had considerable effects on structure, and presumably also on conformation, which might have further influenced MS detection. Improvement of this detection might be achieved by MS optimization with non-reductively 2-AB labeled C4-oxized gluco-oligosaccharide standards, which can be obtained via the method described by Westereng *et al*. [8].

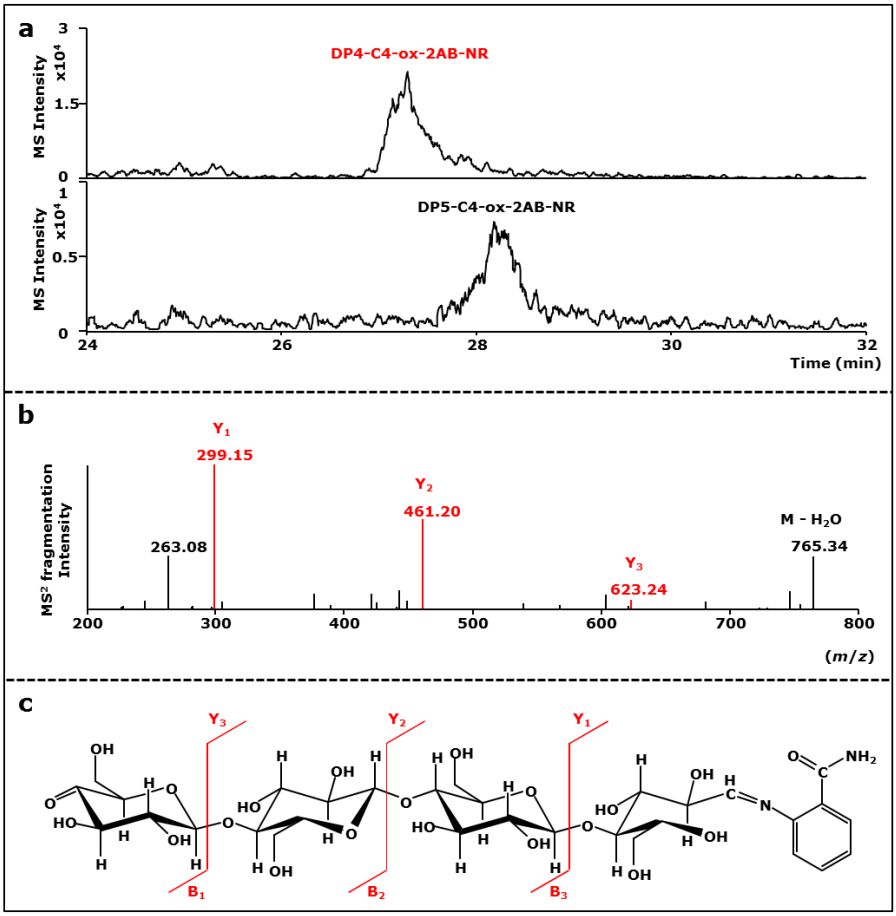

Figure 4.4 Identification of non-reductively labeled C4-oxidized gluco-oligosaccharides. The non-reductively labeled C4-oxidized gluco-oligosaccharides were analyzed by RP-UHPLC-UV-MS/MS **a** EIC of non-reductively 2-AB labeled C4-oxidized cellotetraose (upper graph, DP4-C4-ox-2AB-NR) and cellopentaose (lower graph, DP5-C4-ox-2AB-NR) with the *m/z* values of 783 and 945, respectively (**Table 4.1**). **b** MS^n spectrum, recorded in positive mode, showing determined B- and Y-fragments of non-reductively labeled C4-oxidized cellotetraose (DP4-C4-ox-2AB-NR, *m/z* 783). **c** Fragmentation pattern of non-reductively labeled C4-oxidized cellotetraose based on determined MS^n fragments. See Methods for labeling procedure and RP-UHPLC-UV-MS/MS determination.

Nevertheless, the unambiguous identification of C4-oxidised gluco-oligosaccharides was achieved by using this novel non-reductively labeling method. Similar to PGC-LC, we only determined C4-oxidised gluco-oligosaccharides with a lower DP [8]. A possible solution would be the addition of a *β*-glucosidase, which is able to hydrolyze the β-(1→4)-linkage from the reducing end and thereby forming C4-oxidized gluco-oligosaccharides with a lower DP. The separation of non-oxidized and C4-oxidized gluco-oligosaccharide using RP-UHPLC did not require, as described for the PGC-LC method, the use of buffered mobile phases and therefore, multiple salt adduct formation and reduced MS sensitivity could be limited [8]. In addition, the combination of 2-AB labeling and RP-UHPLC-MS allows, compared to the use of HILIC-MS only, a clear separation of C4-oxidised gluco-oligosaccharides from their non-oxidized counterparts [8]. This challenging separation has been, so far, a limiting factor for the analysis of C4-oxidised gluco-oligosaccharides [8].

Hence, 2-AB labeling can be applied to LPMO reaction mixtures, in which identification of C4-oxidized oligosaccharides is required. An example is LPMO activity towards xyloglucan, where identification of C4-oxidised branched oligosaccharides is required to understand LPMO-cleavage patterns. Here, our method could be a potential alternative to the so far used MALDI-TOF MS method or direct injection in combination with UHPLC-MS [11, 28]. Nevertheless, to allow quantification of LPMO-generated C4-oxidised oligosaccharides, alternative or optimized procedures are still needed.

We considered other labeling compounds, such as phenylhydrazine labeling, which does not require an additional reduction step [29]. However, (over) reactivity of phenylhydrazine was observed: a single gluco-oligosaccharide resulted in numerous singly or multiply labeled gluco-oligosaccharides (data not shown). Therefore, this method was not further developed. Another considered alternative approach was the use of deuterated borohydride (BD_4) instead of STAB for the reductive amination of gluco-oligosaccharides with 2-AB. BD_4 reacted with the 4-keto group of C4-oxized gluco-oligosaccharides following a similar mechanism as STAB (**Additional Figure 4.2**). In the presence of STAB, C4-oxized gluco-oligosaccharides were reduced to their non-oxidized counterparts, identical to the products of hydrolytic cleavage. By BD_4 reduction a deuterium ion is inserted into C4-oxidized gluco-oligosaccharides, which led to the formation of non-oxidized gluco-oligosaccharide with a 1 Da higher mass compared to 'normal' non-oxidized gluco-oligosaccharides. Hence, both non-oxidized and 'modified deuterated C4-oxidized' 2-AB labeled gluco-oligosaccharides could be distinguished by RP-UHPLC-UV-ESI-MS. However, the strong reducing capacity of BD4 led to the formation of alditols (data not shown) that cannot be labeled anymore. Therefore, we suggest a 'two-step-labeling-approach', where in a first step C4-oxidized gluco-oligosaccharides are 2-AB labeled and in a second step BD4 is added in equimolar amounts of expected imines.

Finally, we conclude that 2-AB labeling by selective deuterated reducing agents combined with RP-UHPLC-MS analysis could be a good approach for both identification and, when optimized further, quantification.

Table 4.1 Identification of 2-AB labeled non-oxidized and C4-oxidized gluco-oligosaccharides by RP-UHPLC-UV-ESI-MS.

Gluco-oligosaccharide	Abbreviation	$[M+H]^+$ (*m/z*)	Signature fragments (MS^n) positive mode
Reductively 2-AB labeled[a]			
Non-oxidized			
Cellobiose	DP2-2AB	463.2	301.1, 284.1, 248.1
Cellotriose	DP3-2AB	625.2	463.2, 301.1, 284.1, 248.1
Cellotetraose	DP4-2AB	787.3	625.2, 463.2, 301.1
Cellopentaose	DP5-2AB	949.4	787.3, 625.2, 463.2, 301.1
C4-oxidized			
n.d.[b]	n.d.[b]	n.d.[b]	n.d.[b]
Non-reductively 2-AB labeled[c]			
Non-oxidized			
Cellobiose	DP2-2AB-NR	461.1	299.1, 263.1, 215.0
Cellotriose	DP3-2AB-NR	623.2	461.1, 299.1, 263.1, 215.0
Cellotetraose	DP4-2AB-NR	785.2	623.4, 461.3, 299.2
Cellopentaose	DP5-2AB-NR	947.3	767.3, 623.4, 461.3, 299.1
C4-oxidized			
4-keto-cellotetraose	DP4-C4-ox-2AB-NR	783.3	623.1, 461.2, 299.1
4-keto-cellopentaose	DP5-C4-ox-2AB-NR	945.3	783.4, 623.1, 461.3, 299.1

[a] Gluco-oligosaccharide labeled in the presence of STAB and 2-AB in DMSO:acetic acid (85:15, v/v)

[b] n.d., not determined by RP-UHPLC-UV-ESI-MS due to reduction of the C4 position of the 4-ketoladose by STAB (**Additional Figure 4.2**)

[c] Gluco-oligosaccharide labeled in the absence of STAB and 2-AB in DMSO:acetic acid (85:15, v/v) with **1 M** ascorbic acid addition during labeling

4.3. Conclusions

Here, we describe the use of non-reductive 2-AB labeling for the separation and identification of non-oxidized and C4-oxidized gluco-oligosaccharides in combination with RP-UHPLC-UV-ESI-MS detection. Non-oxidized and C4-oxidized gluco-oligosaccharides were separated by using non-buffered eluents. The imines formed allowed identification by UV and mass spectrometry. The addition of non-selective reducing agents such as STAB during 2-AB labeling led to loss of the ketone of the C4 carbon atom of C4-oxidized gluco-oligosaccharides. Ascorbic acid addition prior to labeling improved the yield of determined non-reductively labeled non-oxidized and C4-oxidized gluco-oligosaccharides. Our results show that the combination of RP-UHPLC-UV-ESI-MS and non-reductively 2-AB labeling is a suitable technique for the separation and identification of LPMO-generated C4-oxidized gluco-oligosaccharides.

4.4. Methods

4.4.1 Enzyme expression, production and purification

*Mt*LPMO9C was expressed and purified according to a previously described procedure [20].

4.4.2 Cellulose substrate, standards and labeling chemicals

Regenerated amorphous cellulose (RAC) was prepared from Avicel PH-101 as described previously [20]. Ascorbic acid, glucose, cellobiose, sodium triacetoxyborohydride (STAB) and deuterated sodium borohydride were purchased from Sigma-Aldrich (Steinheim, Germany). Cellotriose, cellotetraose, cellopentaose and cellohexaose were purchased from Megazyme (Bray, Ireland). Phenylhydrazine hydrochloride, 2-aminobenzamide (2-AB) and dried dimethyl sulfoxide (DMSO) were purchased from VWR International (Radnor, PA, USA).

4.4.3 Incubation conditions for *Mt*LPMO9C

Regenerated amorphous cellulose (2 mg mL^{-1}) was dissolved in 50 mM ammonium acetate buffer (pH 5.0), with or without addition of ascorbic acid (final concentration 1 mM). The enzyme concentration of *Mt*LPMO9C was 15.0 µg protein per mg^{-1} of substrate. Samples were incubated in triplicate for various time points (0, 3, 6, 18, 24, 30, 48 and 72 h) at 50°C in a head-over-tail rotator in portions of 5 mL of total volume (Stuart rotator, Bibby Scientific, Stone, UK) at 20 rpm.

4.4.4 Oligosaccharide analysis

Oligosaccharides were analyzed by high-performance anion-exchange chromatography (HPAEC) with pulsed amperometric detection (PAD) using a HPAEC system (ICS-5000, Dionex, Sunnyvale, CA, USA) as described previously [20].

4.4.5 2-AB labeling of non-oxidized and C4-oxidized gluco-oligosaccharides by using reductive amination

Non-oxidized and C4-oxidized gluco-oligosaccharides were reductively 2-AB labeled as previously described [16, 30] by using a modified protocol [23]. The supernatant (250 µL) obtained from the incubation of RAC with *Mt*LPMO9C in the presence of ascorbic acid after 48 h was used for the reductive labeling by 2-AB. In addition, an equimolar stock solution of a 10 µL mixture of glucose, cellobiose, cellotriose, cellotetraose and cellopentaose (DP1-DP5) was prepared at total amount of 0.5 µmol (0.1 µmol per compound). Duplicates of the standard stock solution and the 250 µL supernatant from the RAC- *Mt*LPMO9C-incubation were dried by using a SpeedVac Savant ISS110 concentrator (Thermo Scientific, San Jose, CA, USA). The dried samples were mixed with a freshly prepared 2-AB solution 12.5 µL (191 mg mL^{-1} DMSO containing 15% (v/v) acetic acid). Subsequently, 37.5 µL of STAB (143 mg mL^{-1} DMSO containing 15% (v/v) acetic acid) was added. The final molar ratio of gluco-oligosaccharides and 2-AB was 1:35 during labeling (10 mM and 350 mM, respectively). All samples were vortexed for 30 sec and centrifuged (3 min, 15,000 x *g*, 20°C) to ensure liquid concentration at the bottom of the tube. All samples were incubated for 2 h at 65°C under continuous shaking at 750 rpm (ThermoMixer Comfort, Eppendorf, Hamburg, Germany). After incubation, samples were cooled to room temperature (20°C), centrifuged (1 min, 15,000 x *g*, 20°C) and dried overnight (SpeedVac Savant ISS110 concentrator).

The dried samples were dissolved in 1 mL 90% (v/v) acetonitrile in water before solid phase extraction (SPE) clean-up with Bond Elut Cellulose columns (300 mg, 3 mL; Agilent, Santa Clara, CA, USA) according to a previous method [16, 30], which was modified. Briefly, the column was conditioned with 2 x 2 mL water and afterwards equilibrated with 3 x 2 mL 90% (v/v) acetonitrile in water. Samples (500 µL) were subsequently loaded. Vacuum was applied 2 min after the first loading and 5 min after the second loading. The column was subsequently washed with 2 x 3 mL 90% (v/v) acetonitrile in water before the analytes were eluted with 2 x 2 mL water with 5 min gravitational elution before vacuum was applied. Obtained samples (4 mL) were dried under a stream of nitrogen overnight at room temperature (20°C). Subsequently, samples were wetted with methanol (1 µL), vortexed for 0.5 min and centrifuged (1 min, 15,000 x *g*, 20°C) and dissolved in 100 µL water. Samples were 10 times diluted prior to RP-UHPLC-UV-ESI-MS analysis.

4.4.6 Non-reductive 2-AB labeling of non-oxidized and C4-oxidized gluco-oligosaccharides

Aliquots of 250 µL supernatant containing non-oxidized and C4-oxidized gluco-oligosaccharides from the incubation of RAC with *Mt*LPMO9C (48 h, **Figure 4.1**) were prepared by using two different sample preparations. One preparation included 250 µL of the RAC-*Mt*LPMO9C-incubation supernatant without additional ascorbic acid addition. The other sample preparation was enriched to yield an ascorbic acid concentration of 1 M during labeling, by addition of fresh ascorbic acid prior to labeling. The same protocol as described above was used for sample preparation with the following modifications: 1) After drying, all samples were mixed with 50 µL freshly prepared 2-AB solution without addition of STAB. 2) Samples were not diluted prior to RP-UHPLC-UV-ESI-MS analysis.

4.4.7 RP-UHPLC-UV-ESI-MS analysis of reductively 2-AB labeled non-oxidized and C4-oxidized gluco-oligosaccharides

All samples were subjected to an Accela reversed phase high-performance liquid chromatography (RP-UHPLC) system coupled to electron spray ionization (ESI) mass spectrometry (Thermo Scientific, San Jose, CA, USA). Injected samples (5 µL) were separated using a Aquidity BEH C18 (2.1 x 150 mm, 1.7 µm particle size) coupled to an Acquity UHPLC BEH C18 Vanguard guard column (2.1 x 5 mm, 1.7 µm particle size). Both columns were purchased from Waters (Milford, MA, USA). Elution with eluent A (H_2O + 0.1% (v/v) formic acid) and eluent B (methanol + 0.1% (v/v) formic acid) was performed according to the following steps: From 0 to 1 min an isocratic elution of 5% B, from 1 to 31 min a linear gradient to 20% B, from 31 to 32 min a linear gradient to 100% B, from 31 to 36 min an isocratic elution of 100% B, from 36 to 37 min a linear gradient to 5% B and from 37 to 45 an isocratic elution of 5% B. A flow rate of 300 µL min^{-1} was used. The oven and tray temperature were set at 25°C and 20°C, respectively. The photodiode array detector (PDA) measured a wavelength range of 200-600 nm. UV-absorbance at 254 nm was used for analysis of 2-AB labeled gluco-oligosaccharides.

Samples were further analyzed using an LTQ-Velos mass spectrometer (Thermo Scientific) equipped with an ESI-MS. Data was collected over a *m/z* range of 90 to 1500 in positive (PI) mode. MS settings were optimized with LTQ-tune. Therefore, a 2-AB labeled cellobiose solution (see section above) was diluted 100 times in the correct elution conditions (12.5% (v/v) B). A splitter was used to combine

the flow of sample (10 µL min^{-1}) to the flow of mobile phases (12.5% (v/v) B at 290 µL min^{-1}). The ion optics were optimized on *m/z* 463.1. A capillary temperature of 250°C, a source heater temperature of 200°C, a sheath gas flow rate of 42, an auxiliary gas flow rate of 10, a sweep gas flow rate of 0 and ion spray voltage of 4.0 kV were determined to be optimal.

4.4.8 Identification of non-reductively 2-AB labeling of non-oxidized and C4-oxidized gluco-oligosaccharides

Samples were analyzed by using RP-UHPLC-UV-ESI-MS as described above with a modified elution profile: From 0 to 1 min an isocratic elution of 2% (v/v) B, from 1 to 31 min a linear gradient to 18% (v/v) B, from 31 to 36 min a linear gradient to 100% (v/v) B, from 36 to 37 min an isocratic elution of 100% (v/v) B, from 36 to 37 min a linear gradient to 2% (v/v) B and from 37 to 45 an isocratic elution of 2% (v/v) B. MS settings were used as described above.

4.4.9 Reductive amination of 2-AB labeled C4-oxidised gluco-oligosaccharides using deuterated borohydride

The supernatant (500 µL) obtained from the incubation of RAC incubated with *Mt*LPMO9C was dried under vacuum and labeled according to the protocol of reductive labeling as described above with the following changes. The dried samples were mixed with a freshly prepared 2-AB solution 12.5 µL (19.1 mg mL^{-1} DMSO containing 60% (v/v) acetic acid). Subsequently, 37.5 µL of $NaBD_4$ (1 mg mL^{-1} DMSO only) was added. Upon mixing of the reducing agent solution (37.5 µL) and 2-AB solution (12.5 µL) a final DMSO:acetic acid ratio equal to 85:15 was achieved. Samples were incubated and further purified by using Bond Elute cellulose columns as described above. Samples were analyzed by using RP-UHPLC-UV-ESI-MS as described above with a modified elution profile: From 0 to 1 min an isocratic elution of 5% (v/v) B, from 1 to 31 min a linear gradient to 50% (v/v) B, from 31 to 32 min a linear gradient to 100% (v/v) B, from 32 to 36 min an isocratic elution of 100% (v/v) B, from 36 to 37 min a linear gradient to 5% (v/v) B and from 37 to 45 an isocratic elution of 5% (v/v) B. MS settings were used as described above.

References

1 Vaaje-Kolstad G, Westereng B, Horn SJ, Liu Z, Zhai H, Sorlie M *et al*. An oxidative enzyme boosting the enzymatic conversion of recalcitrant polysaccharides. Sci. 2010;330(6001):219-22.

2 Phillips CM, Beeson WT, Cate JH, Marletta MA. Cellobiose dehydrogenase and a copper-dependent polysaccharide monooxygenase potentiate cellulose degradation by *Neurospora crassa*. ACS Chem. Biol. 2011;6(12):1399-406.

3 Forsberg Z, Vaaje-Kolstad G, Westereng B, Bunaes AC, Stenstrom Y, MacKenzie A *et al*. Cleavage of cellulose by a CBM33 protein. Prot. Sci. : A Publication of the Protein Society. 2011;20(9):1479-83.

4 Westereng B, Ishida T, Vaaje-Kolstad G, Wu M, Eijsink VG, Igarashi K *et al*. The putative endoglucanase *Pc*GH61D from *Phanerochaete chrysosporium* is a metal-dependent oxidative enzyme that cleaves cellulose. PLoS ONE. 2011;6(11):e27807.

5 Frommhagen M, Sforza S, Westphal AH, Visser J, Hinz SW, Koetsier MJ *et al*. Discovery of the combined oxidative cleavage of plant xylan and cellulose by a new fungal polysaccharide monooxygenase. Biotechnol Biofuels. 2015;8:101.

6 Beeson WT, Phillips CM, Cate JH, Marletta MA. Oxidative cleavage of cellulose by fungal copper-dependent polysaccharide monooxygenases. J. Am. Chem. Soc. 2012;134(2):890-2.

7 Quinlan RJ, Sweeney MD, Lo Leggio L, Otten H, Poulsen JC, Johansen KS *et al*. Insights into the oxidative degradation of cellulose by a copper metalloenzyme that exploits biomass components. Proc. Natl. Acad. Sci. U.S.A. 2011;108(37):15079-84.

8 Westereng B, Arntzen MØ, Aachmann FL, Várnai A, Eijsink VGH, Agger JW. Simultaneous analysis of C1 and C4 oxidized oligosaccharides, the products of lytic polysaccharide monooxygenases acting on cellulose. J. Chromatogr. A. 2016:46-54.

9 Isaksen T, Westereng B, Aachmann FL, Agger JW, Kracher D, Kittl R *et al*. A C4-oxidizing lytic polysaccharide monooxygenase cleaving both cellulose and cello-oligosaccharides. J. Biol. Chem. 2014;289(5):2632-42.

10 Westereng B, Agger JW, Horn SJ, Vaaje-Kolstad G, Aachmann FL, Stenstrom YH, Eijsink VG. Efficient separation of oxidized cello-oligosaccharides generated by cellulose degrading lytic polysaccharide monooxygenases. J. Chromatogr. A. 2013;1271:144-152.

11 Agger JW, Isaksen T, Varnai A, Vidal-Melgosa S, Willats WG, Ludwig R *et al*. Discovery of LPMO activity on hemicelluloses shows the importance of oxidative processes in plant cell wall degradation. Proc. Natl. Acad. Sci. U.S.A. 2014;111(17):6287-92.

12 Appeldoorn MM, Kabel MA, Van Eylen D, Gruppen H, Schols HA. Characterization of oligomeric xylan structures from corn fiber resistant to pretreatment and simultaneous saccharification and fermentation. *J. Agric. Food Chem*. 2010;58:11294-11301.

13 Jonathan MC, Bosch G, Schols HA, Gruppen H. Separation and identification of individual alginate oligosaccharides in the feces of alginate-fed pigs. J. Agric. Food Chem. 2013;61:553-560.

14 Kabel MA, van den Borne H, Vincken J-P, Voragen AGJ, Schols HA. Structural differences of xylans affect their interaction with cellulose. Carbohydr. Polym. 2007;69:94-105.

15 Leijdekkers AGM, Huang J-H, Bakx EJ, Gruppen H, Schols HA. Identification of novel isomeric pectic oligosaccharides using hydrophilic interaction chromatography coupled to traveling-wave ion mobility mass spectrometry. Carbohydr. Res. 2015;404:1-8.

16 Ruhaak LR, Steenvoorden E, Koeleman CAM, Deelder AM, Wuhrer M. 2-Picoline-borane: A non-toxic reducing agent for oligosaccharide labeling by reductive amination. Proteomics. 2010;10:2330-2336.

17 Harvey DJ. Derivatization of carbohydrates for analysis by chromatography; electrophoresis and mass spectrometry. J. Chromatogr. B. 2011;879:1196-1225.

18 Abdel-Magid AF, Mehrman SJ. A review on the use of sodium triacetoxyborohydride in the reductive amination of ketones and aldehydes. Org. Process Res. Dev. 2006;10:971-1031.

19 Sato S, Sakamoto T, Miyazawa E, Kikugawa Y. One-pot reductive amination of aldehydes and ketones with α-picoline-borane in methanol, in water, and in neat conditions. Tetrahedron. 2004;60:7899-7906.

20 Frommhagen M, Koetsier MJ, Westphal AH, Visser J, Hinz SWA, Vincken J-P *et al*. Lytic polysaccharide monooxygenases from *Myceliophthora thermophila* C1 differ in substrate preference and reducing agent specificity.Biotechnol. Biofuels. 2016;9:1-17.

21 Bennati-Granier C, Garajova S, Champion C, Grisel S, Haon M, Zhou S *et al*. Substrate specificity and regioselectivity of fungal AA9 lytic polysaccharide monooxygenases secreted by *Podospora anserina*. Biotechnol. Biofuels. 2015;8:90.

22 Vincken J-P, de Keizer A, Beldman G,. Voragen AGJ. Fractionation of xyloglucan fragments and their interaction with cellulose. Plant Physiol. 1995;108:1579-1585.

23 Jonathan MC, van Brussel M, Scheffers MS, Kabel MA. Characterisation of branched gluco-oligosaccharides to study the mode-of-action of a glucoamylase from *Hypocrea jecorina*.Carbohydr. Polym. 2015;132:59-66.

24 Domon B, Costello CE. A systematic nomenclature for carbohydrate fragmentations in FAB-MS/MS spectra of glycoconjugates. Glycoconjugate J. 1988;5:397-409.

25 Ye W, Seneviratne UI, Chao MW, Ravindra KC, Wogan GN, Tannenbaum SR, Skipper PL. Transimination of quinone imines: A mechanism for embedding exogenous redox activity into the nucleosome. Chem. Res. Toxicol. 2012;25:2627-2629.

26 Caesar JP, Sheeley DM, Reinhold VN. Femtomole oligosaccharide detection using a reducing-end derivative and chemical ionization mass spectrometry. Anal. Biochem. 1990;191:247-252.

27 Snovida SI, Chen VC, Perreault H. Use of a 2,5-dihydroxybenzoic acid/aniline MALDI matrix for improved detection and on-target derivatization of glycans: A preliminary report. Anal. Chem. 2006;78:8561-8568.

28 Nekiunaite L, Petrović DM, Westereng B, Vaaje-Kolstad G, Abou Hachem M, Várnai A, Eijsink VGH. *Fg*LPMO9A from *Fusarium graminearum* cleaves xyloglucan independently of the backbone substitution pattern. FEBS Lett. 2016;590(19):3346-3356.

29 Lattová E, Perreault H. The usefulness of hydrazine derivatives for mass spectrometric analysis of carbohydrates. Mass Spectrom. Rev. 2013;32:366-385.

30 Ruhaak LR, Zauner G, Huhn C, Bruggink C, Deelder AM, Wuhrer M. Glycan labeling strategies and their use in identification and quantification. Anal. Bioanal. Chem. 2010;397:3457-3481.

Additional Files

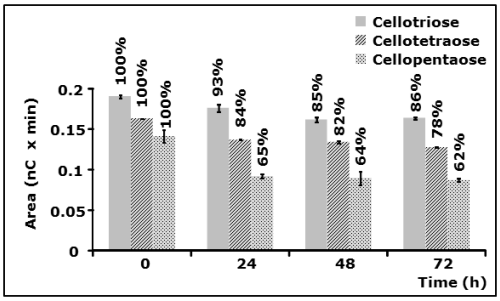

Additional Figure 4.1. Gluco-oligosaccharides incubated with cellulose. Regenerated amorphous cellulose (RAC, 1 mg mL^{-1}) was incubated with either cellotriose, cellotetraose or cellopentaose (2.5 µg mL^{-1}) in the presence of ascorbic acid (1 mM) for 24, 48 and 72 h. The percentages indicate the remaining gluco-oligosaccharide concentrations after an incubation time of 24, 48 and 72 h compared to non-incubated samples (0 h). Samples were incubated in an ammonium acetate buffer pH 5.0 at 50°C. Samples were prepared in duplicate and analyzed by HPAEC (see Methods).

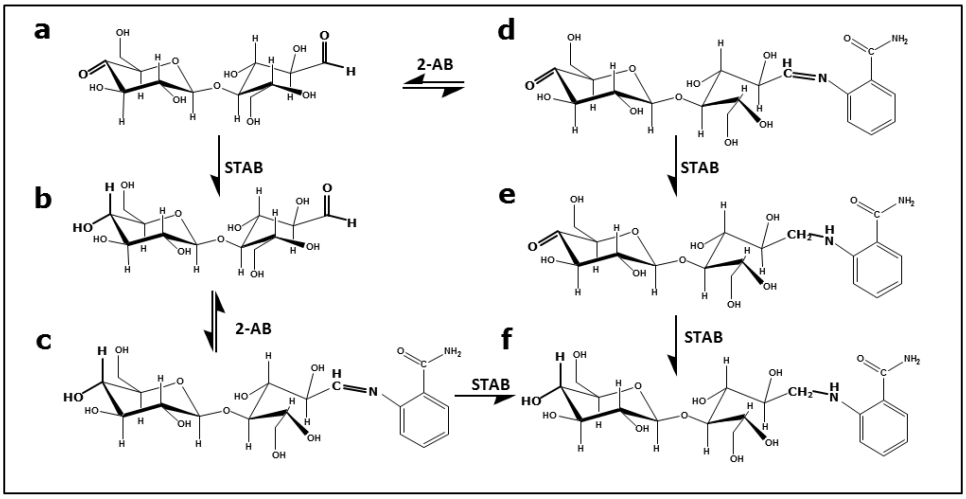

Additional Figure 4.2. Proposed reaction pathways of reductive 2-AB labeling of cellobiose and C4-oxidised cellobiose with STAB as a reducing agent. **a** C4-oxidised cellobiose; **b** cellobiose; **c** non-reduced 2-AB labeled cellobiose; imine; **d** 2-AB labeled C4-oxidized cellobiose; imine; **e** reduced 2-AB labeled C4-oxidized cellobiose; amine; **f** reduced 2-AB labeled cellobiose; amine. Reactive groups are enlarged and indicated in bold.

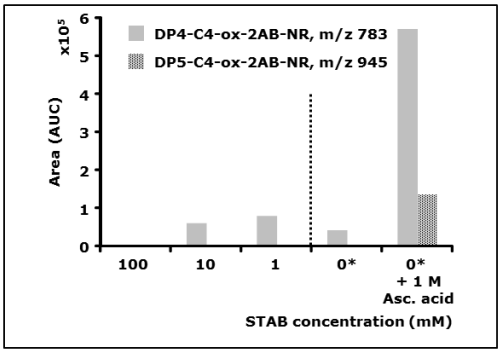

Additional Figure 4.3. Effect of STAB and ascorbic acid on the formation of non-reductively 2-AB labeled C4-oxidized gluco-oligosaccharides. The formed imines of non-reductively 2-AB labeled C4-oxidized gluco-oligosaccharides were analyzed by RP-UHPLC-UV-MS/MS. The areas were obtained from the extracted ion chromatogram (EIC) of non-reductively 2-AB labeled C4-oxidized cellotetraose (grey bar, DP4-C4-ox-2AB-NR, *m/z* 783) and cellopentaose (shaded grey bar, DP5-C4-ox-2AB-NR, *m/z* 945), respectively. In the first experiment, 500 µL of the supernatant from RAC incubated with *Mt*LPMO9C was labeled with 2-AB in the presence of different STAB concentrations (100, 10 and 0 mM). In a second experiment, 250 µL of the supernatant was labeled with 2-AB in the absence of STAB (0 mM, with and without ascorbic acid addition (1 mM)) and the injection volume was 50% compared to the first experiment (marked with *). The results of the two experiments are separated by the dashed line.

Chapter V

Boosting LPMO-driven lignocellulose degradation by polyphenol oxidase-activated lignin building blocks

Based on: Frommhagen M, Mutte SK, Westphal AH, Koetsier MJ, Hinz SWA, Visser J, Vincken J-P, Weijers D, van Berkel WJH, Gruppen H, Kabel MA. Boosting LPMO-driven lignocellulose degradation by polyphenol oxidase-activated lignin building blocks. *Biotechnology for Biofuels*. 2017; 10:121.

Abstract

Many fungi boost the deconstruction of lignocellulosic plant biomass via oxidation by using lytic polysaccharide monooxygenases (LPMOs). The application of LPMOs is expected to contribute to ecologically friendly conversion of biomass into fuels and chemicals. Moreover, applications of LPMO-modified cellulose-based products may be envisaged within the food or material industry.

Here, we show an up to 75-fold improvement in LPMO-driven cellulose degradation by using polyphenol oxidase-activated lignin building blocks. This concerted enzymatic process involves the initial conversion of monophenols into diphenols by the polyphenol oxidase *Mt*PPO7 from *Myceliophthora thermophila* C1, and the subsequent oxidation of cellulose by *Mt*LPMO9B. Interestingly, *Mt*PPO7 shows preference towards lignin-derived methoxylated monophenols. Sequence analysis of genomes of 336 Ascomycota and 208 Basidiomycota reveals a high correlation between *Mt*PPO7 and AA9 LPMO genes.

The activity towards methoxylated phenolic compounds distinguishes *Mt*PPO7 from well-known PPOs, such as tyrosinases, and ensures that *Mt*PPO7 is an excellent redox partner of LPMOs. The correlation between *Mt*PPO7 and AA9 LPMO genes is indicative for the importance of the coupled action of different monooxygenases in the concerted degradation of lignocellulosic biomass. These results will contribute to a better understanding in both lignin deconstruction and enzymatic lignocellulose oxidation and potentially improve the exploration of eco-friendly routes for biomass utilization in a circular economy.

5.1 Background

Fungal carbohydrate converting enzymes are considered important for eco-friendly application in plant biomass degradation. The resulting carbohydrates are sources for the production of biochemicals or biofuels and new enzymatically modified cellulose-based products are envisaged for the future.

Next to carbohydrates, phenolic compounds are also major components of lignocellulosic plant biomass. Phenolic compounds are present either as free molecules or in conjugated form as part of lignin or bound to carbohydrates. Lignin is one of the major constituents of (secondary) plant cell walls, together with the polysaccharides cellulose and hemicellulose. Lignin is composed of the three aromatic monolignol units: coniferyl, sinapyl and *para*-coumaryl alcohol. Cellulose consists of β-(1→4)-linked glucosyl chains that interact with each other via hydrogen bonds and van der Waals forces, which results in the formation of crystalline cellulose fibrils. Unlike cellulose, hemicellulose is a heteropolymer varying in its monosaccharide composition and linkages between the monosaccharides. Examples are xylan, mannan or β-(1→3, 1→4)-linked β-glucan. Hemicellulose interacts with lignin through ester and ether linkages, thereby forming a network that embeds the cellulose microfibrils [1, 2].

Recent studies focused on the function of lytic polysaccharide monooxygenases (LPMOs) have confirmed that these enzymes drive the oxidative degradation of cellulose, and they are considered important for the enzymatic degradation of plant biomass [3]. LPMOs are classified based on their sequence in the Carbohydrate Active enzyme (CAZy;[4]) database as auxiliary activity (AA) families AA9, AA10, AA11 and AA13. In brief, LPMOs have been reported to oxidize β-(1→4)-linked glucan chains at either the C1- or C4-carbon position or both, resulting in the cleavage of glucan chains [3, 5, 6]. Other LPMOs of these AA families have been described to oxidize the (1→4)-linkage of chitin, xylan, hemicellulose such as xyloglucan and glucomannan, soluble cellodextrines and starch [7-11].

In order to oxidize polysaccharides, LPMOs demand electrons to activate molecular oxygen in their copper-containing active site [3, 5, 6]. The electrons can be donated by reducing agents, like low molecular weight compounds (ascorbic acid, gallic acid) or the macromolecule lignin [12-14]. Other ways of providing LPMOs with electrons have been reported, such as flavocytochrome-dependent cellobiose dehydrogenases (CDHs), light induced pigments, light-driven chemical oxidation of water or diphenol regenerating GMC-(glucose-methanol-choline-oxidase/dehydrogenase) oxidoreductases [5, 12, 15, 16]. The mechanistic understanding of electron donation systems is highly relevant in order to enable optimization of LPMO activity, and, thereby, plant biomass degradation.

Phenolic compounds, including small molecular weight compounds that serve as lignin building blocks and lignin, are intrinsically present in plant biomass and are natural electron donors for LPMO activity. However, monophenols are not optimal electron donors for LPMO activity, because of their relatively high redox potential [12]. Compounds with a 1,2-benzenediol or a 1,2,3-benzenetriol moiety have, compared to monophenols, a lower redox potential [13]. Their low redox potential enables them to reduce the copper ion in the active site of LPMOs and enhance the LPMO activity [12].

The enzymatic oxidation of phenolic compounds is a well-known reaction in many natural environments. For example, it causes browning of food products, contributes to taste in tea fermentation and plays a role in plant biomass decomposition [17-19]. These oxidative systems involve the activity of laccases (EC.1.10.3.2), peroxidases (EC.1.11.1), tyrosinases (EC.1.14.18.1) and catechol oxidases (EC 1.10.3.1) [18-20]. In particular tyrosinases, also often referred to as polyphenol oxidases, are of interest due to their ability to hydroxylate phenolic compounds [21]. This so-called monophenolase activity typically involves the *ortho*-hydroxylation of monophenols into *ortho*-diphenols, compounds that comprise a 1,2-benzenediol moiety. Tyrosinases also exhibit diphenolase activity, which is characterized by the oxidation of these *ortho*-diphenols into *ortho*-quinones [22]. With respect to biomass degradation, the diphenolase activity of polyphenol oxidases is not conductive to polysaccharides oxidation since *ortho*-quinones cannot be utilized by LPMOs [12]. Based on their monophenolase activity, tyrosinases have been shown to use non-methoxylated monophenols as substrates, rather than using methoxylated monophenols, that are the predominant structural units of lignin [23].

In this study we investigated if polyphenol oxidases, in particular tyrosinases, can enhance LPMO activity. Therefore, the tyrosinase *Mt*PPO7 from *Myceliophthora thermophila* C1 was used, which showed activity towards phenolic compounds and was obtained from DuPont Industrial Biosciences. In addition, we used the commercially available tyrosinase *Ab*PPO from the white button mushroom *Agaricus bisporus*. Both tyrosinases were each incubated with the previously described *Mt*LPMO9B in the presence of various plant phenolic compounds and cellulose [13, 24]. We found that *Mt*PPO7 is highly active towards methoxylated monophenols, including monomeric lignin building blocks. This activity can strongly boost the release of oxidized gluco-oligosaccharides as catalyzed by *Mt*LPMO9B and thereby the degradation of cellulose. In addition, we found a strong correlation between genes encoding *Mt*PPO like proteins and AA9 LPMOs in fungal genomes of 336 Ascomycota and 208 Basidiomycota.

5.2 Results

5.2.1 *Mt*PPO7 addition improves cellulose oxidation by *Mt*LPMO9B

Our previous results have shown that reducing agents with a 1,2-benzenediol or 1,2,3-benzenetriol moiety gave the highest release of non-oxidized and C1-oxidized gluco-oligosaccharides from regenerated amorphous cellulose (RAC) incubated with three *Mt*LPMOs compared to the incubation with compounds comprising only a single hydroxyl group [13]. Hence, in the current research we hypothesized that *Mt*LPMO activity can benefit from enzymes which have hydroxylating capacity, such as polyphenol oxidases (**Figure 5.1**) [21]. We choose *Mt*PPO7, which originates like the *Mt*LPMO9B employed here, from the thermophilic filamentous fungus *Myceliophthora thermophila* C1. As a reference, the well-studied tyrosinase *Ab*PPO from the edible mushroom *Agaricus bisporus* was used [19, 25, 26-28].

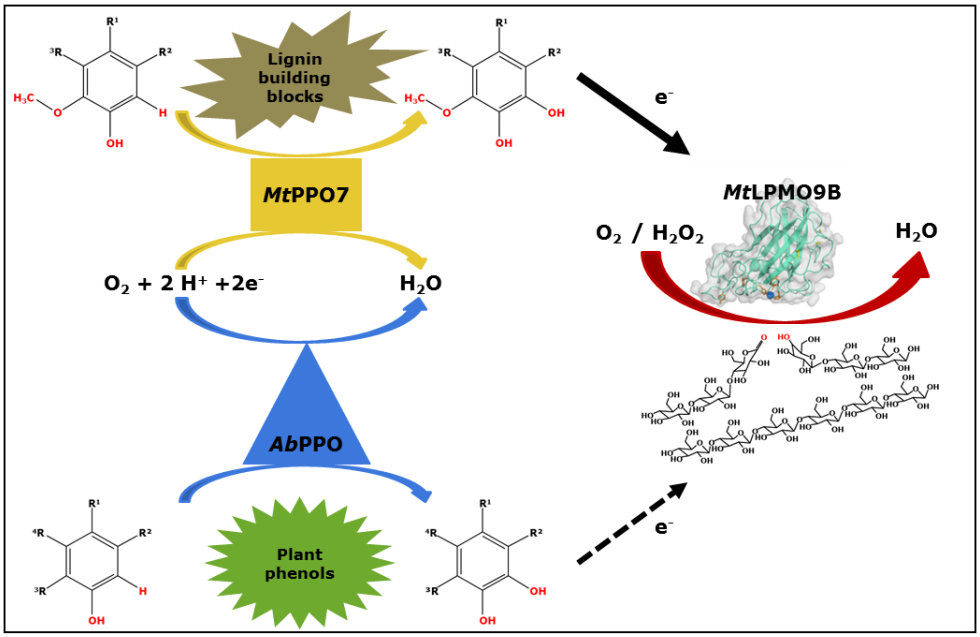

Figure 5.1 Schematic presentation of the concerted action of polyphenol oxidases and LPMOs. Monophenols with a 1-hydroxy, 2-methoxy moiety are hydroxylated by *Mt*PPO7 from *M. thermophila* C1. The resulting methoxylated catechols are excellent electron donors for *Mt*LPMO9B activity. In comparison to *Mt*PPO7, the mushroom tyrosinase *Ab*PPO is able to convert non-methoxylated monophenols into compounds comprising a 1,2-benzenediol moiety. The released compounds comprising a 1,2-benzenediol moiety are able to donate electrons for *Mt*LPMO9B activity. However, *Ab*PPO exhibits a strong diphenolase activity which reduces the available amount of these compounds comprising a 1,2-benzenediol moiety for *Mt*LPMO9B due to further oxidation of these compounds into *ortho*-quinones (indicated by dashed arrow).

The activity of *Mt*LPMO9B towards RAC, with and without addition of *Mt*PPO7, was determined by using 21 phenolic compounds as potential electron donors. Many of these phenolic compounds are methoxylated as these are the predominant structural units of lignin. Results are presented in **Table 5.1** and **Figure 5.2**. The 21 different phenolic compounds used were classified into three groups and further divided into subgroups, as previously described [13]. In short, group I represents compounds comprising one hydroxyl group, group II compounds comprising a 1,2-benzenediol moiety and group III compounds comprising a 1,2,3-benzenetriol moiety (**Figure 5.2**, **Table 5.1**).

As expected, from our previous research [13], monophenols (group Ia) are less efficient electron donors for *Mt*LPMO9B, with the exception of 4-hydroxybenzoic acid (no. 1). The low *Mt*LPMO9B activity towards RAC resulted in a very small amount of released non-oxidized and C1-oxidized gluco-oligosaccharides (**Figure 5.2**, **Table 5.1**, **Additional Figure 5.1**). The addition of *Mt*PPO7 to RAC incubated with *Mt*LPMO9B did not increase the electron donor capacities of this group Ia compounds, except for *para*-coumaric acid (no. 3). In contrast, the addition of *Mt*PPO7 to RAC incubated with *Mt*LPMO9B in the presence of methoxylated monophenols (group Ib, compounds with a 1-hydroxy, 2-methoxy moiety) led in all cases to a high increase (up to ± 75 times, no. 5) in the release of non-oxidized and C1-oxidized gluco-oligosaccharides (**Figure 5.2**, **Additional Figure 5.1**). Similarly, the oxidative cleavage of RAC incubated with *Mt*LPMO9B increased, when *Mt*PPO7

was added to group Ic compounds, which comprise a 1-hydroxy-2,6-dimethoxy moiety. For group IIa, IIb and III phenolic compounds, the addition of *Mt*PPO7 to incubations of RAC with *Mt*LPMO9B led to a moderate increase of non-oxidized and C1-oxidized gluco-oligosaccharides (4 to 39%), with one exception (no. 19) (**Table 5.1**, **Figure 5.2**).

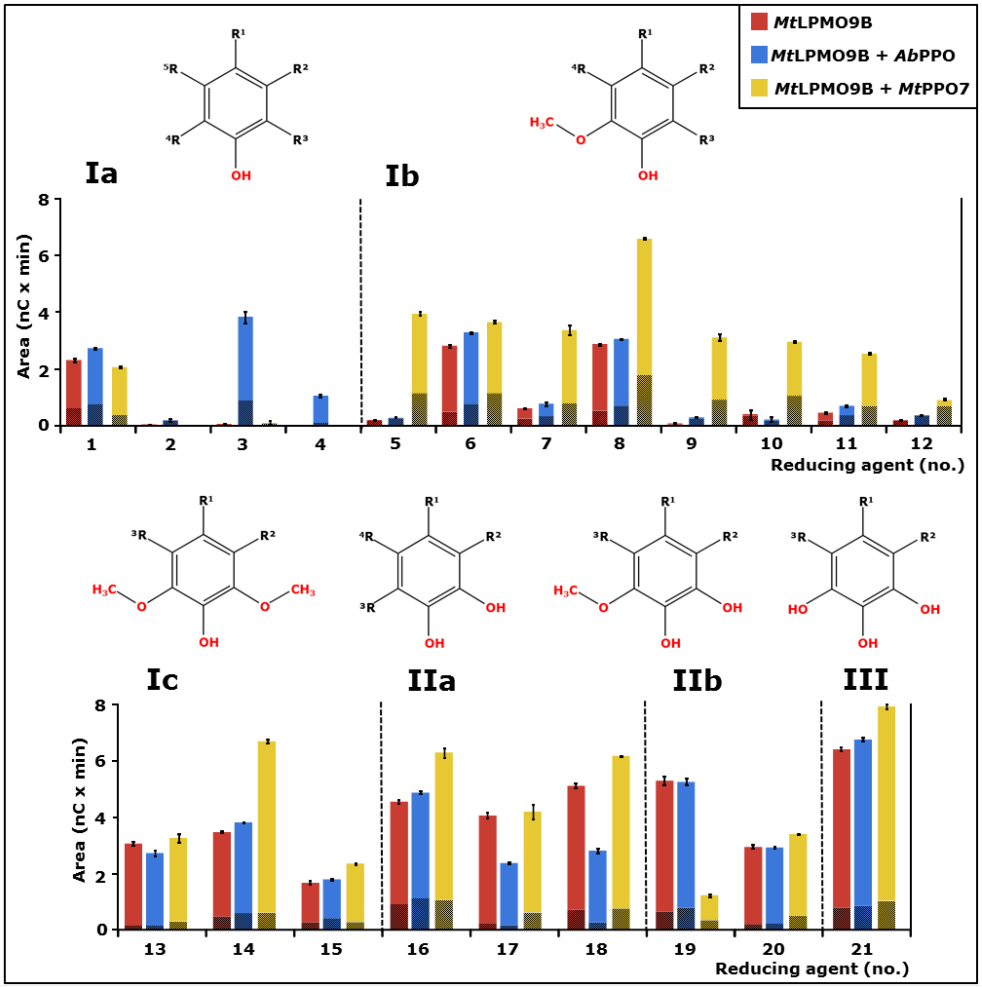

Figure 5.2 RAC incubated with *Mt*LPMO9B with or without *Mt*PPO7 or *Ab*PPO addition in the presence of 21 reducing agents. The numbers are total sums of the integrated peak areas of released non-oxidized (shaded red, blue and yellow) and C1-oxidized (red, blue and yellow) gluco-oligosaccharides after incubation of regenerated amorphous cellulose (RAC; 1.5 mg mL^{-1}) with *Mt*LPMO9B only (red bars) (5.0 µg mL^{-1}), *Mt*LPMO9B together with *Ab*PPO (blue bars, 2.5 µL mL^{-1}) or *Mt*LPMO9B together with *Mt*PPO7 (yellow bars) (5.0 µg mL^{-1}) based on HPAEC. The reducing agents (2 mM) are numbered (X-axis) and specified in **Table 5.1**. Vertical dotted lines separate the reducing agents into groups (I, II, II) and subgroups (a, b, c). Group I, monophenols **Ia**, compounds with a 1-hydroxy,2-methoxy moiety **Ib** or a 1-hydroxy-2,6-dimethoxy moiety **Ic**. Group **II**, compounds with 1,2-benzenediols moiety **IIa** and compounds with a 1,2-dihydroxy-3-methoxy moiety **IIb**. Group III, reducing agents with a 1,2,3-benzenetriol moiety **III**. All incubations were performed in duplicate and the standard deviations are represented by error bars. See Methods for details.

Incubations performed with *Ab*PPO showed deviating results from corresponding experiments with *Mt*PPO7. First, unlike *Mt*PPO7, addition of *Ab*PPO to non-methoxylated monophenols (group Ia) resulted in increased levels of non-oxidized and C1-oxidized oligosaccharides during the incubation of RAC with *Mt*LPMO9B. This different activity was expected on the basis of the known hydroxylating capacity of *Ab*PPO towards non-methoxylated monophenolic compounds. Especially, the addition of *Ab*PPO in the presence of *para*-coumaric acid (no. 3) increased *Mt*LPMO9B-catalysed degradation of RAC compared to the incubation without *Ab*PPO (**Figure 5.2**, **Table 5.1**). Different from *Mt*PPO7, *Ab*PPO addition to group Ib, Ic, II and III compounds did not or, compared to *Mt*PPO7, improved *Mt*LPMO9B catalyzed RAC degradation relatively moderate (5 to 361%, **Table 5.1**), or even decreased RAC degradation by 1 to 44% (**Figure 5.2**, **Table 5.1**).

Table 5.1. RAC incubated with *Mt*LPMO9B only and with *Ab*PPO or *Mt*PPO7 addition in the presence of 21 reducing agnets[a]

Gr.	Sub-group	No.	Reducing agent	Activity [%] *Mt*LPMO9B[b]	Activity [%] *Mt*LPMO9B + *Ab*PPO[c]	Activity [%] *Mt*LPMO9B + *Mt*PPO7[c]
I	a	1	4-hydroxybenzoic acid	100	119	90
		2	*ortho*-cresol	100	**778**	2
		3	*para*-coumaric acid	100	**9,938**	**2,851**
		4	phenol	0[d]	>**0**[d]	0[d]
I	b	5	3-hydroxy-4-methoxycinnamic acid	100	**151**	**7,558**
		6	4-hydroxy-3-methoxyphenylactone	100	117	131
		7	coniferyl aldehyde	100	128	**562**
		8	ferulic acid	100	107	**231**
		9	guaiacol	100	**461**	**5,143**
		10	hesperidin	100	56	**771**
		11	homovanillic acid	100	**156**	**580**
		12	vanillic acid	100	**196**	**495**
I	c	13	4-allyl-2,4-methoxyphenol	100	89	108
		14	sinapic acid	100	110	**195**
		15	syringic acid	100	107	142
II	a	16	3,4-dihydroxybenzoic acid	100	99	139
		17	3-methylcatechol	100	58	104
		18	caffeic acid	100	55	122
II	b	19	3,4-dihydroxy-5-methoxybenzoic acid	100	99	22
		20	3,4-dihydroxy-5-methoxycinnamic acid	100	99	116
III		21	gallic acid	100	105	124

[a]Division based on functional groups of reducing agents (**Figure 5.2**).

[b]Total release of non-oxidized and C1-oxidized gluco-oligosaccharides from RAC incubated with *Mt*LPMO9B set to 100%

[c]Increased (**bold** ≥ 50% increase) or decreased percentage of released non-oxidized and C1-oxidized gluco-oligosaccharides from RAC incubated with *Mt*LPMO9B with addition of either *Ab*PPO or *Mt*PPO7 compared to the release of non-oxidized and C1-oxidized gluco-oligosaccharides from RAC incubated with *Mt*LPMO9B alone. Sum of areas of released non-oxidized and C1-oxidized gluco-oligosaccharides are shown in **Figure 5.2**. See Methods for more information.

[d]No reference due to absent activity of *Mt*LPMO9B towards RAC in the presence of phenol (**Figure 5.2**)

5.2.2 *Mt*LPMO9B-mediated cellulose oxidation in the presence of *Mt*PPO7 by using time-dependent incubations

The ability of *Mt*PPO7 to convert methoxylated phenolic compounds and to increase the oxidative degradation of RAC by *Mt*LPMO9B was further investigated by using time-dependent incubations (24 h). These incubations were performed in the presence of two methoxylated monophenols (guaiacol and ferulic acid, group Ib), as well as in the presence of a non-methoxylated *ortho*-diphenol (3-methylcatechol, group IIa) (**Figure 5.3**, **Additional Figure 5.2**). After 4 hours of incubation, a steady *Mt*PPO7-induced oxidation of guaiacol (no. 9) was observed (**Additional Figure 5.3**). At the same time, the amounts of released non-oxidized and C1-oxidized gluco-oligosaccharides by *Mt*LPMO9B from RAC also increased steadily (**Figure 5.3c**). A similar trend for the release of non-oxidized and C1-oxidized gluco-oligosaccharides was shown for the incubation with ferulic acid (no. 8, **Additional Figure 5.2**). *Mt*PPO7 showed a relatively low efficiency towards 3-methylcatechol (no. 17) compared to guaiacol (**Table 5.1**, **Additional Figure 5.3**). As reported above, no significant increase of *Mt*LPMO9B released non-oxidized and C1-oxidized gluco-oligosaccharides from RAC was observed when comparing incubations with and without *Mt*PPO7 (**Figure 5.3d**). In presence of *Mt*PPO7 though, the initial rate (0 – 6 h) of released non-oxidized and C1-oxidized gluco-oligosaccharides was lower compared to the incubation without *Mt*PPO7 (**Figure 5.3d**).

5.2.3 Activity of *Mt*PPO7 towards methoxylated phenolic compounds

The most striking observation from the experiments described above is the conversion of methoxylated phenolic compounds by *Mt*PPO7 into products, which enhance the oxidative degradation of cellulose by *Mt*LPMO9B. The fate of these phenolic compounds upon *Mt*PPO7 incubation was further studied in the absence of *Mt*LPMO9B by using UHPLC-UV-MS^n.

Based on UV measurements, non-methoxylated phenolic compounds of group Ia, group IIa and group III remained constant in concentration during *Mt*PPO7 incubation, showing that *Mt*PPO7 has a low activity towards compounds comprising a 1,2-benzenediol moiety (**Figure 5.4**, **Additional Table 5.1**). Different from *Mt*PPO7, in previous research *Ab*PPO has been reported to be highly active towards these types compounds [19, 24, 25].

*Mt*PPO7 was active towards *all* eight methoxylated monophenols (group Ib) tested. Based on UV, the concentrations of group Ib compounds decreased during *Mt*PPO7 incubation between 28% and 67% compared to the same compounds incubated without *Mt*PPO7 (**Figure 5.4**). Three types of *Mt*PPO7 reactions were observed based on mass differences between substrate and products formed (**Additional Table 5.1**): A) hydroxylation (*m*/*z* + 16; e.g. no. 5 and 7), B) decarboxylation (*m*/*z* -44, e.g. no. 8) and C) demethylation (*m*/*z* -14, e.g. no. 11). Especially the hydroxylation of methoxylated phenolic compounds is a key reaction, since the products formed comprise a second hydroxyl group. The formed *ortho*-diphenols are known to be efficient electron donors for LPMOs. Decarboxylation and demethylation occurred either in the presence of *Mt*PPO7 or as a result of polymerization reactions in both the presence and absence of *Mt*PPO7. Several group Ib compounds spontaneously formed dimers in the absence of *Mt*PPO7 (no. 8 or no. 11). These dimers were almost absent when group Ib compounds were incubated with *Mt*PPO7 (**Additional Table 5.1**). Similar to group Ib compounds, the concentrations of compounds comprising a 1-hydroxyl-2,6-dimethoxy moiety (group Ic) incubated with *Mt*PPO7 decreased, based on UV, between 6% and 64% compared to the incubation without *Mt*PPO7 (**Figure 5.4**, **Additional Table 5.1**. Again, masses indicating decarboxylation (-44 Da) and demethylation (-14 Da) reactions were formed. *Mt*PPO7 was also able

to convert group IIb compounds (up to 87% substrate conversion, no. 20) that comprise a 1,2-dihydroxy-3-methoxy moiety (**Figure 5.4**). The reactions observed were decarboxylation (*m/z* -44, e.g. no. 19) and dimerization (e.g. no. 20) of group IIb compounds based on masses formed (**Additional Table 5.1**).

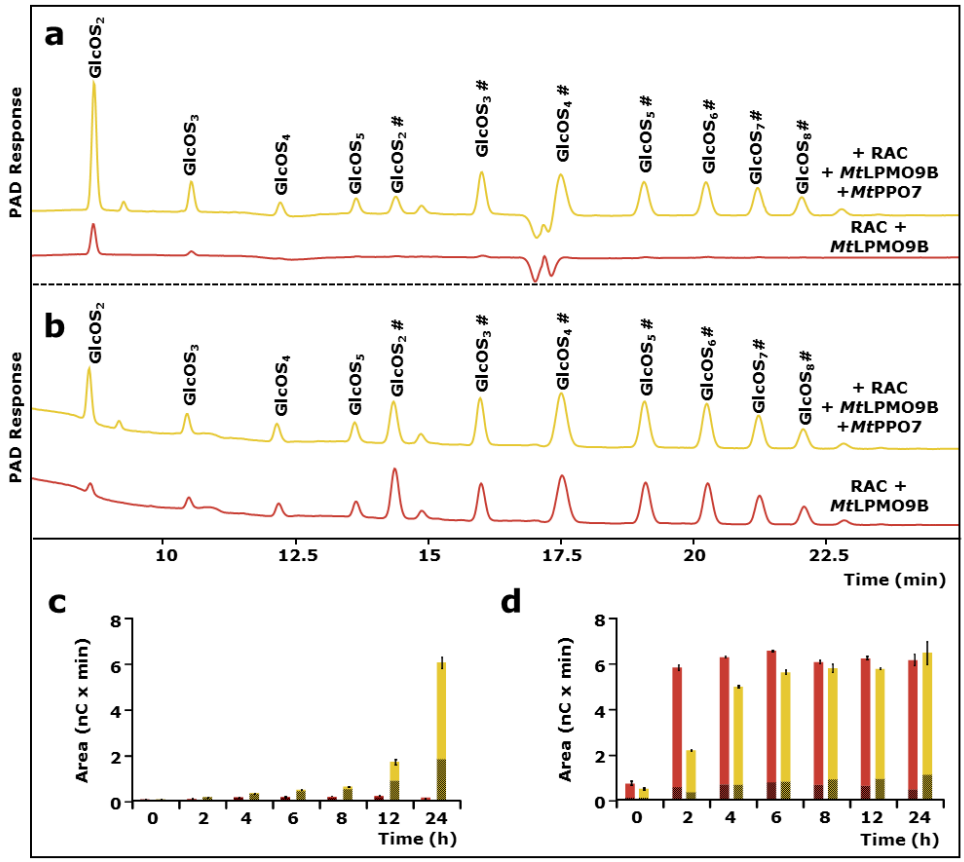

Figure 5.3 Activity of *Mt*LPMO9B towards amorphous cellulose in the presence and absence of *Mt*PPO7. HPAEC elution pattern of regenerated amorphous cellulose (RAC; 1.5 mg mL^{-1}) incubated with *Mt*LPMO9B (5.0 µg mL^{-1}) with (yellow) and without (red) *Mt*PPO7 (5.0 µg mL^{-1}) addition in the presence of **a** guaiacol (no. 9 specified in **Table 5.1**, 2 mM) and **b** 3-methylcatechol (no. 17 specified in **Table 5.1**, 2 mM) after 24 h. The incubation of RAC with *Mt*LPMO9B results in the formation of non-oxidized gluco-oligosaccharides ($GlcOS_n$) and C1-oxidized gluco-oligosaccharides ($GlcOS_n^{\#}$). Based on HPAEC, integrated peak areas are shown as the total sum of released non-oxidized (shaded red and yellow) and C1-oxidized (red and yellow) gluco-oligosaccharides after incubation of RAC (1.5 mg mL^{-1}) with *Mt*LPMO9B only (red bars, 5.0 µg mL^{-1}) and *Mt*LPMO9B together with *Mt*PPO7 (yellow bars, 5.0 µg mL^{-1}) in the presence of **c** guaiacol and **d** 3-methylcatechol. All incubations were performed in duplicate, and the standard deviations are presented as error bars. See Methods for data analysis and details.

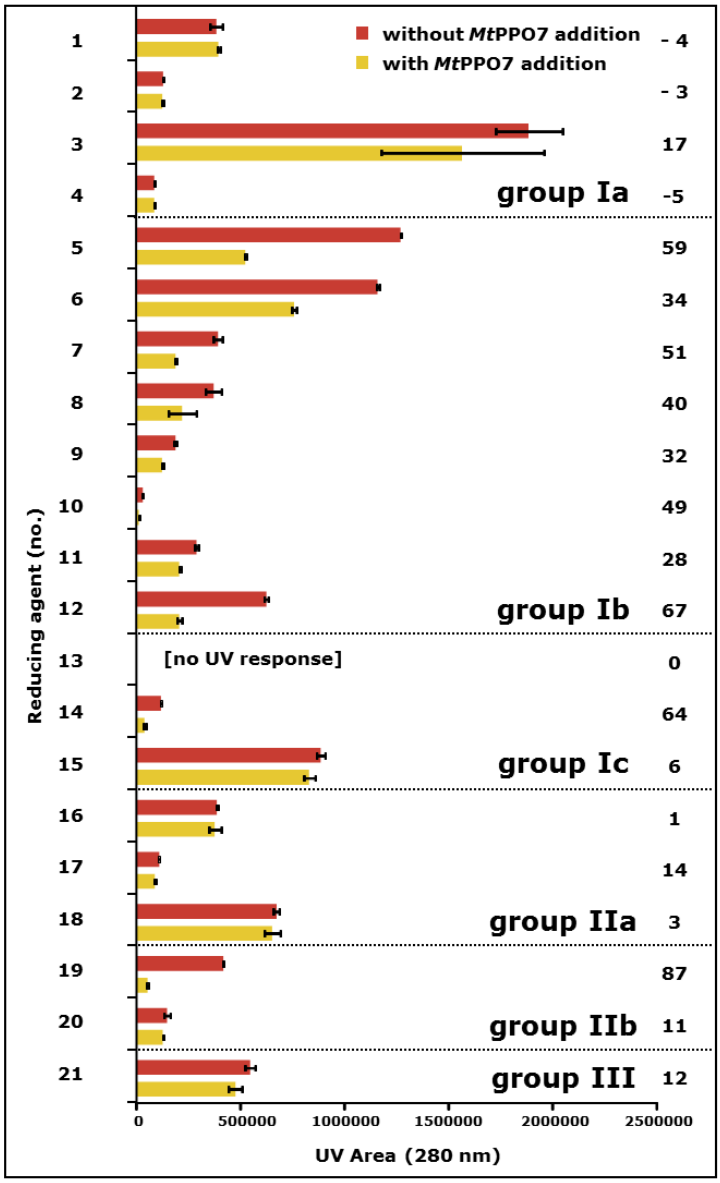

Figure 5.4 UV response areas of 21 reducing agents incubated in the presence and absence of *Mt*PPO7. The total sum is shown of integrated peak areas of 21 reducing agents (2 mM) with (yellow bar) and without (red bar) addition of *Mt*PPO7 (5.0 µg mL^{-1}). The reducing agents are numbered (bold on the left) and specified in **Table 5.1**. Samples were incubated in a 50 mM potassium phosphate buffer (pH 6.0) containing 2.5 µM copper(II)-chloride for 24 h at 50°C and measured by UHPLC-UV (280 nm). Bold numbers on the right: reducing agents conversion (%) by *Mt*PPO7, which is based on the difference of integrated peak areas (UV 280 nm) of the reducing agents incubated with *Mt*PPO7 compared to the incubation of reducing agents only. All incubations were performed in duplicate. See Methods for details.

In general, most phenolic compounds (such as no. 17 and no. 21) that were incubated with *Mt*PPO7 formed insoluble complexes, which likely result from polymerization reactions of *ortho*-quinones formed. These insoluble complexes were not determined by UHPLC-UV-MS^n. The complexation of *ortho*-quinones resulted, obviously, in a decrease of the UV signal of the substrates (**Figure 5.4**, **Additional Figure 5.4**).

5.2.4 Conversion of guaiacol and 3-methylcatechol by *Mt*PPO7

For a better discrimination between monophenolase and diphenolase activity, *Mt*PPO7 conversion of guaiacol and 3-methylcatechol was monitored over a period of 24 hours by UHPLC-UV-MS^n. The conversion of guaiacol by *Mt*PPO7 resulted in the initial formation of 3-methoxycatechol (**Additional Table 5.1**, **Additional Figure 5.4** and **5.5**). Further reactions resulted in the formation of brown pigments indicating that 3-methoxycatechol was oxidized into *ortho*-quinones, which are likely to polymerize and form insoluble complexes. Other masses determined by UHPLC-UV-MS^n indicated the polymerization of guaiacol and compounds originating from the oxidation of guaiacol by *Mt*PPO7 into trimers (*m/z* 399, 401, 415). Based on the masses detected (**Additional Table 5.1** and **Additional Figure 5.4**), a scheme is presented of possible reaction pathways of guaiacol occurring during *Mt*PPO7 incubation (**Additional Figure 5.5**).

The oxidation of guaiacol by *Mt*PPO7 mainly occurred between 4 to 8 hours of incubation, whereas 3-methylcatechol showed to be oxidized by *Mt*PPO7 within the first two hours. During the incubation of 3-methylcatechol with *Mt*PPO7 pink pigments are formed, which precipitate after sample centrifugation. Based on MS^n, masses of 3-methylcatechol (*m/z* 123) and masses indicating the dimerization of 3-methylcatechol (*m/z* 245) were detected upon incubation of both 3-methylcatechol with *Mt*PPO7 and 3-methylcatechol alone (**Additional Table 5.1**). No detectable amounts of new products were formed during the incubation of 3-methylcatechol with *Mt*PPO7 compared to the incubation of 3-methylcatechol only (**Additional Table 5.1**).

5.2.5 Structural model of *Mt*PPO7

A structural model of *Mt*PPO7 was generated based on the available structure of a catechol oxidase from *Aspergillus oryzae* (*Ao*CO4, Protein Data Bank entry: 4j3p) (**Figure 5.5**). *Mt*PPO7 and *Ao*CO4 share 38% amino acid sequence identity. The structural model of *Mt*PPO7 shows a four-helix bundle fold with the presence of six conserved histidines coordinating the two copper ions in the active site, which is typical for PPO-like tyrosinases and catechol oxidases. Six of the seven cysteines are involved in conserved disulfide bridges (Cys47-Cys393, Cys75-Cys134 and Cys196-Cys234) and expected to be relevant for the thermo-tolerance of *Mt*PPO7 (**Figure 5.5**). Based on the model, the large distance (10.5 Å) between the sulfur atom of Cys302 and Cε-atom of His110 prevents formation of a thioether bond, which is present in other PPOs such as *Ab*PPO3 and *Ab*PPO4 [25]. Characteristics of the amino acid sequence and structural model of *Mt*PPO7 are further described in the Discussion section.

5.2.6 Genome-wide analysis of AA9 LPMO, *Ab*PPO and *Mt*PPO7

Sequence annotations of 336 Ascomycota and 208 Basidiomycota genomes [29] were used in this analysis. Some of the numbers of genes obtained encoding AA9 LPMOs, were verified by comparison with published data. For example, we have identified 22 and 18 genes encoding AA9 LPMOs in *M. thermophila* and *T. terrestis*, respectively, which is similar to previously reported results [30]. In total, 277 Ascomycota genomes and 178 Basidiomycota genomes contained AA9 LPMOs encoding

genes (**Figure 5.6**). The two PPOs used in this work are regarded as two different proteins due to their low sequence identity of 12%. The two PPO classes used for the genome analysis were not further divided into short and long tyrosinases [31]. Over 90% of the Ascomycota that comprise genes encoding AA9 LPMOs showed also the presence of genes encoding either *Ab*PPO-like, *Mt*PPO7-like proteins or both (**Figure 5.6a**). In contrast, only around 40% of the AA9 LPMOs encoding Basidiomycota contained genes that encode *Ab*PPO-like, *Mt*PPO7-like proteins or both. The percentage of Ascomycota and Basidiomycota genomes studied that contained neither genes encoding AA9 LPMOs*, Ab*PPOs nor *Mt*PPO7s, were 15% and 8%, respectively (**Figure 5.6a**). The average number of genes found per genome encoding AA9 LPMOs was higher in Ascomycota (13.0) than in Basidiomycota (10.6) (**Figures 5.6b** and **5.6c**). Both the total and the average number of genes encoding *Ab*PPO-like and *Mt*PPO7-like proteins were also higher in Ascomycota compared to Basidiomycota (**Figures 5.6b** and **5.6c**).

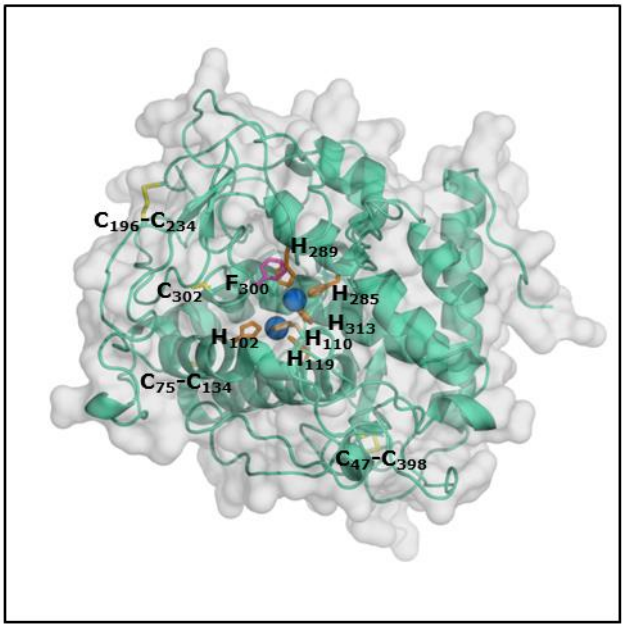

Figure 5.5 Structural model of *Mt*PPO7. The structural model of *Mt*PPO7 was generated based on the crystal structure of a catechol oxidase from *Aspergillus oryzae* (*Ao*CO4, Protein Data Bank entry: 4j3p)[42]. *Mt*PPO7 and *Ao*CO4 share an amino acid sequence identity of 38%. The *Mt*PPO7 model is predominantly α-helical with the catalytic copper site situated in the four-helix bundle. The coordination of the two copper atoms (blue) by six histidine residues (orange) is strictly conserved. The three disulfide bridges Cys47-Cys398, Cys75-Cys134 and Cys196-Cys234 (yellow) are also conserved.

Principal Component Analysis (PCA) was performed on all 336 Ascomycota and 208 Basidiomycota. In addition, we used the numbers which describe the presence of AA9 LPMO, *Mt*PPO7s and *Ab*PPOs encoding genes in each fungal species. The first two components of the PCA explained 69.8% and 19.7% variation in the data, respectively. Correlations of 0.75 and 0.5 were observed between the presence of genes encoding AA9 LPMOs and *Mt*PPO7s in Ascomycota and Basidiomycota, respectively. (**Figure 5.7b**). Lower correlations of 0.59 and 0.34 were observed in the genes encoding

AA9 LPMOs and *Ab*PPOs. No correlation (correlation ≤ 0.25) was observed between *Ab*PPOs and *Mt*PPO7, for both Ascomycota and Basidiomycota. Based on the presence of at least 10 annotated genes that encode cellulose degrading enzymes per fungus, 27 Ascomycota and 23 Basidiomycota genomes were selected (**Additional Table 5.2**, **Additional Table 5.3**) [32]. The selected 27 Ascomycota genomes showed a higher correlation (0.60) between genes encoding AA9 LPMOs and *Mt*PPO7s compared to the 23 selected Basidiomycota (0.53) (**Figure 5.7c**). Also, no correlation was found between genes encoding *Mt*PPO7- and *Ab*PPO-like genes in the selected Basidiomycota species (**Figure 5.7**).

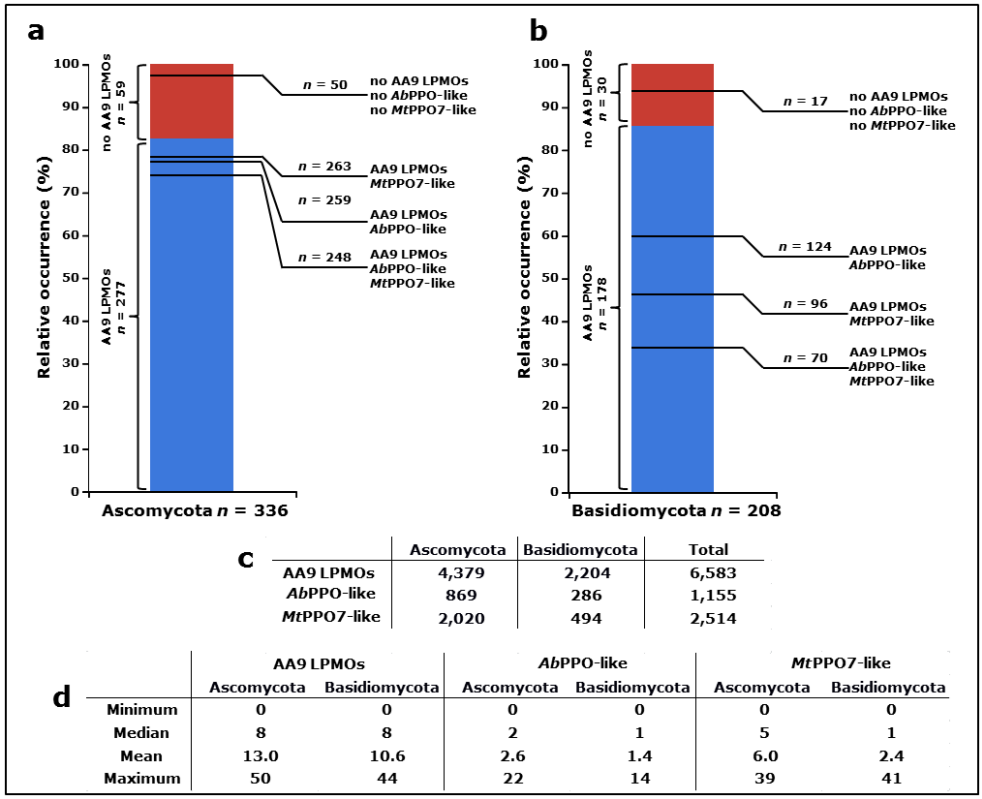

c

	Ascomycota	Basidiomycota	Total
AA9 LPMOs	4,379	2,204	6,583
*Ab*PPO-like	869	286	1,155
*Mt*PPO7-like	2,020	494	2,514

d

	AA9 LPMOs		*Ab*PPO-like		*Mt*PPO7-like	
	Ascomycota	Basidiomycota	Ascomycota	Basidiomycota	Ascomycota	Basidiomycota
Minimum	0	0	0	0	0	0
Median	8	8	2	1	5	1
Mean	13.0	10.6	2.6	1.4	6.0	2.4
Maximum	50	44	22	14	39	41

Figure 5.6 Genome analysis of Ascomycota and Basidiomycota. The protein sequence annotations of 336 Ascomycota and 208 Basidiomycota genomes were used for genome analysis. In total, **a** 277 Ascomycota and **b** 178 Basidiomycota comprise AA9 LPMOs encoding genes (blue column). Next to this occurrence of AA9 LPMOs encoding genes in Ascomycota and Basidiomycota, the co-occurrence of both *Ab*PPO-like and *Mt*PPO7-like, or either *Ab*PPO-like or *Mt*PPO7-like enzymes is indicated on the right of each column. The number of Ascomycota and Basidiomycota without co-occurrence of AA9 LPMOs encoding genes was 59 and 30, respectively (red column). In total, 50 Ascomycota and 17 Basidiomycota species were determined that do not carry any genes encoding AA9 LPMOs, *Ab*PPOs and *Mt*PPO7s. **c** Total number of AA9 LPMOs, *Ab*PPOs and *Mt*PPO7s encoding genes annotated in 336 Ascomycota and 208 Basidiomycota genomes. **d** Distribution of annotated AA9 LPMOs, *Ab*PPOs and *Mt*PPO7s encoding genes within 336 Ascomycota and 208 Basidiomycota genomes. See Methods for details.

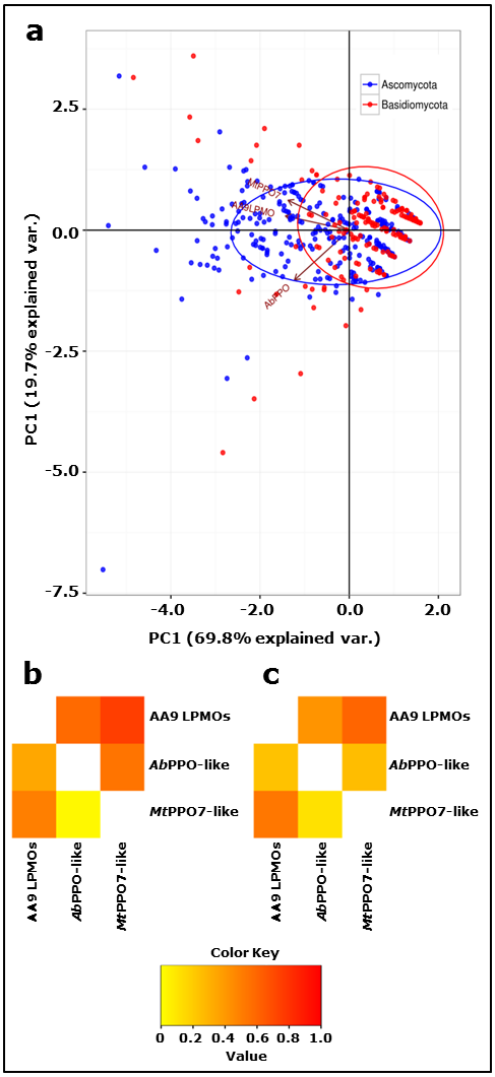

Figure 5.7 Statistical genome analysis of Ascomycota and Basidiomycota. **a** Principal component analysis (PCA) of genes encoding AA9 LPMOs, *Ab*PPOs and *Mt*PPO7s of 336 Ascomycota and 208 Basidiomycota genomes. The numbers which describe the presence of genes encoding AA9 LPMOs, *Mt*PPO7s and *Ab*PPOs in each fungal species were used as variables and are presented as principal components of Ascomycota (red dots) and Basidiomycota (blue dots). The first two components of the PCA explained 69.8% and 19.6% variation in the data, respectively. Vectors (red arrows) with a similar orientation illustrate a high correlation between the gene families (see **b**). The axis legends indicate the overall contribution of the three gene families encoding AA9 LPMOs, *Ab*PPOs and *Mt*PPO7s. **b** Correlation between the three gene families encoding AA9 LPMOs, *Ab*PPOs and *Mt*PPO7s of 336 Ascomycota (upper triangle) and 208 Basidiomycota (lower triangle). **c** Correlation between genes encoding AA9 LPMOs, *Ab*PPOs and *Mt*PPO7s of 27 Ascomycota (upper triangle) and 23 Basidiomycota (lower triangle), which have at least ten annotated genes encoding cellulose degrading enzymes per fungus. Species of both fungal classes are listed in **Additional Table 5.2** and **Additional Table 5.3**. Numerical values of the correlations of **b** and **c** are presented in **Additional Figure 5.6**. See Methods for details.

5.3 Discussion

5.3.1 *Mt*PPO7 enhances cellulose oxidation by *Mt*LPMO9B

Many PPOs, tyrosinases in particular, have been described to oxidize monophenols and various phenolic compounds comprising a 1,2-benzenediol or 1,2,3-benzenetriol moiety. However, none of these tyrosinases show a high activity towards methoxylated compounds (group Ib) such as ferulic acid (no. 8) [33-36]. Importantly, *Mt*PPO7 hydroxylates methoxylated phenolic compounds (group Ib) and thereby improves the activity of *Mt*LPMO9B up to 75 times (no. 5, **Table 5.1**). On the other hand, *Ab*PPO addition to RAC incubated with *Mt*LPMO9B in the presence *non-methoxylated* monophenols also resulted in a significant increase of the *Mt*LPMO9B activity (up to 99 times). Especially the activity of *Mt*PPO7 towards methoxylated phenolic compounds is of high relevance, as these compounds are abundant as structural lignin units and, therefore, intrinsically present during plant biomass degradation. Here, we only determined the effect of polyphenol oxidases on the LPMO-mediated cellulose degradation in the presence of phenolic compounds that are known as lignin building blocks but we did not, for example, investigate the impact of these enzymes in the presence of washed or unwashed pretreated biomass. In comparison to the substrate used in this thesis, we expect a lower effect of *Mt*PPO7-like enzymes on the LPMO-mediated substrate oxidation by using pretreated biomass, since this biomass contains a mixture of multiple potential electron donating compounds, which were described in an earlier study [13].

A recent study described that H_2O_2, in addition to or instead of O_2 (**Figure 5.1**), acts as a co-substrate for LPMOs, while reducing agents are still needed to activate the active site copper [37]. Once copper is activated, LPMOs oxidize substrates under the use of H_2O_2. The latter can be formed by the reduction of O_2 through reducing agents [37]. Considering these recent findings, it can only be hypothesized how *Mt*PPO7 increased the *Mt*LPMO9B-mediated cellulose oxidation, which was investigated in our research. It is possible that the oxidation of the phenolic compounds led to the formation of compounds that have either an enhanced reducing efficiency on *Mt*LPMO9B or led to an enhanced H_2O_2 generation which increased the *Mt*LPMO9B activity.

5.3.2 Activity of *Mt*PPO7 towards phenolic compounds

Based on our results, we conclude that *Mt*PPO7 improves the activity of *Mt*LPMO9B by two main reactions. First, *Mt*PPO7 hydroxylates methoxylated monophenols at the *ortho*-position (monophenolase activity) and forms compounds comprising a 1,2-benzenediol moiety. These compounds have, compared to methoxylated monophenols, a lower redox potential and are known to be good electron donors for LPMOs [12-14]. Secondly, *Mt*PPO7 inhibits the formation of non-enzymatic coupling reactions, which occurred during the incubation of several cinnamic acid derivatives in the absence of *Mt*PPO7, but were not formed when *Mt*PPO7 was present during the incubations (**Additional Table 5.1**). Non-enzymatic coupling reactions of cinnamic acid derivatives of group I, II or III result in the formation of bulky phenolic polymers. The aliphatic acrylic acid (prop-2-enoic acid) group present in cinnamic acid derivatives constitutes an elongation of the conjugated aromatic ring. This group takes part in polymerization reactions, which can be caused by radical formation due to the presence of copper (2.5 µM) [18, 38]. However, it remains unclear, how *Mt*PPO7 prevents (*reduces*) the polymerization of cinnamic acid derivatives.

Importantly, *Mt*PPO7 showed only a low efficiency towards non-methoxylated compounds comprising a 1,2-benzenediol or 1,2,3-benzenetriol moiety. In contrast to *Ab*PPO, *Mt*PPO7 had no inhibitory effect on the *Mt*LPMO9B activity towards RAC in the presence of these phenolic compounds (**Table 5.1**). Although we did not determine the formation of *ortho*-quinones, it is possible that *Mt*PPO7 further oxidizes methoxylated compounds comprising a 1,2-benzenediol moiety into *ortho*-quinones due to the observed pigment formation (**Additional Figure 5.4**, **Additional Figure 5.5**). However, this pigment formation could also partly result from non-enzymatic polymerization reactions or formation of metal-catechol complexes, as indicated in **Figure 5.8** [39]. Still, based on the monophenolase activity we would consider *Mt*PPO7 to be a tyrosinase. The low efficiency of *Mt*PPO7 to convert compounds comprising a 1,2-benzenediol moiety is expected to be an advantage. *Mt*LPMO9B can utilize these compounds as electron donors and improve the oxidative activity towards cellulose. In the case of a strong diphenolase activity, however, the available amount of these compounds comprising a 1,2-benzenediol moiety would rapidly decrease due to further oxidation of these compounds into *ortho*-quinones. Hence, we expect for some other PPOs, such as *Ab*PPO, a negative effect on the LPMO-mediated cellulose oxidation. This effect results from the strong activity of these PPOs towards compounds comprising a 1,2-benzenediol or 1,2,3-benzenetriol moiety, which are potential reducing agents for LPMOs [33, 40, 41]. The *ortho*-quinones formed (no. 17 and 18) (**Figure 5.2**, **Table 5.1**) have been shown to be less efficient electron donors for LPMOs than their *ortho*-diphenol precursors [12].

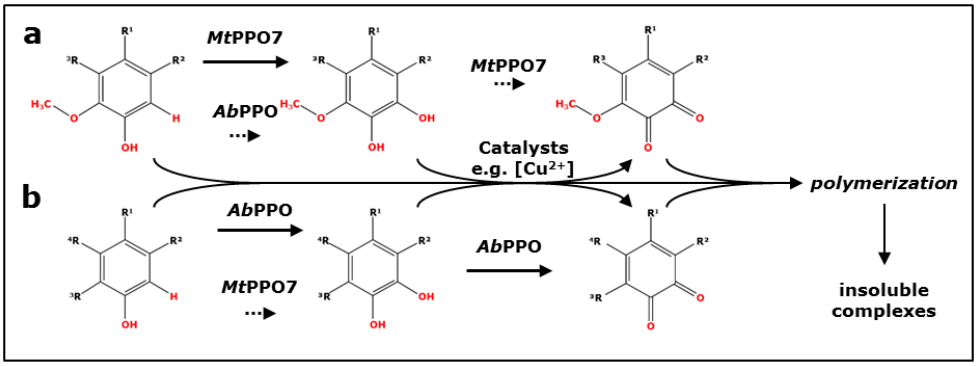

Figure 5.8 Proposed reaction pathway of *Mt*PPO7- and *Ab*PPO-mediated oxidation of phenolic compounds. **a** Phenolic compounds comprising a 2-methoxy moiety are hydroxylated by *Mt*PPO7 from *M. thermophila* C1 at the 6-position. Different from *Mt*PPO7, *Ab*PPO from *A. bisporus* shows a low efficiency (dotted arrows) towards these methoxylated monophenols. The formed compounds comprising a 1,2-dihydroxy-3-methoxy moiety have, compared to the methoxylated monophenols, a lower electron potential and an increased electron donating capacity for LPMOs. **b** Non-methoxylated monophenols are hydroxylated at the *ortho*-position by *Ab*PPO into compounds comprising a 1,2-benzenediol moiety, whereas *Mt*PPO7 shows a low efficiency (dotted arrows) towards non-methoxylated monophenols. The formed compounds comprising a **a** 1,2-dihydroxy-3-methoxy and **b** 1,2-benzenediol moiety are expected to be further oxidized into *ortho*-quinones by either the *Mt*PPO7- and *Ab*PPO-mediated or catalysts-mediated oxidation, such as copper which was present during the incubation. As indicated in **Additional Figure 5.5**, these *ortho*-quinones, including intermediate products formed by the oxidation of phenolic compounds, are expected to polymerize and form insoluble complexes.

5.3.3 Structural characteristics of *Mt*PPO7

The structural model of *Mt*PPO7 shows a four-helix bundle architecture with the presence of six histidine residues coordinating the two copper ions in the active site, which is typical for PPO-like tyrosinases and catechol oxidases (**Figure 5.5**). We clearly showed that the preference of *Mt*PPO7 towards methoxylated phenolic compounds and the low activity towards diphenols is different from reported fungal or plant catechol oxidases and tyrosinases (**Figure 5.4**). Here, we further discuss the structure-function relationship of these PPOs in comparison with the generated model of *Mt*PPO7. However, it should be noted that the structural model of *Mt*PPO7 was generated based on a catechol oxidase from *Aspergillus oryzae* (*Ao*CO4) and both proteins share an overall amino acid sequence identity of only 38% [42]. It has already been shown that marginal structural differences determine whether PPOs exhibit a stronger monophenolase or diphenolase activity [43]. Based on our model, it is possible that structural features discussed below deviate compared to the crystal structure which is, however, not available yet.

Firstly, the presence of a thioether bridge between a cysteine and histidine is assumed to be important for the monophenolase and diphenolase activity. This bond has been described to be present in many fungal PPOs, such as *Ab*PPO3/4 from *A. bisporus*, *Nc*PPO from *Neurospora crassa,* and also in plant catechol oxidases, such as *Ib*CO from *Iponema batatas* [26, 44, 45]. However, similar to *Ao*CO4 from *A. oryzae* [42], *Mt*PPO7 does not form this thioether bond (**Figure 5.5**). Secondly, *Mt*PPO7 shows the presence of the PPO typical 'gate residue' (Phe300 in *Mt*PPO7, Phe261 in *Ib*CO and Val299 in *Ao*CO4). It has been hypothesized that a bulky 'gate residue', such as a phenylalanine, limits the accessibility of monophenols to the copper A ion (CuA) and therefore, might be a limiting factor for the monophenolase activity [44, 46]. However, in *Ao*CO4 the bulky phenylalanine is replaced by Val299 and still *Ao*CO4 shows a rather low activity towards monophenols [31, 42]. Our data suggests, that Phe300 in *Mt*PPO7 does not limit the accessibility for (methoxylated) monophenols. Thirdly, it also has recently been proposed that the presence of certain amino acid residues next to the CuB-coordinating histidines indicates whether a tyrosinase or catechol oxidase exhibits a stronger monophenolase and a weak diphenolase activity or a weak monophenolase and a strong diphenolase activity [43]. However, none of the described amino acid residues at that specific position (Pro, Asn, Glu and Gln) is present in *Mt*PPO7, which has a tyrosine (Tyr268) at the corresponding position. In *Mt*PPO7 a tyrosine (Tyr268) occupies. Whether Tyr268 is responsible for the observed specificity towards methoxylated monophenols can only be hypothesized at this moment. Fourthly, *Mt*PPO7 shares with tyrosinases and catechol oxidases the characteristic 'tyrosine motif' (Tyr-X-Tyr/Phe or Tyr/Phe-X-Tyr; in *Mt*PPO7 residues 399-401). This motif is highly conserved among plants and fungi [31, 42, 47]. Fifthly, *Mt*PPO7 does not contain the 'YG motif' (Gly-Tyr motif), which is a typical feature of fungal tyrosinases and catechol oxidases [47]. In conclusion, based on substrate specificity (**Figure 5.1**) and modelled structure (**Figure 5.5**), we do not classify *Mt*PPO7 as a typical tyrosinase or catechol oxidase.

5.3.4 Genome analysis

Based on genome analysis, we found a positive correlation between genes encoding AA9 LPMOs and *Mt*PPO7-like enzymes in Ascomycota and Basidiomycota, which has not been shown previously. Interestingly, this correlation strengthens the evidence that fungi benefit from the concerted activity of AA9 LPMOs and *Mt*PPO7-like enzymes in nature, which is in agreement with major findings obtained from the experimental data of this work. The proportion of annotated AA9 LPMOs within

Ascomycota and Basidiomycota (82 and 86%, respectively) is about 5-10% lower with the findings of a recent study (92% in Ascomycota and Basidiomycota), which may result from the different species chosen (**Figure 5.6**) [12]. The two PPOs (*Mt*PPO7 and *Ab*PPO) used in this work share only a low sequence identity and, therefore, are considered to belong to different subgroups of polyphenol oxidases. It is important to realize that active tyrosinases, such as the mushroom tyrosinase *Ab*PPO3, have been described to consist of large (H) and small (L) subunits [45, 48]. We focused for the genome analysis on genes encoding the protein of the catalytic H subunit, which contains the highly conserved binuclear copper site. The function of the L subunit is so far not known [45]. All purified enzymes used in this work are secreted. However, we did not differentiate between secreted and non-secreted fungal AA9 LPMOs and PPOs in the genome analysis. It may be that most of the enzymes detected here take part in the external fungal metabolism, as can be deducted from the high abundance of the annotated *Mt*PPO7s and *Ab*PPOs throughout Ascomycota and Basidiomycota. We, therefore, specifically selected genomes of plant biomass degrading fungi that contain at least ten genes encoding known cellulose degrading enzymes per fungus and found again a similar correlation between genes encoding AA9 LPMOs, *Ab*PPOs and *Mt*PPO7s (**Figure 5.7**) [32, 49]. In contrast to *Mt*PPO7s, genes encoding *Ab*PPOs showed a weak correlation with AA9 LPMOs in Ascomycota and Basidiomycota (**Figure 5.7**), especially for the selected cellulose degrading Basidiomycota (**Figure 5.7c**). One possible explanation is that a cellulose rich environment is associated with the abundance of lignin as seen in soft- and hardwoods. Still, there may be considerable variation in the substrate specificity and specific activity of PPOs within the *Mt*PPO7- or *Ab*PPO-like gene families. The latter seems to be consistent with the low sequence identity among PPOs and, in addition, by the diverse substrate specificities of PPOs that have only marginal differences in their amino acid sequence [31, 43, 50].

5.4 Conclusions

For the first time, we demonstrate the importance of the coupled action of different monooxygenases in the concerted degradation of plant biomass. We demonstrated that *Mt*PPO7 is particularly active towards methoxylated phenolic compounds that are the predominant structural units of lignin. This feature distinguishes *Mt*PPO7 from the well-known mushroom tyrosinase *Ab*PPO, which stimulates the LPMO activity via its ability to hydroxylate non-methoxylated monophenols. However, its strong diphenolase activity limits the applicability of this tyrosinase for producing electron donating capacity for LPMOs. In addition, we established that genes encoding *Mt*PPO7-like enzymes and AA9 LPMOs are highly correlated throughout Ascomycota and Basidiomycota, suggesting that AA9 LPMOs benefit from the activity of *Mt*PPO7-like enzymes in nature. Further understanding in both lignin deconstruction and enzymatic lignocellulose oxidation will lead to more eco-friendly routes for biomass utilization, which is seen as a prerequisite for a circular economy.

5.5 Methods

5.5.1 Enzyme expression, production and purification

*Mt*PPO7 (UniProt: KX772412) was over-expressed in the a homologous *Myceliophthora thermophila* C1 strain. A low protease/low (hemi-)cellulase producing *M. thermophila* C1 strain was used to produce *Mt*PPO7 [51, 52]. The *Mt*PPO7-containing culture broth was fractionated to obtain a pure *Mt*PPO7 preparation. This preparation was provided by DuPont Industrial Biosciences. *Mt*LPMO9B was expressed and purified as described in [13].

5.5.2 Protein identification

The pure *Mt*PPO7 fraction was analyzed by LC–mass spectrometry confirming the presence of the *Mt*PPO7 by 'The Scripps Research Institute' (San Diego, CA, USA).

5.5.3 Purification and identification of mushroom tyrosinase

Tyrosinase from the edible button mushroom *Agaricus bisporus* was purified from a commercial enzyme preparation (Sigma-Aldrich, Steinheim, Germany) as described previously [25]. The purified enzyme preparation (referred to as *Ab*PPO) was shown to contain the isoforms PPO3 and PPO4 [25].

5.5.4 Cellulose substrate and reducing agents

Regenerated amorphous cellulose (RAC) was prepared from Avicel PH-101 as described previously [7, 53]. All reducing agents used throughout this study (**Table 5.1**) were purchased from Sigma-Aldrich (Steinheim, Germany).

5.5.5 Incubation conditions for *Mt*LPMO9B, *Mt*PPO7 and *Ab*PPO

Regenerated amorphous cellulose (1-2 mg mL^{-1}, see Figure captions) was dissolved in a 50 mM ammonium acetate buffer (pH 5.0), with or without addition of reducing agents (final concentration of 2 mM). The standard enzyme concentrations of *Mt*LPMO9B, *Mt*PPO7 and *Ab*PPO used in this work were 5.0, 5.0 and 0.7 µg protein mg^{-1} substrate, respectively. All samples were incubated for 20 h at 50°C in a head-over-tail rotator in portions of 1 mL total volume (Stuart rotator, Bibby Scientific, Stone, UK) at 20 rpm. Supernatants of all incubations were analyzed by HPAEC and RP-UHPLC-UV-ESI-MS^n.

5.5.6 Oligosaccharide analysis

Oligosaccharides were analyzed by high-performance anion exchange chromatography (HPAEC) with pulsed amperometric detection (PAD) using a HPAEC system (ICS-5000, Dionex, Sunnyvale, CA, USA) as described previously [7].

5.5.7 RP-UHPLC-UV-ESI-MS^n analysis

Supernatants of all incubations were subjected to an Accela reversed phase high-performance liquid chromatography (RP-UHPLC) system coupled to electron spray ionization mass spectrometry (Thermo Scientific, San Jose, CA, USA). Injected samples (5µL) were separated using a Aquidity C18 column (2.1 x 150 mm, 1.7 µm particle size) with an Acquity UHPLC Shield RP18 Vanguard guard column (2.1 x 5 mm, 1.7 µm particle size). Both columns were purchased from Waters (Milford, MA, USA). Gradient elution with eluent A (H_2O + 1% (v/v) acetonitrile + 0.1% (v/v) HOAc) and eluent B (acetonitrile + 0.1% (v/v) HOAc) was performed according to the following steps: From 0 to 17.7 min a linear gradient from 5% to 60% B; from 17.7 to 21.7 min, isocratic 100% B, and from 21.7 to 26

min, isocratic 5% B. The flow rate and the injection volume were 0.4 mL min^{-1} and 5 µL, respectively. The column temperature was set to 30°C and the photodiode array detector was operated in the range of 200-400 nm.

Samples were further analyzed by using an LTQ-Velos mass spectrometer (Thermo Scientific) equipped with a ESI-MS. Data was collected over a *m/z* range of 90 to 1500 in both negative (NI) and positive (PI) mode. The collision energy was set to 35%.

5.5.8 Structural modelling

An alignment was made of the amino acid sequence of *Mt*PPO7 and the amino acid sequence of catechol oxidase from *Aspergillus oryzae* (*Ao*CO4), which scored highest in a Blast search using the *Mt*PPO7 sequence against the Protein Data Bank (38% amino acid identity). Using this alignment and the available structure of *Ao*CO4 (PDB-id: 4J3P) as template, structural models were obtained for *Mt*PPO7 using the Modeller program version 9.16. One hundred comparative models were generated, after which the model with lowest corresponding DOPE score was selected for inspection and image generation using Pymol (Pymol, The PyMOL Molecular Graphics System, version 1.5.0.4 Schrödinger, LLC, New York, NY, USA).

5.5.9 Genome-wide analysis

Fungal genomes were obtained from the JGI MycoCosm portal [29]. In total, protein sequence annotations of 336 Ascomycota and 208 Basidiomycota genomes were used. BLAST databases for those protein sequences were created using 'makeblastdb' program in BLAST+ v2.2.30 [54]. The protein BLAST was performed separately by using ten *Mt*PPO7 sequences (PDB id: 4J3P and closely related *Mt*PPO7s: Q2UNF9, *Aspergillus oryzae* (strain ATCC 42149); G2QC95, *Myceliophthora thermophila* (ATCC 42464); Q2H7I7, *Chaetomium globosum* (ATCC 6205); G0SFX8, *Chaetomium thermophilum* (DSM 1495); L7IAQ4, *Magnaporthe oryzae* (strain Y34); L7JMT9, *Magnaporthe oryzae* (strain P131); G4N2I5, *Magnaporthe oryzae* (strain 70-15); A0A084GCK1, *Scedosporium apiospermum*; A0A0C4DYF2, *Magnaporthiopsis poae* (ATCC 64411); J3P591, *Gaeumannomyces graminis var. tritici* (strain R3-111a-1)), ten AA9 LPMO sequences (PDB id: 4D7U and closely related LPMOs: Q7SHI8, *Neurospora crassa* (strain ATCC 24698); G2QCJ3, *Myceliophthora thermophila* (strain ATCC 42464); F7W1P4, *Sordaria macrospora* (strain ATCC MYA-333); G2RB73, *Thielavia terrestris* (strain ATCC 38088); Q2H8N9, *Chaetomium globosum* (strain ATCC 6205); G0S408, *Chaetomium thermophilum* (strain DSM 1495); F8MLY8, N*eurospora tetrasperma* (strain FGSC 2508); T0L448, *Colletotrichum gloeosporioides* (strain Cg-14); A0A0H4K9X4 and A0A1C9CXI0, *Myceliophthora thermophila* C1) and four *Ab*PPOs (*Ab*PPO1, *Ab*PPO2, *Ab*PPO3 and *Ab*PPO4 [55, 56]) as query sequences. Resulting sequences below E-value cut-off of 0.001 with query coverage above 60% for AA9 LPMOs, 65% for *Mt*PPO7s and 85% for *Ab*PPOs were considered for further analysis. Selection of cellulase-rich Ascomycota and Basidiomycota was based on the presence of at least 10 genes encoding cellulose degrading enzymes, which are classified in the CAZy database as glycosyl hydrolase families GH1, GH3, GH5, GH6, GH7, GH12, GH45. The GH gene families were selected based on Kubicek *et al*. (2014) [57]. Previous data [32] was used to determine the number of annotated genes encoding cellulose degrading enzymes. Based on this selection, 27 Ascomycota and 23 Basidiomycota species were selected for the Pearson correlation analysis (**Figure 5.7**, **Additional Table 5.2**, **Additional Table 5.3**). All the statistical analyses were performed in R [58].

References

1. Lam TBT, Kadoya K, Iiyama K. Bonding of hydroxycinnamic acids to lignin: ferulic and *p*-coumaric acids are predominantly linked at the benzyl position of lignin, not the β-position, in grass cell walls. Phytochemistry. 2001;57(6):987-92.
2. Takahashi N, Koshijima T. Ester linkages between lignin and glucuronoxylan in a lignin-carbohydrate complex from beech (*Fagus crenata*) wood. Wood Sci. Technol. 1988;22(231-241):231-41.
3. Vaaje-Kolstad G, Westereng B, Horn SJ, Liu Z, Zhai H, Sorlie M *et al*. An oxidative enzyme boosting the enzymatic conversion of recalcitrant polysaccharides. Sci. 2010;330(6001):219-22.
4. Lombard V, Golaconda Ramulu H, Drula E, Coutinho PM, Henrissat B. The carbohydrate-active enzymes database (CAZy) in 2013. Nucleic Acids Res. 2014:42;D490–5.
5. Phillips CM, Beeson WT, Cate JH, Marletta MA. Cellobiose dehydrogenase and a copper-dependent polysaccharide monooxygenase potentiate cellulose degradation by *Neurospora crassa*. ACS Chem. Biol. 2011;6(12):1399-406.
6. Quinlan RJ, Sweeney MD, Lo Leggio L, Otten H, Poulsen JC, Johansen KS *et al*. Insights into the oxidative degradation of cellulose by a copper metalloenzyme that exploits biomass components. Proc. Natl. Acad. Sci. U.S.A. 2011;108(37):15079-84.
7. Frommhagen M, Sforza S, Westphal AH, Visser J, Hinz SW, Koetsier MJ *et al*. Discovery of the combined oxidative cleavage of plant xylan and cellulose by a new fungal polysaccharide monooxygenase. Biotechnol. Biofuels. 2015;8:101.
8. Vu VV, Beeson WT, Span EA, Farquhar ER, Marletta MA. A family of starch-active polysaccharide monooxygenases. Proc. Natl. Acad. Sci. U.S.A. 2014;111(38):13822-7.
9. Isaksen T, Westereng B, Aachmann FL, Agger JW, Kracher D, Kittl R *et al*. A C4-oxidizing lytic polysaccharide monooxygenase cleaving both cellulose and cello-oligosaccharides. J. Biol. Chem. 2014;289(5):2632-42.
10. Forsberg Z, Rohr AK, Mekasha S, Andersson KK, Eijsink VG, Vaaje-Kolstad G *et al*. Comparative study of two chitin-active and two cellulose-active AA10-type lytic polysaccharide monooxygenases. Biochem. 2014;53(10):1647-56.
11. Agger JW, Isaksen T, Varnai A, Vidal-Melgosa S, Willats WG, Ludwig R *et al*. Discovery of LPMO activity on hemicelluloses shows the importance of oxidative processes in plant cell wall degradation. Proc. Natl. Acad. Sci. U.S.A. 2014;111(17):6287-92.
12. Kracher D, Scheiblbrandner S, Felice AKG, Breslmayr E, Preims M, Ludwicka K *et al*. Extracellular electron transfer systems fuel cellulose oxidative degradation. Sci. 2016.
13. Frommhagen M, Koetsier MJ, Westphal AH, Visser J, Hinz SWA, Vincken J-P *et al*. Lytic polysaccharide monooxygenases from *Myceliophthora thermophila* C1 differ in substrate preference and reducing agent specificity. Biotechnol. Biofuels. 2016;9(1):1-17.
14. Westereng B, Cannella D, Wittrup Agger J, Jørgensen H, Larsen Andersen M, Eijsink VGH *et al*. Enzymatic cellulose oxidation is linked to lignin by long-range electron transfer. Sci. Rep. 2015;5:18561.
15. Bissaro B, Forsberg Z, Ni Y, Hollmann F, Vaaje-Kolstad G, Eijsink VGH. Fueling biomass-degrading oxidative enzymes by light-driven water oxidation. Green Chem. 2016;18, 5357-5366.
16. Cannella D, Mollers KB, Frigaard NU, Jensen PE, Bjerrum MJ, Johansen KS *et al*. Light-driven oxidation of polysaccharides by photosynthetic pigments and a metalloenzyme. Nat. Commun. 2016;7:11134.
17. Gao Z-J, Liu J-B, Xiao X-G. Purification and characterisation of polyphenol oxidase from leaves of *Cleome gynandra L*. Food Chem. 2011;129(3):1012-8.
18. Dec J, Haider K, Bollag J-M. Decarboxylation and demethylation of naturally occurring phenols during coupling reactions and polymerization. Soil Sci. 2001;166(10):660-71.
19. Kuijpers TFM, van Herk T, Vincken J-P, Janssen RH, Narh DL, van Berkel WJH *et al*. Potato and mushroom polyphenol oxidase activities are differently modulated by natural plant extracts. J. Agric. Food Chem. 2014;62(1):214-21.
20. Beloqui A, Pita M, Polaina J, Martínez-Arias A, Golyshina OV, Zumárraga M *et al*. Novel polyphenol oxidase mined from a metagenome expression library of bovine rumen: biochemical properties, structural analysis, and phylogenetic relationships. J. Biol. Chem. 2006;281(32):22933-42.
21. Lerch K. *Neurospora* tyrosinase: structural, spectroscopic and catalytic properties. Mol, Cell. Biochem. 1983;52(2):125-38.
22. Konrad L. Tyrosinase: molecular and active-site structure. Enzymatic browning and its prevention. ACS Symposium Series: Am. Chem. Soc. 1995. p. 64-80.
23. Vanholme R, Demedts B, Morreel K, Ralph J, Boerjan W. Lignin biosynthesis and structure. Plant Physiol. 2010;153(3):895-905.
24. Kuijpers TFM, Narváez-Cuenca C-E, Vincken J-P, Verloop AJW, van Berkel WJH, Gruppen H. Inhibition of enzymatic browning of chlorogenic acid by sulfur-containing compounds. J. Agric. Food Chem. 2012;60(13):3507-14.

25. Kuijpers TFM, Gruppen H, Sforza S, van Berkel WJH, Vincken J-P. The antibrowning agent sulfite inactivates *Agaricus bisporus* tyrosinase through covalent modification of the copper-B site. FEBS J. 2013;280(23):6184-95.
26. Mauracher SG, Molitor C, Al-Oweini R, Kortz U, Rompel A. Latent and active *ab*PPO4 mushroom tyrosinase cocrystallized with hexatungstotellurate(VI) in a single crystal. Acta Crystallogr., Sect. D. 2014;70(9):2301-15.
27. Mauracher SG, Molitor C, Al-Oweini R, Kortz U, Rompel A. Crystallization and preliminary X-ray crystallographic analysis of latent isoform PPO4 mushroom (*Agaricus bisporus*) tyrosinase. Acta Crystallogr., Sect. F: Struct. Biol. Commun. 2014;70(Pt 2):263-6.
28. Wu J, Chen H, Gao J, Liu X, Cheng W, Ma X. Cloning, characterization and expression of two new polyphenol oxidase cDNAs from *Agaricus bisporus*. Biotechnol. Lett. 2010;32(10):1439-47.
29. Grigoriev IV, Nikitin R, Haridas S, Kuo A, Ohm R, Otillar R *et al*. MycoCosm portal: gearing up for 1000 fungal genomes. Nucleic Acids Res. 2014;42(Database issue):D699-D704.
30. Berka RM, Grigoriev IV, Otillar R, Salamov A, Grimwood J, Reid I *et al*. Comparative genomic analysis of the thermophilic biomass-degrading fungi *Myceliophthora thermophila* and *Thielavia terrestris*. Nat. Biotechnol. 2011;29(10):922-7.
31. Gasparetti C, Faccio G, Arvas M, Buchert J, Saloheimo M, Kruus K. Discovery of a new tyrosinase-like enzyme family lacking a C-terminally processed domain: production and characterization of an *Aspergillus oryzae* catechol oxidase. Appl. Biochem. Microbiol. 2010;86(1):213-26.
32. Zhao Z, Liu H, Wang C, Xu J-R. Comparative analysis of fungal genomes reveals different plant cell wall degrading capacity in fungi. BMC Genomics. 2013;14(1):1-15.
33. Selinheimo E, NiEidhin D, Steffensen C, Nielsen J, Lomascolo A, Halaouli S *et al*. Comparison of the characteristics of fungal and plant tyrosinases. J. Biotechnol. 2007;130(4):471-80.
34. Zhou P, Smith NL, Lee CY. Potential purification and some properties of *Monroe* apple peel polyphenol oxidase. J. Agric. Food Chem. 1993;41(4):532-6.
35. Paul B, Gowda LR. Purification and characterization of a polyphenol oxidase from the seeds of field bean (*Dolichos lablab*). J. Agric. Food Chem. 2000;48(9):3839-46.
36. Zou Y, Hu W, Jiang A, Ma K. Partial purification and characterization of a novel extracellular tyrosinase from *Auricularia auricula*. Appl. Biochem. Biotechnol. 2013;172(3):1460-9.
37. Bissaro B, Rohr AK, Skaugen M, Forsberg Z, Horn SJ, Vaaje-Kolstad G *et al*. Fenton-type chemistry by a copper enzyme: molecular mechanism of polysaccharide oxidative cleavage. bioRxiv. 2016.
38. Rosazza JPN, Huang Z, Dostal L, Volm T, Rousseau B. Review: biocatalytic transformations of ferulic acid: an abundant aromatic natural product. J. Ind. Microbiol. 1995;15(6):457-71.
39. Schweigert N, Zehnder AJB, Eggen RIL. Chemical properties of catechols and their molecular modes of toxic action in cells, from microorganisms to mammals. Environ. Microbiol. 2001;3(2):81-91.
40. Raymond J, Rakariyatham N, Azanza JL. Purification and some properties of polyphenoloxidase from sunflower seeds. Phytochemistry. Int. J. Plant Biochem. 1993;34(4):927-31.
41. Lee CY, Smith NL, Pennesi AP. Polyphenoloxidase from *DeChaunac* grapes. J. Sci. Food Agric. 1983;34(9):987-91.
42. Hakulinen N, Gasparetti C, Kaljunen H, Kruus K, Rouvinen J. The crystal structure of an extracellular catechol oxidase from the ascomycete fungus *Aspergillus oryzae*. JBIC J. Biol. Inorg. Chem. 2013;18(8):917-29.
43. Solem E, Tuczek F, Decker H. Tyrosinase versus catechol oxidase: one asparagine makes the difference. Angew. Chem., Int. Ed. 2016;55(8):2884-8.
44. Klabunde T, Eicken C, Sacchettini JC, Krebs B. Crystal structure of a plant catechol oxidase containing a dicopper center. Nat. Struct. Biol. 1998;5(12):1084-90.
45. Ismaya WT, Rozeboom HJ, Weijn A, Mes JJ, Fusetti F, Wichers HJ *et al*. Crystal structure of *Agaricus bisporus* mushroom tyrosinase: identity of the tetramer subunits and interaction with tropolone. Biochemistry. 2011;50(24):5477-86.
46. Decker H, Schweikardt T, Tuczek F. The first crystal structure of tyrosinase: all questions answered? Angew. Chem., Int. Ed. 2006;45(28):4546-50.
47. Marusek CM, Trobaugh NM, Flurkey WH, Inlow JK. Comparative analysis of polyphenol oxidase from plant and fungal species. J. Inorg. Biochem. 2006;100(1):108-23.
48. Strothkamp KG, Jolley RL, Mason HS. Quaternary structure of mushroom tyrosinase. Biochem. Biophys. Res. Commun. 1976;70(2):519-24.
49. Kubicek CP, Kubicek EM. Enzymatic deconstruction of plant biomass by fungal enzymes. Curr. Opin. Chem. Biol. 2016;35:51-7.
50. Goldfeder M, Kanteev M, Adir N, Fishman A. Influencing the monophenolase/diphenolase activity ratio in tyrosinase. Biochim. Biophys. Acta, Proteins Proteomics. 2013;1834(3):629-33.
51. Visser H, Joosten V, Punt PJ, Gusakov AV, Olson PT, Joosten R *et al*. Development of a mature fungal technology and production platform for industrial enzymes based on a *Myceliophthora thermophila* isolate, previously known as *Chrysosporium lucknowense* C1. Ind. Biotechnol. 2011;7:214–23.

52. Punt PJ, Burlingame RP, Pynnonen CM, Olson PT, Wery J, Visser J, Heinrich *et al*. *Chrysosporium lucknowense* protein production system. 2010. Patent WO/2010/107303.
53. Zhang YHP, Cui J, Lynd LR, Kuang LR. A transition from cellulose swelling to cellulose dissolution by *o*-phosphoric acid: evidence from enzymatic hydrolysis and supramolecular structure. Biomacromolecules. 2006;7(2):644-8.
54. Camacho C, Coulouris G, Avagyan V, Ma N, Papadopoulos J, Bealer K *et al*. BLAST+: architecture and applications. BMC Bioinformatics. 2009;10(1):1-9.
55. Wichers HJ, Recourt K, Hendriks M, Ebbelaar CEM, Biancone G, Hoeberichts FA *et al*. Cloning, expression and characterisation of two tyrosinase cDNAs from *Agaricus bisporus*. Appl. Biochem. Microbiol. 2003;61(4):336-41.
56. Li N-y, Cai W-m, Jin Q-l, Qin Q-p, Ran F-l. Molecular cloning and expression of polyphenoloxidase genes from the mushroom, *Agaricus bisporus*. Agric. Sci. China. 2011;10(2):185-94.
57. Kubicek CP, Starr TL, Glass NL. Plant cell wall–degrading enzymes and their secretion in plant-pathogenic fungi. Annu. Rev. Phytopathol. 2014;52(1):427-51.
58. Team RC. R: A language and environment for statistical computing. R Foundation for Statistical Computing, Vienna, Austria. 2016. https://www.R-project.org.

Addtitional Files

Additional Table 5.1 Compounds detected after incubation of 21 reducing agents without or with *Mt*PPO7 by UHPLC/UV-MS. Submitted as online file only (open access)
http://biotechnologyforbiofuels.biomedcentral.com/articles/10.1186/s13068-017-0810-4

Additional Table 5.2 Selected cellulase rich Ascomycota from the JGI database[a].

No.	Class	Fungi	Species Description	JGI Abbreviation
1	Ascomycota	*Arthrobotrys oligospora*	*Arthrobotrys oligospora* ATCC 24927	Artol1
2	Ascomycota	*Aspergillus clavatus*	*Aspergillus clavatus* NRRL 1 from AspGD	Aspcl1
3	Ascomycota	*Aspergillus flavus*	*Aspergillus flavus* NRRL3357	Aspfl1
4	Ascomycota	*Aspergillus fumigatus*	*Aspergillus fumigatus* A1163	Aspfu_A1163_1
5	Ascomycota	*Aspergillus niger*	*Aspergillus niger* ATCC 1015 v4.0	Aspni7
6	Ascomycota	*Aspergillus oryzae*	*Aspergillus oryzae* RIB40	Aspor1
7	Ascomycota	*Aspergillus terreus*	*Aspergillus terreus* NIH 2624	Aspte1
8	Ascomycota	*Cladonia grayi*	*Cladonia grayi Cgr* DA2myc ss v2.0	Clagr3
9	Ascomycota	*Cladosporium fulvum*	*Cladosporium fulvum* v1.0	Clafu1
10	Ascomycota	*Cochliobolus sativus*	*Cochliobolus sativus* ND90Pr v1.0	Cocsa1
11	Ascomycota	*Debaryomyces hansenii*	*Debaryomyces hansenii*	Debha1
12	Ascomycota	*Dothistroma septosporum*	*Dothistroma septosporum* NZE10 v1.0	Dotse1
13	Ascomycota	*Fusarium graminearum*	*Fusarium graminearum* v1.0	Fusgr1
14	Ascomycota	*Fusarium oxysporum*	*Fusarium oxysporum f. sp. lycopersici* 4287 v2	Fusox2
15	Ascomycota	*Fusarium verticillioides*	*Fusarium verticillioides* 7600 v2	Fusve2
16	Ascomycota	*Gaeumannomyces graminis*	*Gaeumannomyces graminis var. tritici* R3-111a-1	Gaegr1
17	Ascomycota	*Magnaporthe poae*	*Magnaporthiopsis poae* ATCC 64411	Magpo1
18	Ascomycota	*Myceliophthora thermophila*	*Myceliophthora thermophila/Sporotrichum thermophile* v2.0	Spoth2
19	Ascomycota	*Neosartorya fischeri*	*Neosartorya fischeri* NRRL 181	Neofi1
20	Ascomycota	*Neurospora crassa*	*Neurospora crassa* OR74A v2.0	Neucr2
21	Ascomycota	*Penicillium chrysogenum*	*Penicillium chrysogenum* v1.0	Pench1
22	Ascomycota	*Pyrenophora teres*	*Pyrenophora teres f. teres*	Pyrtt1
23	Ascomycota	*Sclerotinia sclerotiorum*	*Sclerotinia sclerotiorum* v1.0	Sclsc1
24	Ascomycota	*Talaromyces stipitatus*	*Talaromyces stipitatus* ATCC 10500	Talst1_2
25	Ascomycota	*Trichoderma reesei*	*Trichoderma reesei* RUT C-30 v1.0	TrireRUTC30_1
26	Ascomycota	*Tuber melanosporum*	*Tuber melanosporum* Mel28 v1.0	Tubme1
27	Ascomycota	*Verticillium dahliae*	*Verticillium dahliae* v1.0	Verda1

[a] The presented Ascomycota contain at least 10 genes encoding cellulose degrading enzymes, which are classified in the CAZy database as glycosyl hydrolase families GH1, GH3, GH5, GH6, GH7, GH12, GH45. The GH gene families were selected based on Kubicek *et al*. (2014). The data published by Zhao *et al*. (2013) was used to determine the amount of annotated genes encoding cellulose degrading enzymes. Based on this selection, a protein BLAST was performed for *Ab*PPOs, AA9 LPMOs and *Mt*PPOs using the protein sequence annotations from the JGI database. The outcome is presented in **Figure 5.7**. See Methods for more information.

Additional Table 5.3 Selected cellulase rich Basidiomycota from the JGI database[a]

No	Class	Fungi	JGI Species Description	JGI Abbreviation
1	Basidiomycota	*Botryobasidium botryosum*	*Botryobasidium botryosum* v1.0	Botbo1
2	Basidiomycota	*Coniophora puteana*	*Coniophora puteana* v1.0	Conpu1
3	Basidiomycota	*Coprinopsis cinerea*	*Coprinopsis cinerea* AmutBmut pab1-1 v1.0	Copci_AmutBmut1
4	Basidiomycota	*Cryptococcus neoformans*	*Cryptococcus neoformans var neoformans* JEC21	Cryne_JEC21_1
5	Basidiomycota	*Dichomitus squalens*	*Dichomitus squalens* v1.0	Dicsq1
6	Basidiomycota	*Fomitiporia mediterranea*	*Fomitiporia mediterranea* v1.0	Fomme1
7	Basidiomycota	*Fomitopsis pinicola*	*Fomitopsis pinicola* FP-58527 SS1 v3.0	Fompi3
8	Basidiomycota	*Ganoderma sp.*	*Ganoderma sp.* 10597 SS1 v1.0	Gansp1
9	Basidiomycota	*Gloeophyllum trabeum*	*Gloeophyllum trabeum* v1.0	Glotr1_1
10	Basidiomycota	*Gymnopus luxurians*	*Gymnopus luxurians* v1.0	Gymlu1
11	Basidiomycota	*Hebeloma cylindrosporum*	*Hebeloma cylindrosporum* h7 v2.0	Hebcy2
12	Basidiomycota	*Hypholoma sublateritium*	*Hypholoma sublateritium* v1.0	Hypsu1
13	Basidiomycota	*Jaapia argillacea*	*Jaapia argillacea* v1.0	Jaaar1
14	Basidiomycota	*Laccaria amethystina*	*Laccaria amethystina* LaAM-08-1 v2.0	Lacam2
15	Basidiomycota	*Laccaria bicolor*	*Laccaria bicolor* v2.0	Lacbi2
16	Basidiomycota	*Melampsora laricis-populina*	*Melampsora laricis-populina* v2.0	Mellp2_3
17	Basidiomycota	*Moniliophthora perniciosa*	*Moniliophthora perniciosa* FA553	Monpe1_1
18	Basidiomycota	*Paxillus involutus*	*Paxillus involutus* ATCC 200175 v1.0	Paxin1
19	Basidiomycota	*Postia placenta*	*Postia placenta* MAD-698-R-SB12 v1.0	PosplRSB12_1
20	Basidiomycota	*Puccinia graminis*	*Puccinia graminis f. sp. tritici* v2.0	Pucgr2
21	Basidiomycota	*Puccinia triticina*	*Puccinia triticina* 1-1 BBBD Race 1	Puctr1
22	Basidiomycota	*Schizophyllum commune*	*Schizophyllum commune* H4-8 v3.0	Schco3
23	Basidiomycota	*Serpula lacrymans*	*Serpula lacrymans* S7.9 v2.0	SerlaS7_9_2

[a] The presented Basidiomycota contain at least 10 genes encoding cellulose degrading enzymes, which are classified in the CAZy database as glycosyl hydrolase families GH1, GH3, GH5, GH6, GH7, GH12, GH45. The GH gene families were selected based on Kubicek *et al*. (2014). The data published by Zhao *et al*. (2013) was used to determine the amount of annotated genes encoding cellulose degrading enzymes. Based on this selection, a protein BLAST was performed for *Ab*PPOs, AA9 LPMOs and *Mt*PPOs using the protein sequence annotations from the JGI database. The outcome is presented in **Figure 5.7**. See Methods for more information.

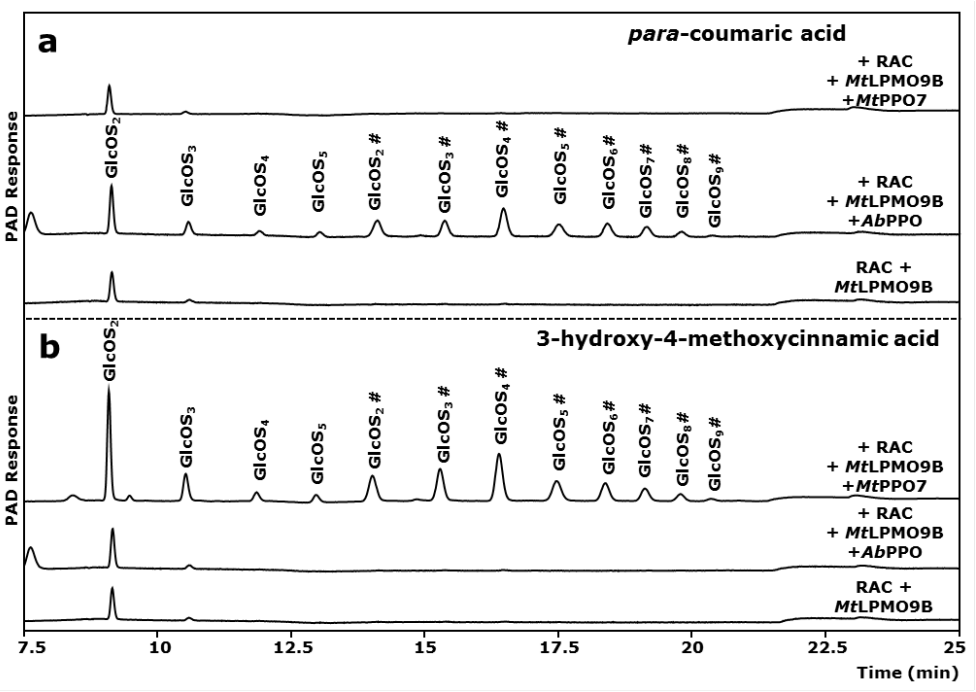

Additional Figure 5.1 Activity of *Mt*LPMO9B towards amorphous cellulose in the presence and absence of *Mt*PPO7 or *Ab*PPO. HPAEC elution pattern of regenerated amorphous cellulose (RAC; 1.5 mg mL^{-1}) incubated with *Mt*LPMO9B (5.0 µg mL^{-1}) only, or with either *Ab*PPO (2.5 µL mL^{-1}) or *Mt*PPO7 (5.0 µg mL^{-1}) in the presence of **a** *para*-coumaric acid (no. 3 specified in **Table 5.1**, 2 mM) and **b** 3-hydroxy-4-methoxycinnamic acid (no. 5 specified in **Table 5.1**, 2 mM). The incubation of RAC with *Mt*LPMO9B results in the formation of non-oxidized gluco-oligosaccharides ($GlcOS_n$) and C1-oxidized gluco-oligosaccharides ($GlcOS_n^{\#}$). See Methods for details.

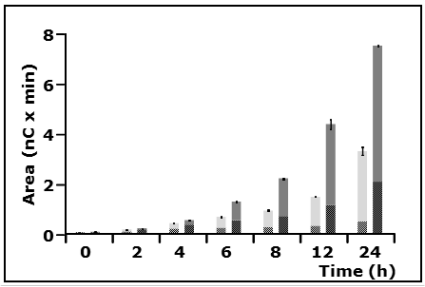

Additional Figure 5.2 Release of oligosaccharides from RAC incubated with *Mt*LPMO9B in the presence and absence of *Mt*PPO7 throughout 24 h. Samples were incubated in the presence of ferulic acid (no. 8 specified in **Table 5.1**). The total sum is shown as integrated peak areas of released non-oxidized (shaded light gray and shaded dark gray) and C1-oxidized (light gray and dark gray) gluco-oligosaccharides after incubation of regenerated amorphous cellulose (RAC; 1.5 mg mL^{-1}) with *Mt*LPMO9B only (light gray bars, 5 mg mL^{-1}) and *Mt*LPMO9B together with *Mt*PPO7 (dark gray bars, 5 mg mL^{-1}) based on HPAEC. All incubations were performed in duplicate, and the standard deviations are presented as error bars. See Methods for details.

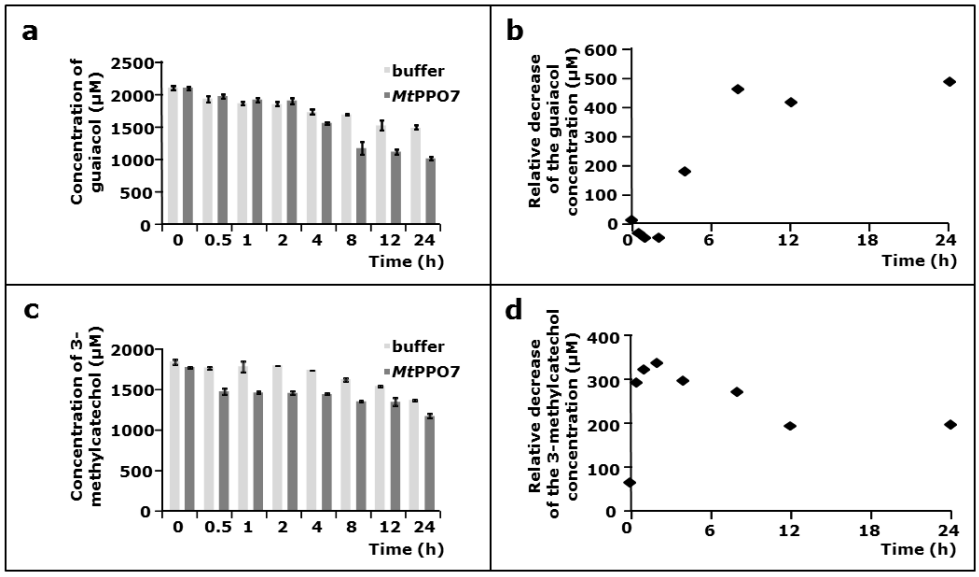

Additional Figure 5.3 Concentration of phenolic compounds incubated in the presence and absence of *Mt*PPO7. **a** guaiacol (no. 9 specified in **Table 5.1**, 2 mM) and **c** 3-methylcatechol (no. 17 specified in **Table 5.1**, 2 mM) were incubated with *Mt*PPO7 (dark gray bar, 5 µg mL^{-1}) or without (light gray bar). Samples were incubated in a 50 mM potassium phosphate buffer (pH 6.0) containing 2.5 µM copper(II)-chloride for 24 h at 50°C. The conversion of guaiacol and 3-methylcatechol by *Mt*PPO7 was calculated by subtracting the determined concentration of the incubation of guaiacol or 3-methylcatechol in the presence of *Mt*PPO7 from the concentration that was determined by the incubation of guaiacol and 3-methylcatechol alone. This conversion was expressed as the relative decrease of the guaiacol and 3-methylcatechol concentration and is shown in **b** and **d**, respectively. See Methods for details.

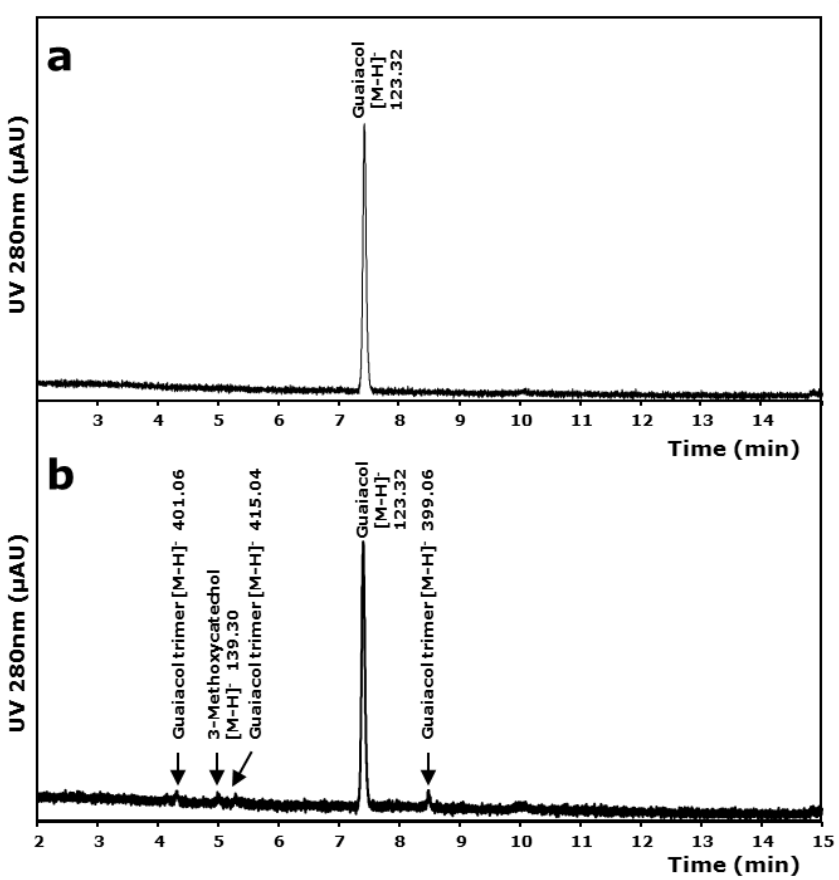

Additional Figure 5.4 UHPLC-UV-MS^n elution profile of guaiacol incubated **a** in the presence and **b** absence of *Mt*PPO7. Guaiacol (no. 9 specified in **Table 5.1**, 2 mM) was incubated with (5 µg mL^{-1}) or without *Mt*PPO7. Samples were incubated in a 50 mM potassium phosphate buffer (pH 6.0) containing 2.5 µM copper(II)-chloride for 24 h at 50°C. Annotation of the peaks based on UV was done by using mass spectrometry (**Additional Figure 5.5**). See Methods for details.

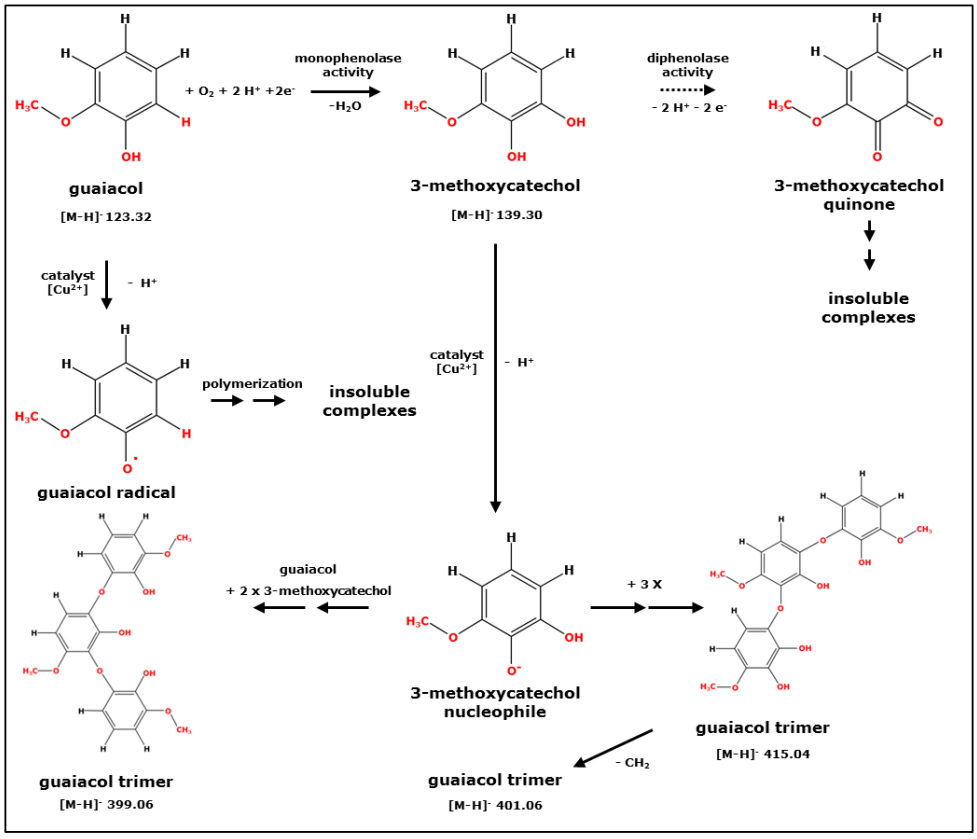

Additional Figure 5.5 Schematic presentation of possible reaction pathways of guaiacol incubated in the presence of *Mt*PPO7. In short, *Mt*PPO7 hydroxylates guaiacol (no. 9 specified in **Table 5.1**) into 3-methoxycatechol (monophenolase activity). Although not determined, it is likely that 3-methoxycatechol is further oxidized by *Mt*PPO7 into the corresponding *ortho*-quinone (diphenolase activity, dashed arrow). These *ortho*-quinones are expected to polymerize and form insoluble complexes. Guaiacol itself forms insolube complexes via auto-oxidation, which results from the presence of copper during the incubation for 24 h at 50°C. The decrease in guaiacol concentration during the incubation of guaiacol without *Mt*PPO7 is also shown in **Additional Figure 5.3a**. The determined masses indicate the presence of multiple trimers (399.06, 401.06 and 415.04) consisting of polymerized 3-methylcatechol and guiacol (**Additional Figure 5.4**). As described above, the polymerization reactions are expected to be catalyzed by copper during the incubation conditions applied. All masses were determined by UHPLC-UV-MS^n after incubation of guaiacol (2 mM) with *Mt*PPO7 (5.0 µg mL^{-1}). Samples were incubated for 24 h at 50°C in 50 mM potassium phosphate, pH 6.0, containing 2.5 µM copper(II)-chloride.

a

	AA9 LPMOs	*Ab*PPOs	*Mt*PPO7s
AA9 LPMOs	1.00	0.59	0.75
*Ab*PPOs	0.59	1.00	0.54
*Mt*PPO7s	0.75	0.54	1.00

b

	AA9 LPMOs	*Ab*PPOs	*Mt*PPO7s
AA9 LPMOs	1.00	0.34	0.50
*Ab*PPOs	0.34	1.00	0.03
*Mt*PPO7s	0.50	0.03	1.00

c

	AA9 LPMOs	*Ab*PPOs	*Mt*PPO7s
AA9 LPMOs	1.00	0.42	0.60
*Ab*PPOs	0.42	1.00	0.26
*Mt*PPO7s	0.60	0.26	1.00

d

	AA9 LPMOs	*Ab*PPOs	*Mt*PPO7s
AA9 LPMOs	1.00	0.24	0.53
*Ab*PPOs	0.24	1.00	0.12
*Mt*PPO7s	0.53	0.12	1.00

Additional Figure 5.6 Correlation of AA9 LPMOs, *Ab*PPOs and *Mt*PPO7s encoding genes in Ascomycota and Basidiomycota. Correlation between the three gene families encoding AA9 LPMOs, *Ab*PPOs and *Mt*PPO7s of **a** 336 Ascomycota and **b** 208 Basidiomycota. Correlation between genes encoding AA9 LPMOs, *Ab*PPOs and *Mt*PPO7s of **c** 27 Ascomycota and **d** 23 Basidiomycota, which have at least ten annotated genes encoding cellulose degrading enzymes. Species of selected fungal classes are listed in **Additional Table 5.2** and **Additional Table 5.3**. Graphical presentations of the correlations of **a** togehter with **b** and **c** and **d** are shown in **Figure 5.7**. See Methods for details.

Chapter VI

Quantification of the catalytic performance of C1-oxidizing cellulose specific lytic polysaccharide monooxygenases

Based on: Frommhagen M, Westphal AH, Hilgers R, Koetsier MJ, Hinz SWA, Visser J, Gruppen H, van Berkel WJH, Kabel MA. Quantification of the catalytic performance of C1-oxidizing cellulose specific lytic polysaccharide monooxygenases. *Under review*.

Abstract

Lytic polysaccharide monooxygenases (LPMOs) have recently been shown to significantly enhance the degradation of recalcitrant polysaccharides and are of interest for the production of biochemicals and bioethanol from plant biomass. The copper-containing LPMOs utilize electrons, provided by reducing agents, to oxidatively cleave polysaccharides. Here, we report the development of a β-glucosidase-assisted method to quantify the release of C1-oxidized gluco-oligosaccharides from cellulose by two C1-oxidizing LPMOs from *Myceliophthora thermophila* C1. Based on this quantification method, we demonstrate that the catalytic performance of both *Mt*LPMOs is strongly dependent on pH and temperature. Further measurements revealed that pH mainly affects the reducing agent dependency, whereas temperature impacts the operational stability of *Mt*LPMOs.

The obtained results indicate that the catalytic performance of LPMOs depends on the interaction of multiple factors, which are affected by pH and temperature.

1. Introduction

The enzymatic degradation of plant biomass is considered to be a green and sustainable approach for the production of biochemicals and biofuels. Plant biomass contains a substantial amount of the plant cell wall material lignocellulose, which is resistant for hydrolytic enzymatic degradation.

Recently, studies have confirmed that lytic polysaccharide monooxygenases (LPMOs) improve the degradation of lignocellulose [1, 2]. Based on their amino acid sequences, LPMOs are classified as auxiliary activity (AA) families AA9, AA10, AA11 and AA13 in the Carbohydrate Active enZyme database [3]. LPMOs contain a coordinated copper atom and require external electrons for the molecular oxygen-driven oxidation of polysaccharides [4, 5]. Recently, also hydrogen peroxide has been shown to be a co-substrate of LPMOs [6].

Lignocellulose is mainly composed of cellulose, hemicellulose and lignin. In addition, free phenolic compounds and phenolic compounds conjugated to hemicellulose are part of lignocellulose. Here we focus on the catalytic performance of two *Mt*LPMOs from *Myceliophthora thermophila* C1. Both *Mt*LPMOs are active towards cellulose, a homogenous linear polymer that consist of β-(1→4)-linked glucosyl chains. These glucosyl chains interact with each other and form crystalline cellulose fibrils via hydrogen bonds and van der Waals forces [7, 8]. In general, cellulose-active LPMOs are able to degrade crystalline cellulose regions by oxidizing the β-(1→4)-linkages at either the C1 or C4 position or at both of these positions [4, 5, 9].

Until now, LPMOs have been characterized for their catalytic mechanism, C1-/C4-regioselectivity, substrate specificity, protein structure and external electron donation systems [5, 6, 10-13]. However, the impact of pH and temperature on the catalytic performance of LPMOs has received little attention. One reason is the difficulty of reliable quantification of released C1- and C4-oxidized gluco-oligosaccharides, which differ in their degree of polymerization (DP) [14, 15]. In addition, commercial standards for oxidized gluco-oligosaccharides are not available. Another reason is that pH and temperature also influence the redox and stability properties of reducing agents [16].

In general, electrons for LPMOs can be provided by multiple sources, such as phenolic compounds (ascorbic acid, gallic acid, lignin) [5, 17, 18], cellobiose dehydrogenase (CDH) [9], photosynthetic pigments and light-driven water oxidation [19, 20]. Also beneficial for the oxidative activity of LPMOs is the co-operation with other enzymes such as GMC-oxidoreductases (glucose-methanol-choline-oxidase/dehydrogenase), or polyphenol oxidases [16, 21]. Obviously, the synergy with other enzymes increases the complexity of analyzing the pH- and temperature-dependent catalytic properties of LPMOs.

In this research, we describe a procedure for quantifying the catalytic performance of *Mt*LPMO9B and *Mt*LPMO9D that oxidize cellulose at the C1 position. Incubation of the released gluco-oligosaccharide products with β-glucosidase from almonds results in a mixture of gluconic and cellobionic acid, which can be quantified by high-performance anion exchange chromatography. The newly developed method was further applied to study the catalytic performance of *Mt*LPMO9B and *Mt*LPMO9D as a function of pH and temperature. Using either ascorbic acid or 3-methylcatechol as electron donor, it is demonstrated that the oxidative cleavage capacity of both *Mt*LPMOs depends

on their operational stability, the pH of the reaction, and the pH-dependent characteristics of the reducing agents.

2. Results

2.1 Degradation of C1-oxidized gluco-oligosaccharides into gluconic and cellobionic acid

As previously described [17], *Mt*LPMO9B activity towards regenerated amorphous cellulose (RAC) results in the formation of non-oxidized and C1-oxidized gluco-oligosaccharides (**Figure 6.1a**). Hence, *Mt*LPMO9B is characterized as a C1-oxidizing LPMO. *Mt*LPMO9D is characterized as a C1-oxidizing LPMO, based on the product pattern determined by HPAEC (**Additional Figure 6.1**) and previous work [22, 23].

The ability of β-glucosidase to further degrade the C1-oxidized gluco-oligosaccharides was tested by adding β-glucosidase to the soluble part of the *Mt*LPMO9B-incubated RAC mixture. Under the applied conditions (50 mM ammonium acetate buffer, pH 5.0, 37°C, 20 h), a complete degradation of the non-oxidized and C1-oxidized gluco-oligosaccharides into glucose (not further analyzed), gluconic acid and cellobionic acid was observed at a dose of 1 U of β-glucosidase (**Figure 6.1b**). In the absence of electron donors no gluconic or cellobionic acid was formed.

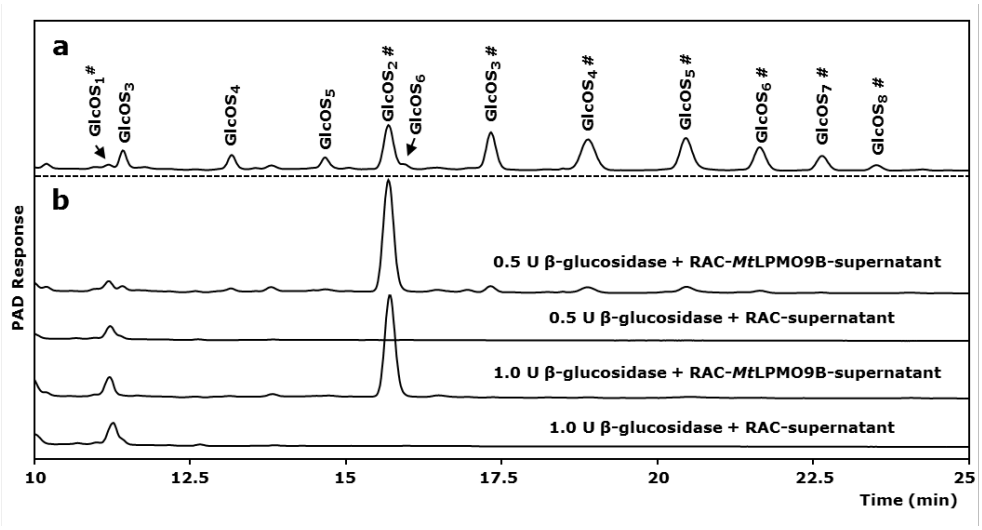

Figure 6.1 Hydrolysis of released (oxidized) gluco-oligosaccharides with β-glucosidase. **a** HPAEC elution pattern of released non-oxidized ($GlcOS_n$) and C1-oxidized ($GlcOS_n^{\#}$) gluco-oligosaccharides after incubation of RAC (2.8 mg mL^{-1}) with *Mt*LPMO9B (3 mg g^{-1} substrate) in the presence of 1 mM ascorbic acid. Samples were incubated in a 50 mM ammonium acetate buffer (pH 5.0) at 50°C for 20 h. **b** Elution profile of the soluble supernatant (250 µL) described under **a**, which was incubated with different amounts of β-glucosidase (0.5 U and 1.0 U per sample). Upon addition of 1 U β-glucosidase, all C1-oxidized gluco-oligosaccharides were degraded into cellobionic acid ($GlcOS_2^{\#}$) and glucose (not shown, elution time at 5 min). Only small amounts of gluconic acid ($GlcOS_1^{\#}$) were formed after the addition of β-glucosidase to the supernatant.

2.2 Linearity verification of the β-glucosidase-assisted method

In order to investigate whether the β-glucosidase-assisted method can be used for the quantification of C1-oxidized gluco-oligosaccharides, a dilution series of the soluble part of the *Mt*LPMO9B-incubated RAC mixture (30 h incubation) was prepared and subsequently incubated with 1 U of β-glucosidase. All non-oxidized and C1-oxidized gluco-oligosaccharides in the supernatant were completely degraded into glucose, gluconic and cellobionic acid. The concentration of gluconic acid and cellobionic acid was proportional to the dilution series from 0 to 59.7 nmol mL^{-1} (R^2 = 0.9945, **Figure 6.2**). Hence, the β-glucosidase-assisted method was seen as suitable to determine the total amount of C1-oxidized gluco-oligosaccharides in a range of 0 to 60 nmol mL^{-1}.

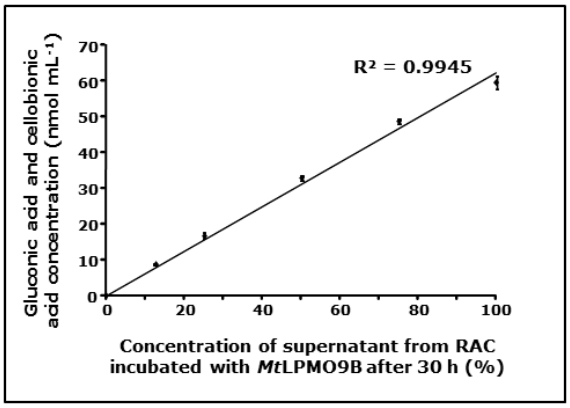

Figure 6.2 Verification of the linearity of the β-glucosidase-assisted method. The soluble fraction obtained from the incubation of RAC (2.8 mg mL^{-1}) with *Mt*LPMO9B (3 mg g^{-1} substrate) in the presence of ascorbic acid after 30 h was diluted to obtain samples with varying concentrations of gluconic acid and cellobionic acid. Each diluted sample was incubated with the same amount of β-glucosidase (1 U per sample). The concentration of gluconic acid and cellobionic acid is proportional to the dilutions series (R^2 = 0.9945).

2.3 Quantification of soluble C1-oxidized gluco-oligosaccharides and insoluble C1-oxidized residues formed by *Mt*LPMO9B

The β-glucosidase-assisted method was applied to determine the release of C1-oxidized gluco-oligosaccharides in the soluble fraction that was obtained after RAC was incubated with *Mt*LPMO9B in the presence of 1 mM ascorbic acid over a time period of 30 h. In the first 2 h, no soluble C1-oxidized gluco-oligosaccharides were formed. From 4 to 30 h, the concentration of C1-oxidized gluco-oligosaccharides steadily increased up to 59.5 nmol mL^{-1} (**Figures 6.3a** and **6.3b**).

In addition to the soluble part, the insoluble part of the *Mt*LPMO9B-incubated RAC mixture was degraded using a β-glucosidase-enriched cellulolytic enzyme cocktail. In contrast to soluble C1-oxidized gluco-oligosaccharides, insoluble C1-oxidized residues were already formed within the first 2 h of the incubation. The concentration of C1-oxidized gluco-oligosaccharides increased in the insoluble residue from 0 to 10 h. Between 10 and 30 h, equal concentrations of C1-oxdized gluco-oligosaccharides were determined in the insoluble part (**Figures 6.3a** and **6.3b**). Interestingly, the concentration of insoluble C1-oxidized residues was higher compared to that of the soluble residues until 8 h of the incubation. The incubation time point at which the concentration of soluble and insoluble C1-oxidized residues is identical was defined as t_{MF} (**Figure 6.3b**).

Notably, the concentration of released C1-oxidized gluco-oligosaccharides from the incubation of RAC with *Mt*LPMO9B did not reach the plateau after 30 h of incubation (**Figure 6.3**). Addition of ascorbic acid after the first 24 h did not increase the product formation (**Additional Figure 6.2**). In contrast, an extra load of *Mt*LPMO9B increased the product formation. Hence, it was concluded that *Mt*LPMO9B lost part of its catalytic performance during incubation (**Additional Figure 6.2**).

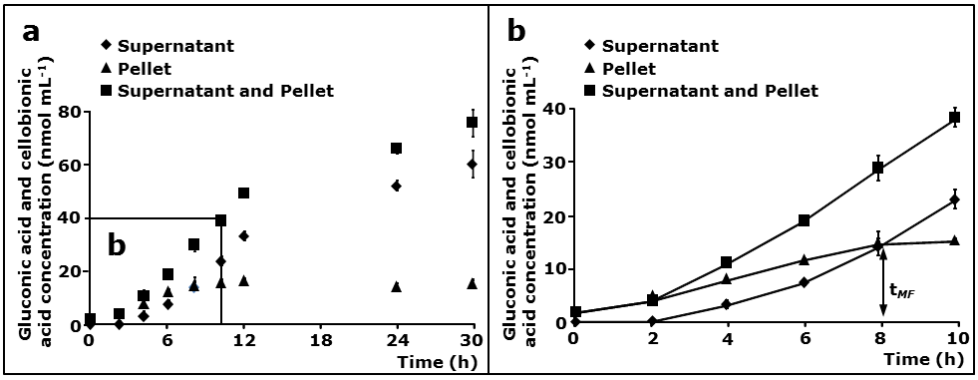

Figure 6.3 Released gluconic acid and cellobionic acid concentration from RAC incubated with *Mt*LPMO9B measured by using the β-glucosidase-assisted method. The incubation of RAC (2.8 mg mL^{-1}) with *Mt*LPMO9B (3 mg g^{-1} substrate) in the presence of ascorbic acid (1 mM) led to the formation of released non-oxidized and C1-oxidzed gluco-oligosaccharides. **a** Soluble fractions obtained from the incubation of RAC with *Mt*LPMO9B were incubated with β-glucosidase (1 U per sample) to yield glucose (not shown), gluconic acid and cellobionic acid only (diamonds). A modified method based on Cannella & colleagues was used to determine the amount of gluconic acid and cellobionic acid in the insoluble pellet after hydrolysis (triangles) [20]. Total amounts of gluconic acid and cellobionic acid obtained from the hydrolysis of soluble and insoluble C1-oxidized gluco-oligosaccharides from RAC incubated with *Mt*LPMO9B in the presence of ascorbic acid (squares). **b** The enlargement highlights the formation of gluconic acid and cellobionic acid from RAC incubated with *Mt*LPMO9B in the first 10 hours. The time point (t_{MF}), at which the concentration of soluble and insoluble C1-oxidized gluco-oligosaccharides is identical was determined at 8 h.

2.4 Catalytic performance of *Mt*LPMO9B and *Mt*LPMO9D as a function of temperature

As a first step to understand the temperature dependency of *Mt*LPMO9B and *Mt*LPMO9D, the β-glucosidase-assisted method was applied to quantify soluble C1-oxidized oligosaccharides formed at various temperatures between 20 and 60°C (**Figure 6.4**).

*Mt*LPMO9B showed the highest release of C1-oxidized gluco-oligosaccharides at 40°C in the presence of ascorbic acid, while most C1-oxidized gluco-oligosaccharides were released at 60°C in the presence of 3-methylcatechol (**Figure 6.4a**). In comparison, *Mt*LPMO9D showed an optimum at 50°C in the presence of ascorbic acid and at 40°C in the presence of 3-methylcatechol (**Figure 6.4b**). In contrast to *Mt*LPMO9D, the catalytic performance of *Mt*LPMO9B between 20 and 40°C was highly different in the presence of ascorbic acid or 3-methylcatechol.

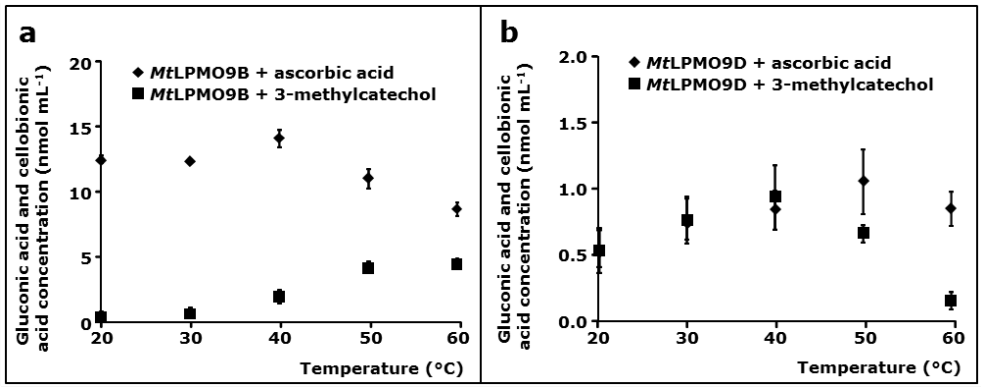

Figure 6.4 Temperature-dependent activity of *Mt*LPMO9B and *Mt*LPMO9D towards RAC. RAC (1.7 mg mL^{-1}) was incubated with **a** *Mt*LPMO9B (3 mg g^{-1} substrate) or **b** *Mt*LPMO9D (1.5 mg g^{-1} substrate) in the presence of ascorbic acid (diamonds) or 3-methylcatechol (squares). Samples were incubated at pH 5.0 for 8 hours. Soluble fractions obtained from the incubation of RAC with either *Mt*LPMO9B or *Mt*LPMO9D were further incubated with β-glucosidase (1 U per sample) to yield glucose (not shown), gluconic acid and cellobionic acid only. Both *Mt*LPMO9B and *Mt*LPMO9D show a reducing agent-dependent temperature optimum.

2.5 Catalytic performance of *Mt*LPMO9B and *Mt*LPMO9D as a function of pH

The above-described incubation of RAC with *Mt*LPMO9B in the presence of ascorbic acid showed an almost linear release of C1-oxidized gluco-oligosaccharides between 6 and 12 h (**Figure 6.3**). Therefore, the effect of pH on the catalytic performance of *Mt*LPMO9B and *Mt*LPMO9D towards RAC was studied within this incubation time frame. Incubations were performed in the presence of ascorbic acid or 3-methylcatechol at their optimum temperature as determined in **Section 2.4**. For both *Mt*LPMOs, an increase in pH enhanced the formation of released C1-oxidized gluco-oligosaccharides regardless of the reducing agent used (**Figure 6.5**). Hence, no pH optimum was observed within the measured pH range between 3.0 and 8.0. Between pH 3.0 and 6.0, the formation of C1-oxidized gluco-oligosaccharides by *Mt*LPMO9B increased between 6 and 12 h (**Figures 6.5a** and **6.5b**). At a higher pH of 7.0 and 8.0, the catalytic performance of *Mt*LPMO9B already reached the maximum within the first 6 h and hardly any increase of C1-oxidized gluco-oligosaccharides was determined thereafter (**Figures 6.5a** and **6.5b**). The latter pattern was also observed for *Mt*LPMO9D for all pH values and no increase in the release of C1-oxidized gluco-oligosaccharides was observed between 6 and 12 h of incubation (**Figures 6.5c** and **6.5d**).

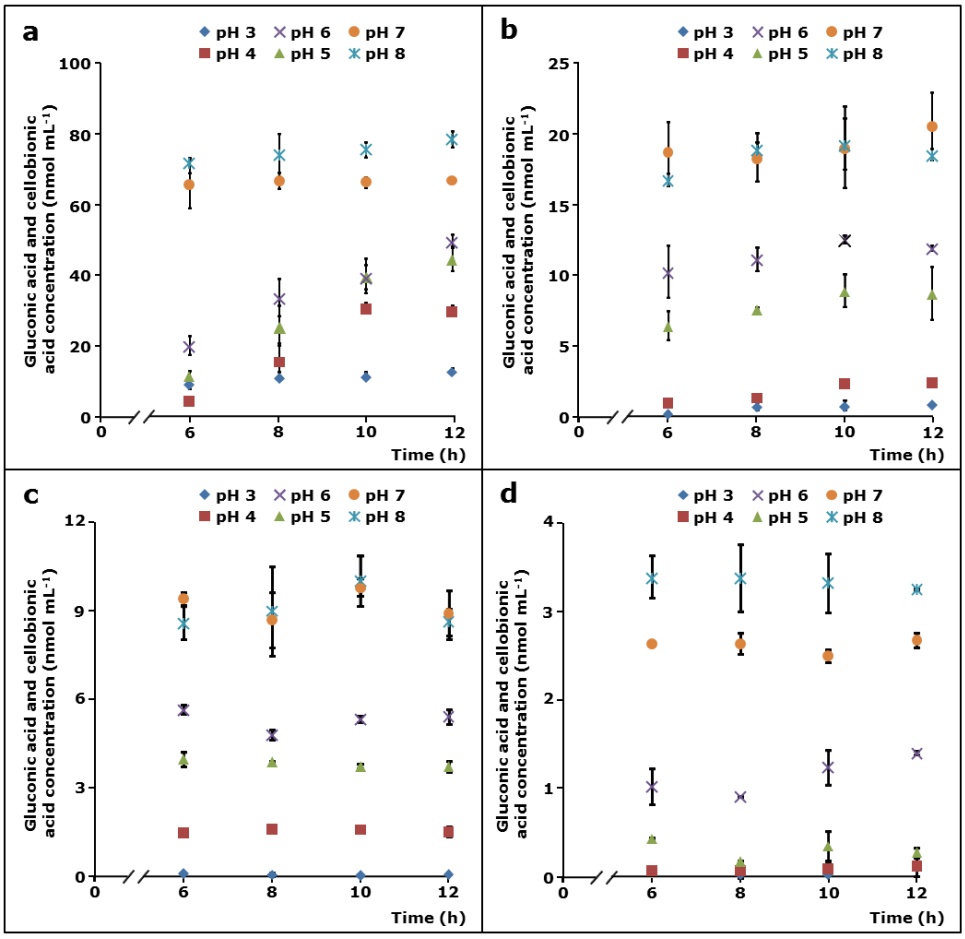

Figure 6.5 *Mt*LPMO9B and *Mt*LPMO9D activity towards RAC at different pH values. RAC (1.7 mg mL^{-1}) was incubated with *Mt*LPMO9B (3 mg g^{-1} substrate) in the presence of **a** ascorbic acid (40°C) and **b** 3-methylcatechol (60°C). **c** and **d** – Incubation of RAC with *Mt*LPMO9D (1.5 mg g^{-1} substrate) in the presence of **c** ascorbic acid (50°C) and **d** 3-methylcatechol (40°C). Samples were incubated at different pH values (see symbols at the top of the graphs) in a 50 mM McIlvaine buffer. Soluble fractions obtained from the incubation of RAC with either *Mt*LPMO9B or *Mt*LPMO9D were incubated with β-glucosidase (1 U per sample) to yield glucose (not shown), gluconic acid and cellobionic acid only. Optimal temperatures were determined from the incubation of RAC with either *Mt*LPMO9B and *Mt*LPMO9D in the presence of ascorbic acid or 3-methylcatechol at pH 5 for 8 h (**Figure 6.4**).

2.6 Ascorbic acid and 3-methycatechol – pH and temperature effects

The observed effects of pH and temperature on the catalytic performance of *Mt*LPMOs raised the question whether and how the reducing agents ascorbic acid and 3-methylcatechol are affected by pH and temperature. Hence, for these two reducing agents, both the stability and their reduction potential were determined at varying pH and temperatures (**Figures 6.6** and **6.7**). Each reducing agent (1000 µM) was incubated for 12 h and the remaining reducing agent concentration reflected its stabilty. In addition, standard calibration curves were prepared at each pH that was used to avoid

errors by UV quantification, since the pH is known to change the absorption maxima of e.g. ascorbic acid [24]. Ascorbic acid remained stable (conc. > 800 µM) between pH 3.0 to 8.0 at 20 and 30°C (**Figure 6.6a**). However, the stability of ascorbic acid decreased at increasing temperature (> 30°C) and at a higher pH. Above 50°C, the concentration of ascorbic acid decreased by more than 60% (conc. < 400 µM) at a pH above 5.0 (**Figure 6.6a**).

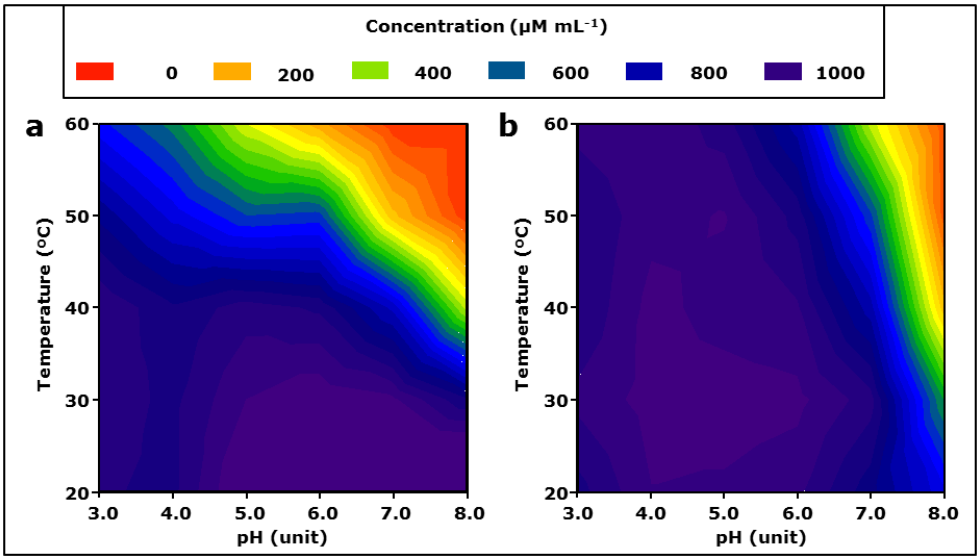

Figure 6.6 Contour plot of the stability of ascorbic acid and 3-methylcatechol as a function of pH and temperature. Samples containing either **a** ascorbic acid (1 mM) or **b** 3-methylcatechol (1 mM) were incubated at different temperatures (20, 30, 40, 50 and 60°C) and pH values (3.0, 4.0, 5.0, 6.0, 7.0, and 8.0) for 12 h. The purple and blue regions indicate the highest ascorbic acid and 3-methylcatechol concentrations in the samples after 12 h of incubation. The ascorbic acid and 3-methylcatechol concentrations were analyzed by using UHPLC-MS. The contour plot was obtained by using SigmaPlot 8.0.

3-Methylcatechol was stable (conc. > 800 µM) between 20 and 60°C and at a pH ranging from 3.0 to 6.0 (**Figure 6.6b**). However, 3-methylcatechol became instable above pH ≥ 7.0, even at low temperatures like 30°C and above. For instance, the 3-methylcatechol concentration decreased about 50% (conc. 516 µM) when incubated at 30°C and pH 8.0 for 12 h (**Figure 6.6b**).

The fate of ascorbic acid and 3-methylcatechol during the incubation in the above mentioned conditions was not further investigated. Although not determined in our analysis, ascorbic acid is known to form degradation products such as furfural, 3-hydroxy-2-pyrone or 2-furoic acid, depending on temperature and pH [25]. In contrast to ascorbic acid, the decline in the 3-methylcatechol concentration was accompanied by the formation of insoluble brown pigments that precepitated after centrifugation (15 min, 15,000 x *g*, 4°C). This pigment formation most likely resulted from the auto-oxidation and polymerization of 3-methylcatechol, which has already been described for other catechol compounds [26].

The reduction potentials of ascorbic acid and 3-methylcatechol were measured using cyclic voltammetry. Determined reduction potentials of electron donating compounds can be used to describe their reducing efficiency on LPMOs. In general, the reducing efficiency of electron-donating

compounds increases as the reduction potential decreases. As previously described [27], the use of cyclic voltammetry to determine the reduction potential of ascorbic acid is incomplete due to an irreversible reduction of this reducing agent. Therefore, the cathodic peak potential E_{pc} was used to illustrate the impact of pH and temperature on the formal reduction potential (E°') of ascorbic acid. A pH increase from 3.0 to 7.0 decreased the cathodic peak potential of ascorbic acid by about 0.25 V at 20°C, which was similar to the determined difference at 30, 40 and 50°C (**Figure 6.7a**). Thus, ascorbic acid has a stronger reducing efficiency on LPMOs at a higher pH. A temperature increase from 20 to 50°C decreased the cathodic peak potential of ascorbic acid by about 0.06 V, which was less compared to the pH-dependent decrease (0.25 V) (**Figure 6.7b**).

For 3-methylcatechol an increase of the pH from 3.0 to 7.0 led to a decrease of up to 0.22 V of the reduction potential of 3-methylcatechol measured at 20, 30, 40 and 50°C (**Figure 6.7c**). Hence, 3-methylcatechol has a stronger reducing efficiency on LPMOs at a higher pH, just like ascorbic acid. As observed for ascorbic acid, an increase of the temperature from 20 to 50°C affected the formal reduction potential of 3-methylcatechol only slightly (~ 0.02 V) (**Figure 6.7d**).

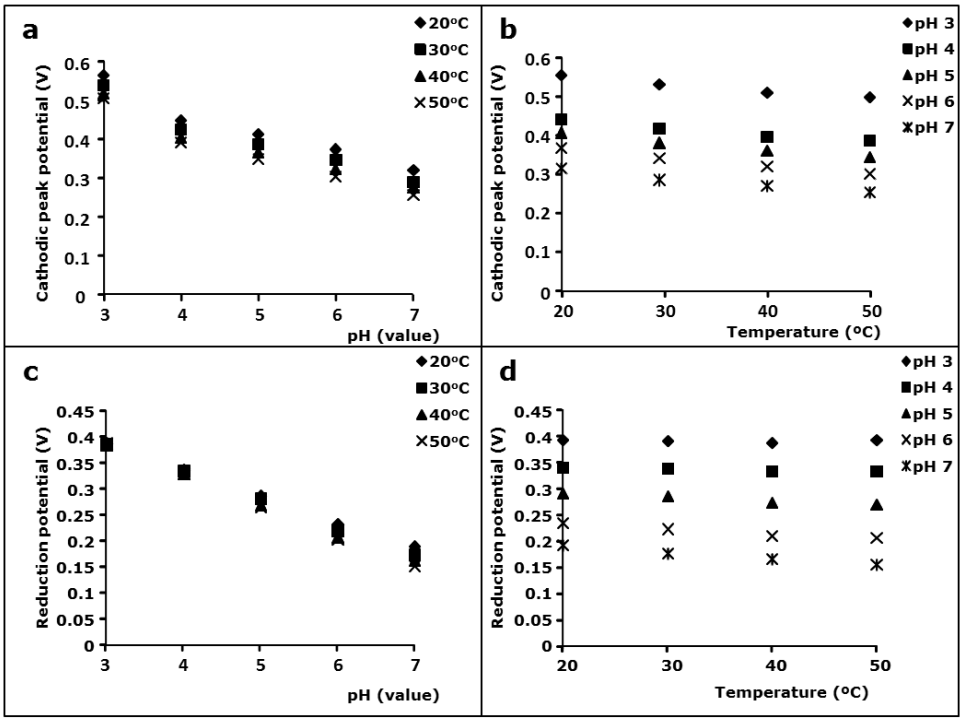

Figure 6.7 Redox potentials of ascorbic acid and 3-methylcatechol. The redox potentials of ascorbic acid (1 mM) and 3-methylcatechol (1 mM) were measured at different pH and temperature values by using cyclic voltammetry. **a** and **b** – Cathodic peak potential E_{pc} of ascorbic acid at **a** pH 3.0 to 7.0 and **b** between 20 and 50°C. The reduction potential (E°') of ascorbic acid was not obtained due to the non-reversible reduction of ascorbic acid during cyclic voltammetry. **c** and **d** – Reduction potential (E°') of 3-methylcatechol at **c** pH 3.0 to 7.0 and **d** between 20 and 50°C. Standard deviations (not presented) are between 0.001–0.026 (median 0.007) and 0.001–0.004 (median 0.001) for ascorbic acid and 3-methylcatechol, respectively. All samples were measured in duplicate.

2.7 Structure-based sequence alignment of *Mt*LPMO9B and *Mt*LPMO9D

*Mt*LPMO9D shares 100% amino acid sequence identity with the recently described *Mt*PMO3*. *Mt*PMO3* is encoded by a gene (gene ID: MYCTH_92668) from *M. thermophila* ATCC 42464, which is a closely related species to *M. thermophila* C1. Furthermore, *Mt*PMO3* was produced via heterologous gene expression in *Neurospora crassa* (FGSC 2489) [22], whereas *Mt*LPMO9D was obtained from homologous gene expression using the native host *M. thermophila* C1. Span & colleagues also obtained the crystal structure of *Mt*PMO3* (pdb ID code 4UFV)[22], which we used to construct a structure-based sequence alignment of *Mt*LPMO9B and *Mt*LPMO9D (**Figure 6.8**). In the alignment, both LPMOs are shown without the signal peptide, while the carbohydrate binding module 1, which is linked to *Mt*LPMO9B, is also not presented. Based on the amino acid sequence, *Mt*LPMO9B has a theoretical molecular weight of 23.8 kDa, whereas the appended CBM-1 has a molecular weight of 6.8 kDa. [17]. The overall amino acid sequence identity of *Mt*LPMO9B (without appended CBM) and *Mt*LPMO9D is 31.8%. Both *Mt*LPMO9B and *Mt*LPMO9D share the β-sheet core that is typical for LPMOs, but differ in their loop regions 'loop 2' (L2, Gly16-Val27), 'loop short' (LS, Gly108-Trp-126), 'loop 8' (L8, Gln162-Pro166) and 'long C-terminal loop' (LC, Gly195-Thr228) that are involved in shaping the substrate-binding surface [22, 28, 29]. The amino acid residues of *Mt*LPMO9B and *Mt*LPMO9D involved in the coordination of the copper are His1-His79-Tyr170 and His1-His75-Tyr169, respectively. Special characteristics of the amino acid sequences of *Mt*LPMO9B and *Mt*LPMO9D are further highlighted in the discussion (**Section 3.4**).

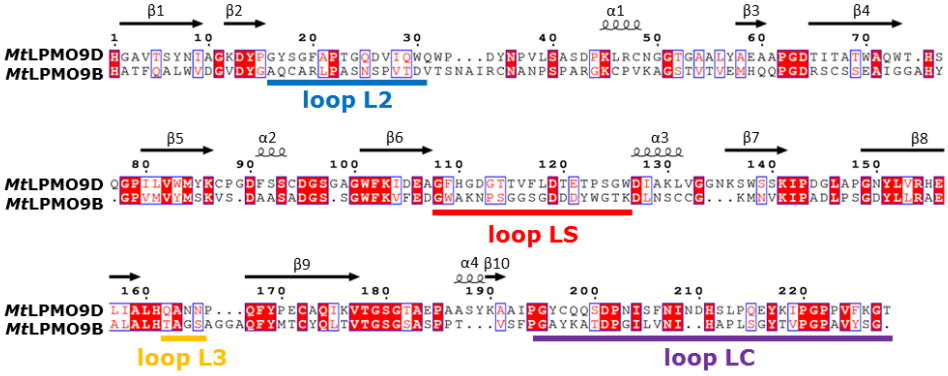

Figure 6.8 Structure-based sequence alignment of *Mt*LPMO9B and *Mt*LPMO9D. The amino acid sequences of *Mt*LPMO9B and *Mt*LPMO9D were aligned with the amino acid sequence of *Mt*PMO3* (PDB ID code 4UFV, 100% amino acid sequence identity with *Mt*LPMO9D) based on [22]. Conserved amino acid residues are presented as white letters on a red background. Amino acid residues that have comparable chemical and physical properties are presented as red letters within blue frames. The secondary structures β-strands (black arrow) and α-helices (black helix) are based on *Mt*PMO3* and shown above the sequences [22]. The amino acid residues of the four loop regions L2 (blue), L3 (yellow), LS (red) and LC (purple) are marked by colored lines below the sequences [22]. Sequences are presented without the signal sequence and start from the N-terminal histidine (His1). The structure-based sequence alignment was obtained by using ESPript [30].

2.8 Conformational stability of *Mt*LPMO9B and *Mt*LPMO9D

The conformational stability of *Mt*LPMO9B and *Mt*LPMO9D as a function of temperature was determined by far-UV circular dichroism (CD). The CD spectra recorded at 20°C (**Figures 6.9a** and **6.9b**) revealed that both *Mt*LPMOs share a high content of antiparallel β-sheets, whereas the content of α-helices and β-turns is relatively low (**Additional Figure 6.3**). The BeStSel method was used because it has been reported to be a reliable tool for the estimation of the secondary structure composition (%) of proteins which contain high amounts of β-structures [31]. It should be noted that the obtained CD-spectrum of *Mt*LPMO9B is likely to be influenced by the secondary structure of the appended CBM-domain. This CBM1 of *Mt*LPMO9B shares an amino acid sequence identity of 59% with the C-terminal cellulose binding domain (pdb ID code: 1CBH) of a cellobiohydrolase I (CT-CBH I). It is noteworthy that this CT-CBH I binding domain comprises three antiparallel β-sheets, which is expected to be similar for the CBM I appended to *Mt*LPMO9B [32].

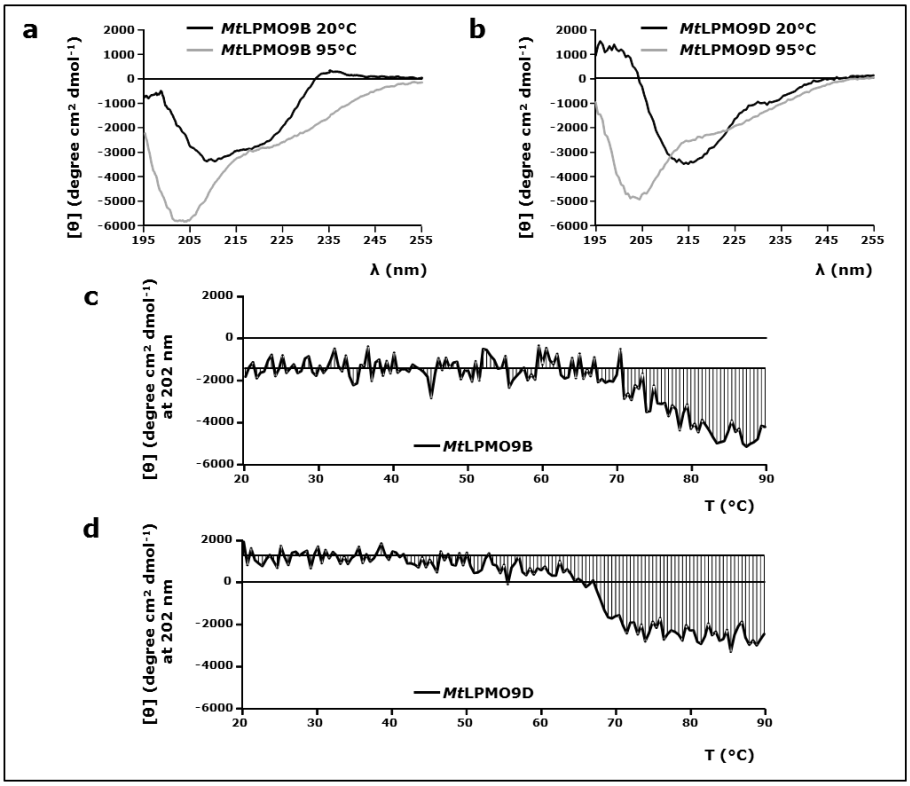

Figure 6.9 Circular dichroism (CD) spectra and conformational stability as a function of temperature of *Mt*LPMO9B and *Mt*LPMO9D. CD spectra (far UV) of **a** *Mt*LPMO9B (0.20 mg mL^{-1}) and **b** *Mt*LPMO9D (0.20 mg mL^{-1}) at 20 and 90°C, respectively. The conformational stability of **c** *Mt*LPMO9B (0.20 mg mL^{-1}) and **d** *Mt*LPMO9D (0.20 mg mL^{-1}) was determined from 20 to 90°C. The temperature was increased at a rate of 1°C min^{-1}. Protein unfolding was monitored at 202 nm by far UV CD. The horizontal line shows the determined mean residue ellipticity [θ] (degree cm^2 $dmol^{-1}$) average between 20 and 40°C, whereas vertical lines illustrate the deviations from this initial [θ] average. The formulas to calculate the mean residue ellipticity [θ] were used as described in Greenfield [33]. Both CD spectra and conformational stability of the *Mt*LPMOs were determined by using a 10 mM potassium phosphate buffer at pH 7.0.

From monitoring the change in CD signal at 202 nm upon heating, it could be deduced that the *Mt*LPMO9B protein structure was stable in a temperature range between 20 and 70°C, and unfolded gradually at higher temperatures (**Figure 6.9c**). Until now it is not clear if the gradual change in CD signal above 70°C is related to the separate unfolding of the *Mt*LPMO9B or appended CBM domain. **Figure 6.9d** shows that the CD spectrum of *Mt*LPMO9D already started to change above 40°C. This gradual change was followed by a sharper transition around 68°C (**Figure 6.9d**). The impact of temperature on the protein structures was further illustrated by the far-UV CD spectra of *Mt*LPMO9B and *Mt*LPMO9D recorded at 90°C (**Additional Figure 6.3**). Both *Mt*LPMOs comprised less β-sheets and α-helices at 90°C, whereas the content of β-turns and undefined secondary structures increased. Notably, both proteins still contained a significant amount of secondary structures, such as β-sheets, at this temperature (**Additional Figure 6.3**). A reverse temperature decrease from 90 to 20°C did not lead to refolding of *Mt*LPMO9B or *Mt*LPMO9D to their native state (data not shown).

3. Discussion

3.1 Quantification of soluble and insoluble C1-oxidized gluco-oligosaccharides

In this research, we used a β-glucosidase-assisted method to quantify released C1-oxidized gluco-oligosaccharides in order to evaluate the catalytic properties of two C1-oxidizing *Mt*LPMOs (**Figure 6.1**, **Additional Figure 6.1**) [17]. A comparable method has been described earlier, but was aimed at the quantification of released C1-oxidized chito-oligosaccharides from chitin by the AA10 CBP21 [34]. Other studies applied multiple enzymes or enzyme cocktails to enable quantification or to ease the analysis of oxidized gluco-oligosaccharides released by LPMOs [15, 20, 35, 36]. So far, these methods have not been used to discriminate between soluble and insoluble C1-oxidized gluco-oligosaccharides. Additionally, these methods have not been applied to investigate the pH and temperature dependency of LMPOs, which was the aim of the present study. Hereto, it was verified that our β-glucosidase-assisted method is suitable for the quantification of different C1-oxidized gluco-oligosaccharides in a range of 0 to 60 nmol mL^{-1} (**Figure 6.2**). The β-glucosidase from almonds, which was used for this method, did not show a significant activity towards cellobionic acid, since we only determined a minor amount of gluconic acid (**Figure 6.1**). In addition, a considerable dose (1 U) of β-glucosidase was needed to cleave released non-oxidized and C1-oxidized gluco-oligosaccharides into glucose, gluconic acid and cellobionic acid only. It is likely that known inhibitors of β-glucosidases, such as glucose, 1,5-gluconolactone and gluconic acid, also suppressed the activity of the β-glucosidase from almonds used for this method [37, 38].

3.2 Time-dependent cellulose oxidation by *Mt*LPMO9B

We showed that the initial reaction products of *Mt*LPMO9B-mediated oxidation of cellulose are insoluble and that they precede the generation of soluble C1-oxidized gluco-oligosaccharides (**Figure 6.3**). In the incubations with *Mt*LPMO9B (**Figure 6.3**), it took approximately 8 h until more soluble than insoluble C1-oxidized products were formed. This finding is in agreement with the previously described cleavage pattern of *Nc*LPMO9F, which was imaged by atomic force microscopy (AFM) [39]. Although the activity of *Nc*LPMO9F was tested towards crystalline cellulose, AFM imaging showed a degradation of non-soluble cellulose structures, followed by the formation of smaller fragments, which dissolved during the ongoing degradation. We studied *Mt*LPMOs on RAC only, but it can be expected that the time until soluble products are released differs between LPMOs. This expectation

is based on the fact that LPMOs show differences in the preference for crystalline and amorphous regions of cellulose [39-41]. Obviously, the substrate morphology and the length of glucosyl chains in particular [8, 42], will influence the time-dependent release of C1-oxidized gluco-oligosaccharides.

3.3 Catalytic performance of *Mt*LPMO9B and *Mt*LPMO9B as a function of pH and temperature

Here, we show that the pH and temperature dependency of *Mt*LPMO9B and *Mt*LPMO9D is influenced by multiple factors such as type of reducing agent, reducing agent stability and operational stability of the LPMO enzyme. All these factors need to be considered when evaluating the catalytic properties of LPMOs.

At pH 5.0, both *Mt*LPMO9B and *Mt*LPMO9D showed a reducing agent-dependent temperature optimum. The catalytic performance of *Mt*LPMO9B was highest at 40 and 60°C in the presence of ascorbic acid and 3-methylcatechol, respectively (**Figure 6.4**). The decrease in the catalytic performance of *Mt*LPMO9B above 50°C in the presence of ascorbic acid likely resulted from the accompanying decline in ascorbic acid stability (**Figure 6.6a**). In contrast, 3-methylcatechol was stable over the whole temperature range (20-60°C) and, consequently, did not influence the temperature optimum of *Mt*LPMO9B (**Figure 6.6b**). It is noteworthy that the efficiency of both reducing agents was hardly affected by the temperature (**Figures 6.7a** and **6.7c**). In addition, no alterations in the secondary structure of *Mt*LPMO9B were determined between 20 and 70°C based of CD measurements at pH 7.0, which illustrates the conformational stability of *Mt*LPMO9B in this temperature range (**Figure 6.9c**). In contrast to *Mt*LPMO9B, *Mt*LPMO9D was less active at higher temperatures in the presence of both reducing agents (**Figure 6.4**). From the observed conformational changes of *Mt*LPMO9D at temperatures above 40°C (**Figure 6.9d**), it is most likely that the reduced catalytic performance at higher temperatures is determined by the relatively poor operational stability of this enzyme. Considering the above, quantitative results reported in literature with various LPMOs should be interpreted cautiously, since most of the reported conversions have been performed using only one single time point, at one temperature and pH value.

Next to the temperature dependency, the pH dependency of the catalytic performance of *Mt*LPMOs was investigated. In general, in the presence of both ascorbic acid and 3-methylcatechol, a higher pH enhanced the catalytic performance of *Mt*LPMO9B and *Mt*LPMO9D (**Figure 6.5**). One explanation for this behavior is the decrease in redox potential, and thus a stronger reducing power of both electron donors at higher pH (**Figure 6.7**). A positive relation between the reducing power of various reducing agents and an improved catalytic performance of LPMOs (LPMO-02916) has already been described before [16]. Nevertheless, as we do not know the rate-limiting step of catalysis, it is possible that other steps in the reaction cycle contribute to the pH dependency of the activities of both *Mt*LPMO enzymes, such as the impact of pH on protonation reactions that occur during the LPMO-catalyzed substrate oxidation [43]. Moreover, it is not known what effect pH and temperature have on the reaction pathway when hydrogen peroxide (H_2O_2) acts as co-substrate instead of molecular oxygen (O_2) [6].

Interestingly, the increase in the catalytic performance of *Mt*LPMO9B at higher pH values was already at its maximum after 6 h of incubation (**Figures 6.5a** and **6.5b**). This indicates that *Mt*LPMO9B was inactivated within the first 6 h at pH values above 6.0. One possible explanation is

that the enhanced tendency of reducing agents to donate electrons led to an increased production of reactive oxygen species (ROS). Previous research already reported that the inactivation of LPMOs by ROS can occur within minutes [6]. It was concluded that the formation of ROS in the catalytic center during LPMO activity led to oxidative modification of the catalytic histidine and neighboring residues, which results in LPMO inactivation. In addition, the limited stability of ascorbic acid and 3-methylcatechol above pH 7 at higher temperatures (40-60°C) also affects the catalytic performance of *Mt*LPMOs (**Figures 6.5** and **6.6**).

For *Mt*LPMO9D, the incubation conditions were found to be even more critical for optimal performance. This enzyme was inactivated within the first 6 h of incubation at most pH values tested, or alternatively showed hardly any catalytic performance at a low pH (3.0-5.0; **Figures 6.5c** and **6.5d**).

3.4 Structural features of *Mt*LPMO9B and *Mt*LPMO9D

Although the C1-oxidizers *Mt*LPMO9B and *Mt*LPMO9D originate from the same fungal *M. thermophila* C1 strain, these enzymes share only 32% sequence identity. Intriguingly, *Mt*LPMO9D comprises multiple aromatic amino acid residues (1 x Tyr, 2 x Trp and 1 x Phe) within the L2 loop, whereas other AA9 type LPMOs have been described to contain one or two aromatic residues [44]. In contrast to *Mt*LPMO9D, *Mt*LPMO9B does not contain any aromatic amino acid in the L2 loop. Aromatic amino acids are known to play an important role in shaping the substrate-binding surface, substrate recognition and specificity of LPMOs [44]. Furthermore, it has been reported that single domain LPMOs comprise strong substrate-binding abilities [45-48], whereas LPMOs with CBMs show a decreased substrate affinity [49, 50]. Therefore, it is possible that the aromatic amino acid residues present in the L2 loop of *Mt*LPMO9D enhance the substrate-binding abilities.

Using the developed β-glucosidase-assisted method, we showed that *Mt*LPMO9B has an about five times higher overall activity towards cellulose compared to *Mt*LPMO9D (**Figure 6.4**). Whether this higher activity is related to the presence of CBM1 can only be speculated. So far, a diverse effect of CBMs on the catalytic performance of LPMOs has been shown and this effect seems dependent on the type of substrate or LPMO used [40, 51-53].

The structural features of the *Mt*LPMOs are also illustrated in the far-UV CD spectra. Based on the BeStSel method, the calculated secondary structure composition (%) of both *Mt*LPMOs is typical for AA9 LPMOs (**Additional Figure 6.3**) [1, 4, 13]. Both *Mt*LPMOs share a high content of antiparallel β-sheets and minor amounts of α-helices and β-turns, but differ significantly in their CD spectra (**Additional Figure 6.3**).

It has been shown that proteins which comprise a high amount of β-sheets and a low amount of α-helices have diverse far-UV CD spectral properties, whereas proteins with a high content of α-helices are more similar in their CD spectra [31]. Hence, we used the crystal structure of *Mt*PMO3*, which shares a 100% amino acid sequence identity with *Mt*LPMO9D to control if the secondary structure prediction based on the obtained CD spectra by using the BeStSel method is in agreement with the actual secondary structure [22]. Based on the predicted secondary structure, the percentage of antiparallel β-sheets was overestimated by about 20% whereas the amount of β-turns was underestimated (-25%) (**Additional Figure 6.3**) compared to the actual secondary structure of *Mt*PMO3*. In contrast, the percentage of predicted α-helices corresponded to the amount of α-helices present in *Mt*PMO3*. The deviation between the predicted and the actual secondary

structure is likely to result from the limited CD spectral data obtained below 200 nm, which is of importance to obtain a more accurate secondary structure prediction [54]. Especially the CD spectrum of *Mt*LPMO9B showed an atypical break below 200 nm, which was also observed if a lower protein concentration (0.1 mg mL^{-1}) was used (data not shown). Possibly, the conditions used (e.g. type of buffer and or pH) were suboptimal for determining a more accurate CD spectrum of the *Mt*LPMOs in the lower wavelength range (< 200 nm). Still, the accuracy of the predicted compared to the actual secondary structure is in agreement with values reported in the literature and, therefore, was further used to determine the conformational stability of the *Mt*LPMOs upon heating [31].

Interestingly, the secondary structure of *Mt*LPMO9B hardly altered upon heating until 70°C (**Figure 6.9c**), which is indicative for the high conformational stability of this LPMO. As mentioned in the results section, we do not know to what degree the appended CBM I contributes to the determined structural changes upon heating of *Mt*LPMO9B (**Figure 6.9**). *Mt*LPMO9D on the other hand, already showed minor structural changes between 40 and 60°C and lost most of its native structure at 70°C (**Figure 6.9**). Still, both *Mt*LPMOs maintain a decent amount of structure at 90°C and both CD spectra of *Mt*LPMOs show a collapse in the signal around 200 nm (**Figure 6.9a** and **6.9b**). Intriguingly, similar CD spectra with a strong negative band near 205 nm have been shown for poly(Pro)II helix, which might suggest that the *Mt*LPMOs have turned into a kind of fibrillar state during the heat-induced denaturation process [55, 56].

4. Conclusion

In this research, we successfully developed a β-glucosidase-assisted method to quantify the release of C1-oxidized gluco-oligosaccharides from RAC incubated with *Mt*LPMO9B and *Mt*LPMO9C. The method was applied to determine the impact of pH and temperature on the catalytic performance of *Mt*LPMOs in the presence of ascorbic acid or 3-methylcatechol. It is concluded that the catalytic performance of *Mt*LPMO9B and *Mt*LPMO9C depends on pH and temperature with a different optimum for each reducing agent. Our work demonstrates that pH affects the overall enzymatic rate and reducing agent dependency, while temperature mainly influences the operational stability of these LPMOs.

5. Methods

5.1 Enzyme expression, production and purification

*Mt*LPMO9B was produced and purified as previously described [17]. The homologous expression of *Mt*LPMO9D (UniProt: KY924631) was performed by using a low protease/low (hemi)cellulose producing *Myceliophthora thermophila* C1 strain [57, 58]. The *Mt*LPMO9D-containing crude enzyme preparation from the fermentation broth was dialyzed against a 10 mM potassium phosphate buffer (pH 7.0). *Mt*LPMO9D was purified from the dialyzed enzyme preparation by using an ÄKTA-Explorer preparative chromatography system (GE Healthcare, Uppsala, Sweden). The absorbance was continuously monitored at 220 and 280 nm. The protein content of *Mt*LPMO9D-containing fractions was determined as previously described using a BCA Protein Assay Kit [12].

*Mt*LPMO9D was purified in five subsequent chromatographic steps. First, hydrophobic interaction chromatography (HIC) was applied by loading the *Mt*LPMO9D-containing enzyme preparation on a self-packed Phenyl Sepharose Fast Flow column (450 mL, GE Healthcare). The column was pre-equilibrated with 3 column volumes of a 20 mM potassium phosphate buffer (pH 7.8) containing 0.9 M ammonium sulphate. After sample loading, a linear gradient from 0.9 to 0 M ammonium sulphate in a 20 mM potassium phosphate buffer (pH 7.8) was applied at a flow rate of 5 mL min^{-1} over 4 column volumes. All fractions were collected and immediately stored on ice. Peak fractions were, based on UV (280 nm), pooled and concentrated by ultrafiltration (Amicon Ultra, molecular mass cut-off of 3 kDa, Merck Millipore, Cork, Ireland) at 4°C. The concentrated pools were analyzed by SDS-PAGE to determine the *Mt*LPMO9D-containing pool (expected molecular mass 25.4 kDa). The second purification step was applied by using anion exchange chromatography (AEC). The *Mt*LPMO9D-containing fraction was loaded on a Source 30 Q column (50 mL, GE Healthcare) and the column was equilibrated with a 20 mM potassium phosphate buffer (pH 7.8) at a flow rate of 5 mL min^{-1} for 2 column volumes. The elution was performed by using a linear gradient from 0 to 1 M potassium chloride in 20 mM potassium phosphate buffer (pH 7.8) at a flow rate of 5 mL min^{-1} for 10 column volumes. Fractions obtained (10 mL) were immediately stored on ice. Peak fractions were pooled, concentrated and analyzed by SDS-PAGE as described above. In a third purification (HIC) step, the *Mt*LPMO9D-containing pool was loaded on a Phenyl Sepharose Fast Flow column (50 mL, GE Healthcare). The column was pre-equilibrated with a 1.2 M ammonium sulphate in a 20 mM potassium phosphate buffer (pH 7.8). The elution was performed using a linear gradient elution from 1.2 to 0 mM ammonium sulphate in a 20 mM potassium phosphate buffer (pH 7.8) at a flow rate of 5 mL min^{-1} for 4 column volumes. Again, all fractions were immediately stored on ice. The obtained peak fractions were pooled, concentrated and analyzed by SDS-PAGE to determine the *Mt*LPMO9D-containing pool as described above. As a fourth purification step, size exclusion chromatography (SEC) was applied. The *Mt*LPMO9D-containing pool was subjected to a Superdex 75 (250 mL column, GE Healthcare). The equilibration and isocratic elution (2 and 1.5 column volumes, respectively) was performed using a 20 mM potassium phosphate buffer at a flow rate of 3 mL min^{-1}. Fractions were immediately stored on ice. Peak fractions were pooled, concentrated and analyzed by SDS-PAGE to determine the *Mt*LPMO9D-containing pool as described above. In a fifth purification step, the *Mt*LPMO9D-containing fraction was loaded on a Resource Q column (30 x 16 mm internal diameter, GE Healthcare). A 20 mM potassium phosphate buffer (pH 7.0) was used to pre-equilibrate the column. Elution was performed using a linear gradient from 0 to 1 M NaCl in a 20 mM potassium phosphate buffer (pH 7.0) at a flow rate of 6 mL min^{-1} over 20 column volumes and monitored at 220 and 280 nm. All fractions were collected and immediately stored on ice. The fractions of the most abundant peak contained purified *Mt*LPMO9D. Finally, these fractions were pooled, concentrated and stored at -20°C.

5.2 Enzymes, carbohydrates and reducing agents

Regenerated amorphous cellulose (RAC) was prepared from Avicel PH-101 as previously described [12, 42]. D-glucose, D-gluconic acid, ascorbic acid and 3-methylcatechol were purchased from Sigma-Aldrich (Steinheim, Germany). D-cellobionic acid ammonium salt was obtained from Toronto Research Chemicals (Toronto, Ontario, Canada). Almond β-glucosidase was purchased from Sigma-Aldrich and had, according to the suppliers information, a specific activity of 6 U mg^{-1} lyophilized

powder. Commercial cellulase mixtures Celluclast 1.5l and Novozym 188 were obtained from Novozymes A/S (Bagsværd, Denmark).

5.3 Catalytic performance of *Mt*LPMO9B and *Mt*LPMO9D: β-glucosidase-assisted quantification

Regenerated (RAC) amorphous cellulose was dissolved in a 50 mM ammonium acetate buffer (pH 5.0) to a concentration of 2.8 mg mL^{-1} and incubated with *Mt*LPMO9B (3 mg of protein mg^{-1} substrate) in the absence or presence of ascorbic acid (1 mM). Samples were incubated between 0 and 30 h at 50°C in a head-over-tail Stuart rotator (Bibby Scientific, Stone, UK) at 20 rpm. After incubation, all samples were heated for 10 min at 100°C in a water bath (TW20 Water Bath, JULABO GmbH, Seelbach, Germany) and afterwards cooled down to room temperature (20°C). Subsequently, all samples were centrifuged (15 min, 15,000 x *g*, 4°C) and 250 µL of the supernatant was dissolved in 750 µL of a 50 mM ammonium acetate buffer (pH 5.0). Finally, 1 U of β-glucosidase was added to each sample. All samples were incubated for 20 h at 37°C under continuous shaking at 750 rpm (ThermoMixer Comfort, Eppendorf, Hamburg, Germany). After incubation, samples were cooled on ice, centrifuged (1 min, 15,000 x g, 20°C) and analyzed by using HPAEC. The same protocol as described above was used to determine pH and optimal temperature of *Mt*LPMO9B and *Mt*LPMO9D with the following modifications: i) RAC was incubated with either *Mt*LPMO9B (3.0 µg of protein mg^{-1} substrate) or *Mt*LPMO9D (1.5 µg of protein mg^{-1} substrate) in the absence or presence of ascorbic acid (1 mM) or 3-methylcatechol (1 mM); ii) all incubations were performed in a McIlvaine buffer at pH 3.0, 4.0, 5.0, 6.0, 7.0, and 8.0, respectively; iii) the pH of all supernatants was adjusted to pH 5.0 prior to β-glucosidase addition. Therefore, 250 µL McIlvaine buffer with a corresponding molarity (50 mM) and a pH between 3.0 and 8.0 was added to 250 µL supernatant until the final pH of the mixture reached precisely pH 5.0. Afterwards, 500 µL McIlvaine buffer (50 mM, pH 5.0) containing 1U β-glucosidase was added to each sample, which yielded a total volume of 1 mL. All incubations of RAC with and without enzyme addition were performed in triplicate. Samples were diluted 10 times prior to HPAEC analysis.

5.4 Enzymatic hydrolysis of cellulose obtained from the incubation of RAC with *Mt*LPMO9B

The total cellulose (or RAC) hydrolysis was performed by using a previously described method [20] with the following modifications. Samples (triplicates), obtained from the incubation of RAC with *Mt*LPMO9B in the presence and absence of ascorbic acid, were heated for 10 min at 100°C in a water bath and cooled down to room temperature (20°C) afterwards. Samples were then centrifuged (15 min, 15,000 x *g*, 4°C) and the complete supernatant was removed. The remaining pellet was dissolved in 1000 µL of a 75 mM ammonium acetate buffer (pH 5.0) and stirred vigorously. Subsequently, Celluclast 1.5l (0.9%, w/v) and Novozym 188 (0.18%, w/v) were added to each sample. All samples were incubated at 50°C for 20 h. After incubation, samples were centrifuged (15 min, 15,000 x *g*, 4°C) and the supernatant was diluted twenty times prior to HPAEC analysis.

5.5 HPAEC analysis of mono- and oligosaccharides

D-Glucose, gluconic acid, cellobionic acid and (oxidized) oligosaccharides were analyzed by high-performance anion exchange chromatography (HPAEC) with pulsed amperometric detection (PAD) using a Dionex ICS-5000 system (Sunnyvale, CA, USA) as described previously [12] with the following

modification. The temperature of the auto sampler was set to 6°C. A gradient elution program of 35 min was used for the quantification of C1-oxidized gluco-oligosaccharides. In brief, 0–21 min, linear gradient 0-0.25 M NaOAc; 21-25 min, linear gradient 0.25-1 M NaOAc; 25-28 min isocratic gradient 1 M NaOAc; followed by equilibration (7 min) of the column with the starting conditions. Gluconic acid and cellobionic acid were used for calibration in a range of 0 to 50 µg mL^{-1}.

5.6 RP-UHPLC-UV-ESI-MS analysis of ascorbic acid and 3-methylcatechol

Ascorbic acid (1 mM) and 3-methylcatechol (1 mM) were dissolved in a 50 mM McIlvaine buffer ranging from pH 3.0 to 8.0. These samples were incubated at different temperatures (20, 30, 40, 50 and 60°C) under continuous shaking at 750 rpm (ThermoMixer Comfort) for 12 h. Afterwards, all incubates were centrifuged (15 min, 15,000 x g, 4°C) and the supernatant was diluted fifty times in the starting eluent A (H_2O + 1% (v/v) acetonitrile + 0.1% (v/v) HOAc) prior to analysis. The samples were analyzed by using an Accela reversed phase high-performance liquid chromatography (RP-UHPLC) system coupled to electron spray ionization mass spectrometry (Thermo Scientific, San Jose, CA, USA) as described previously [21]. The concentration of ascorbic acid and 3-methylcatechol was determined spectrophotometrically, using an UV-VIS-spectrophotometer (CPS-240A, Shimadzu, Kyoto, Japan). Ascorbic acid was quantified by measuring the absorption at 265 nm [24]. The maximum absorbance of 3-methylcatechol was determined at 262 nm at pH 5.0. The use of different pH values during the incubations led to different absorption maxima of measured samples. Therefore, standard calibration curves were created for all six different pH values for both ascorbic acid and 3-methylcatechol in a range of 0 to 1 mM.

5.7 Reduction potential of ascorbic acid and 3-methylcatechol.

Voltammetry experiments were performed by using an Autolab PGSTAT100 Potentiostat (Metronohm, Utrecht, The Netherlands). Both ascorbic acid and 3-methylcatechol (1 mM) were dissolved in a 50 mM McIlvaine buffer ranging from pH 3.0 to 7.0. Temperature-dependent measurements (20-50°C) were conducted by pre-heating samples in a water bath prior to analysis. Samples were analyzed in duplicate. A three-electrode configuration was used consisting of an Ag/AgCl reference electrode, a glassy carbon working electrode and a platinum plate counter electrode. Scans were made from -300 to 800 mV with a scan rate of 50 mV s^{-1}.

5.8 Structure-based sequence alignment

Structure-based sequence alignments of *Mt*LPMO9B and *Mt*LPMO9D were constructed by using the amino acid sequence and 3D-structure of *Mt*PMO3* (pdb ID code 5UFV) from *M. thermophila* (ATCC 42464) based on [22]. *Mt*PMO3* and *Mt*LPMO9D share a 100% amino acid sequence identity. The final alignment was obtained by using ESPript [30].

5.9. Secondary structure analysis

Changes in secondary structure as a function of temperature of both *Mt*LPMOs were measured by using far UV circular dichroism. *Mt*LPMO concentrations and the conditions are described in the figure captions. Measurements were performed using a J-715 spectropolarimeter (Jasco Corp., Tokyo, Japan) with a sensitivity of 100 mdeg and a bandwidth of 2 nm. All obtained CD spectra of the *Mt*LPMOs have been corrected by subtracting the CD spectra of the buffer. Samples were measured by using quartz cuvettes with an optical path length of 0.1 cm. Secondary structure compositions (%) were calculated by using the online software BeStSel [59]. The calculation of the secondary structure composition (%) of *Mt*PMO3* was based on a method described previously [60,

61]. In brief, the secondary structure composition was calculated by using the number of amino acids involved in the formation of secondary structures (based on the DSSP file of the pdb ID code 5UFV) and the total number of amino acid residues based on the *Mt*PMO3* sequence.

References

1. Harris PV, Welner D, McFarland KC, Re E, Navarro Poulsen JC, Brown K *et al*. Stimulation of lignocellulosic biomass hydrolysis by proteins of glycoside hydrolase family 61: Structure and function of a large, enigmatic family. Biochemistry. 2010;49(15):3305-16.
2. Merino ST, Cherry J. Progress and challenges in enzyme development for biomass utilization. In: Biofuels. Olsson L, editor. Berlin, Heidelberg: Springer Berlin Heidelberg; 2007; p. 95-120.
3. Lombard V, Golaconda Ramulu H, Drula E, Coutinho PM, Henrissat B. The carbohydrate-active enzymes database (CAZy) in 2013. Nucleic Acids Res. 2014:42;D490–5.
4. Quinlan RJ, Sweeney MD, Lo Leggio L, Otten H, Poulsen JC, Johansen KS *et al*. Insights into the oxidative degradation of cellulose by a copper metalloenzyme that exploits biomass components. Proc. Natl. Acad. Sci. U.S.A. 2011;108(37):15079-84.
5. Vaaje-Kolstad G, Westereng B, Horn SJ, Liu Z, Zhai H, Sorlie M *et al*. An oxidative enzyme boosting the enzymatic conversion of recalcitrant polysaccharides. Science. 2010;330(6001):219-22.
6. Bissaro B, Rohr AK, Skaugen M, Forsberg Z, Horn SJ, Vaaje-Kolstad G *et al*. Fenton-type chemistry by a copper enzyme: molecular mechanism of polysaccharide oxidative cleavage. bioRxiv. 2016.
7. Parthasarathi R, Bellesia G, Chundawat SPS, Dale BE, Langan P, Gnanakaran S. Insights into hydrogen bonding and stacking interactions in cellulose. J. Phys. Chem. A. 2011;115(49):14191-202.
8. Jarvis M. Chemistry: Cellulose stacks up. Science. 2003;426(6967):611-2.
9. Phillips CM, Beeson WT, Cate JH, Marletta MA. Cellobiose dehydrogenase and a copper-dependent polysaccharide monooxygenase potentiate cellulose degradation by *Neurospora crassa*. ACS Chem. Biol. 2011;6(12):1399-406.
10. Agger JW, Isaksen T, Varnai A, Vidal-Melgosa S, Willats WG, Ludwig R *et al*. Discovery of LPMO activity on hemicelluloses shows the importance of oxidative processes in plant cell wall degradation. Proc. Natl. Acad. Sci. U.S.A. 2014;111(17):6287-92.
11. Frandsen KEH, Simmons TJ, Dupree P, Poulsen J-CN, Hemsworth GR, Ciano L *et al*. The molecular basis of polysaccharide cleavage by lytic polysaccharide monooxygenases. Nat. Chem. Biol. 2016;12(4):298-303.
12. Frommhagen M, Sforza S, Westphal AH, Visser J, Hinz SW, Koetsier MJ *et al*. Discovery of the combined oxidative cleavage of plant xylan and cellulose by a new fungal polysaccharide monooxygenase. Biotechnol. Biofuels. 2015;8:101.
13. Karkehabadi S, Hansson H, Kim S, Piens K, Mitchinson C, Sandgren M. The first structure of a glycoside hydrolase family 61 member, Cel61B from *Hypocrea jecorina*, at 1.6 A resolution. J. Mol. Biol. 2008;383(1):144-54.
14. Frommhagen M, van Erven G, Sanders M, van Berkel WJH, Kabel MA, Gruppen H. RP-UHPLC-UV-ESI-MS/MS analysis of LPMO generated C4-oxidized gluco-oligosaccharides after non-reductive labeling with 2-aminobenzamide. Carbohydr. Res. 2017; 448:191-199.
15. Westereng B, Arntzen MØ, Aachmann FL, Várnai A, Eijsink VGH, Agger JW. Simultaneous analysis of C1 and C4 oxidized oligosaccharides, the products of lytic polysaccharide monooxygenases acting on cellulose. J. Chromatogr. A. 2016;1445:46–54.
16. Kracher D, Scheiblbrandner S, Felice AKG, Breslmayr E, Preims M, Ludwicka K *et al*. Extracellular electron transfer systems fuel cellulose oxidative degradation. Science. 2016;27;352(6289):1098-101.
17. Frommhagen M, Koetsier MJ, Westphal AH, Visser J, Hinz SWA, Vincken J-P *et al*. Lytic polysaccharide monooxygenases from *Myceliophthora thermophila* C1 differ in substrate preference and reducing agent specificity. Biotechnol. Biofuels. 2016;9(1):1-17.
18. Westereng B, Cannella D, Wittrup Agger J, Jørgensen H, Larsen Andersen M, Eijsink VGH *et al*. Enzymatic cellulose oxidation is linked to lignin by long-range electron transfer. 2015;5:18561.
19. Bissaro B, Forsberg Z, Ni Y, Hollmann F, Vaaje-Kolstad G, Eijsink VGH. Fueling biomass-degrading oxidative enzymes by light-driven water oxidation. Green Chem. 2016; 18, 5357-5366.
20. Cannella D, Mollers KB, Frigaard NU, Jensen PE, Bjerrum MJ, Johansen KS *et al*. Light-driven oxidation of polysaccharides by photosynthetic pigments and a metalloenzyme. Nat. Commun. 2016; (4)7:11134.
21. Frommhagen M, Mutte SK, Westphal AH, Koetsier MJ, Hinz SWA, Visser J *et al*. Boosting LPMO-driven lignocellulose degradation by polyphenol oxidase-activated lignin building blocks. Biotechnol. Biofuels. 2017;10(1):121.

22. Span EA, Suess DLM, Deller MC, Britt RD, Marletta MA. The role of the secondary coordination sphere in a fungal polysaccharide monooxygenase. ACS Chem. Biol. 201;12(4):1095-1103.
23. Vu VV, Beeson WT, Phillips CM, Cate JH, Marletta MA. Determinants of regioselective hydroxylation in the fungal polysaccharide monooxygenases. J. Am. Chem. Soc. 2014;136(2):562-5.
24. Hernanz A. High-performance liquid chromatographic determination of ascorbic acid in serum using paired-ion chromatography and UV spectrophotometric detection. J. Clin. Chem. Clin. Biochem. 1988;26(7):459-61.
25. Yuan J-P, Chen F. Degradation of ascorbic acid in aqueous solution. J. Agric. Food Chem. 1998;46(12):5078-82.
26. Yang J, Cohen Stuart MA, Kamperman M. Jack of all trades: Versatile catechol crosslinking mechanisms. Chem. Soc. Rev. 2014;43(24):8271-98.
27. Liu Y, Tomiuk S, Rozoy E, Simard S, Bazinet L, Green T *et al*. Thermal oxidation studies on reduced folate, L-5-methyltetrahydrofolic acid (L-5-MTHF) and strategies for stabilization using food matrices. J. Food Sci. 2012;77(2):C236-C43.
28. Li X, Beeson I William T, Phillips CM, Marletta MA, Cate JHD. Structural basis for substrate targeting and catalysis by fungal polysaccharide monooxygenases. Structure. 2012;20(6):1051-61.
29. Wu M, Beckham GT, Larsson AM, Ishida T, Kim S, Payne CM *et al*. Crystal structure and computational characterization of the lytic polysaccharide monooxygenase GH61D from the Basidiomycota fungus *Phanerochaete chrysosporium*. J. Biol. Chem. 2013;288(18):12828-39.
30. Robert X, Gouet P. Deciphering key features in protein structures with the new ENDscript server. Nucleic Acids Res. 2014;42(Web Server issue):W320-4.
31. Micsonai A, Wien F, Kernya L, Lee Y-H, Goto Y, Réfrégiers M *et al*. Accurate secondary structure prediction and fold recognition for circular dichroism spectroscopy. Proc. Natl. Acad. Sci. U.S.A. 2015;112(24):E3095-E103.
32. Kraulis PJ, Clore GM, Nilges M, Jones TA, Pettersson G, Knowles J *et al*. Determination of the three-dimensional solution structure of the C-terminal domain of cellobiohydrolase I from *Trichoderma reesei*. A study using nuclear magnetic resonance and hybrid distance geometry-dynamical simulated annealing. Biochemistry. 1989;28(18):7241-57.
33. Greenfield NJ. Using circular dichroism spectra to estimate protein secondary structure. 2007;1(6):2876-90.
34. Loose JSM, Forsberg Z, Fraaije MW, Eijsink VGH, Vaaje-Kolstad G. A rapid quantitative activity assay shows that the *Vibrio cholerae* colonization factor GbpA is an active lytic polysaccharide monooxygenase. FEBS Lett. 2014;588(18):3435-40.
35. Cannella D, Hsieh C-wC, Felby C, Jørgensen H. Production and effect of aldonic acids during enzymatic hydrolysis of lignocellulose at high dry matter content. Biotechnol. Biofuels. 2012;5(1):26.
36. Müller G, Várnai A, Johansen KS, Eijsink VGH, Horn SJ. Harnessing the potential of LPMO-containing cellulase cocktails poses new demands on processing conditions. Biotechnol. Biofuels. 2015;8(1):1-9.
37. Kara HE, Turan Y, Er A, Acar M, Tümay S, Sinan S. Purification and characterization of β-glucosidase from greater wax moth *Galleria mellonella* L. (Lepitoptera: Pyralidae). Arch. Insect. Biochem. Physiol. 2014;86(4):209-19.
38. Michlmayr H, Schümann C, da Silva NM, Kulbe KD, del Hierro AM. Isolation and basic characterization of a β-glucosidase from a strain of *Lactobacillus brevis* isolated from a malolactic starter culture. J. Appl. Microbiol. 2010;108(2):550-9.
39. Eibinger M, Ganner T, Bubner P, Rosker S, Kracher D, Haltrich D *et al*. Cellulose surface degradation by a lytic polysaccharide monooxygenase and its effect on cellulase hydrolytic efficiency. J. Biol. Chem. 2014;289(52):35929-38.
40. Bennati-Granier C, Garajova S, Champion C, Grisel S, Haon M, Zhou S *et al*. Substrate specificity and regioselectivity of fungal AA9 lytic polysaccharide monooxygenases secreted by *Podospora anserina*. Biotechnol. Biofuels. 2015;8:90.
41. Villares A, Moreau C, Bennati-Granier C, Garajova S, Foucat L, Falourd X *et al*. Lytic polysaccharide monooxygenases disrupt the cellulose fibers structure. Sci. Rep. 2017;7:40262.
42. Zhang Y-HP, Lynd LR. Toward an aggregated understanding of enzymatic hydrolysis of cellulose: Noncomplexed cellulase systems. Biotechnol. Bioeng. 2004;88(7):797-824.
43. Walton PH, Davies GJ. On the catalytic mechanisms of lytic polysaccharide monooxygenases. Curr. Opin. Chem. Biol. 2016;31:195-207.
44. Vaaje-Kolstad G, Forsberg Z, Loose JSM, Bissaro B, Eijsink VGH. Structural diversity of lytic polysaccharide monooxygenases. Curr. Opin. Struct. Biol. 2017;44:67-76.
45. Nakagawa YS, Kudo M, Loose JSM, Ishikawa T, Totani K, Eijsink VGH *et al*. A small lytic polysaccharide monooxygenase from *Streptomyces griseus* targeting α- and β-chitin. FEBS J. 2015;282(6):1065-79.
46. Suzuki K, Suzuki M, Taiyoji M, Nikaidou N, Watanabe T. Chitin binding protein (CBP21) in the culture supernatant of *Serratia marcescens* 2170. Biosci., Biotechnol., Biochem. 1998;62(1):128-35.
47. Vaaje-Kolstad G, Houston DR, Riemen AH, Eijsink VG, van Aalten DM. Crystal structure and binding properties of the *Serratia marcescens* chitin-binding protein CBP21. J. Biol. Chem. 2005;280(12):11313-9.
48. Zeltins A, Schrempp H. Specific interaction of the streptomyces chitin-binding protein Chb1 with α-chitin. Eur. J. Biochem. 1997;246(2):557-64.

49. Forsberg Z, Nelson CE, Dalhus B, Mekasha S, Loose JS, Crouch LI *et al*. Structural and functional analysis of a lytic polysaccharide monooxygenase important for efficient utilization of chitin in *Cellvibrio japonicus*. J. Biol. Chem. 2016; 291(14):7300-12..
50. Forsberg Z, Rohr AK, Mekasha S, Andersson KK, Eijsink VG, Vaaje-Kolstad G *et al*. Comparative study of two chitin-active and two cellulose-active AA10-type lytic polysaccharide monooxygenases. Biochemistry. 2014;53(10):1647-56.
51. Crouch LI, Labourel A, Walton PH, Davies GJ, Gilbert HJ. The contribution of non-catalytic carbohydrate binding modules to the activity lytic polysaccharide monooxygenases. J. Biol. Chem. 2016; 291(14):7439-49.
52. Borisova AS, Isaksen T, Dimarogona M, Kognole AA, Mathiesen G, Varnai A *et al*. Structural and functional characterization of a lytic polysaccharide monooxygenase with broad substrate specificity. J. Biol. Chem. 2015; 290(38):22955-69.
53. Forsberg Z, Mackenzie AK, Sørlie M, Røhr ÅK, Helland R, Arvai AS *et al*. Structural and functional characterization of a conserved pair of bacterial cellulose-oxidizing lytic polysaccharide monooxygenases. Proc. Natl. Acad. Sci. U.S.A. 2014;111(23):8446-51.
54. Kelly SM, Jess TJ, Price NC. How to study proteins by circular dichroism. Biochim. Biophys. Acta, Proteins Proteomics 2005;1751(2):119-39.
55. Sreerama N, Woody RW. Computation and analysis of protein circular dichroism spectra. Methods Enzymol. Academic Press; 2004. p. 318-51.
56. Jenness DD, Sprecher C, Johnson WC. Circular dichroism of collagen, gelatin, and poly(proline) II in the vacuum ultraviolet. Biopolymers. 1976;15(3):513-21.
57. Punt PJ, Burlingame RP, Pynnonen CM, Olson PT, Wery J, Visser J, Heinrich *et al*. *Chrysosporium lucknowense* protein production system. 2010. Patent WO/2010/107303.
58. Visser H, Joosten V, Punt PJ, Gusakov AV, Olson PT, Joosten R *et al*. Development of a mature fungal technology and production platform for industrial enzymes based on a *Myceliophthora thermophila* isolate, previously known as *Chrysosporium lucknowense* C1. Ind. Biotechnol. 2011;7:214–23.
59. Kardos J, Micsonai A. BeStSel. Department of Biochemistry, Institute of Biology, Eötvös Loránd University, Budapest, Hungary. http://bestsel.elte.hu/contact.php. Accessed February 2017.
60. Kabsch W, Sander C. Dictionary of protein secondary structure: Pattern recognition of hydrogen-bonded and geometrical features. Biopolymers. 1983;22(12):2577-637.
61. Touw WG, Baakman C, Black J, te Beek TA, Krieger E, Joosten RP *et al*. A series of PDB-related databanks for everyday needs. Nucleic Acids Res. 2015;43(Database issue):D364-8.

Additional Files

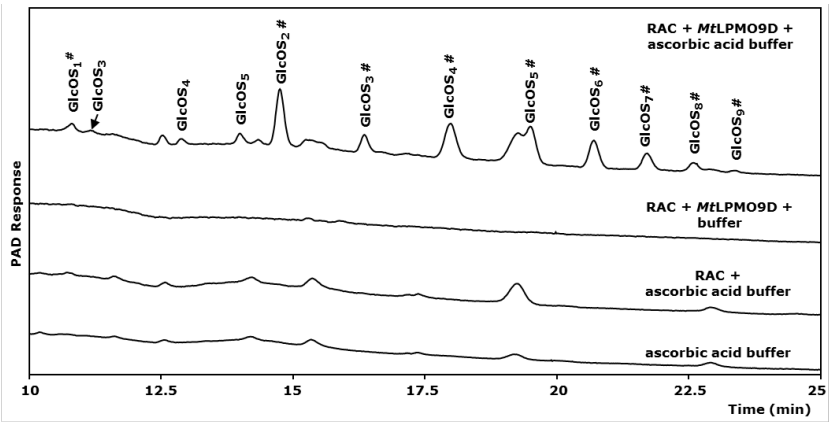

Additional Figure 6.1 Activity of *Mt*LPMO9D towards amorphous cellulose. HPAEC elution pattern of regenerated amorphous cellulose (RAC) after incubation with *Mt*LPMO9D (2.5 mg g^{-1} substrate). Nomenclature used: $GlcOS_n$, non-oxidized gluco-oligosaccharides and $GlcOS_n^{\#}$, gluco-oligosaccharides oxidized at the C1 carbon atom. Only in the presence of ascorbic acid, C1-oxidized $GlcOS_n^{\#}$ are formed by *Mt*LPMO9D. Samples were incubated in a 50 mM ammonium acetate buffer (pH 5.0) at 52°C for 24 h in the absence or presence of ascorbic acid (1 mM).

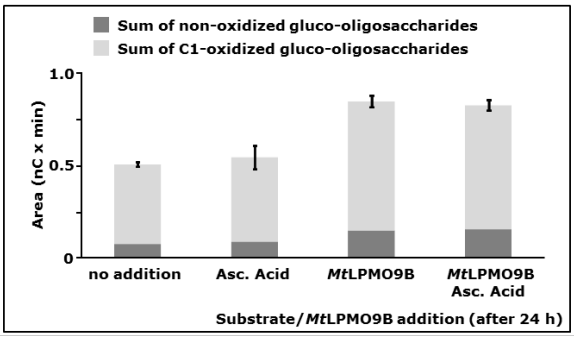

Additional Figure 6.2 Activity of *Mt*LPMO9B towards amorphous cellulose. The figure shows the sum of integrated peak areas of released C1-oxidized and non-oxidized gluco-oligosaccharides after incubation of RAC with *Mt*LPMO9B (5 mg g^{-1} substrate) with RAC (1.5 mg mL^{-1}) in the presence of ascorbic acid (1 mM) based on HPAEC. Samples were incubated in 50 mM ammonium acetate buffer (pH 5.0) at 50°C for 48 h. The incubation was interrupted after 24 h and samples were divided into four batches with the following treatments: first batch, no addition of ascorbic acid and no addition of *Mt*LPMO9B; second batch, another addition of 1 mM ascorbic acid but no addition of *Mt*LPMO9B; third batch, no ascorbic acid addition but another addition of *Mt*LPMO9B (5 mg g^{-1} substrate); fourth batch, another addition of 1 mM ascorbic acid and another addition of *Mt*LPMO9B (5 mg g^{-1} substrate). All incubations were performed in duplicate. The standard deviation is represented by error bars, which correspond to one cumulated SD (error bar = ± SDtot; with SDtot = √SD1 2 + SD2 2 +…).

a

Secondary structure (%)	*Mt*LPMO9B 20°C	*Mt*LPMO9B 95°C	*Mt*LPMO9D 20°C	*Mt*LPMO9D 95°C
Helix	8.5	2.8	7.2	4.3
Antiparallel	38.3	25.7	32.4	28.5
Parallel	0	0	0	0
Turn	12.9	16.3	12.7	16.2
Others	40.3	55.1	47.7	51

b

Secondary structure (%)	*Mt*PMO3* (5UFV)	*Mt*LPMO9D (BeStSel)
Helix	6.3	7.2
Antiparallel	26.9	32.4
Parallel	0	0
Turn	16.8	12.7
Others	50	47.7

Additional Figure 6.3 Secondary structure composition of *Mt*LPMO9B and *Mt*LPMO9D. **a** The secondary structure composition (%) is based on the obtained CD spectra (far UV) of *Mt*LPMO9B (0.20 mg mL^{-1}) and *Mt*LPMO9D (0.20 mg mL^{-1}) at 20 and 90°C, respectively (see **Figure 6.9a** and **6.9b**). The calculation of the secondary structure composition was based on the BeStSel method [59]. **b** Comparison of the predicted secondary structure composition (%) of *Mt*LPMO9D, which was based on the obtained CD spectra and BeStSel method, with the actual secondary structure composition based on *Mt*PMO3* (pdb ID code 5UFV) [22]. See Methods for details.

Chapter VII

General Discussion

7.1 Diversity of LPMOs

7.1.1 *Myceliophthora thermophila* C1 LPMOs differ in their C1-/C4-regioselectivity and substrate specificity

In this thesis we investigated LPMOs from *M. thermophila* C1 (*Mt*LPMOs). In total, this fungus encodes 26 putative LPMO genes. Based on sequence annotation, 22 are classified as AA9 and 4 as AA11 LPMOs, respectively (**Chapter I**). At the start of our research, it was hypothesized that the 26 *Mt*LPMOs are involved in the breakdown of a range of polysaccharides and therefore, differ in their mode of action.

Indeed, we found that all seven investigated *Mt*LPMOs differ in their C1-/C4-regioselectivity and substrate specificity, as summarized in **Table 7.1**. The C1-/C4-regioselectivities and substrate specificities of *Mt*LPMO9E, *Mt*LPMO9F and *Mt*LPMO9G are presented as new data in this discussion, as these data have not been part of one of the previous thesis chapters. All seven *Mt*LPMOs studied oxidize regenerated amorphous cellulose (**Table 7.1** and **Figure 7.1**).

Table 7.1 Characterized LPMOs from *M. thermophila* C1 (this thesis)

***Mt*LPMO**	**Regioselectivity**	**Substrate specificity**	**Chapter**
*Mt*LPMO9A	C1/C4	RAC, xylan associated to cellulose, xyloglucan[a], mixed β-(1→3, 1→4)-linked glucan[a]	II, III
*Mt*LPMO9B	C1	RAC	III, V, VI
*Mt*LPMO9C	C4	RAC, xyloglucan[a], mixed β-(1→3, 1→4)-linked glucan[a]	III, IV
*Mt*LPMO9D	C1	RAC	VI
*Mt*LPMO9E	C4	RAC, Xyloglucan, soluble gluco-oligosaccharides	VII
*Mt*LPMO9F	C4	RAC[b]	VII
*Mt*LPMO9G	C4	RAC[b]	VII

[a] Minor activity

[b] LPMO activity tested on RAC only, data not shown in this thesis

One of the most important findings of this thesis project was the demonstration of the oxidative cleavage of xylan associated to cellulose by *Mt*LPMO9A (**Chapter II**). The other *Mt*LPMOs tested did not have this ability. Apart from xylan, other hemicelluloses could also be oxidized, in particular by *Mt*LPMO9A, *Mt*LPMO9C and *Mt*LPMO9E, which were shown to oxidize mixed β-(1→3, 1→4)-linked glucans and xyloglucan (**Table 7.1**, **Figure 7.2**). Out of the tested *Mt*LPMOs, only *Mt*LPMO9E exhibits activity towards soluble gluco-oligosaccharides having a degree of polymerization (DP) of 5 or higher (**Table 7.1**, **Figure 7.2**). We also established that *Mt*LPMO9A oxidizes the C1- and C4-carbon atom, whereas *Mt*LPMO9B and *Mt*LPMO9D oxidize the C1-carbon atom of the β-(1→4)-linked glucan. Four *Mt*LPMOs (*Mt*LPMO9C, *Mt*LPMO9E, *Mt*LPMO9F, *Mt*LPMO9G) cleave the β-(1→4)-linked glucan chain by oxidizing the C4-carbon atom (**Table 7.1**).

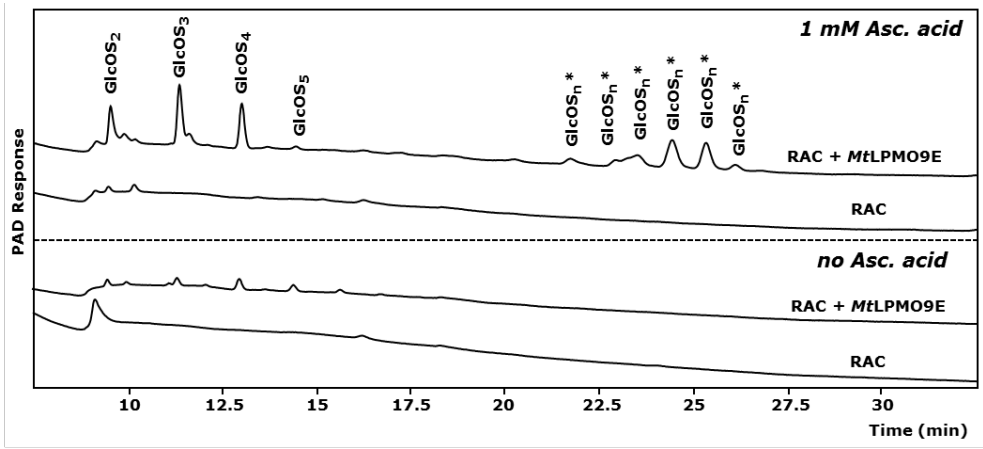

Figure 7.1 HPAEC elution pattern of regenerated amorphous cellulose (RAC) incubated with *Mt*LPMO9E. RAC (1.5 mg mL^{-1}) was incubated with *Mt*LPMO9E (5 mg g^{-1} substrate) in the presence (1 mM) and absence of ascorbic acid in an ammonium acetate buffer (50 mM, pH 5.0) at 50°C for 24 h. RAC incubated with *Mt*LPMO9E led to the formation of non-oxidized ($GlcOS_n$) and C4-oxizidized gluco-oligosaccharides ($GlcOS_n$*). Small amounts of non-oxidized gluco-oligosaccharides were released from RAC incubated with *Mt*LPMO9E in the absence of ascorbic acid, indicating a low hydrolytic background activity.

*Mt*LPMOs from *M. thermophila* C1 were expected to differ in their C1-/C4-regioselectivity and substrate specificity since the ability of a fungus like *M. thermophila* C1 to efficiently degrade a variety of complex lignocelluloses most likely depends on its enzymatic 'toolbox'. Furthermore, depending on the exact composition of the substrate, *M. thermophila* C1 has been shown to express different *Mt*LPMOs during growth to specifically target the degradation of the polysaccharides present [3].

The C1-/C4-regioselectivity is, possibly, the result of how the LPMO binds to the substrate, meaning that different LPMOs may bind to differently exposed cellulose-fiber surfaces. For instance, cellulose is structurally polymorph and consists of several features such as varying microfibril structures, hydrophobic and hydrophilic sides, and ranges in the degree of crystallinity [4-6]. Diverse intra- and intermolecular hydrogen bonds and bridges between oxygen atoms (*O*2, *O*3, *O*5 and *O*6) influence the conformation and, therefore, shape and compactness of the β-(1→4)-linked glucan chains and units [4, 5, 7, 8]. As a result, the accessibility of the C1- or C4-carbon atom may vary depending on these conformational features, which is a possible explanation for the evolution of LPMOs exhibiting different regioselectivities.

The substrate specificity of LPMOs defines which substrate is oxidized. All AA9 *Mt*LPMOs which have been used in this research oxidize cellulose. Apparently, these LPMOs are important to attack, in particular, the cellulose in lignocellulosic plant cell walls (**Chapter I**). Furthermore, it became apparent that hemicelluloses known to interact with cellulose, such as xylan and xyloglucan, were the other main substrates of the studied LPMOs. The ability of LPMOs to attack these polysaccharides indicates that they have an important function in opening up the lignocellulose matrix to assist subsequent extensive degradation by hydrolytic enzymes.

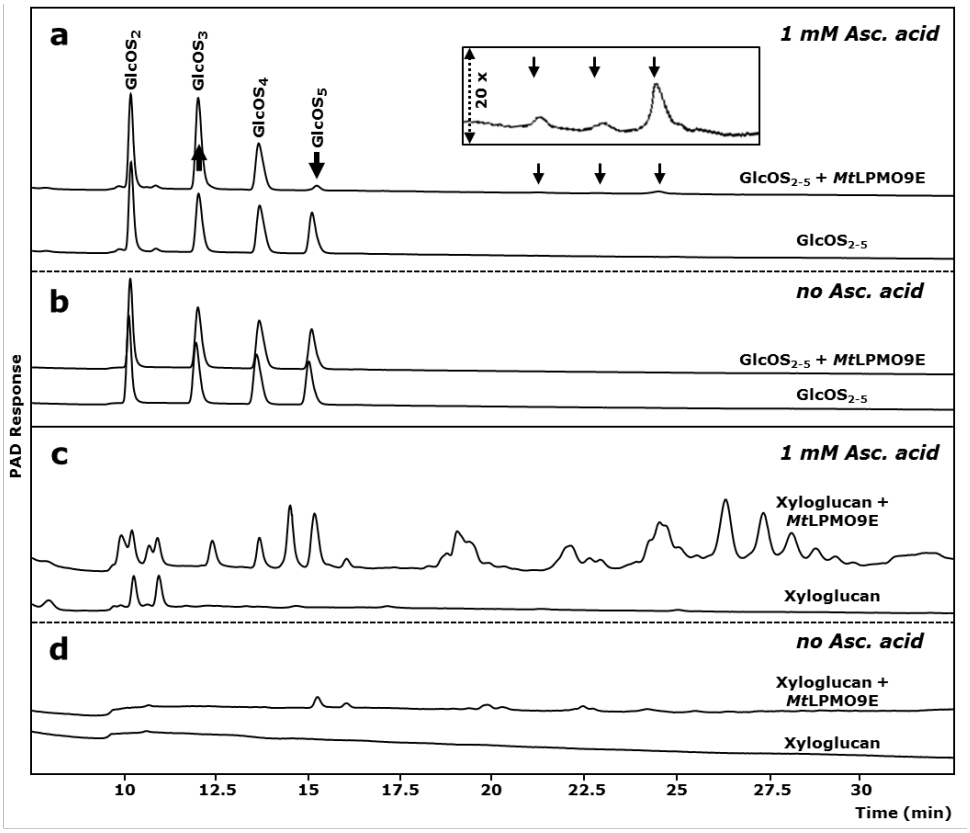

Figure 7.2 HPAEC elution profiles of soluble gluco-oligosaccharides and xyloglucan incubated with *Mt*LPMO9E. Soluble gluco-oligosaccharides (DP2-5 ($GlcOS_{2-5}$), 0.25 mg mL^{-1} per compound) were incubated with *Mt*LPMO9E (5 mg g^{-1} substrate) in **a** the presence (1 mM) and **b** absence of ascorbic acid. The incubation of gluco-oligosaccharides with *Mt*LPMO9E led to the formation of cellotriose and 4-keto-cellobiose through the oxidation of cellopentaose. The enlargement of part of the elution profile of **Figure 7.2a** shows the formation of three new compounds, which are most likely tautomerization products of 4-keto-cellobiose as described by Isaksen *et al*. [1]. *Mt*LPMO9E showed no activity towards soluble gluco-oligosaccharides in the absence of ascorbic acid. Xyloglucan from tamarind seed (1.5 mg mL^{-1}) was incubated with *Mt*LPMO9E (5 mg g^{-1} substrate) in **c** the presence (1 mM) and **d** absence of ascorbic acid. The oxidization of xyloglucan by *Mt*LPMO9E in the presence of ascorbic acid **c** led to the formation of multiple different substituted non-oxidized and oxidized xyloglucan-oligosaccharides, which indicates that *Mt*LPMO9E oxidizes xyloglucan independently of the background substitution [2]. In the absence of ascorbic acid **d**, low amounts of non-oxidized xylogluco-oligosaccharides are formed, which are the result of a low hydrolytic background activity in the used *Mt*LPMO9E-fraction. All samples were incubated in an ammonium acetate buffer (50 mM, pH 5.0) at 50°C for 24 h.

The investigation of structural features of LPMOs bearing different regioselectivities and substrate specificities is a continuous process in the LPMO field. As a result, several characteristics of LPMOs were identified such as the presence and shape of loops, highly conserved amino acid residues or the presence of aromatic amino acid residues in the flat surface [9-12]. Further investigations of phylogenetic relationships between structural features and regioselectivity of LPMOs led to the

implementation of an AA9 subclassification (PMO-I, PMO-II and PMO-III) [9, 11]. However, some AA9 members could be categorized into more than one of these AA9 subclasses [10, 13]. Hence, the classification of AA9 LPMOs in AA9-subfamilies is inadequate to predict their function. In particular, the classification of LPMOs is challenging due to the high diversity and overall low sequence identity of these enzymes [10, 13]. Similarly, our investigated *Mt*LPMOs (**Chapter II-VII**) have a low sequence identity ranging from 22-36% (**Figure 7.3**).

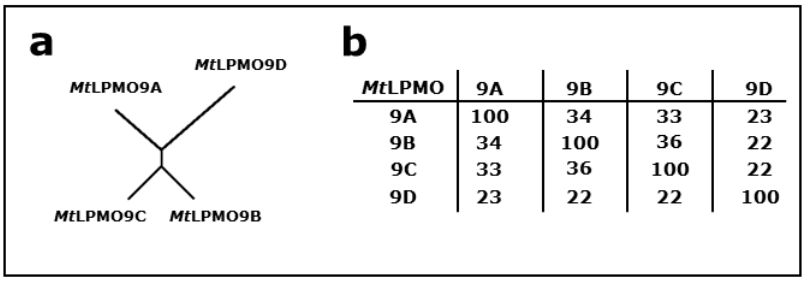

*Mt*LPMO	9A	9B	9C	9D
9A	100	34	33	23
9B	34	100	36	22
9C	33	36	100	22
9D	23	22	22	100

Figure 7.3 Sequence alignment of four *Mt*LPMOs investigated in this thesis. **a** Unrooted phylogenetic tree of *Mt*LPMO9A, *Mt*LPMO9B, *Mt*LPMO9C and *Mt*LPMO9D. **b** Sequence identity among these four *Mt*LPMOs (%). Multiple Sequence Alignments were obtained by using CLUSTALW. Sequences were used without signal peptide and, in the case of *Mt*LPMO9B, without the sequence that encodes the CBMI (**Chapter III**).

7.1.2 LPMOs characterized among fungal species

Based on published findings since 2011, fungal AA9 LPMOs are known to oxidize cellulose and LPMOs characterized between 2011 and 2013 are listed in **Chapter I** (**Table 1.4**) [14-16]. Here, a summary is presented of published AA9 LPMOs that have been characterized between 2013 and the beginning of 2017 (**Table 7.2**).

Until 2013, it was only published that LPMOs oxidize insoluble substrates. In 2014, Isaksen *et al*. were the first to publish findings of a fungal LPMO (*Nc*LPMO9C) that oxidizes soluble substrates, in particular, soluble cello-oligosaccharides [1]. A follow-up study described the activity of *Nc*LPMO9C towards hemicellulose structures such as xyloglucan and mixed β-(1→3, 1→4)-linked glucan [17]. We extended the description of possible substrates for LPMOs with our demonstration of the xylan oxidizing *Mt*LPMO9A in 2015 (**Chapter II**) [18]. The discovery of LPMOs such as *Mt*LPMO9A which are active towards hemicellulose structures, led to a paradigm shift in the understanding of plant cell wall degradation. Until now, only nine out of thirty (including *Mt*LPMOs) AA9 LPMOs have been shown in literature to be active towards hemicellulose or soluble gluco-oligosaccharides (**Table 7.2**). For comparison, we identified over 6500 putative AA9-encoding genes in the known genome sequences of Ascomycota and Basidiomycota (**Chapter V**). Only when more of these putative LPMOs are characterized, their function can be understood better.

7.1.3 Substrate specificity and planar surface of AA9 *Mt*LPMOs

All LPMOs feature a planar surface that possibly enables them to oxidize less accessible substrates (see **Figures 1.7**, **1.8** and **1.9**, **Chapter I**) [47]. In contrast, glycosyl hydrolases (GHs) interact with their substrates via a pocket, a cleft or a tunnel [48, 49]. Hence, the enhancing effects of LPMOs with glycosyl hydrolases may relate to the possibility that LPMOs make the substrate accessible for further and faster degradation by GHs (**Chapter II**) [47]. The latter is not only beneficial for cellulose

Table 7.2 AA9 LPMOs and their C1-/C4-regioselectivity and substrate specificity[a,b]

Organism	Enzyme name	Regioselectivity	Substrate specificity	References
Aspergillus nidulans	*AN*3046	C1[c]	Cellulose (PASC), xyloglucan	[19]
Fusarium graminearum	*Fg*LPMO9A	C1/C4	Cellulose, xyloglucan, longer xylogluco-oligosaccharides	[2]
Gloeophyllum trabeum	*Gt*LPMO9A-2	C1/C4	Cellulose, Carboxymethylcellulose, xyloglucan, glucomannan	[20]
Lentinus similis	*Ls*(AA9)A	C4	Cellulose, soluble gluco-oligosaccharides	[21]
Myceliophthora thermophila	MYCTH_92668	C1	Cellulose	[22]
Neurospora crassa	NCU01050, PMO-2, *Nc*PMO-2	C4	Cellulose	[11, 14]
	NCU07898, PMO-3, *Nc*LPMO9M	C1/C4	Cellulose	[11, 14, 22]
	NCU08760, PMO-08760, LPMO-08760	C1	Cellulose	[14, 23, 24]
	*Nc*LPMO9C, NCU02916, *Nc*GH61-3, PMO-02916, LPMO-02916	C4	Cellulose, soluble gluco-oligosaccharides, xyloglucan, glucomannan, mixed β-(1→3, 1→4)-linked glucan, carboxymethyl cellulose	[1, 17, 20, 23-29]
	NCU07760	C1/C4	Cellulose	[22]
	PMO-03328, *Nc*LPMO9F, NCU03328, LPMO-03328	C1	Cellulose	[23, 24, 30]
	NCU02240, GH61-1	C4	Cellulose	[22, 31]
	LPMO-1867	C1	Cellulose	[24]
Pestalotiopsis sp. NCi6	*Ps*LPMOA	C1/C4	Cellulose	[32]
	*Ps*LPMOB	C1/C4	Cellulose	[32]
Phanerochaete chrysosporium	*Pc*GH61D, GH61D, PcLPMO9D	C1	Cellulose	[16, 33-36]

Organism	Enzyme name	Regioselectivity	Substrate specificity	References
Podospora anserina	*Pa*GH61A, *Pa*LPMO9A	C1/C4	Cellulose	[13, 37]
	*Pa*GH61B	C1/C4[d]	Cellulose	[37]
	*Pa*LPMO9E	C1	Cellulose	[13, 38]
	*Pa*LPMO9H	C1/C4	Cellulose (PASC only), soluble gluco-oligosaccharides, xyloglucan, glucomannan, lichenan, mixed β-(1→3, 1→4)-linked glucan	[13, 39, 40]
Thermoascus aurantiacus	*Ta*GH61, *Ta*GH61A, *Tau*GH61A, *Ta*AA9, *Ta*LPMO9A	C1/C4	Cellulose	[15, 28, 41-43]
Thielavia terrestris	*TtAA9E, TtGH61E, TtLPMO9E*	C1	Cellulose	[42-44]
Trichoderma reesei	*Tr*Cel61A, EGIV	C1/C4	Cellulose	[45, 46]

[a] without *Mt*LPMOs investigated in this thesis

[b] only AA9 LPMOs with known C1-/C4-regioselectivity and substrate specificity are listed

[c] inconclusive, C1 proposed

[d] C1 only with CDH as reducing agent

fiber degradation, but also for the degradation of cellulose-associated hemicelluloses. Two examples are xylan and xyloglucan, which are non-covalently associated with cellulose within plant cell walls (**Chapter I**; [50, 51]). The planar surface of LPMOs may enable them to oxidize these less accessible regions, which is followed by a disruption of the cellulose and hemicellulose structure and thereby enhances the accessibility for hydrolases. As shown in **Chapter I** and **VII**, *M. thermophila* C1 expresses LPMOs, which are active towards xylan associated to cellulose (*Mt*LPMO9A) and towards xyloglucan (*Mt*LPMO9E). Additionally, *M. thermophila* C1 is known to comprise a plethora of hemicellulose-degrading enzymes [52]. The concerted action of LPMOs and glycosyl hydrolases improves plant cell wall degradation, which can be seen as a benefit for fungi such as *M. thermophila* C1. These benefits of LPMOs in the plant biorefinery field will be further discussed in **Section 7.5**.

7.1.4 Beyond regioselectivity and substrate specificity of *Mt*LPMOs

Here, we suggest that the current discrimination of LPMOs by only their substrate preference and C1-/C4-regioselectivity is not complete. We expect that LPMOs are exhibiting further modes of action, similar to glycosyl hydrolases, which can range from random to processive hydrolytic cellulose cleavage (**Chapter I**).

Certainly, AA9 LPMOs do oxidize cellulose, but we propose that this cellulose specificity potentially ranges from the preferred oxidation of highly crystalline to completely amorphous regions. Furthermore, LPMOs that are active towards crystalline cellulose may further be distinguished by their preference for microfibrils comprising the I_α or I_β crystal form [5, 7, 8]. A similar scenario has already been described for carbohydrate binding modules (CBMs) and some members have, for example, been shown to be able to bind hardwood cellulose but not bacterial cellulose [53]. Another example is shown by a recent study in which the cleaving behavior of *Nc*LPMO9F on the cellulose surface is revealed by using time-resolved atomic force microscopy (AFM) [30]. This LPMO oxidized the surface layer of the crystalline cellulose region only, which resulted in the formation of a patch, but amorphous regions were not oxidized (**Table 7.2**). Moreover, this LPMO mainly oxidized the surface layer, but vertical degradation of subjacent layers was hardly determined. In comparison, another study described the activity of *Pa*LPMO9H, which was only active towards amorphous cellulose, but not towards crystalline cellulose fibers [39] (**Table 7.2**).

We also hypothesize that LPMOs and their preference for either crystalline or amorphous cellulose regions will be influenced by CBMs. Recent studies already showed that the LPMO domain of “natural” LPMOs with appended CBMs have a lower LPMO-mediated binding affinity towards substrates compared to single domain LPMOs, which could strengthen the hypothesis that CBMs influence the LPMO cleavage capability [54-59]. In addition, CBMs exhibit different binding behaviors and preferences towards potential substrates [53, 60, 61]. It is therefore possible that the CBM binding nature will influence the positioning of the specific LPMOs to which the CBM is appended to. Hereby, the CBM could promote either a random or more processive cellulose oxidation, which is similar to random and processive glycosyl hydrolases.

7.2 *Mt*LPMOs and electron donors

7.2.1 *Mt*LPMOs and non-enzymatic reducing agents

In this work we investigated multiple potential reducing agents that can efficiently reduce *Mt*LPMOs from *M. thermophila* C1. We hypothesized that the *Mt*LPMOs differ in their reducing agent specificity. A summary of analyzed *Mt*LPMOs' reducing agent specificities is shown in **Table 7.3**, which is based on the results of **Chapters III** and **V** and on new data (**Figure 7.4**). Indeed, *Mt*LPMOs varied in their ability to oxidize cellulose with varying reducing agents, of which many are considered as lignin building blocks. Regardless of these differences, ascorbic acid was a good reducing agent for all seven investigated *Mt*LPMOs. Furthermore, *Mt*LPMO9A, *Mt*LPMO9B, *Mt*LPMO9C and *Mt*LPMO9D were all active in the presence of 3-methylcatechol (**Table 7.3**).

Notably, *Mt*LPMO9B oxidized cellulose in the presence of lignin (**Figure 7.4**), whereas *Mt*LPMO9A and *Mt*LPMO9C did not show any catalytic performance in the presence of this aromatic biopolymer (**Table 7.3**).

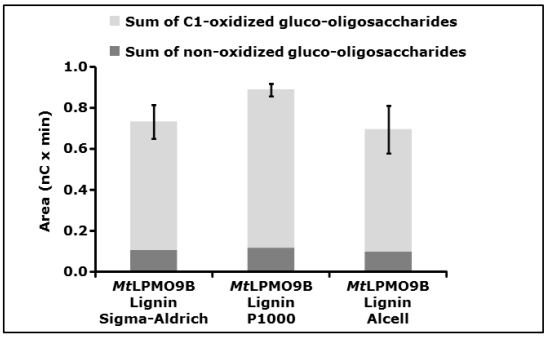

Figure 7.4 Release of non-oxidized and C1-oxidized gluco-oligosaccharides from RAC incubated with *Mt*LPMO9B in the presence of three different lignin fractions. RAC (1.5 mg mL^{-1}) was incubated with *Mt*LPMO9B (5 mg g^{-1} substrate) in the presence of alkaline-extracted lignin (Sigma-Aldrich, Steinheim Germany), soda P1000 and Alcell (2 mg mL^{-1}) in an ammonium acetate buffer (50 mM, pH 5.0) at 50°C for 24 h. Both Protobind 1000 (P1000) soda lignin and Alcell have been characterized previously [62]. The figure shows the total sum of integrated peak areas of released C1-oxidized and non-oxidized gluco-oligosaccharides after the incubation of RAC with *Mt*LPMO9B. All incubations were performed in duplicates and the standard deviations are represented by error bars, which correspond to one cumulated SD (errorbar = ± SDtot; with SDtot = $\sqrt{SD_1^2 + SD_2^2 + \ldots}$).

Today in 2017, it has been reported that LPMOs such as *Mt*LPMOs receive electrons from different types of reducing agents. However, there were only few studies published about the effect of reducing agents on the catalytic performance of LPMOs in the beginning of our research project [16]. Next to our findings summarized above, other studies have already reported a variety of reducing agents that can be used to determine the catalytic performance of LPMOs, such as ascorbic acid, gallic acid and reduced glutathione [1, 15, 16, 63]. Westereng *et al*. showed that lignin acts as electron donor for *Tt*LPMO9E [44]. Hence, it is shown that the catalytic performance of different LPMOs depends on the type of reducing agent that is present during the incubation [24, 44, 64].

In summary, both our research and that of others demonstrate that different types of reducing agents do not only influence the catalytic performance of LPMOs, but also that LPMOs differ in their reducing agent specificity.

Table 7.3 Overview of non-enzymatic reducing agents tested in this thesis

Gr.[a]	Subgr.[a]	No.	Reducing agent	*Mt*LPMO				Chapter
				9A[b] (pH5.0)	9B[b] (pH5.0)	9C[b] (pH5.0)	9B[c] (pH 6.0)	
I	a	1	4-hydroxybenzoic acid	-	-	-	+	V
		2	naringin	-	-	-	n.d.	III
		3	*o*-cresol	n.d.	n.d.	n.d.	+	V
		4	*p*-coumaric acid	-	-	-	+	III, V
		5	phenol	n.d.	n.d.	n.d.	-	V
I	b	6	3-hydroxy-4-methoxycinnamic acid	-	-	-	+	III, V
		7	4-hydroxy-3-methoxyphenylacetone	n.d.	n.d.	n.d.	+	V
		8	coniferyl aldehyde	n.d.	n.d.	n.d.	+	V
		9	ferulic acid	n.d.	n.d.	n.d.	+	V
		10	guaiacol	n.d.	n.d.	n.d.	+	V
		11	hesperidin	n.d.	n.d.	n.d.	+	V
		12	homovanillic acid	-	-	-	+	III, V
		13	vanillic acid	-	-	-	+	III, V
I	c	14	4-allyl-2,6-dimethoxyphenol	n.d.	n.d.	n.d.	+	V
		15	sinapic acid	+	+	+	+	III, V
		16	syringic acid	-	-	-	+	III, V
II	a	17	(-)-epicatechin	+	+	+	n.d.	III
		18	(+)-catechin	+	+	+	n.d.	III
		19	3,4-dihydroxybenzaldehyde	+	-	-	n.d.	III
		20	3,4-dihydroxybenzoic acid	+	+	+	+	III, V
		21	3,4-dihydroxycinnamic acid	-	+	-	n.d.	III
		22	3,4-dihydroxyphenylacetic acid	+	+	+	n.d.	III
		23	3-methylcatechol[d]	+	+	+	+	III, V, VI
		24	4-chlorocatechol	+	+	+	n.d.	III
		25	caffeic acid	+	+	-	+	III, V
		26	carminic acid	+	-	+	n.d.	III
		27	catechol	+	+	+	n.d.	III
		28	chlorogenic acid	+	+	-	n.d.	III

Gr.[a]	Subgr.[a]	No.	Reducing agent	*Mt*LPMO				Chapter
				9A[b] (pH5.0)	9B[b] (pH5.0)	9C[b] (pH5.0)	9B[c] (pH 6.0)	
II	a	29	dopamine hydrochloride	+	+	+	n.d.	III
		30	1,4-dihydroxybenzene	+	+	+	n.d.	III
		31	L-3,4-dihydroxyphenylalanine	+	+	+	n.d.	III
		32	quercetin	-	-	-	n.d.	III
		33	resorcinol (meta)	-	-	-	n.d.	III
		34	taxifolin	-	+	+	n.d.	III
II	b	35	3,4-dihydroxy-5-methoxybenzoic acid	n.d.	n.d.	n.d.	+	V
		36	3,4-dihydroxy-5-methoxycinnamic acid	n.d.	n.d.	n.d.	+	V
III		37	(-)-epigallocatechin-gallate	+	+	+	n.d.	III
		38	gallic acid	+	+	+	+	III, V
IV		39	allyl iso-thiocyanate	-	-	-	n.d.	III
		40	D-methionine	-	-	-	n.d.	III
		41	L-cysteine	+	+	+	n.d.	III
		42	reduced glutathione	-	+	+	n.d.	III
V		43	ascorbic acid[e]	+	+	+	+	II-VII
		44	D-quinic acid	-	-	-	n.d.	III
Hetero-		45	lignin Alcell[f]	n.d.	+	n.d.	n.d.	VII
polymers		46	lignin soda P1000[f]	n.d.	+	n.d.	n.d.	VII
		47	lignin, alkali-extracted[g]	-	+	-	n.d.	VII
		48	tannic acid	-	+	-	n.d.	III

[a] Reducing agents were classified into groups and subgroups: Group I, monophenols (Ia), compounds with a 1-hydroxy-2-methoxy moiety (Ib) or a 1-hydroxy-2,6-dimethoxy moiety (Ic); Group II, aromatic compounds with 1,2- or 1,4-dihydroxy moiety (IIa) and compounds with a 1,2-dihydroxy-6-methoxy moiety (IIb); Group III, aromatic compounds with a 1,2,3-trihydroxy moiety (III); Group IV, sulfur-containing compounds (IV); Group V, compounds with neither a phenolic ring nor sulfur atom; Group IV, heteropolymers comprising phenolic compounds as structural units (VI)

[b] *Mt*LPMO-activity was tested in a 50 mM ammonium acetate buffer pH 5.0

[c] *Mt*LPMO9B-activity was tested in a 50 mM potassium phosphate buffer pH 6.0

[d] *Mt*LPMO9D was also active towards RAC in the presence of 3-methylcatechol (**Chapter VI**)

[e] all seven *Mt*LPMOs (**Table 7.1**) were active in the presence of ascorbic acid

[f] Lignin Alcell and Lignin soda P1000 were previously described by Constant *et al.* [62]

[g] Lignin, alkali extracted, obtained from Sigma-Aldrich (Steinheim, Germany)

Based on the current results, we can draw two main conclusions that will be further discussed below: 1) LPMOs can receive electrons from a variety of reducing agents with a relatively low redox potential (≤ 250 mV); 2) LPMOs comprise a reducing agent preference which is the result of their three-dimensional protein structure.

1) Phenolic compounds comprising structural features like the 1,2-dihydroxy (IIa), 1,2-dihydroxy-6-methoxy (IIb) and 1,2,3-trihydroxy moiety (III) have been shown to efficiently reduce *Mt*LPMOs (**Chapter III** and **V**, **Table 7.3**). In addition, compounds that do not comprise the above-mentioned features have also been shown to reduce LPMOs such as ascorbic acid, glutathione and L-cysteine or the macromolecule lignin (**Table 7.3**). In comparison, monophenols (Ia-c) are less efficient electron donors for *Mt*LPMOs (**Table 7.3**). The reducing efficiency of a compound can be determined experimentally by cyclic voltammetry and expressed as the reduction potential. Phenolic compounds comprising a second hydroxyl group attached to the benzene ring have a relatively low reduction potential (≤ 250 mV), whereas monophenols have a relatively high reduction potential (≥ 400 mV) [24]. Kracher *et al*. have already shown that a lower reduction potential of reducing agents resulted in a higher catalytic performance of LPMOs [24]. Hence, based on the structure and associated reduction potential of a compound and the reduction potential of a LPMO, it seems possible to predict if it is an efficient reducing agent for a LPMO or not. Deviating from this general rule are exceptions, such as quercetin. In the presence of this compound, all three tested *Mt*LPMOs were not active towards cellulose (**Table 7.3**).

2) The differences in the reducing agent preference of *Mt*LPMOs results from the structural diversity of these enzymes. However, the mechanism of LPMOs interacting with potential reducing agents and how the electrons are transferred to the copper ion in the histidine brace is not clear (**Chapter I**). In 2012, it has been hypothesized that LPMOs interact with the reducing agent via a surface patch centered around the Pro-Gly-Pro triad or a narrow patch around the amino acid residues that coordinate the copper ion [11, 26, 65]. We have shown that the amino acid residues present in these two regions differ in their surface charge distribution among *Mt*LPMO9A, *Mt*LPMO9B and *Mt*LPMO9C (**Chapter III**). Therefore, it is plausible that the interaction between these residues and reducing agents is different for each of these *Mt*LPMOs.

In addition, the reduction potential of a number of LPMOs has been determined to be around + 250 mV (vs. SHE), but some members show deviating values which are either higher (+ 326 mV vs. SHE) or lower (+ 155 mV vs. SHE) [17, 24, 38, 66]. These deviating values may result from differences in the protein structure. Thus, LPMOs comprising a low reduction potential (e.g. below + 250 mV (vs. SHE)) are likely to require compounds with an even lower reduction potential in order to receive electrons. In contrast, LPMOs with a high reduction potential (e.g. above + 250 mV (vs. SHE)) can also receive electrons from reducing agents which comprise a reduction potential that is, for example, around + 250 mV (vs. SHE).

Notably, the above-mentioned properties such as surface charge of the enzyme or reduction potential are influenced by incubation conditions like pH, temperature or the type of buffer used (**Chapter VI** and Katja S. Johansen, 1st LPMO Symposium, Copenhagen, Denmark, 2016). Furthermore, high concentrations of reducing agents, in particular the ones with a low reduction potential, have been reported to inactivate LPMOs within minutes by forming reactive oxygen species (ROS) [35]. Altogether, the electron donating system or reducing agent type should be

carefully considered when studying the biochemical characteristics of LPMOs, such as pH or temperature optima (**Chapter VI**).

7.2.2 Mapping enzymatic and non-enzymatic electron-donating systems

In our work the beneficial effect of polyphenol oxidases on the LPMO-driven cellulose degradation is demonstrated for the first time. More specifically, we show that the polyphenol oxidase *Mt*PPO7 from *M. thermophila* C1 converts methoxylated phenolic compounds into compounds comprising a 1,2-dihydroxy moiety and, thereby, enhances the catalytic performance of *Mt*LPMO9B (**Chapter V**). This finding is of high relevance, since methoxylated phenolic compounds are present as lignin-building blocks in the plant cell wall. Furthermore, we show that polyphenol oxidases comprising a strong diphenolase activity are less beneficial for LPMO activity due to the subsequent strong oxidation of diphenols into quinones, which have a low reducing efficiency on LPMOs (**Chapter V**). Furthermore, sequence analysis of genomes of 336 Ascomycota and 208 Basidiomycota reveals a high correlation between genes encoding *Mt*PPO7-like proteins and AA9 LPMOs (**Chapter V**). This correlation between *Mt*PPO7 and AA9 LPMO genes is indicative for the importance of the coupled action of different monooxygenases in the concerted degradation of lignocellulosic biomass.

In addition to our finding that PPOs can have a positive effect on the electron donating system of LPMOs, other new enzymatic and non-enzymatic electron-donating systems were uncovered *in vitro*, too. Based on these new findings reported in the latest literature and our own research (**Chapter V**), we propose four electron-donating systems (I, II, III and IV) that enable LPMO activity, which are discussed in the text below and summarized in **Figure 7.5**. The relevance of these systems on the LPMO activity *in vivo* will be discussed later in this section and their possible role for the application in biorefinery is described in **Section 7.4**. Electron donating system I includes compounds and enzymes that directly donate electrons to LPMOs, such as cellobiose dehydrogenases (CDHs) (**Figure 7.5**, **A – E** and **G**). Electron donating system II comprises enzymes that release and modify reducing agents which influence the activity of LPMOs, such as the polyphenol oxidase *Mt*PPO7 (**Chapter V**; **Figure 7.5**, **F**, **H** and **I**). Electron donating system III includes light-induced non-enzymatic electron-donating systems (**Figure 7.5**, **J**). Finally, electron-donating system IV comprises enzymes that alter superoxide or hydrogen peroxide levels to affect the catalytic performance of LPMOs (**Figure 7.5**, **K, L** and **M**).

It should be noted that some members of electron donating system I, such as CDH, can also be part of system II and *vice versa*, dependent on the activity. In **Figure 7.5**, the black arrows and fonts indicate published systems and in red we hypothesize new routes to promote LPMO activity.

Electron donating system I: compounds and enzymes that directly donate electrons to LPMOs

Electron donating system I includes compounds that have already been described in **Section 7.2.1**, such as plant phenols and lignin building blocks (**A** - **D**, **Figure 7.5**). CDH (**Figure 7.5**, **E**) was the first enzyme that has been shown to reduce LPMOs directly, as demonstrated for three *N. crassa* LPMOs (NCU01050, NCU07898 and NCU08760) [14]. Furthermore, gene expression studies revealed a correlation between the expression of CDH and LPMO genes [24].

CDH is a member of the GMC (glucose-methanol-choline oxidase/dehydrogenase) oxidoreductase family. Next to CDH, other GMC members (**G**, **Figure 7.5**), such as glucose oxidase (GOx), glucose dehydrogenase (GDH), pyranose dehydrogenase (PDH), aryl-alcohol quinone oxidoreductases (AAQO), aryl-alcohol oxidase (AAO) and an isolated flavodehydrogenase domain (DH), have been

shown to donate electrons directly to LPMOs. These flavoproteins can also regenerate electron-donating plant phenols and lignin building blocks [24, 35, 38], in that respect they also belong to '*Electron donating system II*'. In addition, some GMC family members (**G**, **Figure 7.5**) (e.g. AAO, CDH) are reported to interact either via electron donation or H_2O_2 formation with other enzymes, such as laccases and peroxidases (**F**, **Figure 7.5**), which may affect the catalytic performance of LPMO indirectly [67-69].

Electron donating system II: enzymes that release and modify reducing agents

Peroxidases, such as manganese peroxidases (MnP), lignin peroxidases (LiP) and versatile peroxidases (VP) as well as laccases (**F**, **Figure 7.5**) are known to oxidize plant phenols, lignin building blocks and lignin and, therefore, are hypothesized to effect the electron donation of these compounds towards LPMOs [70-76]. As already described in this thesis, polyphenol oxidases (**H**, **Figure 7.5**), such as *Mt*PPO7 and *Ab*PPOs, affect the activity of LPMOs indirectly by their monophenolase and diphenolase activity (**Chapter V**). Furthermore, we propose that the simultaneous use of ferulic acid esterases (**I**, **Figure 7.5**) in combination with polyphenol oxidases is another possible electron donating system for LPMOs. Ferulic acid esterases have been shown to release coumaric acid and ferulic acid from plant cell wall hemicelluloses, like in grains and grasses [77]. Both of these cinnamic acid derivatives are hydroxylated by polyphenol oxidases, such as *Mt*PPO7, into compounds comprising 1,2-dihydroxy moieties, which are efficient electron donors for LPMOs (**Chapter V**).

Electron donating system III: light-induced non-enzymatic electron-donating systems

In 2016, Cannella *et al*. reported that light in combination with photosynthetic pigments (**J**, **Figure 7.5**), such as thylakoids or chlorophillin, are very efficient electron-donating systems for the reduction of LPMOs [43]. Next to these pigments, chemical photocatalysts (**J**, **Figure 7.5**) like vanadium-doped titanium dioxide (V-TiO_2) can also efficiently reduce LPMOs. Above all, these systems comprise the advantage of a switch-on/off possibility and, therefore, are a useful tool for investigating the catalytic mechanism of LPMOs [35, 36, 43, 78].

Electron donating system IV: Enzymes that alter superoxide or hydrogen peroxide levels

Catalase and superoxide dismutase (**K**, **Figure 7.5**) can affect the LPMO activity or stability in an indirect way due to altering superoxide or hydrogen peroxide concentrations during the incubation [35, 79]. As an example, the catalase from *Thermoascus aurantiacus* (Accession DD046677) reportedly decreased the inactivation of AA9 LPMOs during biomass degradation [79]. Apart from that, both superoxide dismutase and catalase may also be involved in most of the non-enzymatic and enzymatic electron-donating systems, since superoxide and hydrogen peroxide are released during the oxidation/reduction (redox) reactions [35]. Details concerning the role of hydrogen peroxide during LPMO activity will be discussed separately in **Section 7.2.4**. Furthermore, the hydrogen peroxide generating xanthine oxidase (XOD) and also, to a minor extent, xanthine only (**L**, **Figure 7.5**) have been shown to reduce *Sc*LPMO10C, which led to the oxidation of cellulose [35]. The same AA10 LPMO was also active towards cellulose in the presence of chemical superoxide generating systems, such as potassium superoxide (KO_2) (**M**, **Figure 7.5**) [35].

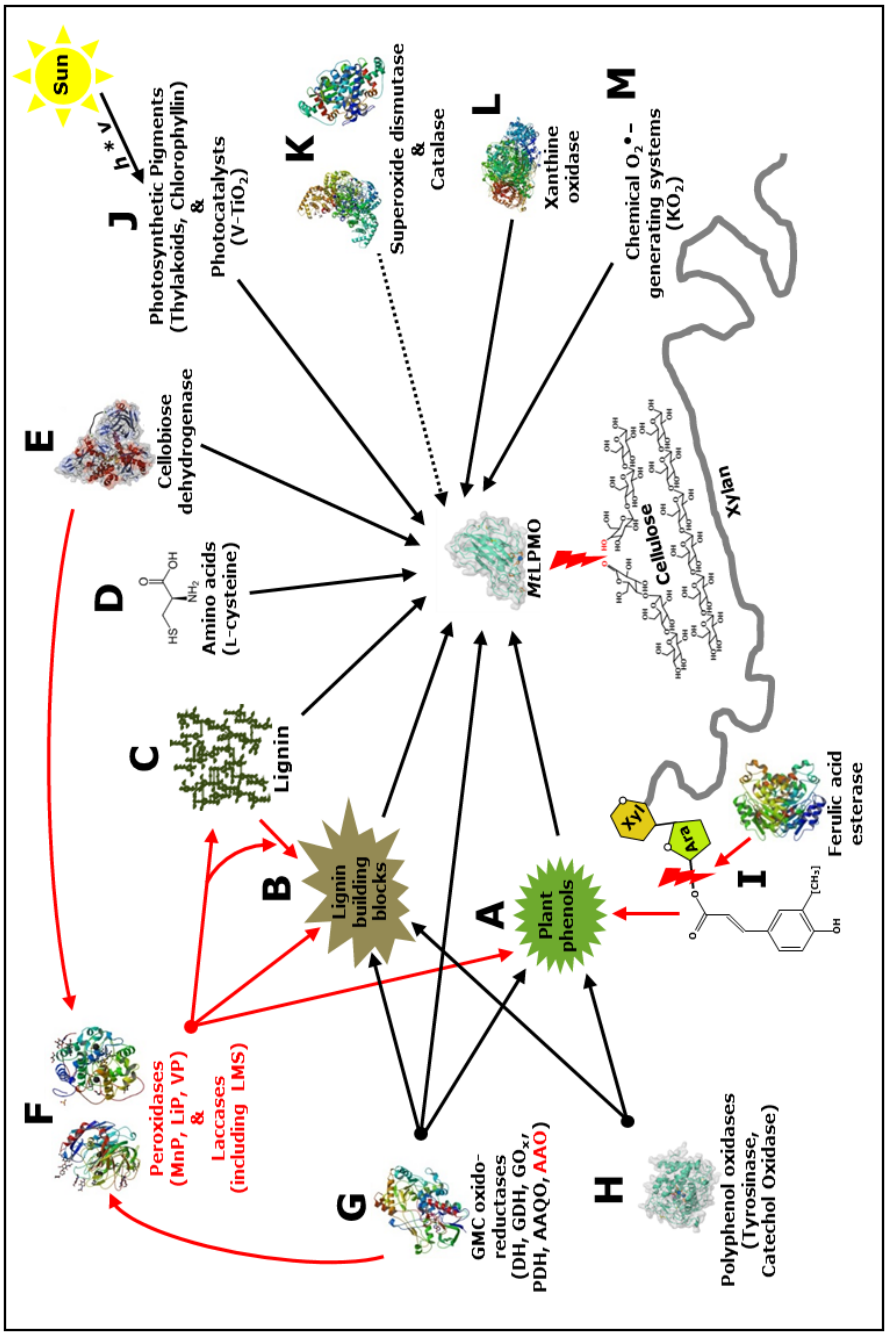

Figure 7.5 Interactions between non-enzymatic and enzymatic electron-donating systems and their effect on LPMOs. Black arrows and fonts represent published systems and in red new systems are hypothesized. Details are described in **Section 7.2.2**. This scheme is simplified and co-substrates such as hydrogen peroxide or oxygen are not included. In addition, aerobic and anaerobic conditions are not further considered.

7.2.3 Electron-donating systems *in vivo*

So far, most of the above-mentioned electron-donating systems have been determined *in vitro*. In general, LPMOs used for the degradation of lignocellulosic biomass are secreted enzymes, which oxidize polysaccharides outside of the fungal cell. To understand the variety of possible electron-donating systems it is necessary to consider that fungi exhibit different modes of life-style, which may influence how LPMOs are used to degrade certain biomasses.

For instance, saprophytic fungi such as *M. thermophila* C1 mainly feed on dead biomass, which often contains high amounts of lignin and other phenolic compounds, next to polysaccharides. For these saprophytic fungi, LPMOs are likely to receive electrons from lignin and lignin-building blocks (**A, B** and **C**, **Figure 7.5**). In addition, we expect that LPMOs benefit from other *secreted* lignocellulose-degrading enzymes during the concerted degradation of biomass, such as GMC oxidoreductases (e.g. CDH), polyphenol oxidases and, as proposed, laccases and peroxidases (**F,G** and **H**, **Figure 7.5**). We do not expect that the light-induced non-enzymatic electron-donating system (**J**, **Figure 7.5**) will act as an efficient electron providing system for LPMOs, which are secreted by saprophytic fungi. Notably, most of these fungi are able to decompose biomass in the absence of light (e.g. in the soil or ground level of a forest) or degrade parts of the plant that do not contain photosynthetic pigments (e.g. stamp of hardwoods). Also intracellular reducing agents, such as ascorbic acid and reduced glutathione, are not expected to play a major role as reducing agents for LPMOs, since dead biomass will not comprise intact cells that contain these rather instable compounds.

In contrast to *Saprophytes*, pathogenic fungi are known to attack the plant cell wall of living cells. LPMOs secreted by these types of fungi are possibly used to disrupt the cell wall in order to improve the penetration of the fungi into the plant cell. Thereby, LPMOs are likely to get in contact with the intracellular matrix of the plant cell (e.g. in leaves) and endogenous electron donors are available for LPMOs, such as ascorbic acid, L-cysteine (**D**, **Figure 7.5**) or reduced glutathione. Moreover, it is likely that photosynthetic pigments, such as chlorophyll, are released from the chloroplast during the decay of the plant cell and donate electrons for LPMOs. However, based on the current knowledge it remains debatable to what extent the latter system will contribute to the LPMO-assisted plant cell wall degradation *in vivo*.

Enzymes that alter hydrogen peroxide or superoxide concentrations, such as catalases and superoxide dismutases (System IV, **K**, **Figure 7.5**), are present inside and outside of the plant cell and, therefore, will be of importance for different fungi in general. As already described above, these enzymes are expected to influence electron-donating systems to avoid the formation of ROS, which potentially decreases the inactivation of LPMOs. The usefulness of these electron-donating systems in terms of applications is discussed in **Section 7.4**.

7.2.4 Mechanism of electron transfer

Much published work about the catalytic mechanism of LPMOs was based on the assumption that electrons are somehow transferred from a donor to the LPMO and that molecular oxygen is involved to enable the oxidation of cellulose (**Chapter I**). Besides these commonly accepted modes of action, many questions were still unanswered. For example, are electrons transferred from a donor to the Cu(II)-LPMO via a surface patch around the Pro-Gly-Pro triad or via a surface patch in the vicinity of the copper atom? Which amino acids are involved in the electron transfer? Is the Cu(II)-LPMO first reduced to Cu(I)-LPMO and binds oxygen afterwards or does the LPMO first bind to the substrate

and then to oxygen? Still these questions cannot be answered completely, although a number of proposed catalytic mechanisms have been addressed recently [80].

An intriguing recent finding by Bissaro *et al*., shows that H_2O_2 could be a co-substrate of LPMOs [35]. These authors also propose that reducing agents are only needed for the 'priming reduction' to reduce the LPMO-Cu(II) to LPMO-Cu(I). At the reduced stage, the LPMO-Cu(I) could bind H_2O_2 and thereby lead to the formation of hydroxyl radicals, which is similar to the reaction reported during Fenton chemistry [35]. The hydroxyl radical is expected to attack the glucosyl bonds in cellulose, which will lead to the cleavage of the glucan chain. Bissaro *et al*. also showed that H_2O_2 is formed in the presence of reducing agents, such as ascorbic acid [35]. Although still heavily debated, these new insights into the catalytic mechanism of LPMOs can be expected to change our view of the interaction between reducing agents and LPMOs.

In this thesis, we did not study the formation of hydrogen peroxide during the LPMO reactions. It is likely that reducing agents, such as diphenols, are also able to stimulate the formation of H_2O_2. This could have influenced the *Mt*LPMO activities. In addition, the reducing agent preference among *Mt*LPMOs might also be influenced by the sensitivities of *Mt*LPMOs for H_2O_2. Clearly, more insight is needed on the reactivity of *Mt*LPMOs with H_2O_2. For instance, at this point it cannot be excluded that the susceptibility of *Mt*LPMO9D for enzyme inactivation is caused by a relatively high sensitivity for H_2O_2 (**Chapter VI**).

There are several other enzymes that oxidize potential substrates under the use of external electrons and molecular oxygen or alternatively H_2O_2. As an example, the cytochrome P450 peroxygenase $OleT_{JE}$ catalyzes the oxidative decarboxylation or hydroxylation of fatty acids [81-83]. Similar as described for LPMOs, $OleT_{JE}$ requires oxygen and two electrons as well as a protonation step to form a ferric-hydroperoxo (Fe(III)-OOH) intermediate in order to oxidize the fatty acid [81]. This reduction step is described as the canonical pathway. An alternative pathway is the 'peroxide shunt', which describes the formation of the ferric-hydroperoxo intermediate directly via H_2O_2 and thus no molecular oxygen is needed for the oxidation of the fatty acid [81]. It is possible that LPMOs can also follow two oxidative routes as seen for the P450s. Other enzymes might also bear features similar to those reported of LPMOs that involve oxygen or H_2O_2, such as the 'mono-peroxygenase pathway' or 'peroxidase route' of unspecific peroxygenases (UPOs) [84]. Nevertheless, H_2O_2 formation by reducing agents, H_2O_2 sensitivity, and the reduction of LPMO-Cu(II) to LPMO-Cu(I) will be influenced by the structure of the reducing agent and *Mt*LPMO. Therefore, the two main conclusions stated in **Section 7.2.1** are still applicable.

7.3 Qualitative and quantitative analysis of the catalytic performance of LPMOs

7.3.1 Analysis of non-oxidized, C1- and C4-oxidized oligosaccharides released by *Mt*LPMOs

In this thesis, the formation of non-oxidized, C1- and C4-oxidized oligosaccharides is detected by mainly using two techniques: high-pressure anion exchange chromatography (HPAEC) and matrix-assisted laser desorption ionization-time of flight mass spectrometry (MALDI-TOF MS) (**Chapter II-VII**). In addition, we developed a β-glucosidase-assisted method for the quantification of released C1-oxidized gluco-oligosaccharides from the incubation of RAC with *Mt*LPMO9B and *Mt*LPMO9C

(**Chapter VI**; **Table 7.1**). Moreover, non-oxidized and C4-oxidized gluco-oligosaccharides, which were released from the incubation of RAC with *Mt*LPMO9C, were detected by combining non-reductive 2-aminobenzamide (2-AB) labeling with reverse phase-ultra high-performance liquid chromatography (RP-UHPLC) (**Chapter IV**).

Until now, HPAEC is the technique that is used most to determine the C1-/C4-regioselectivity and substrate specificity of LPMOs. In the beginning of our project, the catalytic performance of LPMOs was determined using the sum of the total peak areas of released non-oxidized and oxidized gluco-oligosaccharides measured by HPAEC (**Chapter III-V**) [13, 85]. Non-oxidized and oxidized oligosaccharides with varying DPs differ regarding their response factors. To enable the quantification of C1-oxidized compounds, the released oligosaccharides were hydrolyzed by enzymes, such as β-glucosidases from almonds (**Chapter VI**) and *An*Cel3A from *Aspergillus niger* or cellulases like *Tf*Cel5A from *Thermobifida fucosa* and *Tr*Cel7A from *T. reesei*. [31, 35].

Here, we present new results which show that the developed β-glucosidase-assisted method (**Chapter VI**) can be applied to quantify released soluble C1-oxidized gluco-oligosaccharides from RAC incubated with *Mt*LPMO9B in the presence of 21 reducing agents (**Figure 7.6**). We determined the same order of reducing agents that are suitable as electron donors for *Mt*LPMO9B by using the earlier method (sum of the total peak areas, **Chapter III**) compared to the β-glucosidase-assisted method that actually allows quantification of the catalytic performance (**Figure 7.6**). The highest concentration of released C1-oxidized gluco-oligosaccharides was achieved when RAC was incubated with *Mt*LPMO9B in the presence of ascorbic acid and approximately 1% of the total glucosyl moieties of RAC were oxidized.

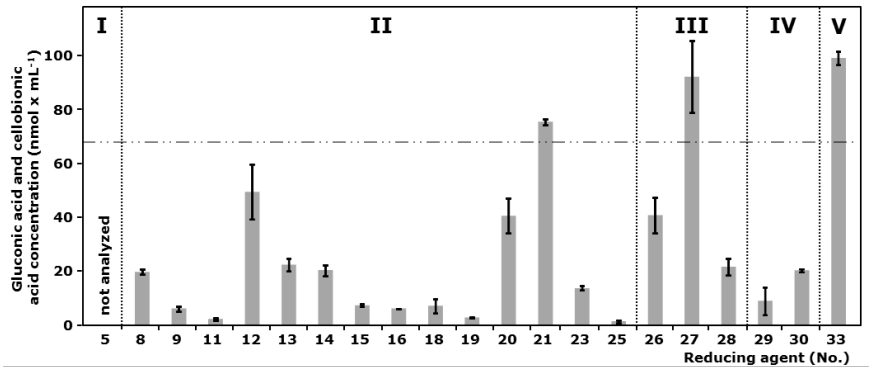

Figure 7.6 Released gluconic acid and cellobionic acid concentration from RAC incubated with *Mt*LPMO9B using different reducing agents, measured by using the β-glucosidase-assisted method. Regenerated amorphous cellulose (RAC; 1.5 mg mL^{-1}) was incubated with *Mt*LPMO9B (5 mg g^{-1} substrate) in an ammonium acetate buffer (pH 5.0) at 50°C for 24 h. Soluble fractions obtained from the incubation of RAC with *Mt*LPMO9B were incubated with β-glucosidase (1.5 U per sample) to yield glucose (not shown), gluconic acid and cellobionic acid only. The reducing agents (1 mM) are numbered and specified in **Table 3.2** (**Chapter III**). Vertical dotted lines separate reducing agents of the five structural groups (**Figure 3.4**; **Chapter III**). The threshold (horizontal dashed dotted line) is set to 70 % of the released products from RAC incubated with *Mt*LPMO9B in the presence of ascorbic acid (no. 33). All incubations were performed in duplicate, and standard deviations are represented through error bars. Details about the analysis are further described in **Chapter III** and **VI**.

7.3.2 Challenges in the qualitative and quantitative analysis of oligosaccharides released by LPMOs

We summarized the methods that were used to determine the catalytic performance of LPMOs until 2013 in **Chapter I**. Now in 2017, more methods are available to determine the activity of LPMOs towards soluble hemicelluloses in particular, such as a glycan microarray using substrate-specific monoclonal antibodies, direct infusion electrospray ionization-mass spectrometry (ESI-MS), or atomic force microscopy [25, 30, 39, 40]. Above that, more methods are being developed that enable the quantification of non-oxidized and C1-oxidized oligosaccharides released from cellulose or chitin incubated with C1-oxidizing LPMOs either by the degradation of the soluble fraction or both the insoluble and soluble fraction (**Chapter V**) [35, 36, 43, 86]. In contrast, the quantification of C4-oxidized oligosaccharides has not been shown, yet (**Chapter VI**) [31] and remains to be developed to further understand the kinetics of C4-oxidizing LPMOs.

The identification and quantification of LPMO-released non-oxidized and oxidized oligosaccharides is restricted by: I) their stability, II) their solubility and III) lack of standards.

I) As an example, C4-oxidized gluco-oligosaccharides released from cellulose through the action of LPMOs, can be determined by HPAEC. However, the high pH of the solvents causes an on-column decomposition of the C4-oxidized gluco-oligosaccharides into non-oxidized compounds and, furthermore, the peaks detected by HPAEC represent C4-oxidized gluco-oligosaccharides in their geminal diol form [31]. Moreover, C4-oxidized gluco-oligosaccharides undergo tautomerization, which leads to the formation of multiple new components and challenges the interpretation of obtained chromatograms (**Figure 7.2a**) [25]. As an alternative, the separation of C4-oxidized gluco-oligosaccharides by using porous graphitized carbon (PGC) or reverse phase columns in combination with milder solvents keeps the C4-ketone intact. However, these separation techniques are often coupled to UV or charged aerosol detection (CAD), which are less sensitive for the detection of non-oxidized and oxidized oligosaccharides compared to the pulsed amperometric detector (PAD) which is used in combination with HPAEC [31, 87] (**Chapter IV**). To overcome the lower sensitivity, we used derivatization methods, such as 2-aminobenzamide (2-AB) labeling, to enable UV detection (**Chapter IV**). But, labeling of the C4-ketone had to be performed under non-reducing conditions to avoid the reduction of the C4-ketone, as already described in detail in **Chapter IV**.

II) Released non-oxidized and oxidized oligosaccharides, formed by LPMOs from various substrates, differ in their solubility. As we already described in **Chapter VI**, the oxidation of RAC by *Mt*LPMO9B starts at the beginning of the incubation. However, released soluble products are measured after approximately 2 h of the incubation (**Chapter VI**). Depending on the substrate, we expected that the release of soluble oligosaccharides by LPMOs will take longer for substrates that have a very high DP, such as cotton (DP ≥ 10.000), compared to substrates with a lower DP like RAC (DP ≤ 500) [88, 89]. Substrates that comprise glucan chains with a high DP demand more oxidative cleavages until the first oligosaccharides are released compared to substrates which are built of glucan chains with a low DP. Possibly, the latter characteristic of LPMOs can be described by the parameter t_{MF}, the time point at which the concentration of soluble and insoluble C1-oxidized glucosyl residues is identical (**Chapter VI**).

Solubility is also dependent on the technique that is used to determine LPMO-released non-oxidized and oxidized oligosaccharides. As an example, oligosaccharides up to a DP of 8 or more can be

determined by using HPAEC whereas HILIC-MS or RP-UHPLC-MS have been used to detect oligosaccharides with a DP between 2 and 5 (**Chapter IV**) [31]. Enzymes that shorten non-oxidized and oxidized oligosaccharides released by LPMOs, such as endoglucanases and β-glucosidases, have been shown to be useful for reducing the amount of compounds and thereby help to overcome a limited detection range (**Chapter VI**) [31, 35, 36, 90].

III) Until now, qualitative and partly quantitative analysis has been carried out for released non-oxidized and oxidized oligosaccharides that comprise a linear structure, such as gluco-oligosaccharides from cellulose. As mentioned above, LPMOs are also active towards hemicelluloses, such as xyloglucan and xylan, which comprise multiple substitutions of the β-(1→3, 1→4)-linked glycosyl backbone (**Table 7.2**). In addition, hemicelluloses are often associated with cellulose (**Chapter I**). The LPMO-mediated oxidation of these rigid regions is expected to enhance the accessibility for hydrolytic enzymes and, therefore, is seen as a key step for efficient plant biomass degradation. However, the LPMO-mediated release of non-oxidized and oxidized oligosaccharides from these substrates can only be analyzed qualitatively by using techniques such as HPAEC, MALDI-TOF MS or direct infusion ESI-MS [18, 25, 40]. The quantification of the catalytic performance of LPMOs that are active towards hemicelluloses is currently not possible due to a lack of appropriate standards, such as non-oxidized and oxidized standards, which comprise side chain substitutions.

Here, we propose that derivatization techniques are suitable alternatives for the identification and quantification of LPMO-released oligosaccharides that are structurally diverse or not soluble. Derivatization techniques using (isotope) labeling have already been applied for the identification and quantification of complex non-oxidized oligosaccharides [91-98]. So far, only two studies have been published that describe the use of derivatization techniques to determine released oligosaccharides by LPMOs. One of these studies made use of fluorescence-labeling to investigate the catalytic performance of the C1-oxidizing *Pc*LPMO9D towards bacterial microcrystalline cellulose (BMCC) [34]. For that, the *Pc*LPMO9D-generated carboxyl groups of BMCC were first activated with 1-ethyl-3-[3-(dimethylamino)propyl]carbodiimide (EDAC) and then labeled with the fluorescence dye ANDA (7-amino-1,3-naphthalenedisulfonic acid). The labeled soluble fraction was analyzed by HPAEC-PAD and the insoluble fraction by X-ray photoelectron spectroscopy (XPS), which enabled the complete analysis of *Pc*LPMO9D-oxidized oligosaccharides [34]. In this thesis, we described the use of non-reductive 2-aminobenzamide labeling in combination with RP-UHPLC-UV-MS^n for the identification of released non-oxidized and C4-oxidized gluco-oligosaccharides from RAC incubated with *Mt*LPMO9C (**Chapter IV**). Next to 2-aminobenzamide, we investigated other labeling procedures using phenyl hydrazine or deuterated sodium borohydride. The latter showed a high potential for further development of the method (**Chapter IV**). In summary, labeling techniques have a high potential for the identification and quantification of LPMO-released non-oxidized and oxidized oligosaccharides.

7.3.4 Progress of LPMO-mediated substrate degradation

At the beginning of our research project, we proposed a three-step model to visualize the progress of the LPMO-mediated substrate degradation (**Figure 7.7**).

The first step of the reaction describes the reduction of the LPMO and the continuous oxidation of the substrate under the simultaneous consumption of electrons. This electron consumption leads to the oxidation of, for example, a diphenol into a quinone, and, thereby, to a decrease of the reducing

agent (diphenol) concentration. To determine the electron consumption of LPMOs, we used 3-methylcatechol since this reducing agent is stable during the standard incubation conditions (50°C, 24 h, pH 5.0) used in this thesis (**Chapter V** and **VI**). However, in 2014 we did not measure a significant difference in the reducing agent concentration during the incubation of RAC with the C1-oxidizing *Mt*LPMO9B by using UHPLC-UV-MS (data not shown). Nevertheless, we hypothesized that the consumption of the electron donor and the LPMO-mediated substrate oxidation will take place before the substrate conversion actually starts (**Figure 7.7**).

The second step of the LPMO reaction describes the continuous oxidation of the substrate, which leads to multiple chain cleavages. Subsequently, these multiple chain cleavages lead to the conversion of the substrate, which is accompanied by the reduction of size and hydrodynamic volume. The determination of the conversion of non-soluble substrates like cellulose or RAC by LPMOs in time is limited by the low solubility of these substrates. The conversion of cellulose was first demonstrated by Eibinger *et al*., who published the cleaving behavior of *Nc*LPMO9F towards crystalline cellulose using time-resolved atomic force microscopy (AFM) (see **Section 7.1.7**) [30]. Our discovery that certain *Mt*LPMOs are active towards soluble hemicelluloses such as xyloglucan or mixed β-(1→3, 1→4)-linked glucans (**Chapter II**) opens new possibilities to determine this time-dependent substrate conversion by using well-implemented techniques, such as high performance size exclusion chromatography (HPSEC).

The third step of the LPMO reaction describes the release of soluble non-oxidized and oxidized oligosaccharides, which is expected to take place after the substrate has already undergone multiple chain cleavages and is partly converted. We measured the delay by incubating RAC with *Mt*LPMO9B in the presence of ascorbic acid. To that end, a β-glucosidase-assisted method was developed to quantify the amount of oxidized gluco-oligosaccharides in the soluble fraction of RAC incubated with *Mt*LPMO9B (**Chapter VI**). In addition, a previously developed method by Cannella *et al*. [43] was used to quantify the amount of oxidized gluco-oligosaccharides in the insoluble fraction (**Chapter VI**). Indeed, we showed that *Mt*LPMO9B oxidizes cellulose from the start of the incubation, whereas soluble oxidized oligosaccharides are released after 2 h of the incubation (**Chapter VI**).

This difference in time between the oxidation of an insoluble substrate and the release of soluble oligosaccharides is useful to characterize LPMOs regarding their substrate specificity, as mentioned above. Again, the time point t_{MF} at which the concentration of soluble and insoluble C1-oxidized glucosyl residues is identical, could be a good parameter to describe such a substrate specificity (**Chapter VI**). As a result, LPMOs with a high catalytic performance towards crystalline or higher DP cellulose are expected to have larger t_{MF} values compared to LPMOs that preferably oxidize amorphous or lower DP cellulose. Obviously, t_{MF} will also depend on the enzyme and substrate concentration, which should be included in the parameter definition.

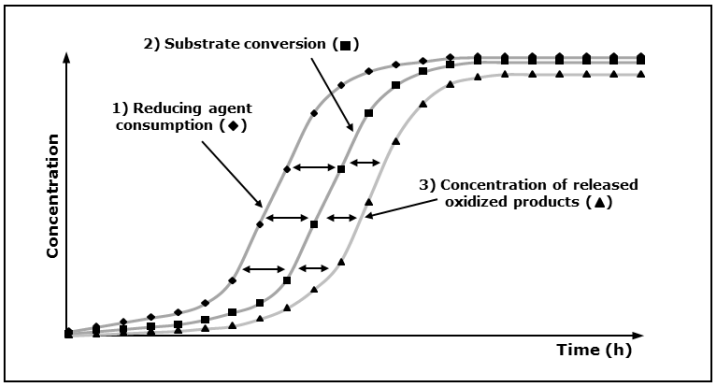

Figure 7.7 Model of the progress of LPMO-mediated substrate degradation. First, LPMOs are reduced under consumption of reducing agents (diamonds) and oxidize an insoluble substrate, such as cellulose. In a second step, the ongoing substrate oxidation leads to multiple chain cleavages and to the conversion (squares) of the substrate, like a reduction of the average DP. In the last stage, oxidized oligosaccharides become shorter until they are released as soluble oligosaccharides. The reactions occur in a delay, which is indicated by the horizontal arrows between the curves.

7.4 LPMOs in the biorefinery

In 2007, Merino *et al*. published a study that described an effect of adding GH61 members from *T. terrestis* to a cellulolytic enzyme cocktail of *T. reesei* [90, 99]. The supplementation of the cellulolytic enzyme cocktail with 5% (w/w) GH61B increased the cellulose conversion 1.4-fold [99]. In 2010, similar results were reported by Harris *et al.* who showed a 2-fold reduction of the enzyme load when AA9 LPMOs were incorporated in the genome of a *T. reesei* strain which was used for enzyme production [47]. Commercial enzyme cocktails have been developed, like Cellic CTec2 and CTec3, which are enriched with LPMOs to varying amounts. As an example, the incubation of hydrothermally pretreated wheat straw with Cellic CTec2 resulted in the oxidation of up to 4% of the original amount of glucosyl units present into gluconic acid [100]. The addition of LPMOs to an enzyme cocktail can be limited because of the formation of gluconic acid, which is a known inhibitor of β-glucosidases. In addition, gluconic acid also inhibits subsequent ethanol fermentation since only a limited amount of this compound can be metabolized by *Saccharomyces cerevisiae* species [100-102].

It has already been shown that the addition of a single LPMO to a cellulolytic cocktail can reduce the required enzyme dose for biomass saccharification [28, 47]. But the structural diversity of the plant biomass will demand the development of 'tailor-made' enzyme cocktails, which comprise LPMOs that differ in, for example, their substrate specificity and C1-/C4-regiospecificity. Moreover, the increase of the hydrolytic activity that can be achieved by the addition of AA9 LPMOs to enzyme cocktails varies depending on the type of LPMO and on the source and type of the substrate [99, 103-105]. Therefore, future enzyme cocktails will contain a more diverse repertoire of AA9 LPMOs, possibly from different fungal sources, such as saprophytic fungi and plant pathogenic fungi. Especially LPMOs that comprise key functions, like the *Mt*LPMO9A-mediated oxidation of xylan, which is non-covalently associated to cellulose, could play an important role to improve biomass

degradation by using enzyme cocktails. Based on these key functions of LPMOs, it remains unclear to what extent LPMOs should be added to a cellulolytic enzyme cocktail. In our opinion, it is not necessary to oxidize cellulose to a maximum extent by using LPMOs. We recommend that LPMOs should be more researched regarding the following questions: How do LPMOs disrupt the crystalline cellulose structure and are there differences between LPMOs? To what extent do hemicellulose-active LPMOs improve lignocellulose degradation? Are specific or unspecific hemicellulose oxidizing LPMOs more beneficial for biomass degradation? Why do fungi express LPMOs which oxidize cello-oligosaccharides? With respect to biorefinery, we see LPMOs as key enzymes that are able to degrade highly rigid polysaccharide structures that are hardly accessible for hydrolytic enzymes. In contrast to biorefinery, other applications such as the production of novel polysaccharides (e.g. oxidized cellulose fibers) would require LPMOs comprising a high specificity towards cellulose.

Based on current knowledge, it is necessary to enlarge the number of LPMOs with known substrate specificities since the characterization of LPMOs regarding their structure-function relationship is just at the beginning. Moreover, more attention needs to be drawn to the investigation of LPMOs that derive from more diverse fungal species which comprise different mode of life-style, such as saprophytic and plant pathogenic Ascomycota and Basidiomycota (see **Section 7.2.3**). We expect that it is of benefit to search *in nature* for the most suitable LPMO which is needed for a selected purpose. Therefore, methods like the analysis of transcription profiles of fungi grown on different substrates have a good potential for the identification of LPMOs with promising substrate specificities [3]. Knowledge about the structure-function relationship of LPMOs can also be combined with protein engineering methods, such as directed evolution. These methods should initially aim at the improvement of the LPMO operational stability, rather than the activity of the enzyme. Bissaro *et al*. already indicated that aromatic amino acids in the active site are susceptible for self-oxidation through ROS, which potentially leads to a fast inactivation of the LPMO [35].

A better understanding of the catalytic mechanism of the LPMO-mediated substrate oxidation will help to improve the implementation of these enzymes in plant biomass degradation. As an example, light-sensitive electron-donating systems have been described to boost the cellulose oxidation of LPMOs up to 100-fold and current developments aim at the implementation of such a system into the biorefinery process [43]. Interestingly, the discovery that H_2O_2 can be a co-substrate of LPMOs and that LPMOs can operate under anaerobic conditions is of high importance for future applications, since biomass degradation at an industrial scale is mainly conducted under oxygen-poor conditions [35]. Moreover, LPMOs changed our view of the role of lignin during plant biomass degradation. Several studies have shown that lignin and lignin-derived phenolic compounds present in lignocellulosic biomass are efficient electron donating compounds for some LPMOs [44, 64]. Furthermore, He *et al*. demonstrated that pretreatments affect the cellulose hydrolysis and thereby also the extent of the LPMO-mediated boosting effect [104]. Therefore, optimization of the plant biomass degradation with LPMO-enriched enzyme cocktails and the simultaneous development of pretreatments should include the focus on the potential of residual lignin as a reducing agent.

Finally, most of the experiments described in this thesis were performed at one pH (5.0) and one temperature (50°C). These conditions were based on the optimal performance of the cellulolytic cocktail produced by *M. thermophila* C1 and turned out to be suitable to determine the activity of *Mt*LPMOs towards a variety of substrates. Nevertheless, future research aimed at the characterization of LPMOs should also include the investigation of the effect of varying incubation

conditions on the LPMO activity, especially in the presence of different reducing agents. This research is of high importance from an applicational point of view, since pH and temperature influence the catalytic performance of LPMOs tremendously (**Chapter VI**).

References

1. Isaksen T, Westereng B, Aachmann FL, Agger JW, Kracher D, Kittl R *et al*. A C4-oxidizing lytic polysaccharide monooxygenase cleaving both cellulose and cello-oligosaccharides. J. Biol. Chem. 2014;289(5):2632-42.
2. Nekiunaite L, Petrović DM, Westereng B, Vaaje-Kolstad G, Abou Hachem M, Várnai A *et al*. *Fg*LPMO9A from *Fusarium graminearum* cleaves xyloglucan independently of the backbone substitution pattern. FEBS Lett. 2016; 590(19):3346-3356.
3. Berka RM, Grigoriev IV, Otillar R, Salamov A, Grimwood J, Reid I *et al*. Comparative genomic analysis of the thermophilic biomass-degrading fungi *Myceliophthora thermophila* and *Thielavia terrestris*. Nat. Biotechnol. 2011;29(10):922-7.
4. Fernandes AN, Thomas LH, Altaner CM, Callow P, Forsyth VT, Apperley DC *et al*. Nanostructure of cellulose microfibrils in spruce wood. Proc. Natl. Acad. Sci. U. S. A. 2011;108(47):E1195-E203.
5. Nishiyama Y, Sugiyama J, Chanzy H, Langan P. Crystal structure and hydrogen bonding system in cellulose Iα from synchrotron x-ray and neutron fiber diffraction. J. Am. Chem. Soc. 2003;125(47):14300-6.
6. Atalla RH, Vanderhart DL. Native cellulose: A composite of two distinct crystalline forms. Science. 1984;223(4633):283-5.
7. Jarvis M. Chemistry: Cellulose stacks up. Nature. 2003;426(6967):611-2.
8. Nishiyama Y, Langan P, Chanzy H. Crystal structure and hydrogen-bonding system in cellulose Iβ from synchrotron x-ray and neutron fiber diffraction. J. Am. Chem. Soc. 2002;124(31):9074-82.
9. Hemsworth GR, Davies GJ, Walton PH. Recent insights into copper-containing lytic polysaccharide mono-oxygenases. Curr. Opin. Struct. Biol. 2013;23(5):660-8.
10. Hemsworth GR, Johnston EM, Davies GJ, Walton PH. Lytic polysaccharide monooxygenases in biomass conversion. Trends Biotechnol. 2015;33(12):747-61.
11. Li X, Beeson WTt, Phillips CM, Marletta MA, Cate JH. Structural basis for substrate targeting and catalysis by fungal polysaccharide monooxygenases. Structure. 2012;20(6):1051-61.
12. Vaaje-Kolstad G, Forsberg Z, Loose JSM, Bissaro B, Eijsink VGH. Structural diversity of lytic polysaccharide monooxygenases. Curr. Opin. Struct. Biol. 2017;44:67-76.
13. Bennati-Granier C, Garajova S, Champion C, Grisel S, Haon M, Zhou S *et al*. Substrate specificity and regioselectivity of fungal AA9 lytic polysaccharide monooxygenases secreted by *Podospora anserina*. Biotechnol. Biofuels. 2015;8:90.
14. Phillips CM, Beeson WT, Cate JH, Marletta MA. Cellobiose dehydrogenase and a copper-dependent polysaccharide monooxygenase potentiate cellulose degradation by *Neurospora crassa*. ACS Chem. Biol. 2011;6(12):1399-406.
15. Quinlan RJ, Sweeney MD, Lo Leggio L, Otten H, Poulsen JC, Johansen KS *et* al. Insights into the oxidative degradation of cellulose by a copper metalloenzyme that exploits biomass components. Proc. Natl. Acad. Sci. U. S. A. 2011;108(37):15079-84.
16. Westereng B, Ishida T, Vaaje-Kolstad G, Wu M, Eijsink VG, Igarashi K *et* al. The putative endoglucanase *Pc*GH61D from *Phanerochaete chrysosporium* is a metal-dependent oxidative enzyme that cleaves cellulose. PloS One. 2011;6(11):e27807.
17. Borisova AS, Isaksen T, Dimarogona M, Kognole AA, Mathiesen G, Varnai A *et* al. Structural and functional characterization of a lytic polysaccharide monooxygenase with broad substrate specificity. J. Biol. Chem. 2015; 290, 22955-22969.
18. Frommhagen M, Sforza S, Westphal AH, Visser J, Hinz SW, Koetsier MJ *et* al. Discovery of the combined oxidative cleavage of plant xylan and cellulose by a new fungal polysaccharide monooxygenase. Biotechnol. Biofuels. 2015;8:101.
19. Jagadeeswaran G, Gainey L, Prade R, Mort AJ. A family of AA9 lytic polysaccharide monooxygenases in *Aspergillus nidulans* is differentially regulated by multiple substrates and at least one is active on cellulose and xyloglucan. Appl. Microbiol. Biotechnol. 2016;100(10):4535-47.
20. Kojima Y, Várnai A, Ishida T, Sunagawa N, Petrovic DM, Igarashi K *et* al. A lytic polysaccharide monooxygenase with broad xyloglucan specificity from the brown-rot fungus *Gloeophyllum trabeum* and its action on cellulose-xyloglucan complexes. Appl. Environ. Microbiol. 2016;82(22):6557-72.
21. Frandsen KEH, Simmons TJ, Dupree P, Poulsen J-CN, Hemsworth GR, Ciano L *et al*. The molecular basis of polysaccharide cleavage by lytic polysaccharide monooxygenases. Nat. Chem. Biol. 2016;12(4):298-303.
22. Vu VV, Beeson WT, Phillips CM, Cate JH, Marletta MA. Determinants of regioselective hydroxylation in the fungal polysaccharide monooxygenases. J. Am. Chem. Soc. 2014;136(2):562-5.
23. Kittl R, Kracher D, Burgstaller D, Haltrich D, Ludwig R. Production of four *Neurospora crassa* lytic polysaccharide monooxygenases in *Pichia pastoris* monitored by a fluorimetric assay. Biotechnol. Biofuels. 2012;5(1):79.

24. Kracher D, Scheiblbrandner S, Felice AKG, Breslmayr E, Preims M, Ludwicka K *et al.* Extracellular electron transfer systems fuel cellulose oxidative degradation. Science. 2016; 27;352(6289):1098-101.
25. Agger JW, Isaksen T, Varnai A, Vidal-Melgosa S, Willats WG, Ludwig R *et al*. Discovery of LPMO activity on hemicelluloses shows the importance of oxidative processes in plant cell wall degradation. Proc. Natl. Acad. Sci. U. S. A. 2014;111(17):6287-92.
26. Courtade G, Wimmer R, Røhr ÅK, Preims M, Felice AKG, Dimarogona M *et al.* Interactions of a fungal lytic polysaccharide monooxygenase with β-glucan substrates and cellobiose dehydrogenase. Proc. Natl. Acad. Sci. U. S. A. 2016;113(21):5922-7.
27. Courtade G, Wimmer R, Dimarogona M, Sandgren M, Eijsink VGH, Aachmann FL. Backbone and side-chain 1H, 13C, and 15N chemical shift assignments for the apo-form of the lytic polysaccharide monooxygenase *Nc*LPMO9C. Biomol. NMR Assignments 2016:1-4.
28. Müller G, Várnai A, Johansen KS, Eijsink VGH, Horn SJ. Harnessing the potential of LPMO-containing cellulase cocktails poses new demands on processing conditions. Biotechnol. Biofuels. 2015;8(1):1-9.
29. Forsberg Z, Mackenzie AK, Sørlie M, Røhr ÅK, Helland R, Arvai AS *et* al. Structural and functional characterization of a conserved pair of bacterial cellulose-oxidizing lytic polysaccharide monooxygenases. Proc. Natl. Acad. Sci. U. S. A. 2014;111(23):8446-51.
30. Eibinger M, Ganner T, Bubner P, Rosker S, Kracher D, Haltrich D *et al*. Cellulose surface degradation by a lytic polysaccharide monooxygenase and its effect on cellulase hydrolytic efficiency. J. Biol. Chem. 2014;289(52):35929-38.
31. Westereng B, Arntzen MØ, Aachmann FL, Várnai A, Eijsink VGH, Agger JW. Simultaneous analysis of C1 and C4 oxidized oligosaccharides, the products of lytic polysaccharide monooxygenases acting on cellulose. J. Chromatogr. A. 2016; 1445 (2016) 46–54.
32. Patel I, Kracher D, Ma S, Garajova S, Haon M, Faulds CB *et* al. Salt-responsive lytic polysaccharide monooxygenases from the mangrove fungus *Pestalotiopsis sp*. NCi6. Biotechnol. Biofuels. 2016;9(1):1-12.
33. Wu M, Beckham GT, Larsson AM, Ishida T, Kim S, Payne CM *et* al. Crystal structure and computational characterization of the lytic polysaccharide monooxygenase GH61D from the Basidiomycota fungus *Phanerochaete chrysosporium*. J. Biol. Chem. 2013;288(18):12828-39.
34. Vuong TV, Liu B, Sandgren M, Master ER. Microplate-based detection of lytic polysaccharide monooxygenase activity by fluorescence-labeling of insoluble oxidized products. Biomacromolecules. 2017;18(2):610-6.
35. Bissaro B, Rohr AK, Skaugen M, Forsberg Z, Horn SJ, Vaaje-Kolstad G *et* al. Fenton-type chemistry by a copper enzyme: molecular mechanism of polysaccharide oxidative cleavage. bioRxiv. 2016.
36. Bissaro B, Forsberg Z, Ni Y, Hollmann F, Vaaje-Kolstad G, Eijsink VGH. Fueling biomass-degrading oxidative enzymes by light-driven water oxidation. Green Chem. 2016; 18, 5357-5366.
37. Bey M, Zhou S, Poidevin L, Henrissat B, Coutinho PM, Berrin JG *et al*. Cello-oligosaccharide oxidation reveals differences between two lytic polysaccharide monooxygenases (family GH61) from *Podospora anserina*. Appl. Environ. Microbiol. 2013;79(2):488-96.
38. Garajova S, Mathieu Y, Beccia MR, Bennati-Granier C, Biaso F, Fanuel M *et al*. Single-domain flavoenzymes trigger lytic polysaccharide monooxygenases for oxidative degradation of cellulose. Sci. Rep. 2016;6:28276.
39. Villares A, Moreau C, Bennati-Granier C, Garajova S, Foucat L, Falourd X *et al*. Lytic polysaccharide monooxygenases disrupt the cellulose fibers structure. Sci. Rep. 2017;7:40262.
40. Fanuel M, Garajova S, Ropartz D, McGregor N, Brumer H, Rogniaux H *et al*. The *Podospora anserina* lytic polysaccharide monooxygenase *Pa*LPMO9H catalyzes oxidative cleavage of diverse plant cell wall matrix glycans. Biotechnol. Biofuels. 2017;10(1):63.
41. Gudmundsson M, Kim S, Wu M, Ishida T, Momeni MH, Vaaje-Kolstad G *et al*. Structural and electronic snapshots during the transition from a Cu(II) to Cu(I) metal center of a lytic polysaccharide monooxygenase by x-ray photoreduction. J. Biol. Chem. 2014;289(27):18782-92.
42. Kim IJ, Seo N, An HJ, Kim J-H, Harris PV, Kim KH. Type-dependent action modes of *Tt*AA9E and *Ta*AA9A acting on cellulose and differently pretreated lignocellulosic substrates. Biotechnol. Biofuels. 2017;10(1):46.
43. Cannella D, Mollers KB, Frigaard NU, Jensen PE, Bjerrum MJ, Johansen KS *et* al. Light-driven oxidation of polysaccharides by photosynthetic pigments and a metalloenzyme. Nat. Commun. 2016; (4)7:11134.
44. Westereng B, Cannella D, Wittrup Agger J, Jørgensen H, Larsen Andersen M, Eijsink VGH *et* al. Enzymatic cellulose oxidation is linked to lignin by long-range electron transfer. Sci. Rep. 2015;5:18561.
45. Pierce BC, Agger JW, Wichmann J, Meyer AS. Oxidative cleavage and hydrolytic boosting of cellulose in soybean spent flakes by *Trichoderma reesei* Cel61A lytic polysaccharide monooxygenase. Enzyme Microb. Technol. 2017; 98, 58–66.
46. Tanghe M, Danneels B, Camattari A, Glieder A, Vandenberghe I, Devreese B *et al*. Recombinant expression of *Trichoderma reesei* Cel61A in *Pichia pastoris*: Optimizing yield and N-terminal processing. Mol. Biotechnol. 2015;57(11-12):1010-7.

47. Harris PV, Welner D, McFarland KC, Re E, Navarro Poulsen JC, Brown K *et al*. Stimulation of lignocellulosic biomass hydrolysis by proteins of glycoside hydrolase family 61: Structure and function of a large, enigmatic family. Biochemistry. 2010;49(15):3305-16.
48. Davies GJ, Williams SJ. Carbohydrate-active enzymes: Sequences, shapes, contortions and cells. Biochem. Soc. Trans. 2016;44(1):79-87.
49. Davies G, Henrissat B. Structures and mechanisms of glycosyl hydrolases. Structure. 1995;3(9):853-9.
50. Vincken JP, de Keizer A, Beldman G, Voragen AGJ. Fractionation of xyloglucan fragments and their interaction with cellulose. Plant Physiol. 1995;108(4):1579-85.
51. Kabel MA, van den Borne H, Vincken J-P, Voragen AGJ, Schols HA. Structural differences of xylans affect their interaction with cellulose. Carbohydr. Polym. 2007;69(1):94-105.
52. Hinz SWA, Pouvreau L, Joosten R, Bartels J, Jonathan MC, Wery J *et al*. Hemicellulase production in *Chrysosporium lucknowense* C1. J. Cereal Sci. 2009;50(3):318-23.
53. Arola S, Linder MB. Binding of cellulose binding modules reveal differences between cellulose substrates. Sci. Rep. 2016;6:35358.
54. Forsberg Z, Nelson CE, Dalhus B, Mekasha S, Loose JS, Crouch LI *et al*. Structural and functional analysis of a lytic polysaccharide monooxygenase important for efficient utilization of chitin in *Cellvibrio japonicus*. J. Biol. Chem. 2016; 1;291(14):7300-12.
55. Forsberg Z, Rohr AK, Mekasha S, Andersson KK, Eijsink VG, Vaaje-Kolstad G *et al*. Comparative study of two chitin-active and two cellulose-active AA10-type lytic polysaccharide monooxygenases. Biochemistry. 2014;53(10):1647-56.
56. Nakagawa YS, Kudo M, Loose JSM, Ishikawa T, Totani K, Eijsink VGH *et* al. A small lytic polysaccharide monooxygenase from *Streptomyces griseus* targeting α- and β-chitin. FEBS J. 2015;282(6):1065-79.
57. Suzuki K, Suzuki M, Taiyoji M, Nikaidou N, Watanabe T. Chitin binding protein (CBP21) in the culture supernatant of *Serratia marcescens* 2170. Biosci. Biotechnol. Biochem. 1998;62(1):128-35.
58. Vaaje-Kolstad G, Houston DR, Riemen AH, Eijsink VG, van Aalten DM. Crystal structure and binding properties of the *Serratia marcescens* chitin-binding protein CBP21. J. Biol. Chem. 2005;280(12):11313-9.
59. Zeltins A, Schrempp H. Specific interaction of the *Streptomyces* Chitin-Binding Protein Chb1 with α-Chitin. Eur. J. Biochem. 1997;246(2):557-64.
60. King JR, Bowers CM, Toone EJ. Specific Binding at the cellulose binding module–cellulose interface observed by force spectroscopy. Langmuir. 2015;31(11):3431-40.
61. Taylor CB, Talib MF, McCabe C, Bu L, Adney WS, Himmel ME *et al*. Computational investigation of glycosylation effects on a family 1 carbohydrate-binding module. J. Biol. Chem. 2012;287(5):3147-55.
62. Constant S, Wienk HLJ, Frissen AE, Peinder Pd, Boelens R, van Es DS *et al*. New insights into the structure and composition of technical lignins: a comparative characterisation study. Green Chem. 2016;18(9):2651-65.
63. Forsberg Z, Vaaje-Kolstad G, Westereng B, Bunaes AC, Stenstrom Y, MacKenzie A *et al*. Cleavage of cellulose by a CBM33 protein. Protein Science : A Publication of the Protein Society. 2011;20(9):1479-83.
64. Rodriguez-Zuniga UF, Cannella D, Giordano RdC, Giordano RdLC, Jorgensen H, Felby C. Lignocellulose pretreatment technologies affect the level of enzymatic cellulose oxidation by LPMO. Green Chem. 2015;17(5):2896-903.
65. Tan T-C, Kracher D, Gandini R, Sygmund C, Kittl R, Haltrich D *et al*. Structural basis for cellobiose dehydrogenase action during oxidative cellulose degradation. Nat. Commun. 2015;(7)6:7542.
66. Aachmann FL, Sorlie M, Skjak-Braek G, Eijsink VG, Vaaje-Kolstad G. NMR structure of a lytic polysaccharide monooxygenase provides insight into copper binding, protein dynamics, and substrate interactions. Proc. Natl. Acad. Sci. U. S. A. 2012;109(46):18779-84.
67. Temp U, Eggert C. Novel interaction between laccase and cellobiose dehydrogenase during pigment synthesis in the white rot fungus *Pycnoporus cinnabarinus*. Appl. Environ. Microbiol. 1999;65(2):389-95.
68. Hildén L, Johansson G, Pettersson G, Li J, Ljungquist P, Henriksson G. Do the extracellular enzymes cellobiose dehydrogenase and manganese peroxidase form a pathway in lignin biodegradation? FEBS Lett. 2000; 477(1-2):79-83.
69. Hernández-Ortega A, Ferreira P, Martínez AT. Fungal aryl-alcohol oxidase: A peroxide-producing flavoenzyme involved in lignin degradation. Appl. Microbiol. Biotechnol. 2012;93(4):1395-410.
70. Adinarayana K, Francisco JP, Antonio B, Miguel A. Laccases and their applications: A patent review. Recent Pat. Biotechnol. 2008;2(1):10-24.
71. Camarero S, Ibarra D, Martínez MJ, Martínez ÁT. Lignin-derived compounds as efficient laccase mediators for decolorization of different types of recalcitrant dyes. Appl. Microbiol. Biotechnol. 2005;71(4):1775-84.
72. Hammel KE, Jensen KA, Mozuch MD, Landucci LL, Tien M, Pease EA. Ligninolysis by a purified lignin peroxidase. J. Biol. Chem. 1993;268(17):12274-81.
73. Hofrichter M. Review: Lignin conversion by manganese peroxidase (MnP). Enzyme Microb. Technol. 2002;30(4):454-66.

74. Pérez-Boada M, Ruiz-Dueñas FJ, Pogni R, Basosi R, Choinowski T, Martínez MJ *et* al. Versatile peroxidase oxidation of high redox potential aromatic compounds: Site-directed mutagenesis, spectroscopic and crystallographic investigation of three long-range electron transfer pathways. J. Mol. Biol. 2005;354(2):385-402.
75. Ruiz-Dueñas FJ, Morales M, García E, Miki Y, Martínez MJ, Martínez AT. Substrate oxidation sites in versatile peroxidase and other basidiomycete peroxidases. J. Exp. Bot. 2009;60(2):441-52.
76. Umezawa T, Higuchi T. Mechanism of aromatic ring cleavage of β-*O*-4 lignin substructure models by lignin peroxidase. FEBS Lett. 1987;218(2):255-60.
77. Kühnel S, Pouvreau L, Appeldoorn MM, Hinz SWA, Schols HA, Gruppen H. The ferulic acid esterases of *Chrysosporium lucknowense* C1: Purification, characterization and their potential application in biorefinery. Enzyme Microb. Technol. 2012;50(1):77-85.
78. Möllers KB, Mikkelsen H, Simonsen TI, Cannella D, Johansen KS, Bjerrum MJ *et al*. On the formation and role of reactive oxygen species in light-driven LPMO oxidation of phosphoric acid swollen cellulose. Carbohydr. Res. 2017, in press.
79. Scott BR, Huang HZ, Frickman J, Halvorsen R, Johansen KS. Catalase improves saccharification of lignocellulose by reducing lytic polysaccharide monooxygenase-associated enzyme inactivation. Biotechnol. Lett. 2016;38(3):425-34.
80. Walton PH, Davies GJ. On the catalytic mechanisms of lytic polysaccharide monooxygenases. Curr. Opin. Chem. Biol. 2016;31:195-207.
81. Matthews S, Belcher JD, Tee KL, Girvan HM, McLean KJ, Rigby SE *et al*. Catalytic determinants of alkene production by the cytochrome P450 peroxygenase OleTJE. J. Biol. Chem. 2017;24;292(12):5128-5143.
82. Grant JL, Mitchell ME, Makris TM. Catalytic strategy for carbon–carbon bond scission by the cytochrome P450 OleT. Proc. Natl. Acad. Sci. U. S. A. 2016;113(36):10049-54.
83. Grant JL, Hsieh CH, Makris TM. Decarboxylation of fatty acids to terminal alkenes by cytochrome P450 compound I. J. Am. Chem. Soc. 2015;137(15):4940-3.
84. Hofrichter M, Kellner H, Pecyna MJ, Ullrich R. Fungal unspecific peroxygenases: Heme-thiolate proteins that combine peroxidase and cytochrome P450 properties. In: Monooxygenase, peroxidase and peroxygenase properties and mechanisms of cytochrome P450. Hrycay EG, Bandiera SM, editors. Cham: Springer International Publishing. 2015; 341-68.
85. Crouch LI, Labourel A, Walton PH, Davies GJ, Gilbert HJ. The contribution of non-catalytic carbohydrate binding modules to the activity lytic polysaccharide monooxygenases. J. Biol. Chem. 2016.
86. Loose JSM, Forsberg Z, Fraaije MW, Eijsink VGH, Vaaje-Kolstad G. A rapid quantitative activity assay shows that the *Vibrio cholerae* colonization factor GbpA is an active lytic polysaccharide monooxygenase. FEBS Lett. 2014;588(18):3435-40.
87. Westereng B, Agger JW, Horn SJ, Vaaje-Kolstad G, Aachmann FL, Stenstrom YH *et al*. Efficient separation of oxidized cello-oligosaccharides generated by cellulose degrading lytic polysaccharide monooxygenases. J. Chromatogr. A. 2013;1271(1):144-52.
88. Mohnen D, Bar-Peled M, Somerville C. Biosynthesis of plant cell walls. In: Biomass Recalcitrance. Himmel M, editor. Oxford: Blackwell Publishing; 2008. p. 94-187.
89. Zhang YHP, Cui J, Lynd LR, Kuang LR. A transition from cellulose swelling to cellulose dissolution by *o*-phosphoric acid: Evidence from enzymatic hydrolysis and supramolecular structure. Biomacromolecules. 2006;7(2):644-8.
90. Vaaje-Kolstad G, Westereng B, Horn SJ, Liu Z, Zhai H, Sorlie M *et al.* An oxidative enzyme boosting the enzymatic conversion of recalcitrant polysaccharides. Science. 2010;330(6001):219-22.
91. Alvarez-Manilla G, Warren NL, Abney T, Atwood IIIJ, Azadi P, York WS *et al*. Tools for glycomics: Relative quantitation of glycans by isotopic permethylation using 13CH3I. Glycobiology. 2007;17(7):677-87.
92. Hitchcock AM, Yates KE, Costello CE, Zaia J. Comparative glycomics of connective tissue glycosaminoglycans. Proteomics. 2008;8(7):1384-97.
93. Jonathan MC, van Brussel M, Scheffers MS, Kabel MA. Characterisation of branched gluco-oligosaccharides to study the mode-of-action of a glucoamylase from *Hypocrea jecorina*. Carbohydr. Polym. 2015;132:59-66.
94. Ridlova G, Mortimer JC, Maslen SL, Dupree P, Stephens E. Oligosaccharide relative quantitation using isotope tagging and normal-phase liquid chromatography/mass spectrometry. Rapid Commun. Mass Spectrom. 2008;22(17):2723-30.
95. Ruhaak LR, Huhn C, Koeleman CAM, Deelder AM, Wuhrer M. Robust and high-throughput sample preparation for (semi-) quantitative analysis of N-glycosylation profiles from plasma samples. In: Quantitative Methods in Proteomics. Marcus K, editor. Totowa, NJ: Humana Press; 2012. p. 371-85.
96. Ruhaak LR, Steenvoorden E, Koeleman CAM, Deelder AM, Wuhrer M. 2-Picoline-borane: A non-toxic reducing agent for oligosaccharide labeling by reductive amination. Proteomics. 2010;10(12):2330-6.
97. Ruhaak LR, Zauner G, Huhn C, Bruggink C, Deelder AM, Wuhrer M. Glycan labeling strategies and their use in identification and quantification. Anal. Bioanal. Chem. 2010;397(8):3457-81.
98. Yuan J, Hashii N, Kawasaki N, Itoh S, Kawanishi T, Hayakawa T. Isotope tag method for quantitative analysis of carbohydrates by liquid chromatography–mass spectrometry. J. Chromatogr. A 2005;1067(1–2):145-52.

99. Merino ST, Cherry J. Progress and challenges in enzyme development for biomass utilization. In: Biofuels. Olsson L, editor. Berlin, Heidelberg: Springer Berlin Heidelberg; 2007. p. 95-120.
100. Cannella D, Hsieh C-wC, Felby C, Jørgensen H. Production and effect of aldonic acids during enzymatic hydrolysis of lignocellulose at high dry matter content. Biotechnol. Biofuels. 2012;5(1):26.
101. Peinado RA, Mauricio JC, Moreno J. Aromatic series in sherry wines with gluconic acid subjected to different biological aging conditions by *Saccharomyces cerevisiae* var. *capensis*. Food Chem. 2006;94(2):232-9.
102. Peinado RA, Moreno JJ, Ortega JM, Mauricio JC. Effect of gluconic acid consumption during simulation of biological aging of sherry wines by a flor yeast strain on the final volatile compounds. J. Agric. Food Chem. 2003;51(21):6198-203.
103. Corrêa TLR, Santos LV, Pereira GAG. AA9 and AA10: from enigmatic to essential enzymes. Appl. Microbiol. Biotechnol. 2015;100(1):9-16.
104. Hu J, Arantes V, Pribowo A, Gourlay K, Saddler JN. Substrate factors that influence the synergistic interaction of AA9 and cellulases during the enzymatic hydrolysis of biomass. Energy & Environ. Sci. 2014;7(7):2308-15.
105. Hu J, Chandra R, Arantes V, Gourlay K, Susan van Dyk J, Saddler JN. The addition of accessory enzymes enhances the hydrolytic performance of cellulase enzymes at high solid loadings. Bioresour. Technol. 2015;186(0):149-53.

Summary

The aim of this project was the characterization of LPMOs from *Myceliophthora thermophila* C1 and their potential use in biomass degradation. Therefore, we purified and investigated seven LPMOs from the fungus *Myceliophthora thermophila* C1 for their mode of action towards plant cell wall materials, such as cellulose.

In total, *M. thermophila* C1 encodes 26 putative LPMOs of which 22 belong to the auxiliary activity (AA) family 9, based on their amino acid sequence identity. We hypothesized that AA9 LPMOs of *M. thermophila* C1 differ in their substrate specificity and mode of action towards plant cell wall polysaccharides. Therefore, the aim of this project was the characterization of seven AA9 *Mt*LPMOs from *M. thermophila* C1 and their potential use in biomass degradation.

In **Chapter I** of this thesis, we describe the background and aim of this project. Therein, we focus on the plant cell wall architecture, which includes the description of the cell wall compartments middle lamella, primary and secondary plant cell wall. In addition, we describe the composition and structure of the cell wall compounds cellulose, hemicellulose and lignin, as well as their interaction within the plant cell wall. Moreover, cell wall degrading enzymes are presented, such as cellulases, hemicellulases and lignin degrading enzymes. In the second part of the introduction, we give an overview of the knowledge about LPMOs at the time of the beginning of our project (2013). Here, the discovery, classification, structural features, substrate specificity, C1-/C4-regioselectivity and electron donating compounds of LPMOs are described. Furthermore, we give an overview of analytical methods that have been used to determine the substrate specificity and C1-/C4-regioselectivity of LPMOs. Finally, we shortly describe the fungus *M. thermophila* C1 and its role in plant biomass degradation.

The first AA9 LPMO of *M. thermophila* C1 that was characterized is *Mt*LPMO9A (**Chapter II**). *Mt*LPMO9A is the only LPMO known so far that oxidizes xylan associated to cellulose. In addition, *Mt*LPMO9A also showed minor activity towards mixed β-(1→3, 1→4)-linked glucan from barley and xyloglucan. Furthermore, *Mt*LPMO9A oxidized the C1 and C4 carbon atom of the β-linked glucan chain. *Mt*LPMO9A showed a synergistic effect with the endoglucanase I (EGI) from *Trichoderma viride*, which led to a 16-fold higher release of detected oligosaccharides compared to the oligosaccharide release of *Mt*LPMO9A and EGI alone.

In **Chapter III**, three *Mt*LPMOs from *M. thermophila* C1 are presented that differ in their substrate specificity, C1-/C4-regioselectivity and reducing agent specificity. Next to the already described *Mt*LPMO9A, we showed that *Mt*LPMO9B releases C1-oxidized and *Mt*LPMO9C C4-oxidized gluco-oligosaccharides from cellulose. *Mt*LPMO9B was only active towards cellulose whereas *Mt*LPMO9C also oxidized, to a minor extent, mixed β-(1→3, 1→4)-linked glucan from oat spelt and xyloglucan. In total, 34 reducing agents, which are mainly plant-derived flavonoids and lignin-building blocks, were studied for their ability to promote LPMO activity. Reducing agents with a 1,2-benzenediol or 1,2,3-benzenetriol moiety gave the highest release of oxidized and non-oxidized gluco-oligosaccharides from cellulose for all three *Mt*LPMOs. Low activities of *Mt*LPMOs towards cellulose were observed in the presence of monophenols and sulfur-containing compounds.

In **Chapter IV** we describe the use of reversed phase (RP)-UHPLC in combination with non-reductive 2-aminobenzamide (2-AB) labeling to separate C4-oxidized gluco-oligosaccharides from their non-oxidized counterparts. Notably, RP-UHPLC did not require buffered mobile phases, which reduce mass spectrometry (MS) sensitivity, and was seen as an advantage over other techniques, such as

hydrophilic interaction liquid chromatography and porous graphitized carbon coupled to MS. Non-reductive labeling kept the ketone at the C4-position of LPMO oxidized oligosaccharides intact, while selective reducing agents such as sodium triacetoxyborohydride (STAB) reduced this ketone group. In addition, alternative labeling approaches including the use of STAB and deuterated sodium borohydride are discussed.

In **Chapter V** we show how polyphenol oxidases (PPOs) boost the LPMO-driven lignocellulose oxidation. The concerted enzymatic process involves the initial conversion of monophenols into diphenols by the polyphenol oxidase *Mt*PPO7 from *M. thermophila* C1, and the subsequent oxidation of cellulose by *Mt*LPMO9B. As a result, the addition of *Mt*PPO7 to the incubation of RAC with *Mt*LPMO9B increased the cellulose oxidation up to 75-fold. Interestingly, *Mt*PPO7 showed preference towards lignin-derived methoxylated monophenols and exhibited low efficiency towards *ortho*-diphenols, thus limiting the generation of unwanted quinones. Sequence analysis of genomes of 336 Ascomycota and 208 Basidiomycota revealed a high correlation between *Mt*PPO7-like and AA9 LPMO-like genes.

The quantification of the catalytic performance of *Mt*LPMO9B and *Mt*LPMO9D, which both oxidize the C1-carbon, is described in **Chapter VI**. Therein, we developed a β-glucosidase-assisted method to quantify the release of C1-oxidized gluco-oligosaccharides from cellulose by both *Mt*LPMOs. We showed that the catalytic performance of both *Mt*LPMOs is strongly dependent on the pH and temperature. We found that pH mainly affected the reducing agent dependency whereas temperature impacted the operational stability of both *Mt*LPMOs. Furthermore, we demonstrated that the *Mt*LPMO9B-mediated cellulose oxidation started immediately at the beginning of the incubation whereas oxidized gluco-oligosaccharides were released after two hours.

Finally (**Chapter VII**), we discuss the relevance of our research in comparison to recently published data. In this chapter, new results are presented such as the substrate specificity of *Mt*LPMO9E, which oxidizes cellulose, xyloglucan, mixed β-(1→3, 1→4)-linked glucan and soluble cellodextrines at the C4-position. In addition, it is shown that *Mt*LPMO9F and *Mt*LPMO9G oxidize cellulose at the C4-carbon position. We present an overview of AA9 LPMOs including their substrate specificities and C1-/C4-regioselectivties, which were published until 2017. Moreover, the reducing agent preferences of *Mt*LPMOs are summarized and various electron donation systems are further discussed. We also describe challenges in the qualitative and quantitative analysis of LPMO-released oligosaccharides. At last, we discuss the impact of LPMOs in second generation biorefinery.

Acknowledgement

I will take this opportunity to express my gratitude to many of you who accompanied me during my PhD thesis project inside and outside Wageningen University over the past four years. Although there is only one name stated on the cover page of this booklet it should be acknowledged that the final outcome of this thesis is a result of the contribution of many of you.

First, I would like to thank my supervisors Harry, Mirjam and Willem for the excellent support during my thesis project.
Harry, thank you for the opportunity to work at the Laboratory of Food Chemistry, one of the most organized and structured departments I have ever visited. The comments that I received from you about my work have always been highly appreciated. I am also grateful that you enabled my colleagues and me to take part in PhD trips and many conferences in different countries around the world, which I really enjoyed. Special thanks to Mirjam for the daily supervision during the past years. We had inspiring and fruitful conversations and I appreciate that you gave me enough freedom during my project. I think we both agree that we had quite some troubles with the project in the beginning of this thesis. Considering the fact that we searched for oxidized products for over a year, I guess we both agree that we can be happy about the final outcome of this thesis during the last three years:). Greetings also to Christiaan. I would also like to express my gratitude to Willem. I think you agree that the collaboration between Food Chemistry and Biochemistry has been very fruitful to tackle LPMO issues. I really appreciate your honest opinion about my work and that you always kept me updated on the latest developments in the field of Oxizymes, which was really helpful for me and made me see the science outside of my PhD bubble.

Thanks to my project partners Sandra and Martijn for the great collaboration that we had together and of course for providing so many enzymes. Jaap, I also like to thank you for being involved in my project, for your supporting ideas and interesting talks during conferences and symposia. I am also happy that we kept in contact throughout the whole time of my project, since your support and experience has always been of a high value.

I also like to express my gratitude to my co-authors. Stefano, Sumanth, Dolf thank you for your involvement in my project, for the great data and ideas that helped a lot improving the outcome of this thesis. Special thanks to Adrie, you were involved as a project partner and colleague over the whole period of my PhD project. Thanks for sharing your knowledge about protein purification, modeling and other techniques.

Thanks to the staff of the Laboratory of Food Chemistry and the pleasant atmosphere created by you. First of all, special thanks to Jolanda, the most important person for PhDs for any kind of questions and organizational issues. You make the life of a PhD-student so much easier. Many thanks to the technicians of Food Chemistry: Margaret, René, Mark, Edwin and Peter for equipment introductions and supervisions as well as for the organizational support. Thanks to Jean-Paul, not only as an essential member of our department but also for our discussions and your involvement in my project.

Special thanks to my (old) Biotechnion office mates Maxime, Tomas, Emma, Anne (also for your support regarding editing and printing my thesis) and (new) Axis-X office mates Frederik, Red, Martijn, Roelant, Madelon and Zhibin for sharing your time and for talks during breaks/work. My lab bench sharers Jesse and Gerald, thank you for the inspiring working time together and for being patient with me while was practicing my first sentences in Dutch. Thanks Red, for being the best guide that I could

have in Taipei and for the fun in our office together with Lingmin and Abishek (to Red, sorry that our humour is not 100% similar, but you will understand). Frederik and Luisa, thanks for sharing not only time during work but also while having dinner and many activities together outside work. I would also like to thank all my former and current colleagues about whom I could still write many words but in short: Thanks for making FCH what it was and still is.

Special thanks to special colleagues and friends. First of all my highly-appreciated paranymph Hugo. If they would know about our drinking evenings in FCH, endless talks (Tokyo...) and many other activities conducted during (mainly) and after working time. Also many thanks to my former flat mate Thibaut, who introduced me even more to the world of French wines and showed me that we should not abandon traditional unhealthy food that tastes very good (I should know as I am a studied Nutritional Scientist). In general, I think YouTube would be nothing without us three weirdos. Thanks to Edita and Gijs (also for being my paranymph), both so different, but still so nice companions during and after work. Yuxi, what should I say? Simply Ajinomoto Panda, you will understand :).

I am grateful for all the BSc and MSc students I had the opportunity to work with. Timo, Ilmi, Gijs, Yiting and Theo. Being your supervisor was a great learning experience for me. I also enjoy to see your development and that some of you decided to continue the scientific career by starting or aiming to start your own PhD project.

Many thanks to the staff and my colleagues of the Laboratory of Biochemistry. Mieke, Tom, Antsje, Gudrun, Joseline, Carlo and Janwillem and many more. Thank you for having a good time not only during work but also during coffee breaks, after work drinks and, of course, conferences and courses addressing OxiZymes.

Many thanks to all participants of the FIF practical of the Food Physics department. Elke, Harry, Tijs, Auke, Pauline, Maria, Marco, Philipp for the nice time during supervision of the FIF practical.

Thanks to our friends from Rhenen, Geraldine and Jacob. We spent a lot of quality time together in Rhenen and (now) Apeldoorn and you helped us to enjoy the life outside “Wageningen bubble”.

Am meisten möchte mich bei meiner Familie und meinen Freunden bedanken, welche mich während meiner Doktorarbeit begleitet haben. Natürlich als allererstes für die Unterstützung von meinen Eltern Karola und Matthias, meinem Bruder Andreas, meiner Großmutter Waltraud :) und Großtante Hannelore. Auch möchte ich mich bedanken bei meiner Freundin Helen, für deine Unterstützung und Hilfe (nicht nur literarischer Art), sowie Hela, Ondra, Wolfgang, Janna und Theo. Zudem vielen Dank für die schöne gemeinsame Zeit mit meinen Freunden aus der Altmark und Magdeburg!

Sincerely,

Matthias

About the Author

About the Author

Matthias Frommhagen was born on April 24th 1986 in Salzwedel, German Democratic Republic. After graduating from the grammar school Friedrich-Ludwig-Jahn-Gymnasium in Salzwedel in 2005, he fulfilled his basic military obligation. In 2006 he started studying Nutritional Science (Diplom-Ernährungswissenschaften) at the Martin-Luther-University Halle-Wittenberg, Germany. At the same department, he conducted his Diploma thesis entitled: "Experimental studies to determine the impact of the maternal vitamin D supply on the body composition and vitamin D status of their offspring" under the supervision of Prof Gabriele Stangl and Dr. Corinna Brandsch. In 2012, he started working as a research assistant on the project "Purification and analysis of catechin metabolites from human urine after the ingestion of green tea" under the supervision of Prof Gary Williamson at the School of Food Science and Nutrition, University of Leeds, United Kingdom. In 2013, he started his PhD research at Wageningen University at the Laboratory of Food Chemistry in cooperation with the Laboratory of Biochemistry and DuPont Industrial Biosciences (formerly Dyadic Nederland B.V.). The results of his PhD research are presented in this thesis. Matthias continues to work at the Laboratory of Food Chemistry as a researcher.

Contact: m.frommhagen@yahoo.de

List of Publications

Frommhagen M, Westphal AH, Hilgers R, Koetsier MJ, Hinz SWA, Visser J, Gruppen H, van Berkel WJH, Kabel MA. Quantification of the catalytic performance of C1-oxidizing cellulose specific lytic polysaccharide monooxygenases. *Under review*.

Frommhagen M, Mutte SK, Westphal AH, Koetsier MJ, Hinz SWA, Visser J, Vincken J-P, Weijers D, van Berkel WJH, Gruppen H, Kabel MA. Boosting LPMO-driven lignocellulose degradation by polyphenol oxidase-activated lignin building blocks. *Biotechnology for Biofuels*. 2017; 10:121.

Frommhagen M, van Erven G, Sanders M, van Berkel WJH, Kabel MA, Gruppen H. RP-UHPLC-UV-ESI-MS/MS analysis of LPMO generated C4-oxidised gluco-oligosaccharides after non-reductive labeling with 2-aminobenzamide. *Carbohydrate Research*. 2017; 448:191-199.

Frommhagen M, Koetsier MJ, Westphal AH, Visser J, Hinz SWA, Vincken J-P, van Berkel WJH, Kabel MA, Gruppen H. Lytic polysaccharide monooxygenases from *Myceliophthora thermophila* C1 differ in substrate preference and reducing agent specificity. *Biotechnology for Biofuels*. 2016; 9:186.

Frommhagen M, Sforza S, Westphal AH, Visser J, Hinz SWA, Koetsier MJ, van Berkel WJH, Gruppen H, Kabel MA. Discovery of the combined oxidative cleavage of plant xylan and cellulose by a new fungal polysaccharide monooxygenase. *Biotechnology for Biofuels*. 2015; 8:101.

Brandsch C, Zibolka J, **Frommhagen M**, Lehmann U, Dierkes J, Kühne H, Hirche F, Stangl GI. Vitamin D is not linked to folate status and mRNA expression of intestinal proton-coupled folate transporter. *European Journal of Nutrition*. 2014; 53(4):1115-1122.

Max D, Brandsch C, Schumann S, Kühne H, **Frommhagen M**, Schutkowski A, Hirche F, Staege MS, Stangl GI. Maternal vitamin D deficiency causes smaller muscle fibers and altered transcript levels of genes involved in protein degradation, myogenesis, and cytoskeleton organization in the newborn rat. *Molecular Nutrition & Food Research*. 2014; 58(2):343-52.

Patent applications

Koetsier MJ, Visser J, Iancu SL, Kabel MA, **Frommhagen M**, Gruppen H, Lange H, Crestini C, Benjelloun-Mlayah B. Polypeptides having demethylating activity. 2017. WO 2016207351 A2.

Koetsier MJ, Visser J, Hinz SWA, Kabel MA, **Frommhagen M**, Gruppen H. Enzymatic activity of lytic polysaccharide monooxygenase. 2016. WO 2016142536 A1.

Overview of completed training activities

Discipline specific activities

Courses

Annual Workshop on Enzymatic Hydrolysis of Insoluble Carbohydrates	University of Copenhagen, Holbæk	2013
Genetics and Physiology of Food-Associated Microorganisms	VLAG, Wageningen	2013
Summer Course of Glycosciences	VLAG, Wageningen	2014 [a]
Applied Biocatalysis	VLAG, Wageningen	2014
Biorefinery of Biomolecules	VLAG, Wageningen	2015
Food and Biorefinery Enzymology	VLAG, Wageningen	2015 [a]

Conferences

Lignin Platform	WUR/FBR, Wageningen	2013
PolyRefNorth – Refining Lignocellulosics to Advance Polymers and Fibers	NordForsk Researcher Network, Copenhagen	2013 [a]
Mini-Symposium WBox2	WUR/BCH, Wageningen	2013
Oxyzymes Conference	BOKU, Vienna	2014
Plant Biomass Utilization by Fungi	CBS-KNAW, Utrecht	2015
PolyRefNorth - Refining Lignocellulosics to Advance Polymers and Fibers	NordForsk Researcher Network, Oslo	2015 [b]
GYSS-Global Young Scientist Summit	Pacific World Meetings, Singapore	2016
Oxyzymes Conference	VLAG/BCH, Wageningen	2016 [b]
Symposium on the Chemistry, Biology and Application of LPMOs	University of Copenhagen, Copenhagen	2016

General Courses

VALD PhD Introduction Week	VLAG, Baarlo	2013
Techniques for Writing and Presenting a Scientific Paper	WGS, Wageningen	2013
IELTS Preparation Course	Wageningen in'to Languages, Wageningen	2013
Mobilizing your Network	Young AFSG, Wageningen	2014
Pitch Yourself	Young AFSG, Wageningen	2014
Know your Neighbor – FBR	Young AFSG, Wageningen	2015
Career Perspectives	WGS, Wageningen	2016
Scientific Writing	Wageningen in'to Languages, Wageningen	2016

Additional Activities

Preparation of the PhD Research Proposal	FCH/BCH, Wageningen	2013
Food Chemistry PhD study trip	FCH, Germany, Denmark, Sweden, Finland	2014 [a,b,c]
Food Chemistry PhD study trip	FCH, Japan	2016 [a,b]
PhD Presentation and Seminars	FCH/BCH/DuPont Industrial Biosciences, Wageningen	2013-2017
BSc and MSc Thesis Student Supervision, Presentation and Colloquiums	FCH, Wageningen	2013-2016

[a] Poster Presentation, [b] Oral Presentation, [c] Organizing Committee

Abbreviations: BCH, Laboratory of Biochemistry; BOKU, University of Natural Resources and Life Sciences, Vienna, Austria; CBS-KNAW, Westerdijk Fungal Biodiversity Institute; FBR, Food & Biobased Research; FCH, Laboratory of Food Chemistry; VLAG, The Graduate School VLAG (Advanced Studies in Food Technology, Agrobiotechnology, Nutrition and Health Sciences); WGS, Wageningen Graduate Schools; WUR Wageningen University & Research.

The work described in this thesis was performed at the Laboratory of Food Chemistry and the Laboratory of Biochemistry of Wageningen University & Research, The Netherlands. This project was sponsored by the Graduate School VLAG (Advanced studies in Food Technology, Agrobiotechnology, Nutrition and Health Sciences).

Financial support from Wageningen University and the Graduate School VLAG for printing this thesis is gratefully acknowledged.

This thesis was printed by Proefschrift-AIO

Cover design by Matthias Frommhagen and Guus Gijben

Edition: 240 copies

Matthias Frommhagen, September 2017